NanoSIMS Analysis and High Resolution Electron Microscopy

of Silicate Stardust Grains from Red Giant Stars and Supernova Explosions

Dissertation

zur Erlangung des Doktorgrades

der Naturwissenschaften

Vorgelegt beim Fachbereich Geowissenschaften

der Johann Wolfgang Goethe – Universität

in Frankfurt am Main

von

Christian Vollmer

aus Essen

Frankfurt 2008

(D30)

Vom Fachbereich Geowissenschaften der

Johann Wolfgang Goethe – Universität als Dissertation angenommen.

Dekan: ....Prof. Dr. Gerhard P. Brey

Gutachter: ....Prof. Dr. Frank E. Brenker

2. Gutachter: ....PD Dr. Peter Hoppe

Datum der Disputation: 17.12.2008

"Now I know why I'm here. Not for a closer look at the Moon, but to look back at our home, the Earth."
(Alfred M. Worden, Apollo 15)

Contents

Deutsche Zusammenfassung

Diese Arbeit beschäftigt sich mit der Analyse „präsolarer" Silikat- und Oxidkörner mit Hilfe hochauflösender Massenspektrometrie- und Elektronenmikroskopie-Techniken. Präsolare Körner im allgemeinen, oder „Sternenstaub", ist durch seine extremen Isotopenanomalien in Sauerstoff, Kohlenstoff oder Stickstoff in primitiver Sonnensystemmaterie (Meteorite, interplanetare Staubpartikel, Kometenproben) zu lokalisieren. Die isotopische Zusammensetzung dieses Staubes ist durch keinen Prozess im Sonnensystem zu erzeugen, sondern deutet auf nukleosynthetische Kernreaktionen im Innern von Sternen hin. Diese Körner sind folglich in den sich abkühlenden Gaswolken sterbender Sterne (rote Riesen und Supernova/Nova-Explosionen) kondensiert und haben dabei den nukleosynthetischen „Fingerabdruck" ihres Muttersterns konserviert. Nach einer gewissen Aufenthaltszeit im interstellaren Medium (ISM) waren diese Körner Teil des solaren Nebels, aus dem schließlich das Sonnensystem entstanden ist. Während der Großteil der Sonnensystemmaterie durch Aufheizung und Homogenisierung diesen ursprünglichen „Fingerabdruck" verloren hat, entgingen einige Staubkörner diesen Prozessen, da ihre Mutterkörper niemals in Kern und Mantel differenzierten und kaum sekundär überprägt worden sind. Sie sind älter als das Sonnensystem und damit „präsolar". Das genaue Alter dieser Proben konnte bisher noch nicht ausreichend präzise ermittelt werden, da nicht genügend Probenmaterial für Datierungen vorhanden ist.

Isotopische, chemische und mineralogische Studien an diesen Körnern erlauben somit die Überprüfung astrophysikalischer Fragestellungen, die ansonsten nur über optische Spektroskopie oder theoretische Modellierungen zugänglich sind – und das mit der hohen Präzision der Analyseverfahren, die in Laboren auf der Erde zur Verfügung stehen. Wie entstehen Elemente in den stellaren Kernreaktoren? Wie kondensieren zirkumstellare Staubkörner in den Winden sterbender Sterne? Wie verändern sich Staubkörner im interstellaren Medium? Wie haben sich die Elemente in der Milchstraße entwickelt (Galaktische chemische Evolution)? Welche Sterne haben Material in unser Sonnensystem geliefert? Die Verteilung und Vermischung von solarer und präsolarer Materie schließlich gibt Aufschlüsse über die Entwicklung des jungen Sonnensystems. Dieses Forschungsgebiet vereint somit so unterschiedliche Disziplinen wie Astrophysik, Kosmochemie, Kernphysik und Mineralogie.

Bei den ersten präsolaren Körnern, die Ende der 80er Jahre identifiziert wurden, handelte es sich um höchst stabile Minerale, wie etwa Siliziumkarbid (SiC) oder Diamant, die durch komplexe chemische und physikalische Methoden aus Meteoriten herausgelöst und angereichert wurden. Dadurch zerstörte man über 99% der Meteoriten, die aus Silikaten und Eisenmineralen bestehen, so dass hauptsächlich dieser präsolare Staub im Residuum zurückblieb. Dieser Vorgang wurde einmal mit der schönen Formulierung beschrieben, dass man den Heuhaufen verbrennt, um die Stecknadel zu finden. Zur Analyse des Sternenstaubs sind dann vor allem Methoden mit einer hohen Ortsauflösung erforderlich. In der „Sekundärionen-Massenspektrometrie" (SIMS) wird die Oberfläche einer festen Probe mit hochenergetischen „Primärionen" (Cs^+ oder O^-) beschossen und die entstehenden „Sekundärionen" in einem Massenspektrometer analysiert. Dadurch kann man z.B. die Verteilung verschiedener Isotope in der

Probe sichtbar machen. Sternenstaub fällt dabei durch seine extremen Isotopenanomalien auf, die um Größenordnungen von jeglicher Sonnensystemmaterie abweichen. Da SIMS keine zerstörungsfreie Technik ist, können je nach Größe der Körner und zu erreichender Präzision verschiedene Isotopensysteme gemessen werden. Präsolare SiC-Körner können sehr groß sein (bis zu 60 μm) und weisen einen sehr hohen Spurenelementgehalt auf, weshalb an ihnen bis heute mit Abstand die meisten Untersuchungen durchgeführt wurden.

Jedoch sind SiC-Körner nicht die häufigste Art von Sternenstaub, da sie nur in kohlenstofffreichen Sternatmosphären kondensieren. Das zirkumstellare C/O-Verhältnis definiert die entstehenden Kornarten, da das CO-Molekül eine derart hohe Bindungsenergie hat, dass es praktisch alle verfügbaren C- und O-Atome bindet, so dass nur die häufigere Atomsorte übrigbleibt. Bei C/O > 1 kondensieren somit kohlenstoffhaltige Minerale wie SiC, Graphit oder Diamant, bei C/O < 1 sauerstoffhaltige, vor allem Silikate, die häufigste Mineralklasse auf der Erde und den festen Himmelskörpern des Sonnensystems. Spektroskopische Untersuchungen haben gezeigt, dass Silikate auch im ISM und in den Winden der weitaus häufigeren sauerstoffreichen Sterne (verglichen mit den kohlenstofffreichen) dominieren. Zumeist sind diese Körner amorph, doch ab Mitte der 90er Jahre konnte durch die Messungen des „Infrared Space Observatory" (ISO) gezeigt werden, dass auch kristalline Silikate in den Winden ferner Sterne entstehen, vor allem Olivin und Pyroxen.

Mit der Entdeckung von Sternenstaub in Meteoriten begann also auch die Suche nach präsolaren Silikaten. Dabei zeigte sich, dass die Ortsauflösung der bisherigen SIMS-Geräte (bis zu 1 μm) für die Identifizierung der Silikate nicht ausreichte. Silikate können außerdem nicht wie refraktäre SiC-Körner und Diamanten chemisch angereichert werden, sondern müssen „in-situ" in der Probe gesucht werden. Die Entwicklung der „NanoSIMS" der Firma CAMECA brachte dabei den Durchbruch: Die wesentlich höhere Ortsauflösung durch ein neues Gerätedesign (< 100 nm Strahldurchmesser) führte 2003 zur Identifizierung der ersten präsolaren Silikate in interplanetaren Staubpartikeln (MESSENGER et al., 2003) und wenig später auch in Meteoriten wie dem Acfer 094 (NGUYEN and ZINNER, 2004; MOSTEFAOUI and HOPPE, 2004). Es zeigte sich jedoch schnell, dass weitere isotopische, chemische und mineralogische Untersuchungen an diesem Sternenstaub eine technische Herausforderung darstellen, da die meisten Körner nur ~300 nm groß und umgeben von Silikaten des Sonnensystems mit „normaler" isotopischer Zusammensetzung sind.

Bei Beginn dieser Arbeit im Oktober 2005 waren seit der Entdeckung der ersten präsolaren Silikate nur drei Jahre vergangen. Es gab einige Daten zur Sauerstoffisotopie der Körner, doch weitere Isotopensysteme wie etwa Silizium waren kaum untersucht worden. Über die chemische und mineralogische Zusammensetzung der Körner wusste man noch erheblich weniger. EDX-Messungen im Rasterelektronenmikroskop (SEM) an diesen Körnern liefern keine präzisen Ergebnisse, da die Anregungsbirne der 5 kV-Elektronen erheblich größer ist als der Durchmesser der Körner. Nur Untersuchungen mit einem Transmissionselektronenmikroskop (TEM) erlauben die komplette Charakterisierung von Mineralen, doch müssen die Proben hierfür elektronentransparent sein, d.h. dünner als ~150 nm. Einige präsolare Silikate wurden in interplanetaren Staubpartikeln gefunden, die bereits mit

Hilfe der Ultramikrotomie in dünne Scheiben geschnitten und vor der NanoSIMS-Messung im TEM charakterisiert waren. Diese Methode liefert folglich Daten aus beiden komplementären Techniken ohne die Notwendigkeit eines weiteren Präparationschrittes. Die meisten präsolaren Silikate sind jedoch in Meteoritendünnschliffen oder Kornseparaten auf Goldfolien detektiert worden, die nicht direkt zugänglich sind für die TEM-Analyse. Diese Körner müssen mit der „focused ion beam" (FIB)-Technik aus dem Dünnschliff oder der Goldfolie herausgeschnitten werden (WIRTH, 2004; ZEGA et al., 2007). Diese Präparation ist extrem zeitaufwendig und risikobehaftet, da das Korn dabei verloren gehen kann. Deshalb gab es kombinierte NanoSIMS/TEM-Arbeiten an präsolaren Silikaten bei Beginn dieses Projekts nur für sieben Körner, wovon wiederum nur drei mit FIB präpariert worden waren (MESSENGER et al., 2003; 2005; YADA et al., 2005; NGUYEN et al., 2005; FLOSS et al., 2006). In dieser Arbeit konnten neun weitere mit Hilfe der FIB-Technik aus dem primitiven Meteoriten „Acfer 094" herausgeschnitten und im TEM untersucht werden. Weiterhin ist mit der „Augerelektronen-Spektroskopie" die Chemie der Körner bestimmt worden, die im Gegensatz zu SEM-EDX sehr viele kleinere Probenvolumina analysieren lässt.

Die Ziele dieser Arbeit lassen sich wie folgt zusammenfassen:

– den silikatischen Sternenstaub in der Matrix des kohligen Chondriten Acfer 094 durch NanoSIMS-Rasteranalyse lokalisieren und die Häufigkeit dieser Sternenstaubklasse im Vergleich zu anderen Kornarten und anderer primitiver Sonnensystemmaterie ermitteln,

– die Verbindung zwischen solarer und präsolarer Materie im frühen Sonnensystem in-situ erforschen und dadurch Rückschlüsse über die Evolution des Sonnensystems erwerben,

– die Ursprünge dieser Körner durch Messung der Sauerstoff- und Silizium-Isotopie untersuchen und dadurch Erkenntnisse über nukleosynthetische Prozesse in Sternen gewinnen,

– die stellaren Quellen, die Material in das Sonnensystem geliefert haben, identifizieren,

– die Körner mit Hilfe kombinierter Auger / FIB / TEM-Messungen mikrostrukurell analysieren, um die Bildung in zirkumstellaren Sternatmosphären zu erforschen,

– nach Anzeichen von Veränderungsprozessen aus dem interstellaren Medium suchen,

– diese Ergebnisse mit astrophysikalischen Beobachtungen und theoretischen Modellen vergleichen,

– einen möglichen Zusammenhang zwischen Isotopie und Mineralogie einiger Körner finden.

Insgesamt sind in dieser Arbeit 142 präsolare Silikate und 20 präsolare Oxide anhand ihrer anomalen Sauerstoffisotopie detektiert worden. Umgerechnet auf die untersuchte Fläche enthält der Acfer 094 demnach 163 ± 14 ppm präsolare Silikate und 26 ± 6 ppm präsolare Oxide. Diese Angaben beruhen auf einer relativ hohen Anzahl gefundener Körner und haben deshalb einen kleinen zählstatistischen Fehler verglichen mit anderen Untersuchungen an demselben Meteoriten (z.B., NGUYEN et al., 2007). In keinem anderen Meteoriten sind bisher mehr präsolare Silikate gefunden worden als in diesem, und zusammen mit wenigen anderen kohligen Chondriten und interplanetaren Staubpartikeln repräsentiert er damit das ursprünglichste Material, das zur Erforschung des frühen Sonnensystems zur Verfügung steht.

Die Sauerstoffisotopendaten lassen sich mit theoretischen Überlegungen (z.B., BOOTHROYD and SACKMANN, 1999) und mit Beobachtungen aus zirkumstellaren Auswürfen (z.B., HARRIS and LAMBERT, 1984) vergleichen. Der Großteil der gefundenen Körner stammt demnach aus roten Riesensternen, die

etwa 1 bis 2.5 Sonnenmassen schwer waren und solare oder sub-solare Metallizität aufwiesen. Metallizität ist der Anteil der Elemente schwerer als Helium in einem Stern in der Astrophysik. In einigen Kernreaktionen, z.B. dem sogenannten CNO-Zyklus, verschmelzen 4 Protonen zu einem He-Kern über verschiedene Zwischenschritte, an denen die CNO-Isotope beteiligt sind. Diese fungieren als Katalysatoren, ihre Häufigkeiten können aber stark verändert werden. ^{17}O wird beispielsweise durch den CNO-Zyklus angereichert, ^{18}O teilweise zerstört. Die Produkte dieser nukleosynthetischen Prozesse werden in „Dredge-Up"-Ereignissen an die Sternoberfläche befördert. Die Menge an ^{17}O, die aus der Tiefe des Sterns an die Oberfläche transportiert wird, ist dabei eine steile Funktion der stellaren Masse. Deshalb lässt sich aus den gemessenen ^{17}O/^{16}O-Verhältnissen auf die Sternmasse zurückschließen. Diese theoretischen Modelle, aber auch die spektroskopischen Messungen korrelieren gut mit den gefundenen Isotopendaten. Dennoch ist die Herkunft einiger Kornklassen mit isotopischen Mustern, die nicht sehr gut mit diesen Modellen übereinstimmen, noch immer nicht hinreichend geklärt. Bei der Untersuchung dieser Körner rätselhafter Herkunft hat diese Arbeit einen entscheidenden Beitrag geleistet, da deren Silizium-Isotopie zum ersten Mal in größerer Zahl analysiert wurde. Einige Silikate sind extrem in ^{17}O angereichert (bis zum 12fachen des solaren Werts), was am oberen Ende der Modellvorstellungen und Beobachtungen liegt. Die Siliziumdaten zeigen, dass diese Körner auch moderat an ^{30}Si angereichert sind, was durch den Ursprung in einem Binärsystem (bestehend aus einem Hauptreihenstern und einem weißen Zwerg oder roten Riesen) erklärt werden könnte. Diese Theorie haben NITTLER et al. (2008) zum ersten Mal postuliert und konnte anhand der Daten in dieser Arbeit unterstützt werden. Eine weitere Klasse ungewöhnlicher Körner, gekennzeichnet durch ^{18}O-Anreicherung, konnte in früheren Arbeiten nicht eindeutig einer bestimmten Quelle zugeordnet werden. Diskutiert wurden ein Ursprung in roten Riesensternen mit einer höheren Metallizität als der Sonne oder in Supernova-Explosionen vom Typ II („Core-collapse Supernovae", SNe). In dieser Arbeit ist zum ersten Mal die Siliziumisotopie einer größeren Anzahl ^{18}O-angereicherter Silikate gemessen worden. Es konnte gezeigt werden, dass diese einen Überschuss an ^{28}Si aufweisen, was auf den Ursprung in SNe hindeutet, in denen dieses Isotop in großer Menge durch Sauerstoffbrennen in tiefen Schalen erzeugt wird. Diese Arbeit hat somit einen deutlichen Hinweis auf die Bildung dieser Körner in SNe geliefert und somit auch astrophysikalische Modelle über die Staubentstehungseffizienz in SNe belegt.

Die Messung der Silizium-Isotopie einer großen Anzahl präsolarer Silikate erlaubte außerdem die Quantifizierung des s-Prozess (= langsame („slow") Anlagerung von Neutronen) für die Siliziumisotope in roten Riesensternen. Dieser Effekt war bisher nur über kernphysikalische Messungen (GUBER et al., 2003) und anhand präsolarer SiC-Körner näher untersucht worden (ZINNER et al., 2006). Während SiC-Körner erst dann kondensieren, wenn bereits viel Kohlenstoff und s-Prozess-Elemente an die Oberfläche des Sterns transportiert worden sind, entstehen Silikate weitaus früher. Ihre Isotopie ist also noch nicht sehr stark durch s-prozess-verändertes Silizium geprägt, sondern noch von der ursprünglichen Silizium-Zusammensetzung des Sterns. Durch den Vergleich der Silizium-Isotope-Verteilungen von Silikaten und SiC-Körnern lässt sich folglich der s-Prozess genauer quantifizieren. Die Resultate in dieser Arbeit stimmen gut mit den Vorhersagen überein.

In dieser Arbeit wurde zum ersten Mal eine große Anzahl präsolarer Silikate im SEM charakterisiert. Außerdem konnte die Chemie von fast der Hälfte aller Körner durch Augerelektronen-Spektroskopie analysiert werden. Der Großteil der Morphologien stimmt demnach mit den Erwartungen aus Kondensationsexperimenten überein, denn die meisten Körner bestehen aus kleinen Sub-Partikeln und sind irregulär. Viele Körner im Acfer 094 sind jedoch durch Anlagerung von Eisenmineralen verändert, deren Ursprung bis heute kontrovers diskutiert wird und auch in dieser Arbeit nicht geklärt werden konnte. Entweder sind diese Eisenminerale zusammen mit den präsolaren Körnern primär kondensiert, oder wurden durch sekundäre Prozesse im ISM, im solaren Nebel oder auf dem Mutterkörper implantiert. Es ist somit nicht abschließend zu sagen, welcher Anteil dieser Eisenminerale primären und welcher sekundären Ursprungs ist. Weiterhin hat terrestrische Alteration, also Verwitterung in der Wüste vor dem Fund des Meteoriten, viele Körner chemisch verändert. Neuere Arbeiten am Acfer 094 (z.B., BLAND et al., 2008) haben ebenso gezeigt, dass dieser Meteorit trotz des hohen Anteils an präsolarem Material terrestrische Alteration (Oxidation, aquatische Verwitterung) erfahren hat. Dies bedeutet entweder, dass präsolare Silikate resistenter gegen diese sekundären Vorgänge sind als bisher angenommen, oder dass der ursprüngliche Anteil präsolaren Materials in Acfer 094 weitaus höher war. Auch die Augerelektronen-Spektroskopie-Analysen ergaben eine sehr heterogene Chemie der präsolaren Silikate im Acfer 094 mit weit streuenden (Mg+Fe)/Si- und Mg/Fe-Verhältnissen, was ebenfalls auf Alteration hindeutet. Jedoch könnten diese Resultate auch das Ergebnis primärer Kondensation sein, die unter Nicht-Gleichgewichtsbedingungen ebenfalls zu eisenreicheren Zusammensetzungen führt.

In den Auger-Messungen wurden zum ersten Mal Silikate mit sehr untypischer, chemischer Zusammensetzung nachgewiesen, die entweder sehr Mg-reich oder sehr Mg-arm sind und sich nicht in die üblichen Silikatkategorien einteilen lassen. Diese Körner könnten entweder erneut ein Hinweis auf Alteration sein (durch „Sputtering" im ISM oder im Sonnensystem), oder auf sehr ungewöhnliche Kondensationsbedingungen. Ein sub-solares Mg/Si-Verhältnis (< 0.5) könnte an eine sehr geringe Metallizität des Muttersterns gekoppelt sein, was Beobachtungen belegen (FERRAROTTI and GAIL, 2001), und ein Teil dieser Körner zeigt in der Tat auch ein sehr geringes $^{18}O/^{16}O$-Verhältnis, was ebenfalls auf eine sehr geringe Metallizität hindeuten könnte. Alternativ könnten diese Körner durch fraktionierte Kondensation entstehen, bei der Silizium in der Gasphase angereichert wird, weil es nicht mehr mit den bereits entstandenen Körnern reagieren kann.

Ein besonders interessantes Ergebnis dieser Arbeit ist der Nachweis komplexer präsolarer Silikate. Da es thermodynamisch schwierig ist, Silikate direkt aus der Gasphase zu kondensieren, wird die Entstehung von Nukleationskeimen bei höheren Temperaturen postuliert. An diese Ca-Al-reichen „refraktären" Minerale wie Korund oder Hibonit kann dann das silikatische Material akkretieren. Theoretisch werden diese komplexen Silikate schon lange vorhergesagt (z.B., SOGAWA and KOZASA, 1999), und auch aus Beobachtungen folgert man, dass Ca-Al-reiche Phasen in Sternatmosphären deshalb so schwer nachzuweisen sind, weil sie mit Silikaten bedeckt sein (DIJKSTRA et al., 2005). Die in dieser Arbeit gefundenen komplexen Silikate sind der erste direkte Nachweis, dass diese Vorhersagen tatsächlich zutreffen. Mit Hilfe der Auger-Technik konnte der Elementgehalt eines dieser Körner analysiert werden.

Die Quantifizierung der Daten führt zu dem Ergebnis, dass dieses Korn aus einem Hibonit/Grossit, einem Ca-haltigen Pyroxen oder Mellilit und einem Fe-reichen Silikat aufgebaut ist. Diese Phasen kondensieren sukzessive bei niedrigeren Temperaturen, und ihre Abfolge lässt sich deshalb mit einer Kondensationssequenz erklären, bei der sich die Zusammensetzung des Gases verändert hat. Der Großteil der analysierten Silikate enthält jedoch keine Subkörner, was darauf hindeutet, dass Silikate möglicherweise auch homogen ohne Nukleationskeime auskondensieren können.

Zum ersten Mal sind eine derart hohe Anzahl präsolarer Silikate (neun) in einer Arbeit mit NanoSIMS / TEM untersucht worden. Der Großteil dieser Körner ist Mg-reich und amorph, was mit den Modellen nicht übereinstimmt, welche kristalline Mg-reiche und amorphe Fe-reiche Silikate postulieren. Die Körner könnten jedoch im ISM sekundär amorphisiert worden sein. Chemisch kennzeichnet die Silikate eher eine pyroxen-ähnliche Zusammensetzung, obwohl amorphe Silikate in Sternatmosphären eher olivin-ähnlich sein sollten. Jedoch könnte dies auch ein Effekt der Amorphisierung sein, denn beim „Sputtering" im ISM wird bevorzugt Mg in die Gasphase überführt. Ein weiteres interessantes Ergebnis dieser koordinierten NanoSIMS/TEM-Arbeiten ist, dass es präsolare Fe-haltige Olivine gibt, die die Theorien und Beobachtungen nicht vorhersagen. In den Modellen und Beobachtungen sind kristalline Silikate grundsätzlich praktisch eisenfrei. In anderen TEM-Arbeiten an präsolaren Silikaten (MESSENGER et al., 2005; KELLER and MESSENGER, 2008) sind jedoch ähnliche Fe-haltige Olivine gefunden worden. Dies zeigt, dass die Interpretation der Infrarotspektren neu überdacht werden sollte und möglicherweise auch mit weniger refraktären kristallinen Silikaten kompatibel ist. Weiterhin überwiegt in den bisherigen TEM-Arbeiten der Anteil der Olivine am kristallinen Silikat-Sternenstaub, während Körner mit Pyroxen-Zusammensetzung bis auf eine Ausnahme amorph sind. Dies unterstützt astrophysikalische Modelle, die auf verschiedene Formationswege dieser beiden Minerale hindeuten (BOUWMAN et al., 2008) und somit auf verschiedene Kristallinität: Während Olivin bei hohen Temperaturen direkt aus der Gasphase kondensiert und deshalb kristallin ist, entsteht Pyroxen durch Reaktion des Olivins mit Si in der Gasphase bei niedrigeren Temperaturen. Dies könnte dazu führen, dass der entstehende Pyroxen amorph bleibt.

Das einzige, bisher gefundene kristalline Silikat mit Pyroxen-Stöchiometrie ist das besonders interessante Korn 1_07: Obwohl seine Chemie auf einen refraktären Enstatit hindeutet (Fe < 1 at.%), mit einem erhöhten Mg-Gehalt im Zentrum, konnte das Beugungsmuster im TEM keiner üblichen Enstatit-Struktur zugeordnet werden. Die beste Übereinstimmung ergab sich mit den d-Werten von Silikat-Perowskit, dem häufigsten Mineral des unteren Erdmantels, das erst ab einem Druck von etwa 23 GPa bei ~1300 K stabil ist. Ein Teil der nachgewiesenen Reflexe sind in der eigentlichen Perowskit-Struktur zwar nicht erlaubt, doch dies könnte dadurch erklärt werden, dass der Perowskit in einer Super-Struktur mit verdoppelten Hauptachsen vorliegt, oder dass die Zonenachse nicht perfekt getroffen wurde.

Wie lässt sich aber ein Hochdruckmineral, das in den Winden eines fernen Sterns unter sehr geringem Druck kondensiert sein sollte, erklären? Die Umwandlung auf dem Meteoritenmutterkörper kann ausgeschlossen werden, da der Acfer 094 ansonsten keinerlei Anzeichen für Schockmetamorphose aufweist. Das Korn könnte demnach im ISM in einer Supernova-Schockwelle, bei der Körner und Gasatome mit hohen Geschwindigkeiten aufeinanderprallen, umgewandelt worden sein. Zwar geht die

Theorie davon aus, dass Staubkörner ein solches Ereignis nicht überleben und entweder verdampfen oder komplett amorphisieren. Doch in den theoretischen Modellen ist es prinzipiell auch möglich, dass ein Bruchteil größerer Körner eine solche Konfrontation als Hochdruck-Modifikation überlebt (TIELENS et al., 1994; JONES et al., 1996). Die ungewöhnliche Isotopie dieses Korns (^{17}O ist extrem angereichert) weist außerdem auf die Möglichkeit einer Bildung in einer Nova-Explosion hin, in der dieses Isotop in großen Mengen durch explosiv ablaufende CNO-Zyklen erzeugt wird. Dies würde eine Erklärung sowohl für die Hochdruck-Struktur als auch die Isotopie liefern, wenn das Korn direkt in der Nova-Schockwelle umgewandelt wurde. Interessanterweise hatte man die schon sehr früh nachgewiesenen präsolaren Nanodiamanten auch zunächst durch Schock zu erklären versucht (TIELENS et al., 1987), doch spätere Untersuchungen deuteten eher auf einen CVD-ähnlichen Kondensations-Prozess in den Sternatmosphären hin (DAULTON et al., 1996). Es wäre also als spekulative Variante möglich, dass auch Silikat-Perowskit unter extrem niedrigem Druck direkt kondensiert, doch diese Hypothese müsste durch Laborexperimente und theoretische Untersuchungen überprüft werden. Die Entdeckung dieses Korns ist in jedem Fall ungewöhnlich, da es bis jetzt das einzige, kristalline, präsolare Silikat mit Pyroxen-Chemie ist. Trotz der hier vorliegenden Ergebnisse steht die Untersuchung präsolarer Silikate noch in den Anfängen. Zukünftige Arbeiten werden sich vor allem auf die Messung weiterer Isotopensysteme wie Al-Mg fokussieren. Auch weitere TEM-Analysen, insbesondere an komplexen Körnern, sind erforderlich, um deren Entstehung zu rekonstruieren. Weiterhin muss die Beziehung zwischen solaren und präsolaren Körnern weiter erforscht werden, um neue Hinweise über die Evolution von Sternenstaub und Sonnensystemmaterie zu gewinnen. Diese Forschungsarbeiten werden weitere wichtige Hinweise auf das ursprüngliche Material unseres Sonnensystems liefern, aus dem schließlich auch unsere Erde hervorgegangen ist.

Outline of Thesis

This thesis deals with microanalytical investigations of silicate and oxide stardust located within the fine-grained matrix of the ungrouped carbonaceous chondrite Acfer 094. This subclass of "presolar" grains has been identified only about six years ago, which means that their characterization has just begun. As these silicates are usually less than ~0.5 μm in diameter, analysis of these grains (e.g., isotopic composition, structure, chemistry) is only possible by means of high-spatial resolution in-situ techniques. This issue is further complicated by the fact that the main component of solar system materials are also silicate grains of similar size. Therefore, investigations of these tiny grains are always hampered by analytical difficulties and are a major challenge in cosmochemistry and astrophysics.

The thesis consists of three parts: In the first part introductory information is given to understand the processes affecting presolar silicates. The focus of this part lies on the formation and composition of cosmic dust in general and of silicate dust in particular. The second part describes the applied analytical techniques and also gives some information about the Acfer 094 meteorite. The third, main part consists of three papers, each of which in its structure for journal submission. Two of these papers have already been published in the Astrophysical Journal. The thesis concludes with a summary and an outlook.

The major fraction of this work was performed at the Max Planck Institute for Chemistry in Mainz and the Geoscience Institute / Mineralogy of the Goethe-University of Frankfurt under the supervision of Peter Hoppe and Frank E. Brenker. Further experiments were carried out at the University of Saarbrücken in collaboration with Christian Holzapfel and Flavio Soldera, the Laboratory for Space Sciences in St. Louis (USA) together with Frank J. Stadermann and his group and with Rhonda M. Stroud from the Naval Research Laboratory in Washington, D.C. (USA).

List of Figures and Tables

List of most common abbreviations

AES – Auger electron spectroscopy

AGB – Asymptotic giant branch

AMM – Antarctic micrometeorite

BF – Brightfield (-TEM)

CAI – Ca-, Al-rich inclusion

CBP – Cool bottom processing

DF – Darkfield (-TEM)

EDX– Energy-dispersive x-ray (analysis)

FIB – Focused ion beam

Ga – Billion years

GCE – Galactic chemical evolution

GEMS – Glass with embedded metal and sulfides

HBB – Hot bottom burning

HR – High resolution

IDP – Interplanetary dust particle

IR – Infrared

ISM – Interstellar medium

Ka – thousand years

LIME – Low-iron, manganese-enriched

Ma – Million years

MRP – Mass resolving power

MS – Mass spectrometer

r – process – rapid neutron capture

RGB – Red giant branch

s – process – slow neutron capture

SAED – Selected area electron diffraction

SEM – Scanning electron microscopy

SIMS – Secondary ion mass spectrometry

SMOW – Standard mean ocean water

SN – Supernova

STEM – Scanning transmission electron microscopy

TEM – Transmission electron microscopy

TDU – third dredge-up

Z – Metallicity

1 Introduction

1.1 The cosmic lifecycle of dust

In the final scene of the Science Fiction movie "Gattaca" the main actor Ethan Hawke is heading off Earth in a rocket to explore faraway stars. And as he is leaving his home planet, we can hear the astronaut's last thoughts: That every atom of his body was once created in the interior of a star, which means that he is now not leaving Earth, but rather flying back home.

This scene illustrates - in a rather over-romantic Hollywood way, of course – one of the most fundamental principles of modern astrophysics: The cosmic lifecycle of dust (Fig. 1.1). This cycle has been discussed already in detail (JONES et al., 1997; DWEK, 1998; JONES, 2004; JONES, 2007; ZHUKOVSKA et al., 2008), but I will use it here as a guideline to summarize the most important processes affecting dust grains.

A new stellar system is born from a molecular cloud made of gas and dust (Sec. 1.1.1), whose composition is inherited from the local interstellar medium (ISM). During its evolution the star produces energy via nucleosynthetic reactions, which alter the initial stellar composition (Sec. 1.1.2). Towards the end of its life, the star expels material progressively into the surrounding medium. In the cooling stellar wind dust grains can condense (Sec. 1.1.3), whose compositions are therefore a mixture of the initial and the nucleosynthetically altered material of the parent star. These dust grains become part of the interstellar medium, where they are subject to different modification processes (Sec. 1.1.4). Finally the dust is incorporated into a new stellar system and the cycle starts again.
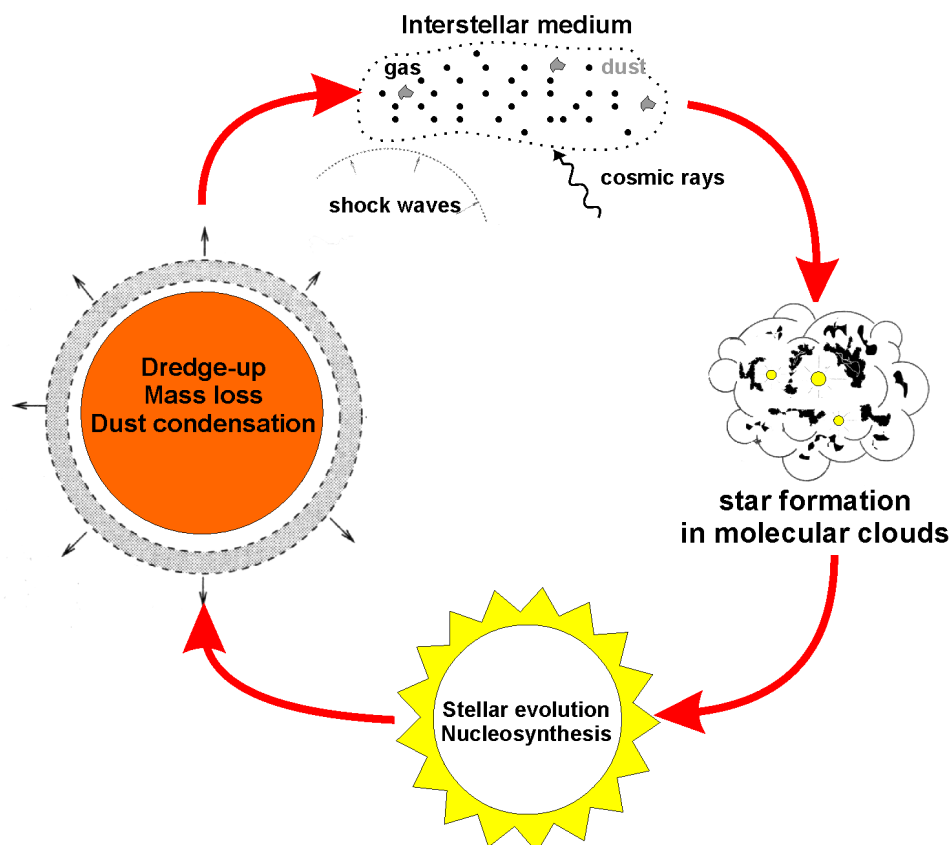
Figure 1. 1 The cosmic lifecycle of dust (after JONES 2004)

As these grains are therefore able to record processes that occur during any of these different cycle stages, their analysis allows us to examine these processes. These investigations have opened up a completely new branch of modern astronomy: "astromineralogy" (JONES, 2007). Originally only based on astronomical observations (Sec. 1.2.1), the discovery of presolar grains as being samples of circumstellar dust that survived formation of the solar system (Sec. 1.2.2) has dramatically increased our knowledge about astrophysical models (HOPPE and ZINNER, 2000; NITTLER, 2003; ZINNER, 2003; CLAYTON and NITTLER, 2004; LODDERS and AMARI, 2005; LUGARO, 2005).

1.1.1 The birth of a star

A star is formed from the gravitational collapse of a dense molecular cloud. Whereas the density in the diffuse ISM is very low (several tens of H atoms per cm^3), cold (~7 – 15 K) molecular clouds contain about 10^3-10^6 H_2 molecules per cm^3. They mainly consist of molecular hydrogen and helium, while heavier elements, which are termed "metals" in astrophysics, are much less abundant (~1 – 2 %). Denser regions in these clouds, so called cloud cores, are sustained against their own gravity by different forces (turbulent motions, magnetic fields, gas pressure and centrifugal forces), but eventually these forces may die down and turn the slow inward transport into a rapidly evolving contraction. Massive stars (> ~8 $M_\odot$) end their lives in supernova (SN) explosions (Sec. 1.1.2.4), and strong shock fronts emerging from these violent events are capable to trigger star formation in neighbouring molecular clouds (BOSS and VANHALA, 2002). This "shock-triggered collapse" model is assumed to play an important role for solar system formation as well. Stars are therefore not single objects that evolve in quiescent molecular clouds separated from each other, but rather form as clusters in stellar nurseries (HESTER et al., 2004).

The cloud then contracts to an even denser and warmer "protostellar cloud" with an optically thick core, the "protostar". Contraction and parallel conservation of angular momentum leads to a higher rotation velocity and advancing collapse. Material from non-equatorial orbits settle down onto the midplane. By then the nebula has adopted a "pancake" shape and is named a "protoplanetary disk". It is noteworthy here, however, that this does not mean that the star is surrounded by planets, and the transition from a protostellar to a "real" protoplanetary disk is not well understood. The central object evolves to a still contracting "pre-main sequence" star, which are mostly low-mass (< 3$M_\odot$) T Tauri stars (other types are the intermediate-mass, but less common Herbig Ae/Be stars). These stars are heated only from gravitational collapse and not from nuclear energy yet. The T Tauri phase is intermediate between the protostar and the final main sequence star and lasts for several Ma until the onset of H burning. During this phase the star has an even higher luminosity than a main sequence star. Finally with the beginning of H burning the star enters the main sequence of the Hertzsprung-Russell (HR)-diagram where it stays for ~90% of its lifetime.

Only ~1% of the initial cloud mass is in the form of sub-μm sized dust. During heating and mixing of the protostellar nebula this dust evaporates, recondenses or may survive unaltered. A major research field of modern astrophysics is how this protostellar dust evolves and how eventually planets may form

(BECKWITH and SARGENT, 1996; VAN BOEKEL et al., 2004). Especially condensation and crystallization of the first grain species in the disk have attracted considerable attention in recent years (HARKER and DESCH, 2002; SCOTT and KROT, 2005). These investigations are crucial in understanding the evolution of the early solar system and the chronology of the formation of solar system bodies such as planets, asteroids and comets. A short introduction to meteorite classification will be presented in Sec. 2.1.1.

1.1.2 Nucleosynthesis and stellar evolution

The first stars that formed in the universe were composed only of those isotopes created during the Big Bang ~13.4 Ga ago: ^{1}H, ^{2}H (=D), ^{3}He, ^{4}He and some ^{7}Li. The isotopes ^{6}Li, ^{9}Be, ^{10}Be and ^{11}B were produced by spallation reactions due to cosmic rays. All other stable isotopes of the elements C to U have been synthesized in stellar interiors via nucleosynthetic fusion reactions. The physics behind these reactions is that nuclei overcome their electrostatic repulsion, the Coloumb barrier, because of extremely high temperatures in stellar interiors. Once the Coloumb barrier is overcome, the strong nuclear force dominates over the electrostatic repulsion. As the mass of the fused nuclei is smaller than the sum of the educts, the mass difference is transformed into energy according to Einstein`s equation E=mc^2. However, this only works up to the Fe group elements, which have the highest binding energies per nucleon. Fusion of higher mass nuclei instead consumes energy, and one of the most fundamental questions of modern physics is the origin of elements heavier than Fe. These elements are created by the capture of neutrons, which are not repelled by electrostatic forces, onto pre-existing seed nuclei. This takes place on a slow (s-process) or a rapid (r-process) timescale (Sections 1.1.2.3 and 1.1.2.4, Tab. 1.1).

Table 1. 1 Nucleosynthetic production mechanisms

Process	Products	T (K)	Site
Hot p-n	H, D, ^{3}He, ^{4}He, ^{7}Li	~10^9	Big Bang
Spallation	^{6}Li, ^{9}Be, ^{10}B, ^{11}B	–	Galactic cosmic rays (GCR)
H burning	^{4}He, ^{13}C, ^{14}N	10^7	Main sequence and red giant stars
Hot CNO	^{13}C, ^{15}N, ^{17}O, F	10^8	Novae
He burning	^{12}C, ^{16}O, ^{18}O	~10^8	Red giant stars
α process (C, Ne, O bruning)	Ne, Na, Mg (C)/ ^{16}O, Mg, Si (Ne)/ Si, S (O)	~10^9	Evolved massive stars, SNe
s process	Some elements heavier than Fe, e.g. Sr, Ba, Pb	~10^8	Red giant stars, massive stars
e process	Fe peak species	~5 x 10^9	SNe
r process	Some elements heavier than Fe, e.g. Xe, Eu, Pt	~10^9	SNe, neutron stars, ?
p process	p-rich isotopes of elements heavier than Fe	~10^9	SNe, ?

The idea that elements are synthesized in stellar interiors was pushed by HOYLE (1946) and later on testified by observations of the unstable isotope ^{99}Technetium (half life 2.1x10^5 a) in some red giant stars (MERRILL, 1952). In their classic work, BURBIDGE et al. (1957) defined the main nucleosynthetic processes and their ideas are still mostly valid today (Tab. 1.1). In the following a rough sketch of stellar evolution is given with an emphasis on those processes important for presolar grain research. For a more detailed review see, e.g., TRURAN and HEGER (2003).

1.1.2.1 Main sequence and H burning

Fusion of protons (=nuclei of H) to α particles (=nuclei of He) is the main process of energy production in stars on the main sequence occurring via so-called "pp chains":

$p + p \rightarrow D + e^+ + \nu$

$D + p \rightarrow {}^3He + \gamma$

${}^3He + {}^3He \rightarrow {}^4He + 2p$
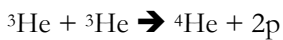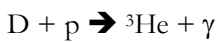
This is the ppI chain, whereas the other two chains (II, III) produce the nuclei ^{7}Be, ^{7}Li, ^{8}Be and ^{8}B in their course. The minimum temperature for these reactions to occur is ~6 x 10^6 K. The net outcome of pp chains is production of ^{4}He, which does not react with protons any more. All other nuclei produced in the course of pp chains rapidly decay or capture protons. It is therefore obvious that elements between He and Si can only be created in fusion reactions occuring at higher temperatures (e.g., He burning, see below). However, if there are initially elements between He and Si present in the star, proton captures do occur via secondary nucleosynthetic reactions (CNO cycle, Sec. 1.1.2.2). The primary mass of elements heavier than He initially present in a star relative to its whole mass defines its metallicity Z. The metallicity of the Sun is 0.016, which means that 1.6% of the solar material consists of elements heavier than H and He. The first generations of stars therefore had a very low metallicity, whereas later generations contained already elements synthesized by these first stars. The metallicity of a star is therefore tightly coupled to the age of the Galaxy, although other aspects may play an important role as well, e.g., a heterogeneous distribution throughout the ISM (NITTLER, 2005). The "Galactic chemical evolution" (GCE) of the elements is a field of its own in astrophysics (TIMMES et al., 1995). The metallicity of a star is, together with its mass, one of the most important parameters determining its later evolution and composition.

1.1.2.2 The CNO cycle

Reactions evolving only from H and He are defined as primary. Secondary reactions start from nuclei that are already present in the star (mainly C, N and O). The net outcome of these reactions is again the fusion of 4 protons into ^{4}He, because the secondary isotopes mainly serve as catalysts. These reactions usually start and end with the same nucleus and are hence termed "cycles". The most important is the CNO cycle, which consists of two sub-cycles, the CN and the NO cycle (Fig. 1.2).
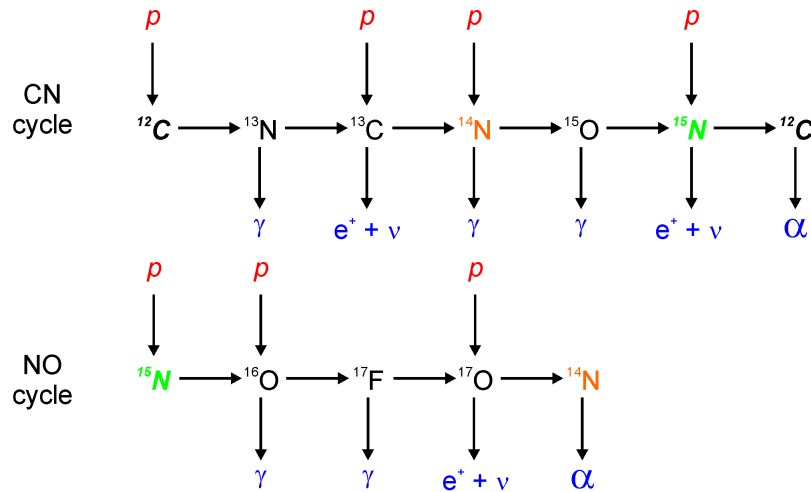
Figure 1. 2 Reaction schemes of the CNO cycle
Educts are in red and products in blue. The NO sidebranch is activated with a probability of ~5x10^{-4}.

The CN circle is activated at ~15 x 10^6 K and usually starts with proton captures on ^{12}C. The NO cycle is activated at ~2 x 10^7 K which starts with proton captures on ^{16}O. The equilibrium result of the CNO cycle is the production of ^{14}N at the expense of C and O. The abundances of the secondary isotopes can be tremendously altered during these reactions. For example, the ^{17}O/^{16}O ratio can vary from 1 x 10^{-4} to 0.02 (solar = 3.83 x 10^{-4}) depending on the temperature; abundances of ^{18}O and ^{19}F are depleted by proton captures. As virtually all stars reach temperatures necessary for the CNO cycle to occur, signatures of the cycle can be detected in all important presolar grain species. The reaction rates, however, strongly depend on temperatures and available nuclei and therefore on the stellar mass and metallicity.

Two other cycles, the NeNa and the MgAl cycle, will not be described here in further detail. The NeNa cycle produces ^{23}Na at the expense of ^{22}Ne, the MgAl cycle ^{26}Al at the expense of ^{25}Mg.

1.1.2.3 Stellar evolution of low- to intermediate-mass stars (< 8 M$_\odot$)

During the main sequence phase, the star is in hydrostatic equilibrium between its strong radiation / gas pressure and its gravitational energy. This phase lasts for ~10 Ga for solar-mass stars and is shorter for more massive stars, which consume their fuel more rapidly. After exhaustion of H in the core (~10% of total mass), the core, now consisting of He, contracts and allows partial H burning in a thin shell above the core due to higher temperatures (Fig. 1.3). The outward pressure rises and the star expands to gain hydrostatic equilibrium again. It therefore has a lower surface temperature (=effective temperature): the star has climbed the "Red giant branch" (RGB) in the HR-diagram, which lasts for ~500 Ma in a solar mass star. This stage is also characterized by deep convection of the stellar envelope: The "first dredge-up", which mixes the ashes of nucleosynthetic reactions into the stellar atmosphere for the first time. When core temperatures reach ~10^8 K, He burning commences in a violent manner, the "He-flash". The star now has a higher effective temperature and lower luminosity and moves back close to the main sequence for ~50 Ma for a solar mass star onto the horizontal branch. He burning mainly produces ^{12}C and ^{16}O via two reactions:

α + α + α ➜ ¹²C ("triple-α" reaction)

¹²C + α ➜ ¹⁶O + γ
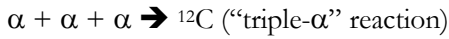
During this stage, two sources therefore generate energy, He core and H shell burning. After exhaustion of core He burning stars of higher mass (> 4 – 5 $M_\odot$) experience a "second dredge-up" event, which again mixes CNO-processed material through the convective envelope to the stellar surface.
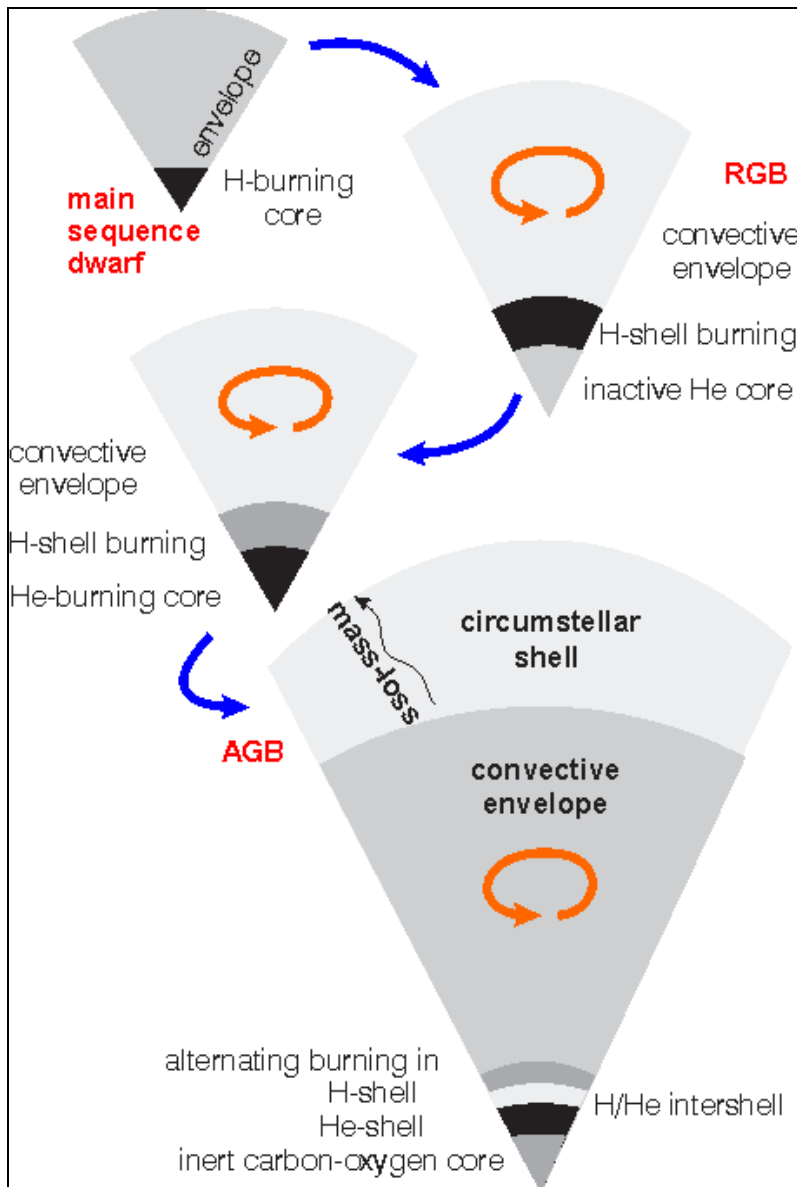
Figure 1. 3 Schematic sketch of a solar mass main sequence star to the AGB phase
(after LODDERS and AMARI 2005, with the permission of Elsevier press)

When He is exhausted in the core, the star follows a similar path as after the end of core H burning: the now degenerate core consisting of C and O contracts and He and H burning commence in thin shells around this core (Fig. 1.3). The star has become an "Asymptotic giant branch" (AGB) star. In stars of higher mass (> ~8 $M_\odot$) further nuclear reactions occur and will be described in the next section. However, the most massive AGB stars (~7.5 – 9.25 $M_\odot$) do ignite C in the core and are termed super-AGB stars (POELARENDS et al., 2008). The main energy of AGB stars is produced in a thin H shell above

an inactive "He intershell". Below the He intershell, a He burning shell lies on top of the inactive CO core. The activation of the two energy producing layers follows a complex alternating path and stellar models are able to calculate the evolution of AGB stars in a more and more accurate way (see e.g. HERWIG, 2005). On the early AGB (E-AGB), He shell burning dominates energy production, which is then overtaken by H shell burning above the inactive He intershell. When the temperature and density are high enough, He burning sets in at the base of the He intershell in an almost explosive way. This instability, known as "thermal pulse", homogenizes the material in the He intershell. In the meantime, the H shell cools and H burning stops. After a few hundred years the thermal pulse is quenched. Following this episode, material from the He intershell (mainly ^{12}C) is then mixed into the stellar envelope and to the surface in so-called "third dredge-up" (TDU) events.

This cycle is repeated $10 - 100$ times, the star has then become a "thermally pulsing" (TP) AGB star. An important aspect of these TDU events is, that they gradually increase the abundance of ^{12}C relative to ^{16}O in the stellar atmosphere. At some point, C dominates over O and the star has become a carbon star. This has significant implications for the types of dust grains to condense (Sec. 1.1.3). However, the efficiency of TDU events strongly depend on stellar mass and metallicity. For example, the TDU is expected to be more efficient in stars of lower-than-solar metallicity due to higher temperatures, whereas a solar-metallicity star needs a minimum mass of 1.5 $M_{\odot}$ to become carbon rich (LATTANZIO, 1989). Furthermore, models show that stars with an initial mass > 4 $M_{\odot}$ experience a deep mixing event named "Hot bottom burning" (HBB) (BOOTHROYD et al., 1995), which prevents the star from becoming carbon rich. In these stars, the base of the convective envelope reaches temperatures high enough for the CN cycle to commence, which converts ^{12}C to ^{14}N. Carbon is therefore never enriched in the stellar atmosphere. ^{18}O is efficiently destroyed by proton captures in this extra mixing event to reach $^{18}O/^{16}O$ ratios down to $10^{-6} - 10^{-7}$, whereas ^{17}O is enriched. Recent cross section determinations of the $^{16}O(p,\gamma)^{17}F$ reaction rate yielded an equilibrium ratio for $^{17}O/^{16}O$ of $\sim 2.5 \times 10^{-3}$ (ILIADIS et al., 2008). A further extra mixing event, "Cool bottom processing" (CBP) has been proposed by models (WASSERBURG et al., 1995; NOLLETT et al., 2003) and was later on testified by presolar grain analyses (e.g., ZINNER et al., 2005). It can be important already during the RGB phase after the first dredge-up. During this non-standard mixing process, material from the convective envelope penetrates the underlying radiative region, where temperatures are high enough to convert some ^{12}C into ^{13}C and deplete ^{18}O via proton captures. ^{17}O is produced via proton captures onto ^{16}O, but also destroyed via the reaction $^{17}O(p,\alpha)^{14}N$, leading to an enhanced equilibrium value for $^{17}O/^{16}O$ of ~ 0.0011 for CBP-processed material (NOLLETT et al., 2003). The exact physical conditions of this process are still largely unknown, but might be due to magnetic mechanisms (BUSSO et al., 2007).

Another important process taking place in the He intershell are slow neutron capture reactions (s-process). The neutron density is very low ($N_n \sim 10^7 - 10^8$ cm^{-3}) and timescales are on the order of thousands of years, which allows unstable nuclei to decay. Typically synthesized nuclei are Ba, Sr, Zr or Y. The rates of these reactions can be experimentally determined by measuring the cross sections of different "s-process paths". As these different paths depend on a large number of nuclear parameters, cross section

determinations applied to astrophysical problems are always hampered by uncertainties. For example, the size of the so-called "^{13}C pocket" at the top of the He intershell, which releases the needed neutrons via the ^{13}C(α,n)^{16}O reaction, heavily influences elemental abundances. The concurring reaction ^{22}Ne(α,n)^{25}Mg is only efficiently activated at temperatures > 3 x 10^8 K, and is therefore more important in more massive (> 5 M$_\odot$) stars. TDU events therefore not only enrich ^{12}C but also s-process elements in the stellar atmosphere.

When mass loss drops after decease of the last thermal pulses, the star evolves to a "post-AGB" star for only 10^2 – 10^3 years, during which the last envelope material is expelled at high velocities (up to 1000 - 4000 km/s) into the surrounding medium. The final stage of stellar evolution is a planetary nebula (PN) with the central degenerate CO core becoming a white dwarf and an enveloping shell of gas and dust.

1.1.2.4 Stellar evolution of high-mass stars (> 8 M$_\odot$)

Stars more massive than ~8 M$_\odot$ evolve differently than AGB stars described above and enter the "red supergiant" phase after cease of core H burning. Most stars heavier than 25 M$_\odot$ pass the "Wolf-Rayet phase", where the star is very hot (T$_{eff}$ between 25000 and 50000 K) and loses most of its envelope in strong stellar winds that exhibit broad emission lines of different elements (mainly C, N, and O). A review on the evolution of massive stars can be found in WOOSLEY et al. (2002). These stars attain higher core temperatures and are therefore able to produce heavier nuclei by a variety of further fusion reactions. As these reactions get more and more complex with increasing mass number, only basic schemes can be sketched here. Most of these objects end their lives in violent "core-collapse Supernova" explosions (Type II SNe or SNeII), which provide the most interesting, but least understood sites of dust grain formation (Sec. 1.1.3.2). Type II SNe are characterized by emission lines of atomic H, which separates them from Type I SNe, that do not exhibit this feature.

The most dominant processes igniting the CO core, after core He burning has died down, is fusion of ^{12}C, which is activated at ~10^9 K via the reactions

^{12}C + ^{12}C ➜ ^{20}Ne + α

^{12}C + ^{12}C ➜ ^{23}Na + p
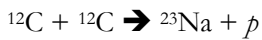
Further α captures on ^{20}Ne and proton captures on ^{23}Na generate ^{24}Mg, and via secondary reactions all stable isotopes of Ne, Na, Mg, Al, Si and P can be produced. At ~1.3 x 10^9 K ^{20}Ne photodisintegrates due to high energy γ photons to ^{16}O and α particles, which react again with ^{20}Ne to form ^{24}Mg ("Ne burning"). At 2 x 10^9 K after core Ne exhaustion O burning sets in and produces mainly ^{28}Si and ^{32}S. By a variety of other reactions, all isotopes of Si, Cl, Ar, K, Ca, Ti and Cr are created as well. C, Ne and O burning reactions are summarized as α-capture processes ("α-process").

Above ~3 x 10^9 K Si burning sets in. This reaction behaves differently than previous fusion schemes, as the most abundant product ^{28}Si photodisintegrates into a large number of nuclei, nucleons, electrons, positrons and photons, that head towards a statistical equilibrium ("e process"). The most stable nuclei are the Fe group elements Cr, Mn, Fe, Co and Ni, which are the final products of e burning.

From these nuclei, no further energy can be produced through nuclear fusion, and eventually the stellar reactor ceases. The pre-SN star has by then developed an "onion-like" structure, as preceding fusion reactions occur in thin shells above the core, which are well homogenized by convection (MEYER et al., 1995) (Fig. 1.4).
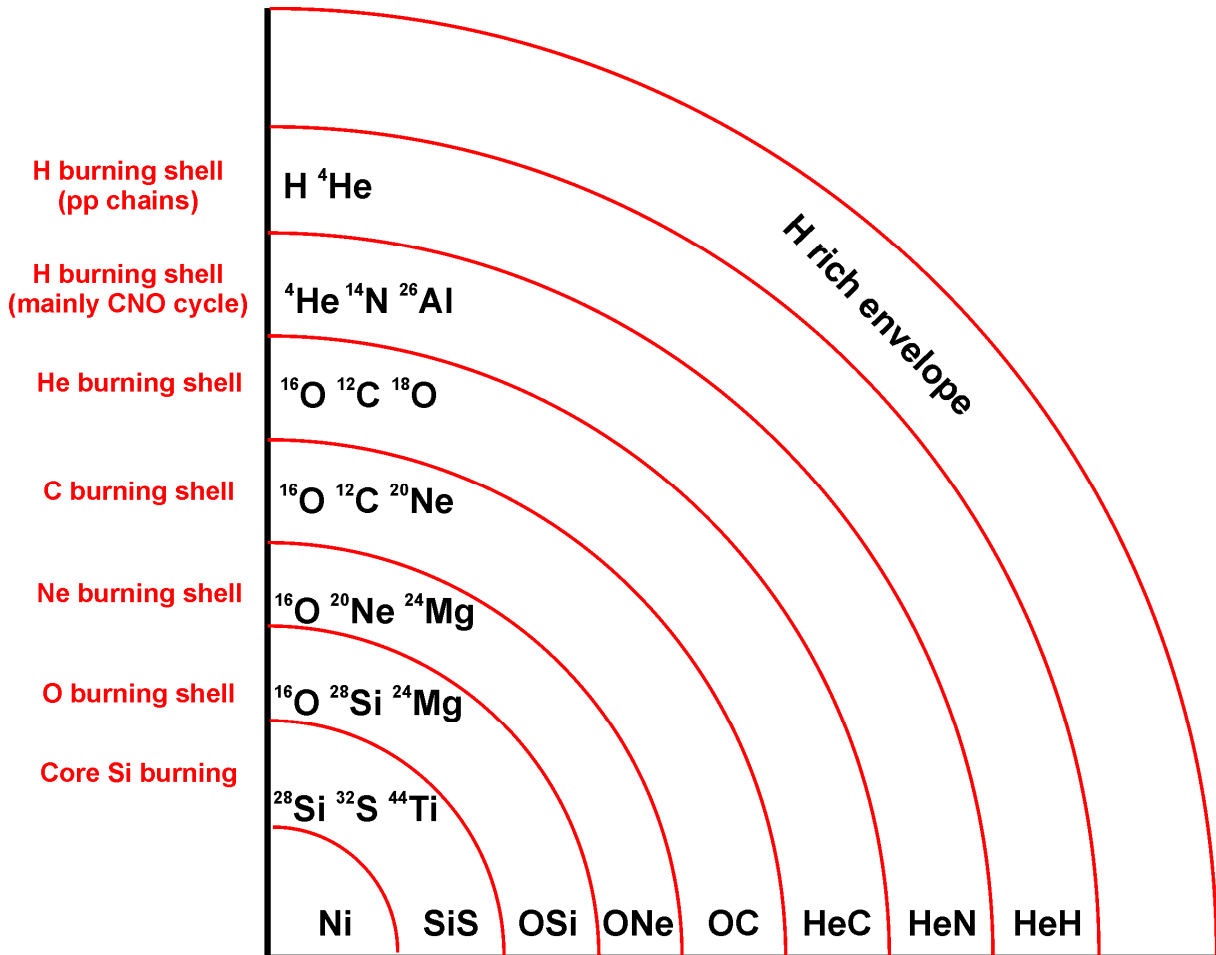
Figure 1. 4 The shell structure of a pre-supernova star
The main nucleosynthetic reactions and products are indicated (after LUGARO 2005). The sizes of the different shells are not to scale.

When the core ceases to produce energy, the gravitational cataclysm is inevitable: The core collapses and partly transforms Fe and Ni into α particles and neutrons, the resulting shock virtually disrupts the whole star. The ejecta are heated by strong neutrino-driven winds emerging from the nascent neutron star. Under the conditions of this outburst explosive nucleosynthesis can modify the composition of the outer layers: "α-rich freeze-out" of O and Si burning leads to the production of α-rich nuclei at very high temperatures such as ^{44}Ti, ^{48}Cr, ^{52}Fe, ^{56}Fe and ^{60}Zn. The remaining core may also become a black hole for the most massive SNe. More elements with mass numbers between 100 – 200 are synthesized via rapid neutron capture reactions ("*r*-process") with neutron densities over 10^{20} cm^{-3} on a much shorter timescale, which prevents β decay of transitional radioactive nuclei. However, the exact astrophysical site of the *r* process is still under debate as its modelling is a complex task (see e.g. ARNOULD et al., 2007 for a recent

review). The "p-process", which includes the γ- and ν-process, is also thought to occur in SNeII and leads to synthesis of proton-rich nuclei such as ^{136,138}Ce or ^{92,94}Mo.

1.1.2.5 Binary stars

About 50% of all stars exist as binary systems (DUQUENNOY and MAYOR, 1991). If their mutual distance is large enough, they can be treated as single stars, but if they evolve very close to each other, mass transfer from one star to the other occurs, which influences their evolution. The most prominent example are novae, where H-rich envelope material from a low-mass main sequence star or a red giant is transferred onto the surface of a white dwarf (see e.g. GEHRZ et al., 1998). During the resulting "thermonuclear runaway" explosion high temperature (several 10^8 K) proton capture reactions under non-equilibrium conditions occur, resulting in the production of large amounts of ^{13}C, ^{15}N and ^{17}O. Luminosities reach $10^4 - 10^5$ times the solar value (JOSÉ and HERNANZ, 2007). Depending on the composition of the white dwarf the outburst is classified into a CO or ONe nova with the latter being more violent with higher peak temperatures and available ^{27}Al as seed nuclei leading, for example, to an enrichment of ^{29,30}Si relative to ^{28}Si. Recently, a distinction between "classical" and "primordial" novae has been suggested (JOSÉ et al., 2007), where nova outbursts evolving from the most primitive, low-metallicity binaries are thought to eject more material than their younger counterparts. These primordial novae display a higher nuclear activity and might play a role for the condensation of certain presolar grains (Sec. 1.1.3.3).

More violent explosions, Type Ia supernovae, occur in close binaries, if the mass of the white dwarf increases over its stability threshold of ~1.4 M$_\odot$ (Chandrasekhar limit). The electron degeneracy pressure can not sustain the gravitational pressure from the accreting matter anymore, and the white dwarf is disrupted in an explosive detonation. C burning and the e process mainly leads to the production of the Fe group elements. Type I SNe do not show H features in their spectra. Massive stars, that have shed virtually their entire H envelope prior to core collapse, comprise the types Ib and Ic SNe. The most violent SNe with kinetic energies over ~10^{52} ergs have been termed "Hypernovae" (NOMOTO et al., 2006) and might have a connection to "Gamma-ray bursts", the most energetic events of our universe since the Big Bang.

1.1.3 Dust condensation in stellar ejecta

1.1.3.1 Condensation around AGB stars

AGB stars are the most important dust producers of our galaxy together with massive stars and novae/supernovae, with the latter being possibly more important in the very young universe. During their final evolutionary stages, mass loss rates can be up to 10^{-4} M$_\odot$ a^{-1}. The chemistry of the stellar atmosphere strongly depends on the abundance ratio C/O, because the CO molecule is extremely stable and virtually combines all available C and O atoms until the more abundant one is left over. Initially, a star inherits an O-rich composition from the ISM, but TDU events enrich the atmosphere progressively with more and more ^{12}C. This evolution can be observed in the spectral types of AGB stars, which gradually evolve from

M (C/O < 1) over S (C/O ~ 1) to C (C/O > 1). Whereas O-rich dust is characterized by silicates and oxides, C-rich dust around carbon stars consists of carbides and sulfides. The dust around intermediate S stars is of peculiar composition (e.g., FeSi) (FERRAROTTI and GAIL, 2002). The dust composition also strongly depends on the mass loss rate and therefore the amount of available gas species (SOGAWA and KOZASA, 1999; JONES, 2007). It has to be noted here, however, that the chemistry of O-rich stars might be more complex than just determined by the C/O ratio (ZIURYS et al., 2007). Furthermore, O-rich dust has been detected around carbon stars as well (MOLSTER and KEMPER, 2005) surviving from evolutionary episodes when the star was still O-rich.

Condensation models calculate with low pressure ranges (~10^{-2} – 10^{-7} bar) and generally assume solar system abundances of the elements in the gas. Program codes like the CONDOR code (LODDERS and FEGLEY JR., 1995) together with thermodynamic properties are able to determine which element condenses at which temperature into which phase taking into account mass balance calculations (GROSSMAN, 1972; LODDERS, 2003). Usually these calculations assume equilibrium conditions, which means that the condensed primary phases and the gas keep reacting and may form secondary phases at lower temperatures and that the chemistry of the gas does not change. However, these equilibrium conditions are not a very realistic assumption for the fast cooling and rapidly diluting outflows and ejecta of AGB stars (GAIL, 2003), although a lot of predictions from these calculations fit well the observations. But new developments in modern condensation theory focus on kinetically controlled condensation conditions, where time is an important factor influencing condensation kinetics in contrast to equilibrium condensation which is given enough time to reach a "steady-state".

Condensation of solid solution series (e.g, Olivine $Mg_{2x}Fe_{2(1-x)}SiO_4$) can be computed as well and usually show that Mg-rich endmembers form under equilibrium conditions at high temperatures (> 1000 K) whereas the Fe-richer species form at lower temperatures under non-equilibrium (e.g. GAIL, 2003).

Most dust species condense via "heteromolecular" growth, which means that the gas composition changes during condensation. Silicates condense heteromolecularly, because the nominal molecule corresponding to the chemical formula of the solid does not exist and the grain is formed from the addition of species such as Si-O and Mg. "Homomolecular" on the opposite means that the composition of the vapour is the same than the one of the condensate. From the most abundant cosmic dust species only solid iron may form via homomolecular growth, i.e. from the addition of Fe atoms from the gas phase.

One of the most important but least understood aspects of dust condensation theory is the formation of "seed nuclei", which can have a different composition than the main condensing species ("heterogeneous condensation"). The surfaces of these seed clusters then act as reaction surfaces onto which the main, lower temperature species condense. For example, tiny carbide grains within presolar carbon-rich phases have been detected (BERNATOWICZ et al., 1996), and these composite grains document a condensation sequence with the higher temperature inclusion condensing first. For silicates, seed nuclei clusters of Al_nO_m or Ti_nO_m are expected by condensation theory (SOGAWA and KOZASA, 1999) and observationally, because Al-rich oxides are coated by silicates at higher mass loss rates (DIJKSTRA et al., 2005). Homogeneous condensation of silicates is also thermodynamically unfavourable. For more detailed

information on condensation theory especially of O-rich dust grains see, e.g., (GAIL and SEDLMAYR, 1999; FERRAROTTI and GAIL, 2001; FERRAROTTI and GAIL, 2002; GAIL, 2003).

1.1.3.2 Condensation around supernovae

Although it is known that SNe contribute dust to the ISM, the exact amount and compositions of these dust grains are poorly constrained. In fact, models dealing with injection rates of SNe sometimes refer to abundances reported by presolar grain researchers (ZHUKOVSKA et al., 2008). Especially the efficiency of dust condensation in the high-energy environment of SNe is difficult to deal with. It has been proposed, that the C/O ratio is not a key parameter anymore around SNe, as the CO molecules are disrupted by high-energy electrons (CLAYTON et al., 1999). Grains may then condense from a gas made of free atoms and not of molecules (EBEL and GROSSMAN, 2001). Conditions are far from equilibrium as the gas from which dust grains condense is merged from different SN zones of variable compositions. Grain condensation conditions are therefore extremely sensitive to the details of mixing (LODDERS, 2006). For example, carbonaceous SN dust grains like low-density graphites and certain SiCs are believed to incorporate material from deep inner SN zones, which are transported into outer C-rich regions by so-called "Rayleigh-Taylor" instabilities proposed by hydrodynamical calculations.

Although the "bulk" composition of SN ejecta is O-rich, a large number of detected presolar SN grains are carbonaceous and mixing calculations for the formation of carbonaceous SN grains are always hampered by the difficulty to obtain a C/O ratio larger than unity (TRAVAGLIO et al., 1999). Nevertheless, heterogeneous mixing of different SN zones can account for the observed isotopic signatures of SN graphite (TRAVAGLIO et al., 1999) and SiC (HOPPE et al., 2000) grains along with C/O > 1 in the ejecta. Fe and other species may be implanted into these grains in the reverse shock of the SN and isotopic compositions may be altered as well in this high-energy environment (DENEAULT and CLAYTON, 2003). Observationally, dust grains have been detected in the ejecta of different SN remnants like 1987a, Cassiopeia A and 2003gd, but the exact amount and composition is still a matter of debate but may range from 0.01 to 1 $M_\odot$ per SN (SUGERMAN et al., 2006; NOZAWA et al., 2007; RHO et al., 2008). Analyses of presolar grains from SNe may help to substantiate possible formation scenarios.

1.1.3.3 Condensation around novae

Novae are common phenomena (~30 events per year, JOSÉ and HERNANZ, 2007), but as only low amounts of material are ejected (~10^{-4} – 10^{-5} $M_\odot$ per outburst), they do not seem to contribute a lot of dust to the ISM (~0.3%, GEHRZ et al., 1998). Up to now, condensation calculations have been performed only for "classical" (=solar metallicity) novae, but grain species and isotopic features of grains from low-metallicity "primordial" novae (JOSÉ et al., 2007) might be different. Predictions for condensing grain species are also different than in AGB stars and include such rare species like cordierite ($Mg_2Al_4Si_5O_{18}$) (JOSÉ et al. 2004). However, more detailed condensation calculations need to be computed. CO novae generally seem to contribute more dust to the ISM, because the expanding shells of the higher mass ONe novae attain higher peak temperatures and lower densities which is not favourable for dust formation. A

discriminating feature of the few nova grains found to date (AMARI, 2002; JOSÉ and HERNANZ, 2007) is an enrichment in ^{30}Si, but only > 1.25 M$_\odot$ ONe nova models display this ^{30}Si enrichment. The mismatch between the lower-than-unity C/O ratio predicted for the bulk nova composition and observed carbonaceous phases (GEHRZ et al., 1998) still provides a puzzle similar to SN calculations. This again might be explained if condensation around novae is not very sensitive to the C/O ratio, but determined by non-equilibrium conditions.

1.1.4 Dust in the interstellar medium (ISM)

Dust grains expelled from AGB stars and supernovae/novae into the ISM are subject to a variety of destruction and modification processes (TIELENS et al., 1994; JONES et al., 1996; JONES, 2004). The grains interact with low- and high-energy photons, where the high-energy photons (down to γ-ray wavelengths) are able to heat and completely vaporize the grain. Interactions with cosmic rays (high energy particles like protons and α particles) may have the same effect if the relative energy between the impacted grain and the impactor is small. At MeV energies cosmic rays merely travel through the grain without causing a lot of damage (JONES, 2004). If the relative energies are in the range of several tens of eV, sputtering becomes important, which means that the impacting ions/atoms remove material from the grain´s surface. Mg for example is preferentially sputtered relative to Si and might therefore be depleted towards the rim of a grain (BRADLEY, 1994). In general, protons and α particles dominate the sputtering process because of their high abundances, but O and C atoms/ions are more effective sputterers because of their higher mass. Another important outcome of these interactions is that crystalline grains may be rendered amorphous.

The impacting particles are usually accelerated by SN shock waves traversing the ISM. In the hot post-shock gas of the propagating shock front, sputtering arises from the thermal velocities of the impacting gas particles, which is one of the dominant processes destroying dust grains (thermal sputtering). On the other hand, inertial sputtering takes place when the gas is rapidly swept up in the shock but the dust grains do not catch up due to their higher inertia. The sputtering yield depends on a variety of parameters such as gas density, temperature, impacted material and impactor.

Although only about 1% of the ISM mass is in the form of dust grains, in areas with higher densities dust grains may collide and interact as well. The resulting effects again depend on the relative velocities, the grain sizes and their compositions. At very low velocities (~1 m/s) grains may stick together and coagulate to form larger aggregates. However, grains affected by shock fronts experience higher relative velocities (at least several km/s) and may be shattered and fragmented into smaller particles. This process preserves the original dust mass, but shifts the peak in the grain size distribution to smaller values. At relative velocities > 20 km/s grains may also be completely vaporized by impacting grains, although it has been shown that this process is less important than shattering independent of the shock velocity (JONES et al., 1996). It is therefore possible that larger grains survive passage of fast shock fronts but may be fragmented into smaller particles.

The estimated lifetime of dust in the ISM experiencing these different destruction processes is estimated to be on the order of $4 - 6 \times 10^8$ years (JONES, 2007). This is somewhat problematic, as on the other hand the estimated reinjection timescale of dust from red giant stars and SNe is on the order of several billion years (DWEK, 1998; JONES, 2007). This could lead to three conclusions: First, dust injection rates are higher than the estimate above and balances the destruction timescale, which might be due to higher injection rates of SNe which are hard to determine. Second, grain destruction in the ISM is not as effective as models might show. This is also conceived by presolar grain researchers, who do not observe any indication of extensive ISM effects like sputtering features in these grains. In fact, microstructures are very well preserved (e.g., STROUD et al., 2004; MESSENGER et al., 2005; KELLER and MESSENGER, 2008). However, this could also be due to a very short residence time in the ISM (OTT et al., 2005). Furthermore, dust grains often accrete icy or carbonaceous mantles, which might protect them from sputtering and destruction and even support coagulation to larger grains (CHOKSHI et al., 1993). Third, there must exist a mechanism for grain formation in the ISM itself. This is also concluded from the fact that refractory elements like Ca and Ti are depleted in the gas phase as derived from observations (SAVAGE and SEMBACH, 1996) and therefore have likely condensed into dust grains. However, the physical process by which dust grains may form under these low temperature / low pressure conditions of the ISM remains a puzzle. It has been proposed that dust grains formed "in-situ" in the ISM are the main component of the ISM dust from which our solar system has emerged (ZHUKOVSKA et al., 2008).

Therefore, a star that forms from the collapse of a dense molecular cloud inherits a complex mixture of gas and dust from the ISM: Dust grains that have condensed at certain stellar sites and retained their stellar fingerprint, dust grains that have been modified and homogenized by diverse processes in the ISM and dust grains that were formed "in-situ" in the ISM and represent a mixture of different stellar sites.

1.2 Analysis of cosmic dust grains

1.2.1 Astronomical observations

Since the early decades of the 20th century it was deduced from the reddening of starlight, that the space between the stars is not empty but filled with gas and dust. With the advent of infrared (IR) astronomy around 1960, information on these dust grains has dramatically increased and analysis of dust properties has opened up a new branch of modern astronomy, "astromineralogy" (JONES, 2007). Especially with the launch of the Short and Long Wavelength Spectrometers (SWS and LWS) on board the infrared space observatory (ISO) in 1996 this field has received growing attention. These two instruments cover the IR spectrum from $2 - 200$ μm, which is sufficient to analyse the most important dust species in space.

Interaction of dust grains with electromagnetic radiation in the ISM occurs via three main processes usually taking place simultaneously: the grains absorb, scatter and emit radiation. The latter is also called "thermal emission" and is one of the most important aspects of IR spectroscopy. The dust grains are heated by optical or UV radiation from stars and release this energy by IR radiation which depends on such parameters like wavelength of light, chemistry, size, shape and crystallinity of the dust grains. By analyzing position, shape and strength of different vibrational resonance bands it is possible to infer these

parameters from the IR spectra. However, this is a complicated task and sophisticated data reduction methods have to be applied to raw spectra. Comparison with spectra of synthetic or natural particles taken in the laboratory, measurements of optical constants and full radiative transfer models allow to a certain degree to determine the chemical and physical properties of the emitting species. However, this strongly depends on the assumption that the used laboratory analogues are representative of the dust grains in space. Also, these theoretical considerations are mostly based on standard grain shapes such as ellipsoids or spheres, whereas dust grains in space might be of irregular morphology. It is therefore important for the analysis and evaluation of IR spectra to bear all these restrictions in mind.

O-rich as well as carbonaceous grains have been detected in interstellar and circumstellar environments. In the following only the properties of O-rich dust, in particular silicates, will be discussed as they are of higher relevance to this thesis. For detailed reviews concerning this subject see, e.g., (TIELENS et al., 1997; MOLSTER and WATERS, 2003; MOLSTER and KEMPER, 2005). Amorphous silicates are the most abundant grain species in interstellar space and around O-rich circumstellar environments. They are characterized by broad bands at 9.7 and 18 μm in the IR spectra, resulting from the Si-O stretch resonance and the Si-O-Si bending resonance of the SiO_4 tetrahedras, respectively. Chemcially they can not be well characterized by IR spectroscopy, but astronomers use the expressions "olivine-like" or "pyroxene-like" for a somewhat more specific description if this is possible.

Crystalline silicates, on the contrary, are characterized by sharp peaks compared to the broad bands of amorphous silicates. They have been detected around evolved and young stars for the first time in spectra taken by the SWS/LWS on board ISO (WAELKENS et al., 1996; WATERS et al., 1996; MALFAIT et al., 1998). Before these discoveries, it was thought that nearly all silicates outside the solar system are amorphous. This is due to the fact that before ISO only wavelengths around 10 μm were accessible for analysis, where the bands of crystalline silicates are overwhelmed by the broad amorphous silicate features. Alternatively, they might be too cold for detectable emission. Crystalline silicates are usually cooler than their amorphous counterparts, which could be the result of their different Fe contents. Crystalline silicates have only been found around stars with very high mass loss rates ($> 10^{-5}$ $M_{\odot}$ a^{-1}), whereas they are absent in stars of low mass loss rates ($< 10^{-6}$ $M_{\odot}$ a^{-1}). However, this could also be due to the same effect mentioned above, because spectra of these thin shells might be dominated by the warmer amorphous silicate bands. Generally, about 10 – 15 % of the total silicate dust mass in evolved stars is in the form of crystalline grains (e.g. MOLSTER et al., 2002), but peculiar objects like binary systems might reach crystallinities up to 75% (MOLSTER and KEMPER, 2005). In the ISM, crystalline silicates have not been detected yet, which is usually explained by amorphization in shock waves. An upper limit to the degree of crystallinity in the ISM was estimated to be on the order of several % (KEMPER et al., 2004; KEMPER et al., 2005).

The sharp IR bands of crystalline grains allows the identification not only of different crystal structures, but also to some extent of chemical details such as the Fe-content of silicate species, which depends on the position of characteristic bands such as the 69 μm feature. It is interesting to note that laboratory experiments on condensation of dust analogues resulted only in either Mg-rich or Fe-rich silicates, but not

in intermediate compositions (MOLSTER and KEMPER, 2005). It is therefore not clear why a ferromagnesian silicate should condense at all in circumstellar environments.

There may be also evidence for the detection of Ca-silicates such as diopside and mellilite in the spectra of the planetary nebula NGC 6302 (MOLSTER et al., 2001; HOFMEISTER et al., 2004). However, these observations are still controversial, because interpretations of band positions strongly depend on the comparison with reliable laboratory species (POSCH et al., 2007). The same nebula might also exhibit the presence of high-temperature condensates such as grossite ($CaAl_4O_7$) and hibonite ($CaAl_{12}O_{19}$). There is also some discussion about the 13 μm feature (DEPEW et al., 2006), which might be attributed to crystalline α-Al_2O_3, spinel ($MgAl_2O_4$) or silica (SiO_2). A broad feature at 11 μm seems to be consistent with amorphous Al_2O_3. $(Mg,Fe)O$, metallic Fe and carbonates (KEMPER et al., 2002) have been detected as well in the spectra of O-rich red giants or PNe. Quantitative analysis is difficult, though, because characteristic bands are often overwhelmed by the much more abundant silicates and particle shape effects play an important role. As this is still a developing branch of modern astronomy, many uncertainties remain concerning the interpretation of IR spectra.

1.2.2 A short history of the discovery of presolar grains

The field of presolar grain research is a very young discipline and started practically in 1987, when Ed Anders and co-workers from St. Louis and Chicago succeeded to isolate the carrier grains of anomalous noble gas components from carbonaceous chondrites (BERNATOWICZ et al., 1987; LEWIS et al., 1987; ZINNER et al., 1987). The search for these tiny grains originating from stars other than the sun ("Stardust") lasted for more than 20 years before these discoveries were made. Already in the 60s of the last century some unusual Ne and Xe components with extreme isotopic anomalies were detected in carbonaceous chondrites upon heating, which could not be explained by origins in the solar sebula (REYNOLDS and TURNER, 1964; BLACK and PEPIN, 1969). In subsequent searches, the isotopic noble gas anomalies were further classified into distinct components (e.g., Ne-E, highly enriched in ^{22}Ne, or Xe-HL, enriched in $^{124}Xe + ^{126}Xe$ (light Xe isotopes) and $^{134}Xe + ^{136}Xe$ (heavy Xe isotopes)). Although it was suggested that the carriers of these anomalous components must be carbonaceous phases, they could not be isolated until the late 80s in a long way of trial and error. For this purpose, the meteorite is subject to a complex procedure of harsh acid treatment and size and density separation (AMARI et al., 1994) after which ~99% of the meteorite is dissolved. Only highly refractory phases survive this procedure and the first presolar grains that were discovered are nanodiamonds (LEWIS et al., 1987), silicon carbide (SiC) (BERNATOWICZ et al., 1987) and graphite (AMARI et al., 1990). Although these carbonaceous presolar grains comprise a minor fraction in the hosting carbonaceous chondrites, the resulting acid-resistant grain separates mainly consist of presolar species.

However, this is only true for carbonaceous phases, whereas meteoritic refractory O-rich grains such as $MgAl_2O_4$ (spinel), Al_2O_3 (corundum and other crystalline structures) or $CaAl_{12}O_{19}$ (hibonite) are dominated by solar system material. To identify presolar grains among O-rich grain separates, ion imaging techniques for secondary ion mass spectrometers (SIMS) had to be developed (HOPPE et al., 1996;

NITTLER, 1996), where presolar grains stand out in digitized ion images by their extremely anomalous O isotopic compositions compared to the majority of isotopically normal grains (Sec. 2.2).

After identification by their anomalous isotopic signatures of major elements, the presolar grains can be further characterized by a variety of other techniques. Additional isotopes of the grains can be measured by SIMS, if enough material is available, their morphology and chemistry can be determined by scanning electron microscopy (SEM), and even their crystal structures may be analyzed by transmission electron microscopy (TEM), if samples are electron transparent. By these investigations it is possible to elucidate the complex histories of these grains: Around which stars did they form? Which nucleosynthetic fingerprints did they inherit from their parent stars? How did they condense? Are there any signs of processing in the ISM? Which solar system materials contain these grains and in what quantities? What stellar sources delivered material to the solar nebula? How did the elements in our Galaxy evolve? In fact, all the processes of the cosmic lifecycle of dust described in Sec. 1.1 may be examined in a laboratory on Earth.

Presolar grains therefore offer the exciting possibility to analyze samples of stardust by high precision analytical techniques to put further constraints on astrophysical questions, i.e., stellar nucleosynthesis and evolution. Therefore they merge together the fields of astrophysics, cosmochemistry, mineralogy, chemistry and nuclear physics. For recent reviews see e.g. HOPPE and ZINNER (2000), NITTLER (2003), ZINNER (2003), CLAYTON and NITTLER (2004), LODDERS and AMARI (2005) and LUGARO (2005).

1.2.3 The discovery of presolar silicate grains

From astronomical observations it was evident already in the mid 90s that silicate material dominates the ISM and circumstellar environments of young and evolved stars (Sec. 1.2.1). Therefore, after the discovery of presolar grains, extensive searches for presolar silicate grains in primitive solar system materials were carried out. These searches had to be performed "in-situ" by SIMS ion imaging without the use of harsh acid treatment, which would have destroyed the presolar silicate material. However, extensive searches remained unsuccessful for a long time (NITTLER, 1996; MESSENGER and BERNATOWICZ, 2000; ALEXANDER et al., 2001). This was explained by the possibility that presolar silicate grains might be preferentially destroyed in the ISM, the solar nebula or the meteorite parent body by secondary alteration. On the other hand, the spatial resolution of the available SIMS instruments by that time only allowed the identification of grains of about > 0.5 μm in size. As it was shown later, presolar silicates are typically only 0.2 – 0.4 μm in size, and it is thus not surprising that they remained hidden in the early searches.

Only the invention of the "NanoSIMS", manufactured by CAMECA in France, made the identification of presolar silicates possible. The main advantage of this instrument is its superior spatial resolution of ~50 nm together with a high transmission at high mass resolving power (Sec. 2.2). It was then only a matter of time until the first presolar silicate grains were discovered by extreme isotopic anomalies in oxygen: First in interplanetary dust particles (IDPs) collected in the stratosphere (MESSENGER et al., 2003), later on in the carbonaceous chondrites Acfer 094 and NWA 530 (MOSTEFAOUI and HOPPE, 2004; NAGASHIMA et al., 2004; NGUYEN and ZINNER, 2004). One of these discoveries was made possible by the use of a special detector system ("SCAPS") attached to an ims 1270 ion probe (NAGASHIMA et al., 2004). Still, it

has to be noted that obtained isotopic ratios are much more strongly diluted by the surrounding isotopically normal silicates than it is the case for the NanoSIMS measurements. It has now turned out that presolar silicates are the most abundant presolar grain species in primitive solar system materials (with the exception of the nanodiamonds, but these might not exclusively be of presolar origin).

1.3 Aims of this study

Up to this research work, only little information on the isotopic composition of elements other than O and on the mineralogy existed about presolar silicate grains. Especially analysis by TEM to investigate microstructural details or the chemical composition was reported only for a handful of grains (MESSENGER et al., 2003; MESSENGER et al., 2005; NGUYEN, 2005; YADA et al., 2005). It was tried to determine the mineralogy of individual grains by SEM/EDX (MOSTEFAOUI and HOPPE, 2004), but this is somewhat problematic, because the excited sample volume usually is larger than the size of the analyzed grains. Therefore, other high spatial resolution techniques such as TEM or Auger electron spectroscopy (AES) have to be applied for this purpose. Furthermore, measurements of additional isotope systems in presolar silicates such as Si or Al-Mg have been reported very rarely (MOSTEFAOUI and HOPPE, 2004; NAGASHIMA et al., 2004; NGUYEN and ZINNER, 2004). Research on this type of presolar grains has just begun to develop.

The main goals of this study are therefore:

– to search for presolar silicates in the matrix of the primitive meteorite Acfer 094 and to determine abundance distributions of different species,

– to put further constraints on the origins of presolar silicate grains by measuring O and Si isotopes in a large number of grains,

– to disentangle stellar sources of material from which our solar system has formed,

– to investigate possible formation mechanisms of these grains in the envelopes of evolved stars and novae/supernovae by microstructural and chemical analyses,

– to look for signs of grain processing or destruction in the ISM,

– to constrain the relationship between solar and presolar material in primitive meteorites,

– to compare our results with observational and theoretical predictions und test proposed formation and alteration scenarios,

– to search for a possible connection between the isotopic composition and the mineralogy.

1.4 References

Alexander C. M. O. D., Nittler L. R., and Tera F. (2001) The search of presolar silicates and the 54Cr carrier. *Lunar and planetary science conference* **32**, 2191.

Amari S. (2002) Presolar grains from novae: Their isotopic ratios and radioactivities. *New Astronomy Reviews* **46**, 519-524.

Amari S., Anders E., Virag A., and Zinner E. (1990) Interstellar graphite in meteorites. *Nature* **345**, 238-240.

Amari S., Lewis R. S., and Anders E. (1994) Interstellar grains in meteorites. I - Isolation of SiC, graphite, and diamond; size distributions of SiC and graphite. *Geochimica et Cosmochimica Acta* **58**, 459-470.

Arnould M., Goriely S., and Takahashi K. (2007) The r-process of stellar nucleosynthesis: Astrophysics and nuclear physics achievements and mysteries. *Physics Reports* **450**, 97-213.

Beckwith S. V. W. and Sargent A. I. (1996) Circumstellar disks and the search for neighbouring planetary systems. *Nature* **383**, 139-144.

Bernatowicz T. J., Cowsik R., Gibbons P. C., Lodders K., Fegley Jr. B., Amari S., and Lewis R. S. (1996) Constraints on stellar grain formation from presolar graphite in the Murchison meteorite. *The Astrophysical Journal* **472**, 760-782.

Bernatowicz T. J., Fraundorf G., Ming T., Anders E., Wopenka B., and Zinner E. (1987) Evidence for interstellar SiC in the Murray carbonaceous chondrite. *Nature* **330**, 728-730.

Black D. C. and Pepin R. O. (1969) Trapped neon in meteorites - II. *Earth and Planetary Science Letters* **6**, 395-405.

Boothroyd A. I., Sackmann I.-J., and Wasserburg G. J. (1995) Hot Bottom Burning in asymptotic giant branch stars and its effect on oxygen isotopic abundances. *The Astrophysical Journal* **442**, L21-L24.

Boss A. P. and Vanhala H. A. T. (2002) Triggering protostellar collapse, injection, and disk formation. *Space Science Reviews* **92**, 13-22.

Bradley J. P. (1994) Chemically anomalous, preaccretionally irradiated grains in interplanetary dust from comets. *Science* **265**(5174), 925-929.

Burbidge E. M., Burbidge G. R., Fowler W. A., and Hoyle F. (1957) Synthesis of the Elements in Stars. *Reviews of Modern Astropysics*(29), 547-650.

Busso M., Wasserburg G. J., Nollett K. M., and Calandra A. (2007) Can extra mixing in RGB and AGB stars be attributed to magnetic mechanisms? *The Astrophysical Journal* **671**, 802-810.

Chokshi A., Tielens A. G. G. M., and Hollenbach D. J. (1993) Dust Coagulation. *The Astrophysical Journal* **407**, 806-819.

Clayton D. D., Liu W., and Dalgarno A. (1999) Condensation of Carbon in radioactive supernova gas. *Science* **283**, 1290-1292.

Clayton D. D. and Nittler L. R. (2004) Astrophysics with presolar stardust. *Annual Reviews Astronomy and Astrophysics* **42**, 39-78.

Deneault E. A.-N. and Clayton D. D. (2003) Supernova reverse shocks: SiC growth and isotopic composition. *The Astrophysical Journal* **594**, 312-325.

DePew K., Speck A. K., and Dijkstra C. (2006) Astromineralogy of the 13 μm feature in the spectra of oxygen-rich asymptotic giant branch stars. I. Corundum and Spinel. *The Astrophysical Journal* **640**, 971-981.

Dijkstra C., Speck A. K., Reid R. B., and Abraham P. (2005) The 10 μm feature of M-type stars in the large magellanic cloud and the dust condensation sequence. *The Astrophysical Journal* **633**, L133-136.

Duquennoy A. and Mayor M. (1991) Multiplicity among solar-type stars in the solar neighbourhood. II - Distribution of the orbital elements in an unbiased sample. *Astronomy and Astrophysics* **248**(2), 485-524.

Dwek E. (1998) The evolution of the elemental abundances in the gas and dust phases of the Galaxy. *The Astrophysical Journal* **501**, 643-665.

Ebel D. S. and Grossman L. (2001) Condensation from supernova gas made of free atoms. *Geochimica et Cosmochimica Acta* **65**(3), 469-477.

Ferrarotti A. S. and Gail H.-P. (2001) Mineral formation in stellar winds II. Effects of Mg/Si abundance variations on dust composition in AGB stars. *Astronomy and Astrophysics* **371**, 133-151.

Ferrarotti A. S. and Gail H.-P. (2002) Mineral formation in stellar winds - III. Dust formation in S stars. *Astronomy and Astrophysics* **382**, 256-281.

Gail H.-P. (2003) Formation and evolution of minerals in accretion disks and stellar outflows. *in: Astromineralogy (ed. Th. Henning)*, 55-120.

Gail H.-P. and Sedlmayr E. (1999) Mineral formation in stellar winds - I. Condensation sequence of silicate and iron grains in stationary oxygen rich outflows. *Astronomy and Astrophysics* **347**, 594-616.

Gehrz R. D., Truran J. W., Williams R. E., and Starrfield S. (1998) Nucleosynthesis in classical novae and its contribution to the interstellar medium. *The Publications of the Astronomical Society of the Pacific* **110**(743), 3-26.

Grossman L. (1972) Condensation in the primitive solar nebula. *Geochimica et Cosmochimica Acta* **36**(5), 597-619.

Harker D. E. and Desch S. J. (2002) Annealing of silicate dust by nebular shocks at 10 AU. *The Astrophysical Journal* **565**, L109-L112.

Herwig F. (2005) Evolution of Asymptotic Giant Branch Stars. *Annual Reviews Astronomy and Astrophysics* **43**, 435-479.

Hester J. J., Desch S. J., Healy K. R., and Leshin L. A. (2004) The Cradle of the Solar System. *Science* **304**, 1116-1117.

Hofmeister A. M., Wopenka B., and Locock A. J. (2004) Spectroscopy and structure of hibonite, grossite, and CaAl2O4: Implications for astronomical environments. *Geochimica et Cosmochimica Acta* **68**(21), 4485-4503.

Hoppe P., Strebel R., Eberhardt P., Amari S., and Lewis R. S. (1996) Type II Supernova matter in a silicon carbide grain from the Murchison meteorite. *Science* **272**, 1314-1316.

Hoppe P., Strebel R., Eberhardt P., Amari S., and Lewis R. S. (2000) Isotopic properties of silicon carbide X grains from the Murchison meteorite in the size range 0.5-1.5 μm. *Meteoritics and Planetary Science* **35**(6), 1157-1176.

Hoppe P. and Zinner E. (2000) Presolar dust grains from meteorites and their stellar sources. *Journal of geophysical research* **105**(A5), 10371-10385.

Hoyle F. (1946) The synthesis of the elements from hydrogen. *Monthly Notices of the Royal Astronomical Society* **106**, 343-383.

Iliadis C., Angulo C., Descouvemont P., Lugaro M., and Mohr P. (2008) New reaction rate for 16O (p,gamma) 17F and its influence on the oxygen isotopic ratios in massive AGB stars. *Physical Review C* **77**, 045802.

Jones A. P. (2004) Dust destruction processes. *Astrophysics of Dust, ASP conference series, edited by Adolf N. Witt, Geoffrey C. Clayton and Bruce T. Draine*, 347.

Jones A. P. (2007) The mineralogy of cosmic dust: astromineralogy. *European Journal of Mineralogy* **19**, 771-782.

Jones A. P., Tielens A. G. G. M., and Hollenbach D. J. (1996) Grain shattering in shocks: The interstellar grain size distribution. *The Astrophysical Journal* **469**, 740-764.

Jones A. P., Tielens A. G. G. M., Hollenbach D. J., and McKee C. F. (1997) The propagation and survival of interstellar grains. *Astrophysical implications of the laboratory study of presolar materials.*

José J., Garcìa-Berro E., Hernanz M., and Gil-Pons P. (2007) The first Nova explosions. *The Astrophysical Journal* **662**, L103-L106.

José J. and Hernanz M. (2007) The origin of presolar nova grains. *Meteoritics and Planetary Science* **42**(7/8), 1135-1143.

Keller L. P. and Messenger S. (2008) Coordinated chemical and isotopic studies of GEMS grains in IDPs. *Lunar and planetary science conference* **39**, abstr.#2347.

Kemper F., Jäger C., Waters L. B. F. M., Henning T., Molster F. J., Barlow M. J., Lim T. L., and De Koter A. (2002) Detection of carbonates in dust shells around evolved stars. *Nature* **415**, 295-297.

Kemper F., Vriend W. J., and Tielens A. G. G. M. (2004) The absence of crystalline silicates in the diffuse interstellar medium. *The Astrophysical Journal* **609**, 826-837.

Kemper F., Vriend W. J., and Tielens A. G. G. M. (2005) Erratum: The absence of crystalline silicates in the diffuse interstellar medium. *The Astrophysical Journal* **633**(1), 534-534.

Lattanzio J. C. (1989) Carbon dredge-up in low-mass stars and solar metallicity stars. *The Astrophysical Journal* **344**, L25-L27.

Lewis R. S., Tang M., Wacker J. F., Anders E., and Steel E. (1987) Interstellar diamonds in meteorites. *Nature* **326**, 160-162.

Lodders K. (2003) Solar system abundances and condensation temperatures of the elements. *The Astrophysical Journal* **591**, 1220-1247.

Lodders K. (2006) They came from the deep in the Supernova: The origin of TiC and metal subgrains in presolar graphite grains. *The Astrophysical Journal* **647**, L37-L40.

Lodders K. and Amari S. (2005) Presolar grains from meteorites: Remnants from the early times of the solar system. *Chemie der Erde* **65**, 93-166.

Lodders K. and Fegley Jr. B. (1995) The origin of circumstellar silicon carbide grains found in meteorites. *Meteoritics* **30**, 661-678.

Lugaro M. (2005) *Stardust from meteorites - An introduction to presolar grains.* World Scientific Publishing Corp.

Malfait K., Waelkens C., Waters L. B. F. M., Vandenbussche B., Huygen E., and de Graauw M. S. (1998) The spectrum of the young star HD 100546 observed with the Infrared Space Observatory. *Astronomy and Astrophysics* **332**, L25-28.

Merrill P. W. (1952) Technetium in stars. *Science* **115**, 484.

Messenger S. and Bernatowicz T. J. (2000) Search for presolar silicates in Acfer 094. *Meeting of the Meteoritical Society* **63**, 5302.

Messenger S., Keller L. P., and Lauretta D. S. (2005) Supernova olivine from cometary dust. *Science* **309**, 737-741.

Messenger S., Keller L. P., Stadermann F. J., Walker R. M., and Zinner E. (2003) Samples of stars beyond the solar system: Silicate grains in interplanetary dust. *Science* **300**, 105-108.

Meyer B. S., Weaver T. A., and Woosley S. E. (1995) Isotope source table for a 25Msun supernova. *Meteoritics* **30**, 325-334.

Molster F. J. and Kemper C. (2005) Crystalline Silicates. *Space Science Reviews* **119**, 3-28.

Molster F. J., Lim T. L., Sylvester R. J., Waters L. B. F. M., Barlow M. J., Beintema D. A., Cohen M., Cox P., and Schmitt B. (2001) The complete ISO spectrum of NGC 6302. *Astronomy and Astrophysics* **372**, 165-172.

Molster F. J. and Waters L. B. F. M. (2003) The mineralogy of interstellar and circumstellar dust. *in: Astromineralogy (ed. Th. Henning)*, 121-170.

Molster F. J., Waters L. B. F. M., and Tielens A. G. G. M. (2002) Crystalline silicate dust around evolved stars II. the crystalline silicate complexes. *Astronomy and Astrophysics* **382**, 222-240.

Mostefaoui S. and Hoppe P. (2004) Discovery of abundant in situ silicate and spinel grains from red giant stars in a primitive meteorite. *The Astrophysical Journal* **613**, L149-L152.

Nagashima K., Krot A. N., and Yurimoto H. (2004) Stardust silicates from primitive meteorites. *Nature* **428**, 921-924.

Nguyen A. N. (2005) Characterization of presolar silicate grains in primitive meteorites by multi-detection raster ion imaging in the Nanosims. Ph. D. thesis, Washington University, St. Louis.

Nguyen A. N. and Zinner E. (2004) Discovery of ancient silicate stardust in a meteorite. *Science* **303**, 1496-1499.

Nittler L. R. (1996) Quantitative isotopic ratio ion imaging and its application to studies of preserved stardust in meteorites. *Ph.D. thesis, Washington University. 210 pp.*

Nittler L. R. (2003) Presolar stardust in meteorites: recent advances and scientific frontiers. *Earth and Planetary Science Letters* **209**, 259-273.

Nittler L. R. (2005) Constraints on heterogeneous galactic chemical evolution from meteoritic stardust. *The Astrophysical Journal* **618**, 281-296.

Nollett K. M., Busso M., and Wasserburg G. J. (2003) Cool bottom processes on the thermally pulsing asymptotic giant branch and the isotopic composition of circumstellar dust grains. *The Astrophysical Journal* **582**, 1036-1058.

Nomoto K. i., Tominaga N., Umeda H., Kobayashi C., and Maeda K. (2006) Nucleosynthesis yields of core-collapse supernovae and hypernovae, and galactic chemical evolution. *Nuclear Physics A* **777**, 424-458.

Nozawa T., Kozasa T., Habe A., Dwek E., Umeda H., Tominaga N., Maeda K., and Nomoto K. i. (2007) Evolution of dust in primordial supernova remnants: Can dust grains formed in the ejecta survive and be injected into the early interstellar medium? *The Astrophysical Journal* **666**, 955-966.

Ott U., Altmaier M., Herpers U., Kuhnhenn J., Merchel S., Michel R., and Mohapatra R. K. (2005) Spallation recoil II: Xenon evidence for young SiC grains. *Meteoritics and Planetary Science* **40**(11), 1635-1652.

Poelarends A. J. T., Herwig F., Langer N., and Heger A. (2008) The Supernova channel of Super-AGB stars. *The Astrophysical Journal* **675**, 614-625.

Posch T., Mutschke H., Trieloff M., and Henning T. (2007) Infrared spectroscopy of Calcium-Aluminium-rich inclusions: analog material for protoplanetary dust? *The Astrophysical Journal* **656**, 615-620.

Reynolds J. H. and Turner G. (1964) Rare gases in the chondrite Renazzo. *Journal of geophysical research* **69**, 3263-81.

Rho J., Kozasa T., Reach W. T., Smith J. D., Rudnick L., DeLaney T., Ennis J. A., Gomez H., and Tappe A. (2008) Freshly formed dust in the Cassiopeia A Supernova remnant as revealed by the Spitzer Space Telescope. *The Astrophysical Journal* **673**, 271-282.

Savage B. D. and Sembach K. R. (1996) Interstellar abundances from absorption-line observations with the Hubble Space Telescope. *Annual Reviews Astronomy and Astrophysics* **34**, 279-330.

Scott E. R. D. and Krot A. N. (2005) Thermal processing of silicate dust in the solar nebula: clues from primitive chondrite matrices. *The Astrophysical Journal* **623**, 571-578.

Sogawa H. and Kozasa T. (1999) On the origin of crystalline silicate in circumstellar envelopes of oxygen-rich asymptotic giant branch stars. *The Astrophysical Journal* **516**, L33-36.

Stroud R. M., Nittler L. R., and Alexander C. M. O. D. (2004) Polymorphism in presolar Al2O3 grains from asymptotic giant branch stars. *Science* **305**, 1455-1457.

Sugerman B. E. K., Ercolano B., Barlow M. J., Tielens A. G. G. M., Clayton G. C., Zijlstra A. A., Meixner M., Speck A., Gledhill T. M., Panagia N., Cohen M., Gordon K. D., Meyer M., Fabbri J., Bowey J. E., Welch D. L., Regan M. W., and Kennicutt jr. R. C. (2006) Massive-Star Supernovae as Major Dust Factories. *Science* **313**, 196-200.

Tielens A. G. G. M., McKee C. F., Seab C. G., and Hollenbach D. J. (1994) The physics of grain-grain collisions and gas-grain sputtering in interstellar shocks. *The Astrophysical Journal* **431**, 321.

Tielens A. G. G. M., Waters L. B. F. M., Molster F. J., and Justtanont K. (1997) Circumstellar silicate mineralogy. *Astrophysics and Space Science* **255**, 415-426.

Timmes F. X., Woosley S. E., and Weaver T. A. (1995) Galactic Chemical Evolution: Hydrogen through Zinc. *The Astrophysical Journal Supplement Series* **98**, 617-658.

Travaglio C., Gallino R., Amari S., Zinner E., Woosley S., and Lewis R. S. (1999) Low-density graphite grains and mixing in type II supernovae. *The Astrophysical Journal* **510**, 325-354.

Truran J. W. and Heger A. (2003) Origin of the Elements. *In: Treatise on Geochemistry (eds. A. M. Davis, H. D. Holland, K. K. Turekian)*(Elsevier), 1-15.

van Boekel R., Min M., Leinert C., Waters L. B. F. M., Richichi A., Chesneau O., Dominik C., Jaffe W., Dutrey A., Graser U., Henning T., de Jong J., Köhler R., De Koter A., Lopez B., Malbet F., Morel S., Paresce F., Perrin G., Preibisch T., Przygodda F., Schöller M., and Wittkowski M. (2004) The building blocks of planets within the "terrestrial" region of protoplanetary disks. *Nature* **432**, 479-482.

Waelkens C., Waters L. B. F. M., De Graauw M. S., Huygen E., Malfait K., Plets H., Vandenbussche B., Beintema D. A., Boxhoorn D. R., Habing H. J., Heras A. M., Kester D. J. M., Lahuis F., Morris P. W., Roelfsema P. R., Salama A., Siebenmorgen R., Trams N. R., van der Bliek N. R., Valentijn E. A., and Wesselius P. R. (1996) SWS observation of young main-sequence stars with dusty circumstellar disks. *Astronomy and Astrophysics* **315**, L245-248.

Wasserburg G. J., Boothroyd A. I., and Sackmann I.-J. (1995) Deep circulation in red giant stars: a solution to the carbon and oxygen isotope puzzles? *The Astrophysical Journal* **447**(L37-40).

Waters L. B. F. M., Molster F. J., De Jong T., Beintema D. A., Waelkens C., Boogert A. C. A., Boxhoorn D. R., De Graauw M. S., Drapatz S., Feuchtgruber H., Genzel R., Helmich F. P., Heras A. M., Huygen R., Izumiura H., Justtanont K., Kester D. J. M., Kunze D., Lahuis F., Lamers H. J. G. L. M., Leech K. J., Loup C., Lutz D., Morris P. W., Price S. D., Roelfsema P. R., Salama A., Schaeidt S. G., Tielens A. G. G. M., Trams N. R., Valentijn E. A., Vandenbussche B., Van den Ancker M. E., Van Dishoeck E. F., Van Winckel H., Wesselius P. R., and Young E. T. (1996) Mineralogy of oxygen-rich dust shells. *Astronomy and Astrophysics* **315**, L361-364.

Woosley S. E., Heger A., and Weaver T. A. (2002) The evolution and explosion of massive stars. *Reviews of Modern Physics* **74**(4), 1015-1071.

Yada T., Stadermann F. J., Floss C., Zinner E., Olinger C. T., Graham G. A., Bradley J. P., Dai Z. R., Nakamura T., Noguchi T., and Bernas M. (2005) Discovery of abundant presolar silicates in subgroups of antarctic micrometeorites. *Lunar and Planetary Science Conference* **36**, 1227.

Zhukovska S., Gail H.-P., and Trieloff M. (2008) Evolution of interstellar dust and stardust in the solar neighbourhood. *Astronomy and Astrophysics* **479**(2), 453-480.

Zinner E. (2003) Presolar Grains. *In: Treatise on Geochemistry (eds. A. M. Davis, H. D. Holland, K. K. Turekian)*(Elsevier), 17-39.

Zinner E., Ming T., and Anders E. (1987) Large isotopic anomalies of Si, C, N and noble gases in interstellar silicon carbide from the Murray meteorite. *Nature* **330**, 730-732.

Zinner E., Nittler L. R., Hoppe P., Gallino R., Straniero O., and Alexander C. M. O. D. (2005) Oxygen, magnesium and chromium isotopic ratios of presolar spinel grains. *Geochimica et Cosmochimica Acta* **69**(16), 4149-4165.

Ziurys L. M., Milam S. N., Apponi A. J., and Woolf N. J. (2007) Chemical complexity in the winds of the oxygen-rich supergiant star VY Canis Majoris. *Nature* **447**, 1094-1097.

2 Samples and Methods

2.1 The Acfer 094 meteorite

2.1.1 Classification scheme of meteorites

Meteorites found on Earth mainly derive from asteroids orbiting the Sun between Mars and Jupiter. They are fragments of these parent bodies released during collisions and then transferred to Earth. About 20000 meteorites heavier than 0.1 kg reach the Earth´s surface every year, most of them in the cm range. Smaller particles evaporate completely during atmospheric entry, and only the smallest dust grains (< 1 mm) slightly sink downwards and are recovered as micrometeorites. This size fraction dominates the total mass that reaches the Earth´s surface every day (~40 t). Only impactors of extremely large dimensions (m to km) can dramatically affect the Earth´s surface (Fig. 2.1).

Figure 2. 1 The Arizona Crater near Flagstaff (USA)
It was created by the impact of an iron meteorite (“Canyon Diablo”) ~50 ka ago.

If the fall of a meteorite (a “meteor” or “falling star”) is witnessed and documented from at least three different points, its approximate landing site can be calculated. These freshly fallen meteorites are then not heavily altered by terrestrial processes. Most meteorites, however, are “finds”. They are collected by professional expedition teams (or private adventurers) in the hot and cold deserts of the Earth, because meteorites merely disintegrate in these extremely dry environments and are also easy to locate on the bright background. On glaciers, meteorites are concentrated by the ice movement which simplifies their

collection. The study of meteorites allows scientists to look deep into the history of the solar system and explore formation and differentiation mechanisms of terrestrial bodies.

If the meteorite parent body experiences high enough temperatures for a longer period of time, it can differentiate into a metal core and a silicate mantle similar to Earth. Heat is produced from accretion and the decay of short-lived radionuclides (e.g., ^{26}Al and ^{60}Fe) and is better retained in larger objects, which therefore more likely differentiate. Fragments from an asteroidal metal core constitute "iron meteorites", fragments from the silicate mantle are called "achondrites" that show the chemical and petrological effects of melting ("cosmic basalts"). Fragments from the boundary layer between the core and the mantle exhibit both metal and silicate material and are called "stony iron meteorites" (pallasites and mesosiderites).

Fragments from "undifferentiated" asteroids, however, have not seen long-term high temperatures that might have erased any previous signature. They are therefore the most pristine samples to study the very first stages of the solar system and are also highly attractive for presolar grain searchers. These "chondrites" are characterized by the presence of mm sized silicate melt droplets called "chondrules" that are dispersed in a fine-grained matrix composed of mainly silicates, metal and sulfides . Their formation mechanism is still not completely understood, but must be connected to a short-term heating event in the early solar system (SCOTT and KROT, 2003). Other objects found in these chondrites are amoeboid olivine aggregates ("AOAs"), Al-rich chondrules ("ARCs"), Fe-Ni metal nuggets and refractory Ca-, Al-rich inclusions ("CAIs"), which are the first solid condensates of the young solar system.

Based on their elemental abundances, mineralogy, O isotope compositions or oxidation states, chondrites are divided into five classes: ordinary chondrites, which are the most abundant meteorites (~80% of all falls), carbonaceous chondrites, which can contain up to several % carbonaceous material, enstatite chondrites, which have a high fraction of pyroxenes and two recently defined classes (Rumuruti, Kakangari). Carbonaceous chondrites are further separated into several subclasses based on chemical and mineralogical attributes, which are named after a type meteorite (e.g., CM after Murchison, CO after Ornans or CI after Ivuna). CI chondrites virtually only consist of matrix material (> 99%), and their chemical composition is best-matched by the composition of the solar photosphere. They therefore are meant to represent the chemically, but not mineralogically most primitive material of the solar system (PALME and JONES, 2003). The "petrologic type" of a chondrite further defines its stage of aqueous alteration and thermal metamorphism after accretion of the parent body. The petrologic type 3 is the least altered in both respects. The meteorite can be further affected by shock metamorphism on the parent body due to impacts and by terrestrial alteration before its recovery. It is therefore obvious that research on these precious samples are always hampered by secondary alteration problems. The least altered samples, on the other hand, are of the highest scientific value.

For presolar grain searchers the most interesting part of a chondrite is its fine-grained matrix in which any presolar material might have survived further alteration processes. Exposure to higher temperatures (> 800 K, petrologic type 4 − 6) likely homogenizes and erases any presolar signature. On the contrary, meteorites of petrologic types 1 − 2 have experienced aqueous alteration on their parent bodies, but no strong thermal alteration (< 370 K). It is interesting that these meteorites have a very high abundance of

presolar carbonaceous phases (like Orgueil, a CI1, or Murchison and Murray, both CM2), which indicates that aqueous alteration does not affect carbonaceous presolar phases very strongly. Recent identifications of highly abundant presolar silicates in the aqueously altered CR2 chondrites QUE 99177 and MET 00426 (FLOSS and STADERMANN, 2008) indicates that this type of presolar mineral also survives slight aqueous modification. In enstatite chondrites, abundances of presolar silicates seems to be very low (10 − 20 ppm) (EBATA et al., 2006; EBATA et al., 2007). Ordinary chondrites contain relatively large amounts of presolar oxide grains (NITTLER et al., 1997; CHOI et al., 1998), but also low amounts of presolar silicates (< 10 ppm) (TONOTANI et al., 2006). It is not clear whether these differences represent heterogeneities of the young solar nebula or differences in destruction efficiency on the meteorite parent bodies.

A recent review on the classification of meteorites can be found in KROT et al. (2003).

2.1.2 The unique carbonaceous chondrite Acfer 094

The Acfer meteorite collection from the Tademait plateau of the Sahara in Algeria has provided cosmochemists since the 90s with a total number of 390 meteorites (see the homepage of the Meteoritical Society). Among these, the 82 g weighing Acfer 094 found in 1990 has turned out to be "unique" in both its characteristics and scientific value. The carbonaceous chondrite breccia could not be classified into one of the known chondrite groups. Its bulk chemical and trace element composition is similar to CM2 chondrites, but in contrast to this group, Acfer 094 lacks any parent body aqueous alteration or thermal metamorphism. Also, it has a distinct carbon and nitrogen isotopic composition and a very low bulk C/N ratio unlike any other meteorite. Its matrix modal abundance and oxygen isotopic composition shows affinities to the CO3 chondrite group. Although this "ungrouped" chondrite has suffered from little terrestrial aqueous alteration (Fig. 2.2), it can be regarded as one of the most primitive meteorites ever collected regarding its alteration state (petrologic type 3.0). Phyllosilicates, usually a sign of aqueous alteration, are virtually absent, and its matrix components are in strong disequilibrium, indicative of very little thermal metamorphism. There are also no signs of shock metamorphism.

Acfer 094 consists of abundant chondrules, ARCs, CAIs, olivine aggregates, chondrule and mineral fragments (hence the term "breccia") embedded in an extremely fine-grained matrix. About 30 − 40 vol.% of the total meteorite consists of grains < 10 μm in diameter (NEWTON et al., 1995). A detailed TEM study of matrix grains < 3 μm (GRESHAKE, 1997) revealed that the matrix mainly consists of amorphous siliceous material (40 vol.%), forsteritic olivine (30 vol.%), Mg-rich/low-Ca pyroxene (20 vol.%) and Fe-Ni-sulfides (5 vol.%), all in the < 500 nm size range. The amorphous groundmass was suggested to have formed by rapid disequilibrium condensation of a nebular reservoir and might have acted as a precursor material to other meteorite groups (GRESHAKE, 1997). Crystalline grains within the groundmass might as well formed by condensation or by crystallization of the amorphous material. A new class of μ-CAIs and an unusual Li-rich phase have been documented as well in a more recent Acfer 094 matrix survey (BLAND et al., 2007). As Acfer 094 virtually represents one of the most primitive solar system samples available, it was thus a prime candidate to search for presolar grains. Indeed, it has turned out that it contains among the highest amounts of presolar SiC grains and nanodiamonds (NEWTON et al., 1995). It was also successfully included in later searches for presolar silicates and was one of the first meteorites in which

this presolar phase has been detected (MOSTEFAOUI and HOPPE, 2004; NAGASHIMA et al., 2004; NGUYEN and ZINNER, 2004).
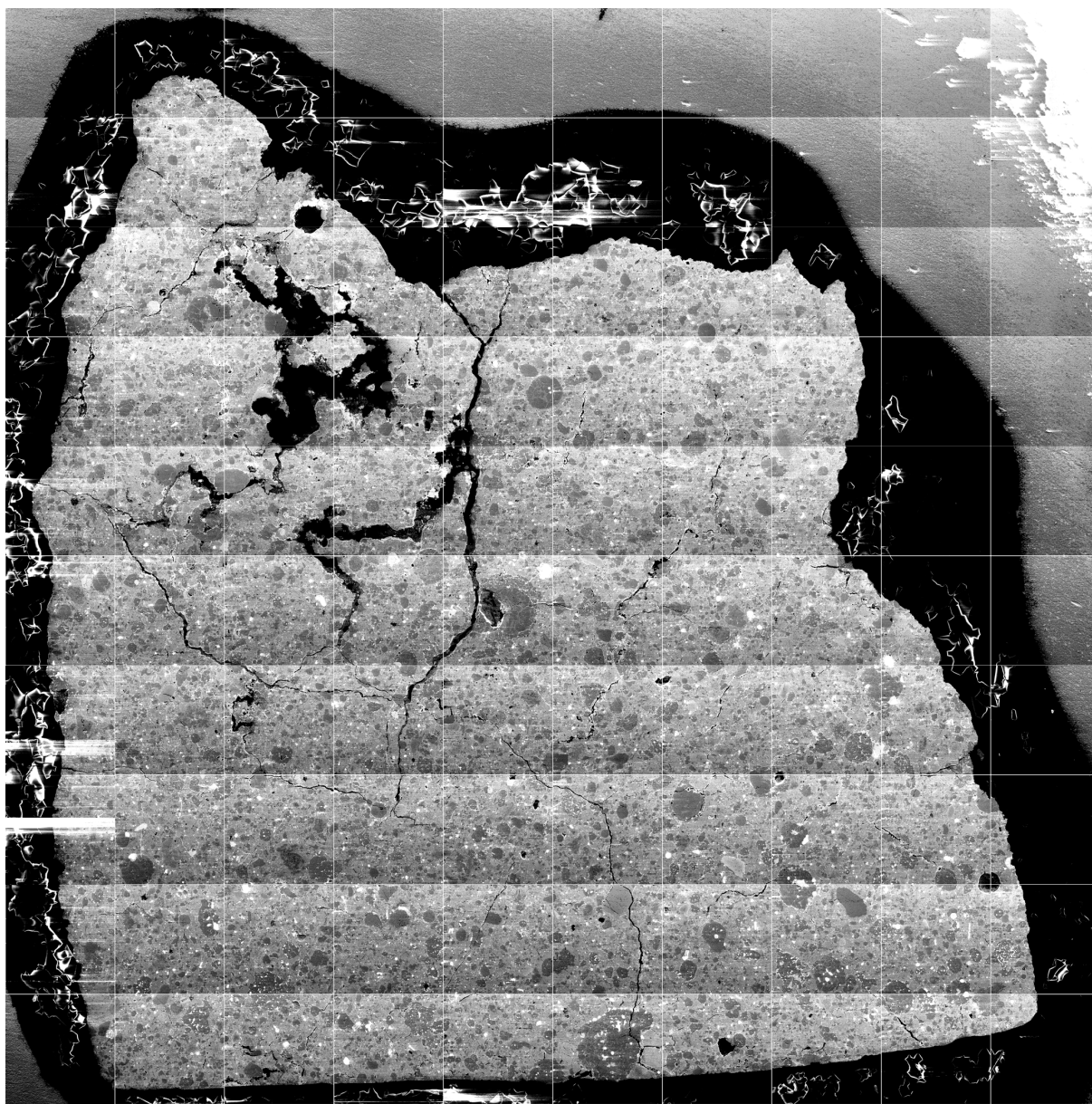
Figure 2. 2 Composed SEM image of the Acfer 094 thin section embedded in epoxy
Visible cracks mainly result from the preparation process, but also indicate terrestrial alteration (image width 1.7 cm).

Although it is now nearly 20 years ago since this meteorite was recovered from the Sahara, new discoveries still arise from this sample. Just recently, a new Fe-rich phase ("cosmic symplectite", COS, previously described as "new-PCP", i.e., new "poorly characterized phase") enriched in heavy O isotopes was detected in the matrix of Acfer 094, which might have a link to nebular water (SAKAMOTO et al., 2007; SETO et al., 2008). To date, Acfer 094 is the only meteorite in which this material has been found. Further research is carried out on fine-grained sulfide minerals, whose origins are still poorly constrained (ZOLENSKY et al., 2008) or carbon-rich globules (BREARLEY, 2008). This meteorite will without doubt play an important role in future work on presolar grains and solar system origin research.

Franz Brandstätter from the Museum of Natural History in Vienna has kindly provided a thin section of this meteorite to the MPI for Chemistry, on which all research work of this thesis has been carried out (Fig. 2.2).

2.2 A SIMS instrument with superior spatial resolution: the NanoSIMS

Secondary Ion Mass Spectrometers (SIMS), also called ion probes, have been a standard tool in geo- and cosmochemistry for nearly 30 years. The technique utilizes a primary beam of accelerated ions (usually O⁻ or Cs⁺) to impact a solid sample surface, which induces a collision cascade in the very first atomic layers. Mono- and polyatomic ions and neutrals are released ("sputtered"), if their kinetic energies exceeds the surface binding energy. This process is enhanced with increasing implantation of primary ions into the sample ("pre-sputtering"), but usually less than ~1% of the sputtered material consists of ions ("ionization efficiency"). The "secondary ion yield" is defined as the number of sputtered secondary ions relative to the number of impacting primary ions and can be as high as 10 – 20 % for certain elements. The secondary ions are accelerated in a strong electric field and transferred into a mass analyzer (usually a quadrupol, a time-of-flight (ToF) or magnetic sector MS). Trace element concentrations down to the ppm level and isotopic ratios with a precision better than 1% may be acquired routinely from H to U of spatially very limited sample volumes. This has the advantage to other mass spectrometers, that the distribution of certain isotopes within a sample may be visualized down to the μm scale on the sample surface (two dimensional ion images) and/or into depth (depth profile). There are also some limitations of the SIMS technique: usually a complex suite of mono- and polyatomic ions is ejected, which may dominate the mass spectra making a quantification of the desired species impossible. Also, the exact physics of the sputtering process are poorly understood, and the sensitivity, i.e., ionization efficiency of an element is strongly dependent on the matrix composition. This makes the use of high quality standards for high precision analyses unavoidable. Elemental relative sensitivity factors have to be determined in each session as they strongly depend on the instrument settings.

Two important parameters of SIMS measurements are the transmission and the mass resolving power. The transmission is defined as the fraction of the actually detected secondary ion current to the emitted secondary ion current. The mass resolving power (MRP) $m/\Delta m$ determines if two mass peaks are separated at their full width half maximum (FWHM) and thus quantifiable. It mainly depends on the widths of the entrance and exit slits of the mass analyzer. Usually the transmission and MRP are inversely correlated, but high performance instruments like the NanoSIMS achieve a high transmission at high MRPs (i.e., ~50% at $m/\Delta m$ ~4000).

Modern SIMS instruments are equipped with a double-focusing magnetic sector MS for best MRP consisting of an electrostatic analyzer (ESA) before the magnet. This design is superior for high precision measurements compared to ToF- or quadrupole MS. As ejected secondary ions have a wide energy spread, and as magnetic sectors separate ions by momentum and not by mass, it is necessary to correct for this energy spread to produce a "clean" spectrum. This is achieved by the ESA located between the

entrance slit and the magnetic sector, which allows only ions of a certain energy spread (usually 20 eV) to pass into the magnet.

The primary beam diameter is mainly controlled by its current and the distance between the extraction lens and the sample surface. In conventional SIMS instruments, the primary and secondary ion columns are in oblique angle to each other, which only allows a certain minimum distance between the extraction lens and the sample surface (usually on the order of ~5 mm in ims series instruments). This design has been dramatically changed for the development of the NanoSIMS in order to achieve a superior spatial resolution of the primary beam: The distance between the sample surface and the extraction lens is only ~300 μm as the primary and secondary ions pass through the same anti-parallel lens system (Fig. 2.3). This reduces the beam diameter at a given current (typically ~0.5 – 1 pA) to ~50 nm compared to ~1 μm in conventional SIMS instruments for Cs^+ primary ions.
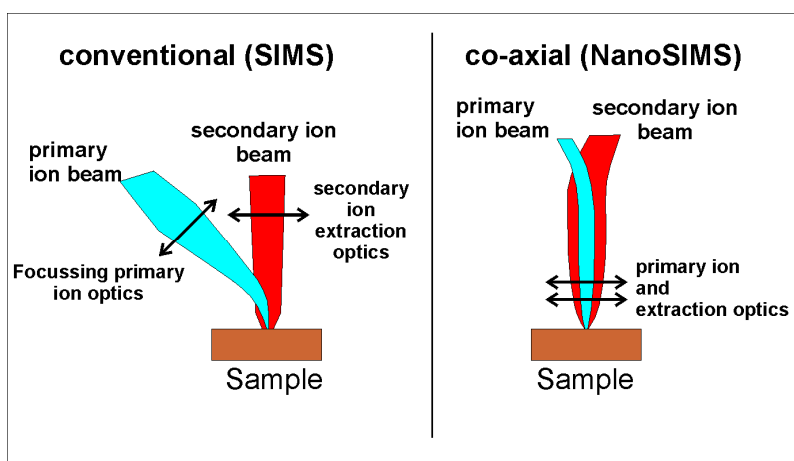
Figure 2. 3 Schematic comparison between conventional and NanoSIMS ion optics (modified after the Cameca NanoSIMS manual)

The NanoSIMS 50 was developed by the French company CAMECA, which also manufactures the ion probe series ims xf, 1270 or 1280. The first two instruments of this kind were installed in 2001 in St. Louis (USA) and Mainz (Fig. 2.4), where the operating scientists and CAMECA engineers worked closely together to improve the design of the machine (HILLION et al., 1994; HOPPE et al., 2004). It also played the key role for the first detection of presolar silicates in IDPs (MESSENGER et al., 2003) and primitive meteorites (NGUYEN and ZINNER, 2004) (Sec. 1.3.3). For a recent detailed review on the NanoSIMS technique and its applications see, e.g., HOPPE et al. (2004) and WINTERHOLLER and HOPPE (2008).

The primary ion source alternatively operates with Cs^+ (beam size down to ~50 nm, analysis of negative secondary ions) and O^- (beam size down to ~200 nm, positive secondary ions). The opposite polarity of the primary and secondary ions is mandatory due to the co-axial setup. Three sets of electrostatic lenses and two apertures determine the width and intensity of the impacting primary beam. The sputtered ions are extracted into the secondary ion column, consisting of scanning plates, deflectors and slit lenses, through the entrance slit (ES), the aperture slit (AS), the energy slit and the ESA into the magnetic sector. The NanoSIMS is designed for high transmission at high MRP, which is due to a high extraction field (± 8 kV), efficient focus of the secondary ions and a "dynamic transfer system". All these innovations

minimize chromatic and angular aberration effects which are inherent to secondary ions. The beam is virtually "squeezed" into the entrance slit thus increasing the transmission.
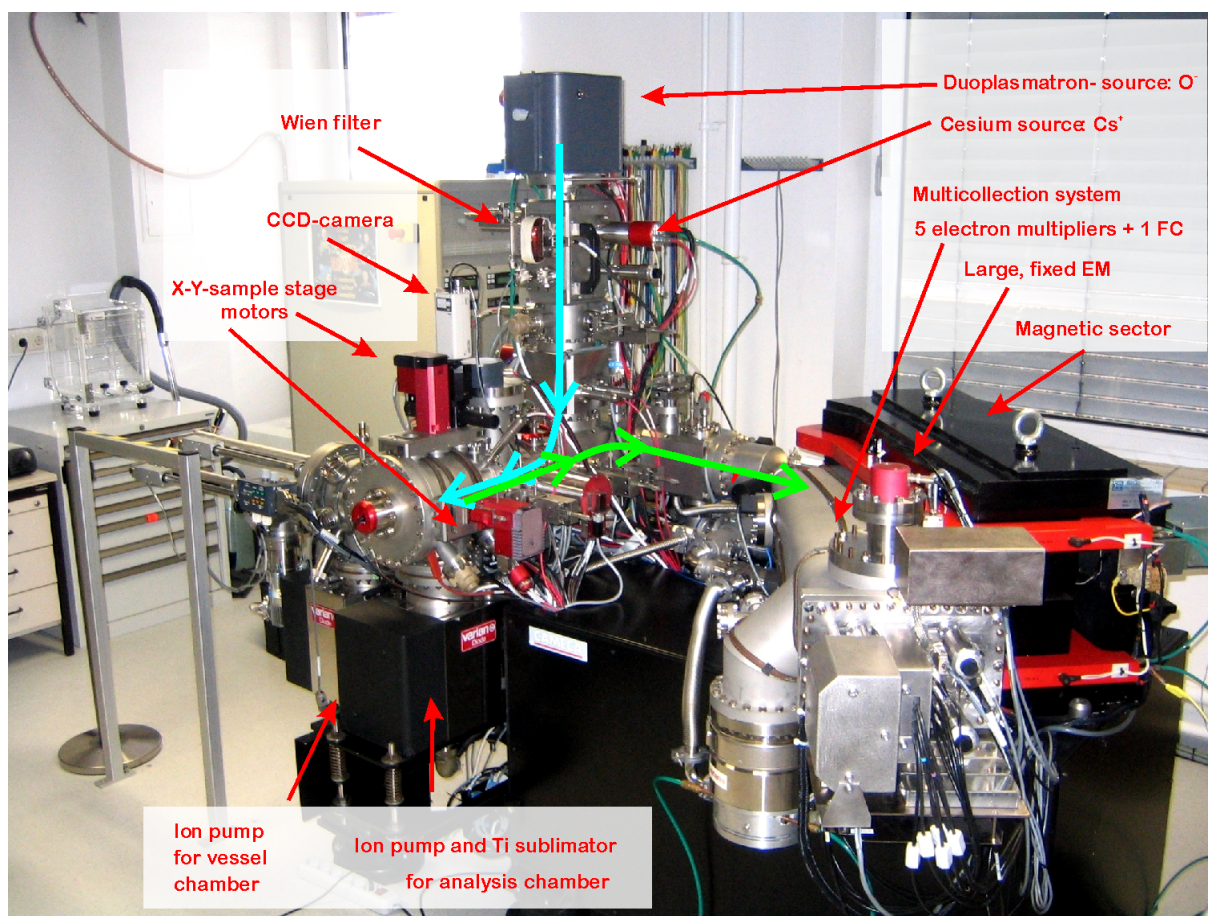
Figure 2. 4 The Mainz NanoSIMS with a description of the main components
The blue arrow indicates the primary beam direction, the green the secondary ion transfer into the magnetic sector (modified after the NanoSIMS Cameca manual).

The magnetic sector is equipped with four movable small electron multipliers (EM), which have been specially designed for the NanoSIMS, one fixed small EM, one fixed Faraday Cup (FC) attached to the EM at the lowest radius and one large EM. This allows to measure 6 masses simultaneously, although only five detectors are used routinely. In the NanoSIMS 50L a larger magnet allows the detection of 7 masses in multicollection mode. The mass dispersion (M_{max} / M_{min}) at a fixed magnetic field is 13.4 in the NanoSIMS 50 (or 14.4 with the large detector). The minimum mass interval between two neighbouring detectors must be M/30, which means that only adjacent masses up to 30 amu can be measured simultaneously. The trajectory of an ion in the magnet is given by the equation R=m*v/B*q, where R (m) is the radius of the curvature, m (kg) the particle´s mass, v (m/s) its velocity, B (T) the magnetic field strength and q (C) the charge of the particle. Each EM is equipped with three different exit slits of 25, 50 and 80 µm width. To resolve the ^{16}OH interference from the ^{17}O mass peak, the smallest exit slit is needed, according to a MRP of ~4500. The deadtime of the EMs is usually taken to be 44 ns, which can be corrected for in data reduction routinely. Only at high count rates, this correction becomes difficult.

Another process which complicates analyses in EMs is quasi-simultaneous arrival (QSA) (SLODZIAN et al., 2004). It occurs if species with a high ionization efficiency and abundance (like ^{16}O and ^{32}S) have to be measured and two incoming secondary ions, emitted by the impact of the same primary ion, are counted as one. QSA therefore undercounts the overabundant species. It can be accounted for by using a FC instead of an EM for the most abundant isotope (SLODZIAN et al., 2003). The number of "lost" secondary ions can be estimated from $(I_S/I_P) * 0.5$. The QSA effect has not been corrected for the values reported in this thesis, as it is only crucial for high precision analyses. The ratio between primary and secondary ion current was usually on the order of $2 - 3$ % (primary beam current ~1 pA = 6.25 x 10^6 cps, typical count rate for ^{16}O ~ 2 x 10^5 cps), the resulting deviation is therefore on the order of $15 - 20$ ‰, which is much less than reported errors ($5 - 10$%). Obtained ratios are not normalized to an external standard, but to the isotopically normal meteorite matrix, which therefore acts as an internal standard. This minimizes the problems resulting from the QSA effect, because it acts on both the surrounding matrix and the measured grain. Normalizing to the matrix also corrects for instrumental mass fractionation (IMF), because the internal standard and the grain are measured under the same analytical conditions.

A program named "Nano50" written by Peter Hoppe and Elmar Gröner in the interactive data language (IDL) was used for data reduction. To obtain an ion image, the focused beam rasters over the sample and the count rate for each isotope on each position, defined by a pixel (px), is converted to a digitized image. Usually 256x256 px^2 ion images of 10 x 10 μm^2 size are acquired in this study. Each px therefore represents ~40 nm of sample surface allowing for a slight overlap of the $50 - 100$ nm sized beam. The dwell time on each px is around 12 ms for a single frame. Usually about five frames are obtained to compensate for beam drift during measurements which can be summed up to one image by the program resulting in ~65 min total counting time per ion image. The counted ions are assumed to follow a Poisson distribution, and the Poisson error, or counting statistical error, of a measurement is determined from the square root of the number of counts. The Poisson error σ of an isotopic ratio A/B then simplifies to $\sigma = \sqrt{(A^{-1} + B^{-1})}$. For the $^{17}O/^{16}O$ ratio, the error is dominated by the much less abundant species ^{17}O ($^{17}O/^{16}O$ = 3.83 x 10^{-4}, the standard mean ocean water reference). A 200 nm sized grain covers about 5x5 px^2 of the whole 256^2 px^2 ion image (or 0.0004). If we assume a typical count rate of 100 cps for ^{17}O on the whole image, we arrive at ~0.04 cps ^{17}O on the grain only. To collect 100 counts of ^{17}O from the grain, resulting in a relative Poisson error of 10%, we have to measure 2500 s or about 40 min. Usually a relative error better than 10% for isotopic ratios of the grain of interest is achieved by the setup explained above. For detection of presolar O-rich grains, $^{16,17,18}O$, ^{28}Si and $^{27}Al^{16}O$ are measured in multicollection mode. For Si isotope measurements ^{16}O, ^{17}O or ^{18}O and $^{28,29,30}Si$ are detected simultaneously. Further analytical details used for the work of this thesis will be described in the experimental sections of the main chapters.

2.3 Auger electron spectroscopy

When accelerated electrons hit the surface of a sample, a variety of elastic and inelastic processes occur in the first µm of the sample. The depth, which is penetrated by the electrons, depends on their energy and the chemical composition ("excitation volume"). One important interaction is the excitation of characteristic x-rays, whose energies/wavelengths can be measured, which is used in x-ray fluorescence (XRF) spectrometers, electron microprobes (EMP) and electron microscopes (SEM/ TEM). However, although modern field emission guns (FEGs) are capable to focus an electron beam to about 1 – 2 nm spot size (at around 5 – 10 kV), the excitation depth from which characteristic x-rays escape is usually in the range of ~500 nm (for a 5 kV beam in a common meteorite matrix). The spatial resolution of such analyses is therefore much worse than determined by the spot size.

The Auger effect was discovered in the 20s of the last century by Lise Meitner and Pierre Auger. When penetrating electrons excite atoms, the released energy after relaxation does not only lead to x-ray emission but also to the escape of low-energy (0.05 – 3 keV) "Auger" electrons from the outer atom bands. Auger electrons are therefore generated in the whole excitation volume within the sample, but only from the very first atomic layers they are not elastically scattered and are able to escape the sample. Auger electron spectroscopy (AES) is therefore a highly surface sensitive technique, which is used routinely in material sciences. As detection limits are in the % range, it is capable to measure major elements and therefore competes with EMP analysis with the advantage of a superior spatial resolution (~10 – 20 nm).

The first Auger instrument for use in the cosmochemistry field was installed in 2006 in St. Louis (USA). The PHI 700™ Scanning Auger Nanoprobe of Physical Electronics is equipped with secondary electron detectors in addition to the Auger detection system allowing for high resolution SEM images. The characteristic elemental peaks of the collected spectra between 0.1 and 2.1 keV can be quantified using relative sensitivity factors obtained from the measurement of mineral standards of similar composition. One major problem of these analyses is that charging of the sample shifts the peak positions to higher values. This was especially a problem with our Acfer 094 thin section, and elemental contents are then harder to quantify. In addition to these chemical analyses of individual grains the Auger technique is also capable to acquire high resolution elemental maps. The information from these maps can not be quantified, but is highly valuable to investigate the distribution of certain elements and thus individual phases.

2.4 The focused ion beam (FIB) preparation technique

One important step from the identification of a presolar grain to further investigations by TEM (Sec. 2.5) is the preparation of electron transparent lamellae including the grain of interest. Although TEM is the most powerful technique to obtain a comprehensive set of structural and chemical information of a sample, its major caveat is that samples have to be electron transparent. The maximum thickness of a sample for usage in TEM depends mainly on the mean density of the sample material and the beam intensity, but should be generally less than ~150 nm. As this is a critical issue in TEM, a diverse set of

preparation techniques have been developed, e.g., crushing, ion milling or cutting with a diamond knife ("ultramicrotoming"). Site specific preparation applying these techniques is a highly difficult and in many cases impossible task, i.e., large areas of the sample are thinned. For the purpose of this work, a different method had to be applied to allow the preparation of slices of submicron sized grains: the "focused ion beam" (FIB) technique was first used in material sciences, and found its way into the geoscience and cosmochemistry field only at the end of the last century. Still, it is far from being a routine technique in this area. Its major advantage rises from the capability to either remove material from the sample and to accrete and weld material by the use of a gas (Pt or C) injection system. Recent reviews on this technique with a focus on geo- and cosmochemical problems can be found in WIRTH (2004) and ZEGA et al. (2007). FIB utilizes a Ga^+ ion beam (usually 30 kV) generated by a liquid metal source (spot size ~10 nm) to cut out precisely defined areas from a specimen. The main part of the FIB work in this thesis was performed at the University of Saarbrücken with a Dual Beam Workstation (Strata DB 235 by FEI). In contrast to single beam stations with ex situ sample transfer, this has the great advantage, that the thinning process can be supervised simultaneously by a high resolution FE-SEM, which minimizes the danger of sample loss during transfer. The grain of interest is first relocated in a LEO 1530 FE-SEM at the MPI for Chemistry by comparison of the NanoSIMS ion image with the SE image. In the FIB, it is marked with a $200 - 300$ nm wide Pt spot to enable later re-identification as this Pt spot is clearly visible in subsequent TEM analyses. A row of holes, ~1 μm deep and ~$100 - 400$ nm wide, are shot with the ion beam into the meteorite matrix along the line of the final TEM section. These holes provide orientation marks for the final thinning process. A protective Pt strap ($10 \times 1 \times 1$ μm³) is then deposited over this line, which is accurately centered above the grain to prevent further damaging by the high energy ion beam. The material on the top and bottom sides of the strap is milled away with the Ga^+-ion beam until a section of $10 \times 5 \times 1$ μm³ is left connected to the matrix only by a tiny bridge on one side. The section is then attached with e-beam assisted Pt deposition to a Cu needle, whose tip has been sharpened previously using the same ion beam. The movement of the needle is controlled by a nanomanipulator (Kleindiek MM3A) and monitored in the ion and electron image. When the section is securely attached to the needle the left-over bridge to the matrix on the other side is cut and the section is lifted out of the meteorite matrix. The section is welded to a half-cut TEM Cu grid and liberated from the needle. This results in a free standing sample whose plane is parallel to the plane of the Cu grid. Alternatively, the tip of the nanomanipulator itself acts as a "microtweezer" (or "End-Effector" manufactured by Ascend Instruments), which can be folded into a geometry compatible with TEM. This technique is used by the FIB group of Rhonda Stroud at the Naval Reasearch Lab (NRL) in Washington (D.C.). The ion beam is then used to polish the section down to a final thickness of $\sim 100 - 150$ nm. The holes in the section provide control points to ensure that the final section follows the originally intended line. This new preparation technique therefore minimizes the problem to accurately center submicron grains in a FIB section and also simplifies later re-identification of the grain. It was developed for the purpose of this study in cooperation with Christian Holzapfel at the University of Saarbrücken (HOLZAPFEL et al., 2008). A series of images illustrating the whole process for FIB preparation is given in Fig. 2.5.
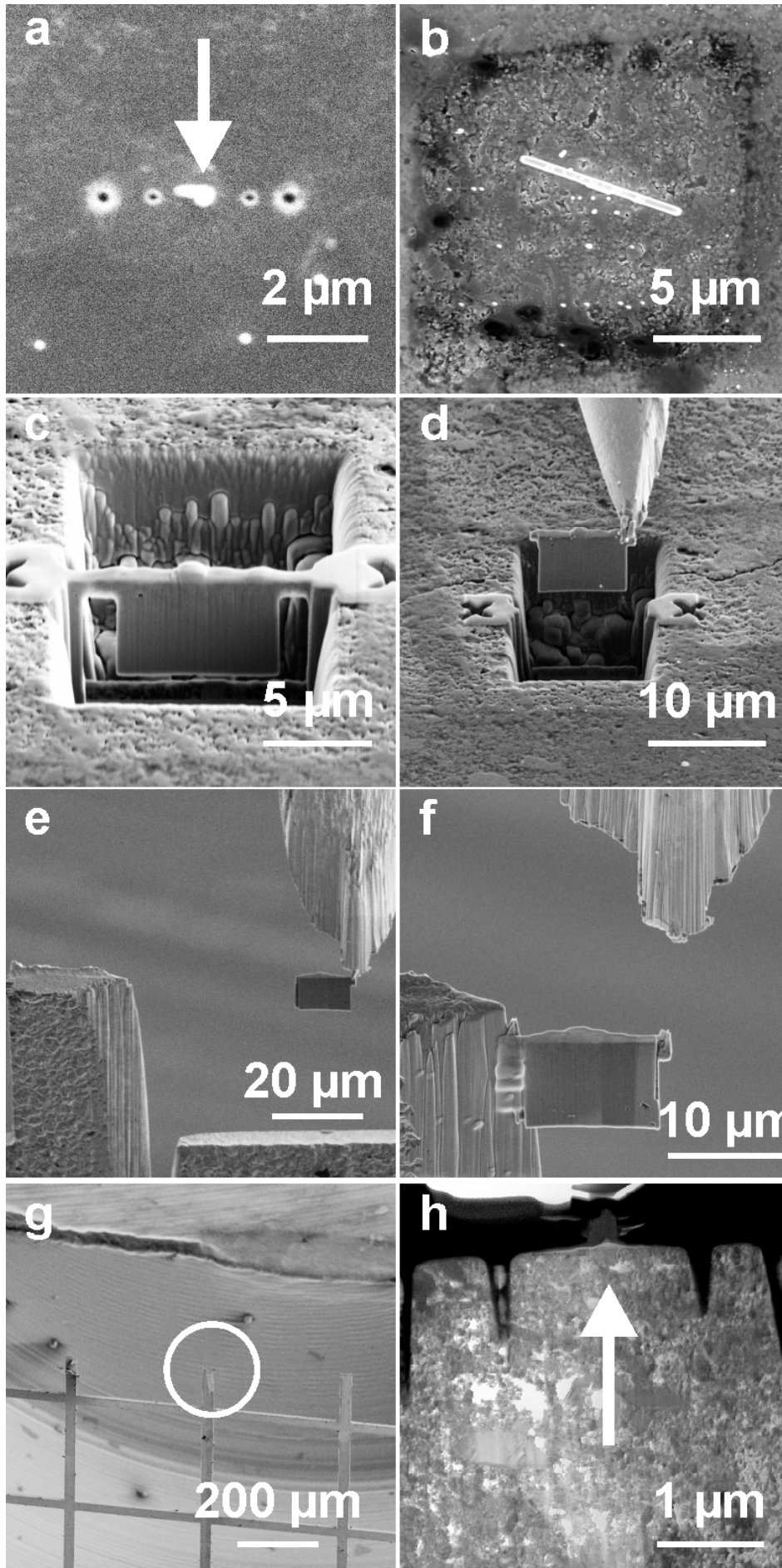
**Figure 2. 5
Procedure to extract a presolar silicate by the FIB technique**

A: The grain of interest is marked (arrow), orientation holes are shot into the matrix,
B: The grain is covered by a protective Pt strap,
C: The material on both sides of the section is milled,
D-G: The section is lifted out of the matrix by a nanomanipulator and welded to a half-cut TEM Cu grid,
H: The grain of interest (arrow) can be relocated by the Pt spot in Scanning TEM mode (18 kV), the holes define the course of the section.

2.5 Transmission electron microscopy (TEM)

The idea that electrons have wave-like properties was first formulated by Louis de Broglie in 1925. The length of these "electron waves" depends on their energy, and is, e.g. , ~0.003 nm for a 200 kV electron beam. That means that in contrast to the use of visible light in optical microscopes much smaller structures down to the atomic scale can be visualized and characterized. The first TEMs were manufactured already in the 30s of the last century, but only when preparation of electron transparent "foils" (~100 nm thickness) was possible in the late 40s, it became a standard tool in material sciences. Still, preparation of samples suitable for TEM analysis is a challenging task in this field (Sec. 2.4).

The typical acceleration voltage in modern TEMs is between $200 - 400$ kV, but voltages over 1000 kV have been applied in some specially designed instruments. Chromatic and spherical aberration effects of the electron beam lead to a decrease in spatial resolution, and modern instrument developments try to correct for these effects (e.g., aberration-corrected TEM or TEAM at the University of Berkeley, resolution down to 0.05 nm). Depending on the thickness of the foil and the stability of the structure, lattice fringes and single atoms or atom groups of a material can be visualized ("High-resolution"-TEM, HR-TEM). Besides imaging techniques such as Brightfield (BF) and Darkfield (DF) TEM, analytical techniques include electron-dispersive x-ray (EDX) analysis for quantitative investigation of major elements, selected area electron diffraction (SAED) and convergent beam electron diffraction (CBED) for determination of the crystal structure, high angle annular dark field (HAADF) detection and energy-filtered TEM (EF-TEM) for qualitative element distributions and electron energy loss spectroscopy (EELS) for studies of the atomic environment and electron states.

The main instrument in this study is a Philips CM 200 TEM (200 kV) at the University of Frankfurt equipped with a LaB_6 Cathode and a post-column GATAN image filter. Standard BF and DF imaging techniques, SAED and EDX spot measurements using an EDAX ultra-thin window spectrometer were applied as routine characterization techniques. Usually the smallest diffraction aperture (25 μm) was selected equivalent to ~200 nm diameter of the sample. This usually resulted in contribution from surrounding phases in the patterns, because measured grains are extremely small. Interplanar spacings were calculated from the SAED patterns using a camera constant, that was calibrated against external synthetic standards and natural minerals or the polycrystalline Pt strap within the same FIB section. EDX spectra were collected at a take-off angle of 20° for ~100s or less (relative 1σ standard deviation on major element integrated intensity < 5%) at a probe current resulting in $~20 - 30\%$ deadtime. Quantification of EDX spectra were performed by applying standard background correction and Cliff-Lorimer thin-film criteria. Two FIB-sectioned grains (14_No2_3a and 18_08) have been further characterized in two other TEM instruments: Grain 14_No2_3a was fibbed at the NRL in Washington, D.C. using a FEI Nova NanoLab 600 and then characterized in a JEOL 2200FS FEG TEM. Grain 18_08 was further analyzed in a FEI Tecnai 200kV FEG-TEM at the MPI for Polymer Chemistry in Mainz for EDX line measurements and HR imaging.

2.6 References

Bland P. A., Stadermann F. J., Floss C., Rost D., Vicenzi E. P., Kearsley A. T., and Benedix G. K. (2007) A cornucopia of presolar and early solar system materials at the micrometer size range in primitive chondrite matrix. *Meteoritics and Planetary Science* **42**(7/8), 1417-1427.

Brearley A. J. (2008) Amorphous Carbon-rich Grains in the Matrices of the primitive carbonaceous chondrites ALHA 77307 and Acfer 094. *Lunar and planetary science conference* **39**, abstr.#1494.

Choi B.-G., Huss G. R., Wasserburg G. J., and Gallino R. (1998) Presolar Corundum and Spinel in Ordinary Chondrites: Origins from AGB stars and a Supernova. *Science* **282**, 1284-1289.

Ebata S., Fagan T. J., and Yurimoto H. (2007) Identification of silicate and carbonaceous presolar grains in the Type 3 enstatite chondrite ALHA81189. *Annual Meeting of the Meteoritical Society* **70**, abstr.#5150.

Ebata S., Nagashima K., Itoh S., Kobayashi S., Sakamoto N., Fagan T. J., and Yurimoto H. (2006) Presolar silicate grains in enstatite chondrites. *Lunar and Planetary Science Conference* **37**, abstr.#1619.

Floss C. and Stadermann F. J. (2008) The Stardust inventory of CR chondrites QUE 99177 and MET 00426, and the distribution of presolar silicate and oxide grains in the early Solar System. *Lunar and planetary science conference* **39**, abstr-#1280.

Greshake A. (1997) The primitive matrix components of the unique carbonaceous chondrite Acfer 094: A TEM study. *Geochimica et Cosmochimica Acta* **61**(2), 437-452.

Hillion F., Daigne B., Girard F., Slodzian G., and Schuhmacher M. (1994) A new high performance instrument: the Cameca "Nanosims 50". *Secondary Ion Mass Spectrometry, Proceedings SIMS IX*, 254-257.

Holzapfel C., Soldera F., Vollmer C., Hoppe P., and Mücklich F. (2008) TEM foil preparation of sub-um sized grains by the Focused ion beam technique. *Journal of Electron Microscopy*, in preparation.

Hoppe P., Ott U., and Lugmair G. W. (2004) NanoSIMS, the new tool of choice: 26Al, 44Ti, 49V, 53Mn, 60Fe and more. *New Astronomy Reviews* **48**, 171-176.

Krot A. N., Keil K., Goodrich C. A., Scott E. R. D., and Weisberg M. K. (2003) Classification of meteorites. *In: Treatise on Geochemistry (eds. A. M. Davis, H. D. Holland, K. K. Turekian)*, 83-128.

Messenger S., Keller L. P., Stadermann F. J., Walker R. M., and Zinner E. (2003) Samples of stars beyond the solar system: Silicate grains in interplanetary dust. *Science* **300**, 105-108.

Mostefaoui S. and Hoppe P. (2004) Discovery of abundant in situ silicate and spinel grains from red giant stars in a primitive meteorite. *The Astrophysical Journal* **613**, L149-L152.

Nagashima K., Krot A. N., and Yurimoto H. (2004) Stardust silicates from primitive meteorites. *Nature* **428**, 921-924.

Newton J., Bischoff A., Arden J. W., Franchi I. A., Geiger T., Greshake A., and Pillinger C. T. (1995) Acfer 094, a uniquely primitive carbonaceous chondrite from the Sahara. *Meteoritics* **30**, 47-56.

Nguyen A. N. and Zinner E. (2004) Discovery of ancient silicate stardust in a meteorite. *Science* **303**, 1496-1499.

Nittler L. R., Alexander C. M. O. D., Gao X., Walker R. M., and Zinner E. (1997) Stellar saphires: The properties and origins of presolar Al2O3 in meteorites. *The Astrophysical Journal* **483**, 475-495.

Palme H. and Jones A. P. (2003) Solar System abundances of the elements. *In: Treatise on Geochemistry (eds. A. M. Davis, H. D. Holland, K. K. Turekian)*, 41-61.

Sakamoto N., Seto Y., Itoh S., Kuramoto K., Fujino K., Nagashima K., Krot A. N., and Yurimoto H. (2007) Remnants of the early Solar System water enriched in heavy oxygen isotopes. *Science* **317**, 231-233.

Scott E. R. D. and Krot A. N. (2003) Chondrites and their components. *In: Treatise on Geochemistry (eds. A. M. Davis, H. D. Holland, K. K. Turekian)*, 143-200.

Seto Y., Sakamoto N., Fujino K., Kaito T., Oikawa T., and Yurimoto H. (2008) Mineralogical characterization of a unique material having heavy oxygen isotope anomaly in matrix of the primitive carbonaceous chondrite Acfer 094. *Geochimica et Cosmochimica Acta* **72**, 2723-2734.

Slodzian G., Hillion F., Stadermann F. J., and Horreard F. (2003) Oxygen isotopic measurements on the Cameca Nanosims 50. *Applied Surface Science* **203-204**, 798-801.

Slodzian G., Hillion F., Stadermann F. J., and Zinner E. (2004) QSA influences on isotopic ratio measurements. *Applied Surface Science* **231-232**, 874-877.

Tonotani A., Kobayashi S., Nagashima K., Sakamoto N., Russell S. S., Itoh S., and Yurimoto H. (2006) Presolar grains from primitive ordinary chondrites. *Lunar and planetary science conference* **37**, abstr.#1539.

Winterholler B. and Hoppe P. (2008) Ion microprobe analysis: basic principles, state-of-the-art instruments and recent applications with emphasis on the NanoSIMS. *in: EMU Notes in Mineralogy. Nanoscopic approaches in Earth and Planetary Sciences (Frank E. Brenker and Guntram Jordan eds.)* **9**, xxx-xxx.

Wirth R. (2004) Focused Ion Beam (FIB): A novel technology for advanced application of micro- and nanoanalysis in geosciences and applied mineralogy. *European Journal of Mineralogy* **16**(6), 863-876.

Zega T. J., Nittler L. R., Busemann H., Hoppe P., and Stroud R. M. (2007) Coordinated isotopic and mineralogic analyses of planetary materials enabled by in situ lift-out with a focused ion beam scanning electron microscope. *Meteoritics and Planetary Science* **42**(7/8), 1373-1386.

Zolensky M., Ohsumi K., Mikouchi T., Hagiya K., and Le L. (2008) Crystallinity of Fe-Ni Sulfides in carbonaceous chondrites. *Lunar and planetary science conference* **39**, abstr.#1676.

3 Si isotopic compositions of presolar silicate grains from red giant stars and supernovae

Christian Vollmer[1*], Peter Hoppe[1] and Frank E. Brenker[2]

[1]Max Planck Institute for Chemistry, Particle Chemistry Dept., 55020 Mainz, Germany; [2]Geoscience Institute / Mineralogy, Goethe-University of Frankfurt, 60054 Frankfurt, Germany.

Abstract

We have measured the silicon isotopic compositions of 38 presolar silicate grains from the carbonaceous chondrite Acfer 094, which have been previously studied for oxygen isotopes. The goals of this study are to further disentangle stellar sources of the ^{18}O enriched (Group IV) and the most ^{17}O enriched (Group I) silicate grains and to put further constraints on the Galactic chemical evolution (GCE) of the Si isotopes. Our results show that the majority (6 out of 8) of the ^{18}O enriched silicates have enhanced ^{28}Si, in qualitative agreement with the signature of presolar silicon carbide (SiC) X grains from supernovae. Three highly ^{17}O enriched grains ($^{17}O/^{16}O > 3 \times 10^{-3}$) have close-to-solar $^{29}Si/^{28}Si$ but enhanced $^{30}Si/^{28}Si$, possibly indicating an origin in binary systems. Alternative stellar sources are 3.5–4 $M_{\odot}$ asymptotic giant branch (AGB) stars. Si isotopic compositions of the majority of presolar silicates fall along the SiC mainstream line, although most grains plot to the ^{30}Si-poor side of this line. Most presolar silicate grains therefore formed in red giant branch (RGB)/AGB stars of roughly solar metallicity and incorporated less (or no) Si processed by slow neutron capture reactions ("*s*-process") than presolar SiC grains, because silicates form before large amounts of ^{12}C and *s*-processed material has been dredged-up to the surface. The inferred shift of the Si isotopes due to the different dredge-up of matter from the He-intershell in C-rich AGB stars is $\Delta^{29}Si = 3‰ - 21‰$ and $\Delta^{30}Si = 17‰ - 30‰$, which is compatible with predictions for $1.5 - 3$ $M_{\odot}$ AGB stars of solar metallicity when C/O > 1.

Subject headings: dust, extinction --- stars: winds, outflows --- stars: late-type --- astrochemistry --- Galaxy: evolution --- supernovae:general

3.1 Introduction

Dust grains from red giant stars and nova/supernova explosions were part of the molecular cloud from which our solar system formed some 4.6 billion years ago. These "presolar" grains are recognized in primitive solar system materials by extreme isotopic anomalies, which can only be explained by nucleosynthetic reactions in stellar interiors. Therefore, they provide precious samples from diverse astrophysical settings (see e.g. LODDERS and AMARI, 2005 for a review). Silicates are the latest addition to the presolar grain collection (MESSENGER et al., 2003). Their discovery was made possible only with the invention of a high spatial resolution mass spectrometer, the Cameca NanoSIMS 50 ion probe (HILLION

et al., 1994). Over 200 presolar silicates have been detected so far by their anomalous O isotopic composition in primitive meteorites (MOSTEFAOUI and HOPPE, 2004, hereafter M04; NAGASHIMA et al., 2004; NGUYEN and ZINNER, 2004; FLOSS and STADERMANN, 2007; NGUYEN et al., 2007, hereafter N07; VOLLMER et al., 2007a), antarctic micrometeorites (YADA et al., 2005; YADA et al., 2006), interplanetary dust particles (MESSENGER et al., 2003; MESSENGER et al., 2005; FLOSS et al., 2006) and in matter from comet Wild 2 collected by the STARDUST-Mission (MCKEEGAN et al., 2006; STADERMANN and FLOSS, 2008).

NITTLER et al. (1997) divided presolar oxides into four different groups based on their O isotope systematics. This classification scheme also applies to presolar silicates. Group I silicates/oxides exhibit enhancements in ^{17}O and close-to-solar or slightly lower-than-solar $^{18}O/^{16}O$ ratios. Most of them apparently come from $1 - 2.5$ $M_\odot$ RGB/AGB stars as inferred from a comparison with astronomical observations (HARRIS and LAMBERT, 1984) and theoretical considerations (BOOTHROYD and SACKMANN, 1999). It is possible, however, that some of the highly ^{17}O enriched silicates ($^{17}O/^{16}O >$ 3×10^{-3}, see Fig. 1) have a different source, as their ^{17}O enrichment lies at the upper end or in some cases even outside the range of model predictions for the first dredge-up in RGB stars and observations. In view of possible dilution of presolar silicate isotopic compositions with surrounding isotopically normal grains the true $^{17}O/^{16}O$ ratios might be even higher than those actually measured (N07). Group II silicates/oxides have strong depletions in ^{18}O and most of the grains are believed to come from RGB/AGB stars that have experienced cool bottom processing (CBP) (WASSERBURG et al., 1995; NOLLETT et al., 2003). Hot bottom burning (HBB) in AGB stars of masses higher than approximately 4 $M_\odot$ (BOOTHROYD et al., 1995) is a distinct possibility to account for low $^{18}O/^{16}O$ ratios in Group II grains but predicted $^{18}O/^{16}O$ and $^{17}O/^{16}O$ ratios from HBB are much lower and higher, respectively, than observed. Evidence for an origin in a massive AGB star has been found only for one presolar spinel grain (LUGARO et al., 2007). However, a recent detailed re-analysis of the ^{16}O (p,γ) ^{17}F reaction rate uncertainties rules out this possibility on the basis of the $^{17}O/^{16}O$ ratio (ILIADIS et al., 2008). Group III grains have ^{16}O excesses and comprise the smallest fraction of presolar silicates/oxides. Based on GCE considerations these grains are thought to come from stars of lower mass and metallicity than the parent stars of the other grains. GCE interpretations of the O isotopes are still hampered by uncertainties, and NITTLER (2007) has pointed out that some of these grains might also come from Type II supernovae (SNeII). To date, there is only little information on the isotopic composition of elements other than O in Group III silicates, and future work should target this population to put further constraints on their origins. Most enigmatic are the Group IV grains, which have moderate to large enhancements in ^{18}O. An origin in SNeII or high-metallicity AGB stars has been considered for these grains (NITTLER et al., 1997; CHOI et al., 1998; MH04). Based on the Si and Fe isotopic compositions of an ^{18}O enriched silicate grain, MH04 favored an origin from a RGB/AGB star of higher-than-solar metallicity, although a SNII origin could not be completely ruled out. One presolar olivine with enhanced ^{18}O (MESSENGER et al., 2005) was found that unequivocally comes from a SNII. This grain is somewhat special because of its low $^{17}O/^{16}O$ ratio, which is not seen in common Group IV grains. However, there is now growing evidence that all or

at least most of the Group IV grains are from SNeII (BLAND et al., 2007; NITTLER, 2007; NITTLER et al., 2008).

The only way to investigate the origins of presolar silicates with unusual O isotopic signatures is to explore other isotope systems such as silicon. Silicon has played a key role in the identification of SiC grains from SNeII and Si isotopic analyses of Group IV grains might help to substantiate the proposed SNII origin. Up to now, Si isotopic data for 27 presolar silicates have been reported (NAGASHIMA et al. 2004; MH04; MESSENGER et al. 2005; N07; BLAND et al. 2007), most of these, however, are from Group I or II. Data by NAGASHIMA et al. (2004) were obtained by low spatial resolution SIMS (compared to the NanoSIMS), and are therefore hampered by large uncertainties. Only four presolar silicates of unusual O isotopic composition, i.e., extreme Group I and Group IV grains, with measured Si isotopes have been reported so far (MH04; MESSENGER et al. 2005; N07; BLAND et al. 2007). Through our ongoing search for presolar silicates in the ungrouped carbonaceous chondrite Acfer 094, we have now established a large sample of presolar silicate grains for further isotope study. The major goal of this work is to disentangle possible stellar sources of Group IV and extreme Group I grains by measuring their Si isotopic compositions.

We also report on Si isotope measurements of Group I and II silicates to put further constraints on the GCE of the Si isotopes. The initial Si isotopic composition in the envelope of an AGB star is altered by slow neutron capture reactions (*s*-process) in the He-intershell and subsequent third dredge-up (TDU) events. Based on most recent cross section determinations (GUBER et al., 2003) the secondary isotopes ^{29}Si and ^{30}Si are expected to evolve along a line of slope $\sim 0.2 - 0.7$ in a Si three-isotope-plot for AGB stars of $1.5 - 3$ M$_\odot$ and solar metallicity (ZINNER et al., 2006). Deconvolving the initial and the *s*-process-altered Si isotope fraction requires precise knowledge of stellar properties such as mass, mass loss, and metallicity, which cannot always be constrained. Silicates condense around RGB/AGB stars when C/O < 1, i.e., before large amounts of ^{12}C and *s*-process material from the He-intershell has been dredged-up to the surface, which leads to C/O > 1 and the formation of carbonaceous grains such as SiC. The Si isotope systematics of presolar silicates should therefore be a more direct measurement of the initial Si isotope composition of a star than can be inferred from presolar SiC. It has been established that the SiC mainstream line obtained from the measurement of thousands of presolar SiC grains (δ^{29}Si/^{28}Si = (1.37 ± 0.01) * δ^{30}Si/^{28}Si – (19.9 ± 0.6) (ZINNER et al., 2007), with $\delta^{29,30}$Si = {{(^{29,30}Si/^{28}Si)$_{Grain}$/(^{29,30}Si/^{28}Si)$_{solar}$ – 1} x 1000}) mostly reflects the GCE of the Si isotopes both in time and space (TIMMES and CLAYTON, 1996; ALEXANDER and NITTLER, 1999; LUGARO et al., 1999) but small imprints of *s*-process Si dredge-up might be present as well.

3.2 Experimental

All presolar silicates in this study were detected by NanoSIMS O isotope mapping on a polished thin section of the Acfer 094 meteorite and subsequently documented in a scanning electron microscope (SEM) (VOLLMER et al., 2006). Si isotope measurements were performed on 3x3 – 6x6 μm² large fields around the grains of interest, for which secondary ions of ^{16}O, ^{17,18}O and ^{28,29,30}Si were acquired in

multicollection mode. Group II and IV grains were relocated by measuring ^{18}O on the second detector, Group I grains by ^{17}O. Measurements were done with mass resolving powers of m/Δm = 2500 (^{16}O, ^{18}O, ^{28}Si, ^{30}Si), 3500 (^{29}Si), and 4500 (^{17}O), sufficient to separate isobaric interferences such as ^{16}OH from ^{17}O and ^{28}SiH from ^{29}Si. To minimize contributions from surrounding isotopically normal silicates, only the innermost 60% − 70% of pixels within the grain of interest were selected for data reduction. As Si isotopic measurements of presolar silicates are hampered by severe dilution with surrounding grains, all anomalies should be seen as a lower limit to the true isotopic composition. The measured Si isotopic ratios of each presolar silicate grain were normalized to those of the whole ion image and expressed as δ-values (see above). Counting statistical errors of the measured δ-values of the grains lie between 10‰ − 50‰ for δ^{29}Si/^{28}Si and 15‰ − 60‰ for δ^{30}Si/^{28}Si.

3.3 Results and discussion

3.3.1 Extreme Group I grains

Three presolar silicates of this study have a ^{17}O/^{16}O ratio larger than 3x10^{-3}. Together with a silicate of uncommon perovskite-like structure found recently (VOLLMER et al., 2007b) and two other highly ^{17}O enriched silicates (HOPPE et al., 2005; N07), this subgroup seems to be separated from the bulk of Group I silicates (Fig. 1). This might be due to the limited data set, but we note that this separation, although not as pronounced as in the silicate data, is also evident from the presolar oxide grain data (NITTLER et al. 2008), for which a similar highly ^{17}O enriched fraction exists. Before our study only one Si isotope measurement of a highly ^{17}O enriched silicate has been done (N07). The large error (54‰ in δ^{30}Si/^{28}Si), however, impeded a definite conclusion in that case. The three grains from this study have an enrichment in ^{30}Si and close-to-solar ^{29}Si/^{28}Si, which is noticeably different from Si isotopic ratios reported for the majority of presolar silicates, which plot close to the SiC mainstream line (Fig. 2). It is therefore possible that these grains have a distinct stellar origin.

The three grains from this study lie in the region occupied by SiC Y or Z grains. The Si isotope characteristics of these rare presolar SiC populations are explained by n-capture reactions in low metallicity AGB stars (HOPPE et al., 1997; AMARI et al., 2001), although a nova origin for the most extreme Z grains cannot be ruled out (AMARI, 2002). The ^{18}O/^{16}O ratios of the three silicate grains, however, favor an origin in an RGB/AGB star of close-to-solar or slightly lower-than-solar metallicity. This interpretation assumes that the ^{18}O/^{16}O ratio increases with time (metallicity) in our Galaxy (TIMMES et al., 1995) and that ^{18}O/^{16}O ratios change only marginally in low-mass RGB stars.

The question is also why the effect of *s*-process Si dredge-up should be seen in silicates that condense during the early evolution on the AGB, i.e., before large amounts of *s*-process Si is mixed into the envelope in TDU events. According to model calculations based on the FRANEC code (STRANIERO et al., 1997) for 1.5 − 3 M$_\odot$ AGB stars with metallicities between 0.003 and 0.02, shifts in Δ^{29}Si (= difference in ‰ to the initial ^{29}Si/^{28}Si ratio) of between 0 and 5 ‰ and in Δ^{30}Si of between 1 ‰ and 10 ‰ are

expected when C/O = 1 (ZINNER et al. 2006), much less than observed in the three grains. Only for a 5 M$_\odot$ AGB star are much larger shifts in the Si isotopic ratios expected, namely, 14 ‰ in Δ^{29}Si and 93 ‰ in Δ^{30}Si at C/O = 1 and for solar metallicity, in good agreement with the grain data.
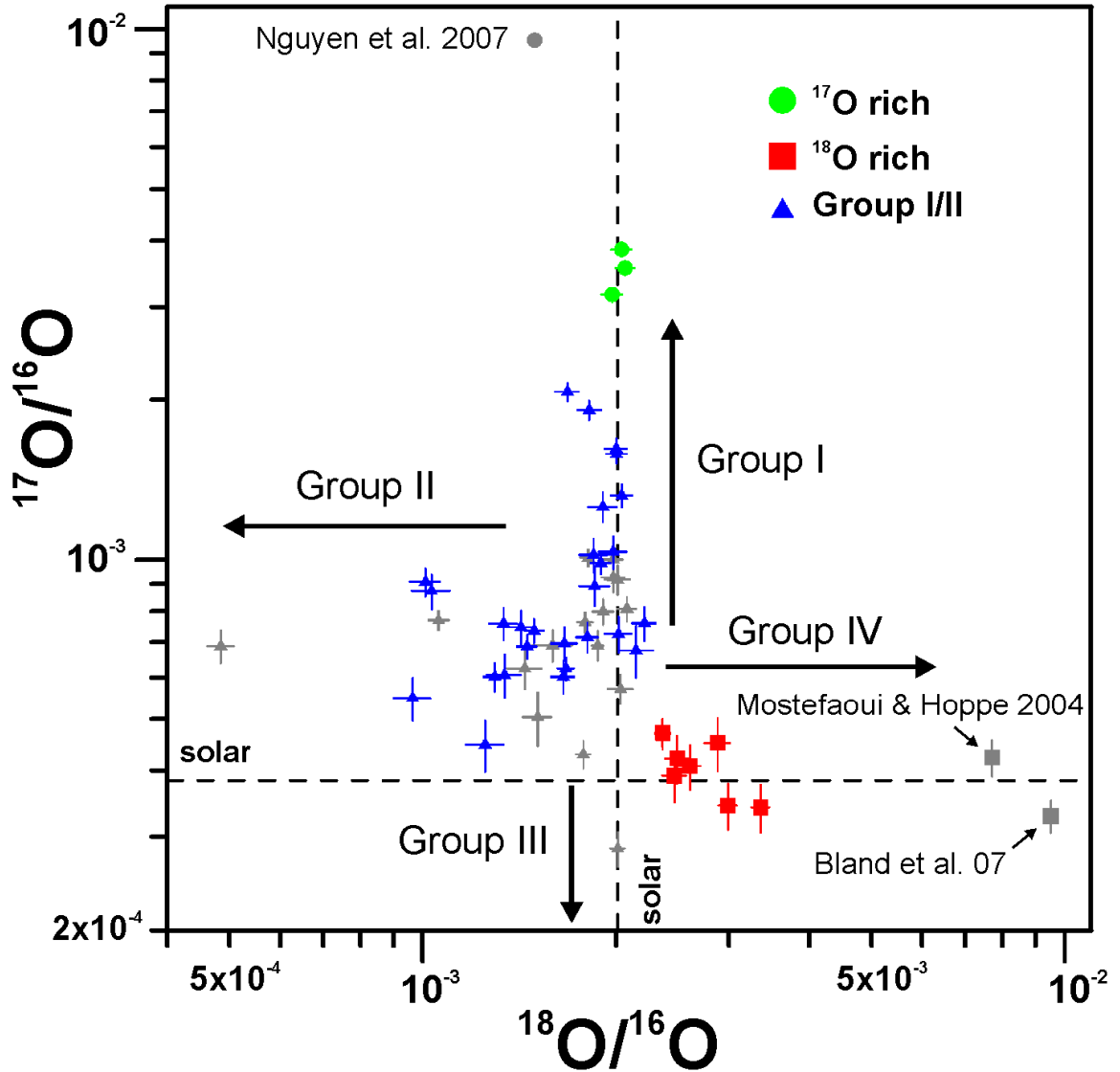
Figure 3. 1 O isotopic ratios of presolar silicate grains for which Si isotopes have also been measured

Data (NanoSIMS only, 1σ error bars) are from this study (colored symbols) and from MOSTEFAOUI and HOPPE (2004), NGUYEN et al. (2007) and BLAND et al. (2007) (gray symbols). Extreme grains discussed in the text are labeled by their source. One ^{17}O depleted grain from NGUYEN et al. (2007) and the SN olivine from MESSENGER et al. (2005) are not shown (as they are off the scale). Arrows indicate main isotopic characteristic of O isotope groups defined by NITTLER et al. (1997).

Models of 5 M$_\odot$ AGB stars, however, predict an ^{17}O/^{16}O ratio about a factor of 2 lower than observed in the three grains. The close-to-solar ^{18}O/^{16}O ratios also rule out the operation of CBP or HBB.
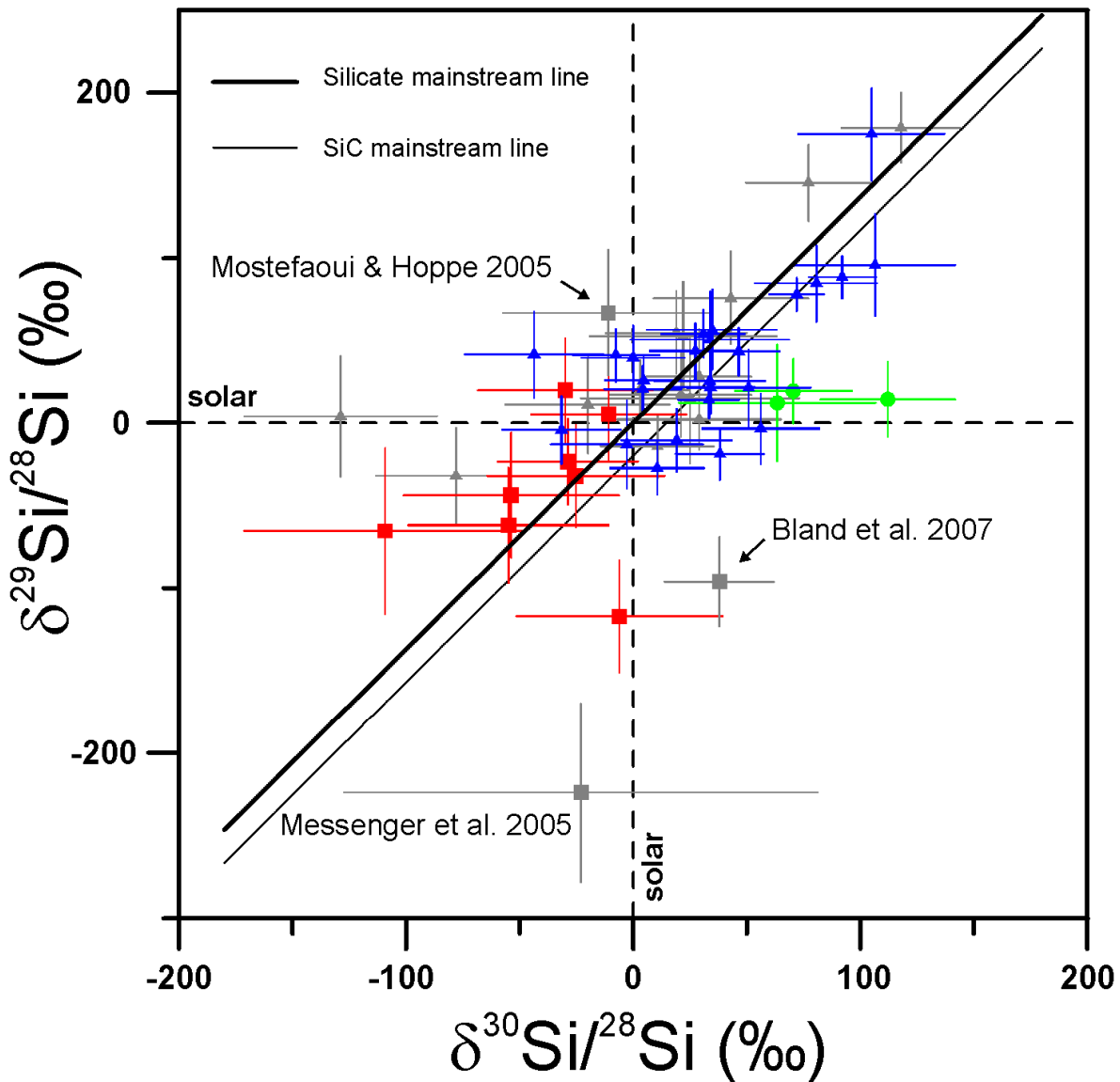
Figure 3. 2 Si isotopic ratios of presolar silicate grains from this study and from the literature

Only those Group I/II grains with an error < 50‰ in $\delta^{30}Si/^{28}Si$ are plotted. Extreme grains are labeled by their source.

See text for details of the definition of the silicate mainstream line. Symbols are the same as in Fig. 3.1, error bars 1σ.

AGB stars with masses between 3 and 5 $M_\odot$, however, deserve further attention as a potential stellar source of the extreme Group I grains. Models of $3.5 - 4$ $M_\odot$ AGB stars with metallicities of 0.02 and 0.008 based on the MONASH code give at C/O = 1 $\Delta^{29}Si = 22‰ - 33$ ‰ and $\Delta^{30}Si = 32‰ - 53$ ‰ (ZINNER et al. 2006). We note that only the low-metallicity case can explain measured Si isotopic ratios within the errors, which is problematic in view of solar $^{18}O/^{16}O$ ratios discussed above. The MONASH models are based on the BAO et al. (2000) Si cross sections for n-capture reactions. With the GUBER et al. (2003) cross sections, $\Delta^{30}Si$ values would increase by several ‰ at C/O = 1, somewhat relaxing the discrepancy between predicted and measured $^{30}Si/^{28}Si$ ratios in the solar metallicity case. Still, $3.5 - 4$ $M_\odot$ AGB stars yield $^{17}O/^{16}O$ ratios that are too low (only up to ~2.6 x 10^{-3} according to BOOTHROYD and SACKMANN, 1999). This might be due to stellar model uncertainties, and it would be interesting to see

whether further modeling will be able to resolve the existing discrepancies. In the context of a possible origin of the extreme Group I grains from low- to intermediate-mass AGB stars, it appears that stars with masses of $3.5 - 4$ M$_\odot$ are the most promising candidates.

NITTLER et al. (1997) have proposed an intermediate-mass star ($> 4 - 5$ M$_\odot$) or a Wolf-Rayet star as the source of the presolar corundum T54 with the highest ^{17}O enrichment ever reported ($^{17}O/^{16}O = 1.4 \times 10^{-2}$). In contrast to the silicates of this study that grain was also characterized by an extreme ^{18}O depletion. This depletion was explained by HBB, but that effect can be ruled out here. NITTLER and HOPPE (2005) have alternatively considered a nova origin for this grain in view of improved model predictions. A nova origin has been discussed as well for a high-pressure structured, extremely ^{17}O enriched silicate found recently (VOLLMER et al. 2007b). Novae have only processed ~0.3% of the interstellar matter (GEHRZ et al., 1998), but the lower mass CO novae in particular are prolific dust producers (JOSÉ and HERNANZ, 2007). The search for nova dust grains among carbonaceous presolar grains has revealed some promising candidates (AMARI, 2002; HECK et al., 2007). For the three extremely ^{17}O-rich presolar silicates of this study, a direct condensation in nova ejecta seems unlikely. ONe nova models can qualitatively account for the observed O and Si isotopic signatures, but a quantitative comparison reveals large discrepancies.

Recently it was proposed that highly ^{17}O-enriched grains could condense around RGB/AGB stars in binary systems in which the RGB/AGB star accreted matter from a nova during the earlier main sequence phase (NITTLER et al. 2008). A mass transfer from an ONe nova could heavily enrich the envelope of the companion star with ^{17}O and ^{30}Si, while leaving the abundances of ^{18}O and ^{29}Si largely unaffected (JOSÉ et al. 2004). Calculations for mixing matter from a main sequence star with solar composition with matter from ONe nova ejecta in a ratio of 100:1 show that if the $^{18}O/^{16}O$, $^{29}Si/^{28}Si$, and $^{30}Si/^{28}Si$ ratios of the silicates are matched, the predicted $^{17}O/^{16}O$ ratio is too high by a factor of 2 (taking the model ONe9 in JOSÉ et al. 2004), which would further increase during the following red giant phase. More recent calculations (JOSÉ and HERNANZ 2007), however, show that larger ^{30}Si enrichments might be possible in nova explosions. This would allow to increase the mixing ratio of 100:1, which might also relax the problem of too much ^{17}O in the envelope of the companion star. The mass-transfer scenario seems promising and it would be desirable to study more grains with strong ^{17}O enrichments for their isotopic compositions of Si and, if possible, other elements to further test this scenario.

3.3.2 Group IV grains

Six out of eight Group IV silicates from this study lie in the lower left quadrant of the Si three-isotope-plot usually occupied by SiC X and graphite grains from SNeII (Fig. 2). The Si isotopic compositions of these grains point to contributions of material from the inner zones of SNeII where ^{28}Si is produced in large quantities through O burning. SNII mixing calculations involving matter from the inner Ni- and Si-rich zones to the outer C-rich zones are able to successfully reproduce many isotopic signatures of low-density graphite grains (TRAVAGLIO et al., 1999) and SiC X grains (HOPPE et al., 2000). It has also been shown that also the O, Mg, and Ca isotopic ratios of Group IV oxide grains can be well reproduced by SNII mixing calculations (NITTLER et al. 2008). The same holds for the O and Si isotopic signatures of

the SN olivine found by MESSENGER et al. (2005), although the $^{30}Si/^{28}Si$ ratio is higher than in typical SiC X and low-density graphite grains. Interestingly, the Group IV silicate described by BLAND et al. (2007) has lower-than-solar $^{29}Si/^{28}Si$ and slightly higher-than-solar $^{30}Si/^{28}Si$ as similarly observed in one grain from this study. A comparison of SiC X and low-density graphite grain data with supernova/hypernova mixing calculations (YOSHIDA et al., 2005) suggests that condensation in the ejecta of < 15 $M_\odot$ SNII or > 20 $M_\odot$ hypernovae more likely produce grains with lower than solar $^{30}Si/^{29}Si$. A small number of grains, however, exhibits higher than solar $^{30}Si/^{29}Si$, which points to formation in more massive SNII (> 15$M_\odot$) or a stronger contribution from the ^{30}Si enriched and ^{29}Si depleted O/Si layer (YOSHIDA et al. 2005). Although the number of Group IV silicate grains analyzed for Si isotopic compositions is still rather small, this could be a hint that the distinction of two populations of SiC X and low-density graphite grains on the basis of their $^{30}Si/^{29}Si$ ratios is also applicable to Group IV silicates (Fig. 2).

To check whether the O and Si isotopic signatures of the Group IV grains of this study can be explained by specific mixing conditions in SNII we have explored the 15 $M_\odot$ model of RAUSCHER et al. (2002) (model s15a28c, see www.nucleosynthesis.org). Following the concept of MEYER et al. (1995), the SNII can be divided into 8 distinct zones. With 0.04 % of matter coming from the Si/S zone, 0.14 % from the O/Ne zone, 1.88 % from the O/C zone, 1.13 % from the He/C zone, 4.78 % from the He/N zone, and 92.03 % from the H zone we obtain $^{17}O/^{16}O = 3.8 \times 10^{-4}$, $^{18}O/^{16}O = 2.9 \times 10^{-3}$, $\delta^{29}Si/^{28}Si = -70$ ‰, and $\delta^{30}Si/^{28}Si = -31$ ‰, in qualitative agreement with the silicate Group IV grain data of this study.

If we consider in contrast high-metallicity, low-mass AGB stars as the source of Group IV grains, one expects to find higher-than-solar $^{18}O/^{16}O$ and roughly solar or higher-than-solar $^{17}O/^{18}O$ ratios based on GCE considerations (TIMMES et al. 1995). This is clearly not the case: the grains of this study have lower-than-solar $^{17}O/^{18}O$ ratios. Even if we consider that the GCE of O isotopic ratios has large uncertainties, additional evidence against high-metallicity stars as sources for the Group IV silicates comes from their Si isotopic ratios. The Si data of Group IV grains plot close to the low-metallicity end of the SiC mainstream line, in the region of inferred initial compositions of the SiC Y and Z grains. Although the meaning of the SiC mainstream line and its relation to metallicity is not yet fully understood, the current interpretation of the origin of SiC Y and Z grains in low-metallicity AGB stars speaks against an origin of Group IV silicates from high-metallicity AGB stars.

It has been argued that an aggregate-like appearance of presolar grains is a qualitative sign of condensation in SNeII ejecta, in contrast to condensation around RGB/AGB stars which more likely leads to single crystals (DAULTON et al., 2002; MESSENGER et al., 2005; NITTLER et al., 2007 and references therein). A presolar Group IV Fe oxide grain found recently (FLOSS et al., 2008) also exhibits such a morphology. High-resolution scanning electron microscope (SEM) imaging of successfully relocated Group IV silicates in this study reveals that most of them show a "polygrain" structure as well (Fig. 3.3). This supports the proposed SNII origin.
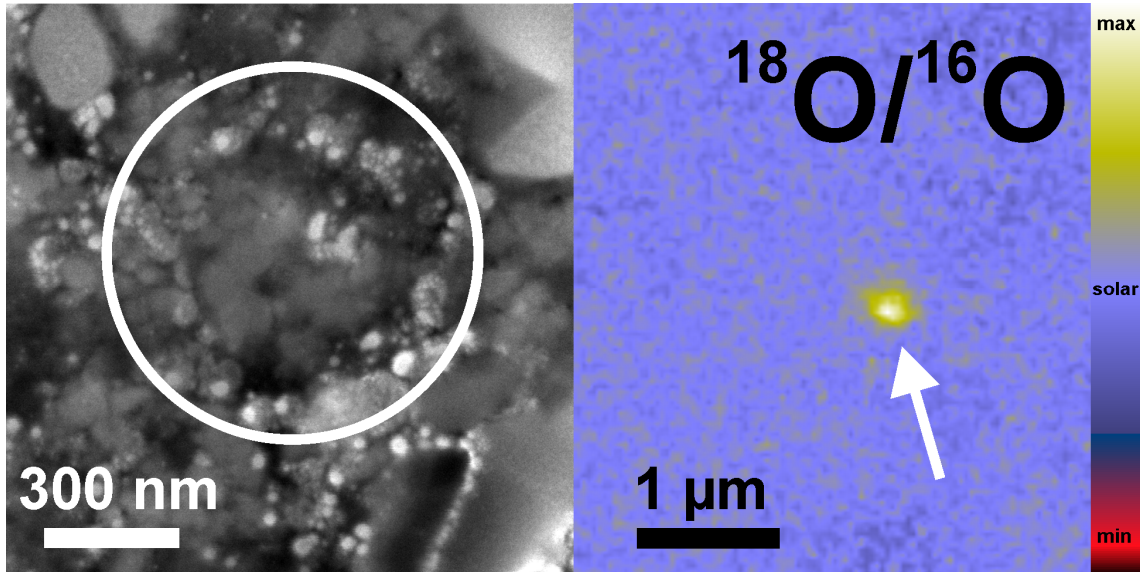
Figure 3. 3 Morphology of a SN grain

SEM image of the presolar silicate 22_10c (left) and the corresponding NanoSIMS $^{18}O/^{16}O$ ratio image after relocation of the grain. The "polygrain" morphology can be clearly recognized in the SEM image.

For the reasons discussed above, we clearly favor a SNII origin for Group IV silicate grains, in agreement with previous suggestions by NITTLER (2007), BLAND et al. (2007), and NITTLER et al. (2008).

3.3.3 Group I/II grains

Most grains of this study are characterized by Group I/II O isotopic compositions (71%). The observed Si isotopic compositions cover a similar range as in previous studies from -30‰ to +180‰ in $\delta^{29}Si/^{28}Si$ and -40‰ to +110‰ in $\delta^{30}Si/^{28}Si$ (Table 1 and Fig. 2). The majority of the silicate grains fall to the left of the SiC mainstream line and it is tempting to calculate a separate "silicate mainstream line" by linear regression, but based on the available data this is difficult, for the following reasons: First, most data cluster around $\delta^{29,30}Si/^{28}Si \sim 20$ ‰ and only a few points lie at the low and high end of the observed range. Second, compared to the observed range the errors are rather large. A linear regression is therefore of little use. However, if we assume that the mainstream SiC and Group I/II silicate grains have the same stellar origin, their Si isotopic ratio distributions should be coupled. We then expect the silicate mainstream line to fall parallel to but shifted to the ^{30}Si-poor side of the SiC mainstream line. The shift between the two lines is determined from the different fractions of *s*-process Si from the He-intershell that is incorporated into the silicate and SiC grains. The amount of *s*-processed Si should be higher in the parent stars of SiC grains than in those of silicate grains because SiC needs C/O > 1 in order to form. Models of $1.5 - 3$ M$_\odot$ AGB stars of solar metallicity show that the shifts in $\Delta^{29}Si$ are < 5 ‰ and in $\Delta^{30}Si$ < 10 ‰ at the time of silicate formation (C/O < 1), and 1‰ − 28 ‰ and 8‰ − 41 ‰, respectively, at the time of SiC formation (ZINNER et al. 2006). We can define a silicate mainstream line in that we shift the SiC mainstream line to the ^{30}Si-poor side in such way that the same number of data points (excluding the extremely ^{17}O-rich grains which may have a distinct source) lies on both sides of the line (Fig. 2).

Interestingly, this line intersects the origin. If we want to quantify the effect of *s*-process Si dredge-up in the parent stars of presolar SiC grains from our data we have to consider the slope of the Si evolution in $Z=Z_\odot$ AGB stars that is between 0.2 (1.5 $M_\odot$) and 0.7 (3 $M_\odot$) in a Si three-isotope-plot. This results in a shift of $\Delta^{29}Si = 3‰ - 21‰$ and $\Delta^{30}Si = 17‰ - 30‰$ which is in good agreement with predictions for *s*-process Si dredge-up in AGB stars when C/O > 1.

Table 3. 1 O and Si isotopic compositions of presolar silicate grains from Acfer 094

Grain	size (nm)	$^{17}O/^{16}O$ (x10^{-4})	$^{18}O/^{16}O$ (x10^{-3})	$\delta^{29}Si/^{28}Si$ (‰)	$\delta^{30}Si/^{28}Si$ (‰)
Chr1_1_2	280x170	4.71 ± 0.28	2.36 ± 0.06	-62 ± 35	-55 ± 44
7_15b	250	3.91 ± 0.42	2.47 ± 0.10	-65 ± 50	-109 ± 62
14_09	250x200	4.07 ± 0.39	2.61 ± 0.10	20 ± 32	-30 ± 38
20_11a	350x180	4.22 ± 0.43	2.49 ± 0.10	-44 ± 38	-54 ± 47
22_10b	310x220	4.51 ± 0.51	2.88 ± 0.13	-32 ± 31	-25 ± 39
22_10c	460x260	3.44 ± 0.34	2.99 ± 0.10	5 ± 27	-11 ± 34
25_22	330x290	3.41 ± 0.35	3.36 ± 0.11	-117 ± 34	-6 ± 45
32_11	340x170	4.69 ± 0.30	2.37 ± 0.07	-23 ± 26	-29 ± 31
13_13	300x200	35.53 ± 0.96	2.07 ± 0.07	14 ± 23	112 ± 30
13_16	350x220	31.67 ± 0.96	1.97 ± 0.07	12 ± 35	63 ± 43
23_15	390x240	38.49 ± 1.06	2.04 ± 0.08	19 ± 20	71 ± 26
Chr_2_1_2b	280x200	6.02 ± 0.37	1.30 ± 0.05	41 ± 16	-8 ± 19
Chr_2_1_7	440x420	7.36 ± 0.38	1.49 ± 0.05	42 ± 26	-44 ± 31
Chr_2_2_1	440x410	5.48 ± 0.51	0.96 ± 0.06	-19 ± 16	38 ± 19
1_15b	300	6.75 ± 0.75	2.15 ± 0.13	143 ± 49	-21 ± 52
6_06	340x180	7.26 ± 0.57	2.02 ± 0.10	25 ± 21	34 ± 24
6_09	350x300	9.87 ± 0.47	1.90 ± 0.06	21 ± 23	51 ± 27
7_03a	400	8.73 ± 0.65	1.03 ± 0.07	14 ± 11	33 ± 13

Grain	size (nm)	$^{17}O/^{16}O$ (x10^{-4})	$^{18}O/^{16}O$ (x10^{-3})	δ^{29}Si/^{28}Si (‰)	δ^{30}Si/^{28}Si (‰)
8_05	330	8.92 ± 0.71	1.85 ± 0.10	44 ± 17	27 ± 20
8_12	470x370	10.21 ± 0.73	1.85 ± 0.09	89 ± 13	92 ± 15
10_03	300	6.96 ± 0.50	1.66 ± 0.08	40 ± 20	0 ± 23
10_06	340x250	7.60 ± 0.55	2.22 ± 0.09	85 ± 23	81 ± 27
11_07	450x150	15.82 ± 0.63	2.00 ± 0.07	-13 ± 26	-3 ± 33
11_10	450x400	10.35 ± 0.72	1.98 ± 0.10	175 ± 28	105 ± 32
13_04	450x380	20.69 ± 0.80	1.68 ± 0.07	-4 ± 21	-32 ± 26
13_23	350x310	6.87 ± 0.36	1.45 ± 0.05	26 ± 14	5 ± 17
14_01	420x340	9.08 ± 0.53	1.01 ± 0.05	22 ± 16	34 ± 19
14_2_1	350x270	6.02 ± 0.43	1.66 ± 0.07	43 ± 15	47 ± 18
15_2_4	400x270	12.58 ± 0.79	1.91 ± 0.10	78 ± 10	72 ± 12
17_02	300	6.24 ± 0.30	1.67 ± 0.05	57 ± 24	35 ± 28
21_09	380x360	7.47 ± 0.56	1.42 ± 0.08	20 ± 14	4 ± 17
21_13a	380	16.17 ± 0.71	2.00 ± 0.08	-10 ± 19	19 ± 24
21_13b	300	7.15 ± 0.44	1.81 ± 0.07	55 ± 14	31 ± 18
22_03	300	4.48 ± 0.49	1.25 ± 0.08	96 ± 31	107 ± 35
23_05	400x300	19.12 ± 0.80	1.82 ± 0.08	-27 ± 16	11 ± 21
23_06	400x330	7.58 ± 0.51	1.34 ± 0.07	51 ± 29	34 ± 35
23_12a	400x310	13.22 ± 0.63	2.04 ± 0.08	43 ± 40	23 ± 50
25_17	240x200	6.07 ± 0.56	1.34 ± 0.08	-3 ± 21	56 ± 26
solar		3.83	2.01	0	0

Note: grains 1-8 – Group IV, grains 9-11 – extreme Group I, remaining grains – Group I and II

3.4 Conclusions

We have measured the Si isotopic compositions of 38 presolar silicate grains that were previously classified according to their O isotope systematics. Our results allow us to draw the following conclusions:

1. Highly ^{17}O enriched Group I silicates ($^{17}O/^{16}O > 3x10^{-3}$) may have a distinct source from the majority of Group I grains, which most likely come from $1 - 2.5$ M$_\odot$ RGB/AGB stars. The three grains from this study are all characterized by an enrichment in ^{30}Si relative to solar and close-to-solar $^{29}Si/^{28}Si$. The combined O and Si isotope systematics of this presolar silicate subgroup might be explained by an origin in binary systems, in which mass was transferred from a nova to a main sequence star (NITTLER et al. 2008), which produced the silicate dust during its later red giant phase. Alternatively, $3.5 - 4$ M$_\odot$ AGB stars might also produce silicate dust with the observed Si isotopic compositions within the errors, although predicted $^{17}O/^{16}O$ ratios for these intermediate-mass stars are slightly too low.

2. Group IV grains more likely derive from SNeII than from higher-than-solar metallicity AGB stars. Six out of eight Group IV grains from our study show enhanced ^{28}Si, which is in qualitative agreement with the signature of presolar SiC X grains from SNeII.

3. The effect of s-process Si dredge-up in the parent stars of presolar SiC grains inferred from the shift between the silicate and the SiC mainstream line is $\Delta^{29}Si = 3‰ - 21 ‰$ and $\Delta^{30}Si = 17‰ - 30 ‰$. This is in good agreement with predictions for *s*-process Si dredge-up in AGB stars when C/O > 1.

3.5 References

Alexander C. M. O. D. and Nittler L. R. (1999) The galactic evolution of Si, Ti, and O isotopic ratios. *The Astrophysical Journal* **519**, 222-235.

Amari S. (2002) Presolar grains from novae: Their isotopic ratios and radioactivities. *New Astronomy Reviews* **46**, 519-524.

Amari S., Nittler L. R., Zinner E., Gallino R., Lugaro M., and Lewis R. S. (2001) Presolar SiC grains of type Y: Origin from low-metallicity asymptotic giant branch stars. *The Astrophysical Journal* **546**, 248-266.

Bao Z. Y., Beer H., Käppeler F., Voss F., Wisshak K., and Rauscher T. (2000) *At. Data Nucl. Data Tables* **76**, 70.

Bland P. A., Stadermann F. J., Floss C., Rost D., Vicenzi E. P., Kearsley A. T., and Benedix G. K. (2007) A cornucopia of presolar and early solar system materials at the micrometer size range in primitive chondrite matrix. *Meteoritics and Planetary Science* **42**(7/8), 1417-1427.

Boothroyd A. I. and Sackmann I.-J. (1999) The CNO isotopes: Deep circulation in red giants and first and second dredge-up. *The Astrophysical Journal* **510**, 232-250.

Boothroyd A. I., Sackmann I.-J., and Wasserburg G. J. (1995) Hot Bottom Burning in asymptotic giant branch stars and its effect on oxygen isotopic abundances. *The Astrophysical Journal* **442**, L21-L24.

Choi B.-G., Huss G. R., Wasserburg G. J., and Gallino R. (1998) Presolar Corundum and Spinel in Ordinary Chondrites: Origins from AGB stars and a Supernova. *Science* **282**, 1284-1289.

Daulton T. L., Bernatowicz T. J., Lewis R. S., Messenger S., Stadermann F. J., and Amari S. (2002) Polytype distribution in circumstellar silicon carbide. *Science* **296**, 1852-1855.

Floss C. and Stadermann F. J. (2007) Very high presolar grain abundances in the CR chondrite QUE 99177. *Meeting of the Meteoritical Society* **70**, 5060.

Floss C., Stadermann F. J., and Bose M. (2008) Circumstellar Fe oxide from the Acfer 094 carbonaceous chondrite. *The Astrophysical Journal* **672**, 1266-1271.

Floss C., Stadermann F. J., Bradley J. P., Dai Z. R., Bajt S., Graham G., and Lea A. S. (2006) Identification of isotopically primitive interplanetary dust particles: A NanoSIMS isotopic imaging study. *Geochimica et Cosmochimica Acta* **70**, 2371-2399.

Gehrz R. D., Truran J. W., Williams R. E., and Starrfield S. (1998) Nucleosynthesis in classical novae and its contribution to the interstellar medium. *The Publications of the Astronomical Society of the Pacific* **110**(743), 3-26.

Guber K. H., Koehler P. E., Derrien H., Valentine T. E., Leal L. C., Sayer R. O., and Rauscher T. (2003) Neutron capture reaction rates for silicon and their impact on the origin of presolar mainstream SiC grains. *Physical Review C* **67**(062802).

Harris M. J. and Lambert D. L. (1984) Oxygen isotopic abundances in the atmospheres of seven red giant stars. *The Astrophysical Journal* **285**, 674-682.

Heck P. R., Marhas K. K., Hoppe P., Gallino R., Baur H., and Wieler R. (2007) Presolar He and Ne isotopes in single circumstellar SiC grains. *The Astrophysical Journal* **656**, 1208-1222.

Hillion F., Daigne B., Girard F., Slodzian G., and Schuhmacher M. (1994) A new high performance instrument: the Cameca "Nanosims 50". *Secondary Ion Mass Spectrometry, Proceedings SIMS IX*, 254-257.

Hoppe P., Annen P., Strebel R., Eberhardt P., Gallino R., Lugaro M., Amari S., and Lewis R. S. (1997) Meteoritic silicon carbide grains with unusual Si-isotopic compositions: evidence for an origin in low-mass, low-metallicity asymptotic giant branch stars. *The Astrophysical Journal* **487**, L101-L104.

Hoppe P., Mostefaoui S., and Stephan T. (2005) Nanosims Oxygen- and Sulfur isotopic imaging of primitive solar system materials. *Lunar and Planetary Science Conference* **36**, 1301.

Hoppe P., Strebel R., Eberhardt P., Amari S., and Lewis R. S. (2000) Isotopic properties of silicon carbide X grains from the Murchison meteorite in the size range 0.5-1.5 μm. *Meteoritics and Planetary Science* **35**(6), 1157-1176.

Iliadis C., Angulo C., Descouvemont P., Lugaro M., and Mohr P. (2008) New reaction rate for 16O (p,gamma) 17F and its influence on the oxygen isotopic ratios in massive AGB stars. *Physical Review C* **77**, 045802.

José J. and Hernanz M. (2007) The origin of presolar nova grains. *Meteoritics and Planetary Science* **42**(7/8), 1135-1143.

Lodders K. and Amari S. (2005) Presolar grains from meteorites: Remnants from the early times of the solar system. *Chemie der Erde* **65**, 93-166.

Lugaro M., Karakas A. I., Nittler L. R., Alexander C. M. O. D., Hoppe P., Iliadis C., and Lattanzio J. C. (2007) On the asymptotic giant branch star origin of peculiar spinel grain OC2. *Astronomy and Astrophysics* **461**, 657-664.

Lugaro M., Zinner E., Gallino R., and Amari S. (1999) Si isotopic ratios in mainstream presolar SiC grains revisited. *The Astrophysical Journal* **527**, 369-394.

McKeegan K. D., Aléon J., Bradley J. P., Brownlee D. E., Busemann H., Butterworth A., Chaussidon M., Fallon S., Floss C., Gilmour J., Gounelle M., Graham G., Guan Y., Heck P. R., Hoppe P., Hutcheon I. D., Huth J., Ishii H., Ito M., Jacobsen S. B., Kearsley A. T., Leshin L. A., Liu M.-C., Lyon I., Marhas K. K., Marty B., Matrajt G., Meibom A., Messenger S., Mostefaoui S., Mukhopadhyay S., Nakamura-Messenger K., Nittler L. R., Palma R., Pepin R. O., Papanastassiou D. A., Robert F., Schlutter D., Snead C. J., Stadermann F. J., Stroud R. M., Tsou P., Westphal A., Young E. D., Ziegler K., Zimmermann L., and Zinner E. (2006) Isotopic compositions of cometary matter returned by Stardust. *Science* **314**, 1724-1728.

Messenger S., Keller L. P., and Lauretta D. S. (2005) Supernova olivine from cometary dust. *Science* **309**, 737-741.

Messenger S., Keller L. P., Stadermann F. J., Walker R. M., and Zinner E. (2003) Samples of stars beyond the solar system: Silicate grains in interplanetary dust. *Science* **300**, 105-108.

Meyer B. S., Weaver T. A., and Woosley S. E. (1995) Isotope source table for a 25Msun supernova. *Meteoritics* **30**, 325-334.

Mostefaoui S. and Hoppe P. (2004) Discovery of abundant in situ silicate and spinel grains from red giant stars in a primitive meteorite. *The Astrophysical Journal* **613**, L149-L152.

Nagashima K., Krot A. N., and Yurimoto H. (2004) Stardust silicates from primitive meteorites. *Nature* **428**, 921-924.

Nguyen A., Stadermann F. J., Zinner E., Stroud R. M., Alexander C. M. O. D., and Nittler L. R. (2007) Characterization of presolar silicate and oxide grains in primitive carbonaceous chondrites. *The Astrophysical Journal* **656**, 1223-1240.

Nguyen A. N. and Zinner E. (2004) Discovery of ancient silicate stardust in a meteorite. *Science* **303**, 1496-1499.

Nittler L. R. (2007) Presolar grain evidence for Low-Mass Supernova injection into the Solar Nebula. *Workshop on the Chronology of Meteorites and the Early Solar System, Kauai* **LPI Contribution No. 1374**, 125-126.

Nittler L. R., Alexander C. M. O. D., Gallino R., Hoppe P., Nguyen A. N., Stadermann F. J., and Zinner E. (2008) Aluminum-, Calcium- and Titanium-rich oxide stardust in ordinary chondrite meteorites. *The Astrophysical Journal* **682**, 1450-1478.

Nittler L. R., Alexander C. M. O. D., Gao X., Walker R. M., and Zinner E. (1997) Stellar saphires: The properties and origins of presolar Al2O3 in meteorites. *The Astrophysical Journal* **483**, 475-495.

Nittler L. R. and Hoppe P. (2005) Are presolar silicon carbide grains from novae actually from supernovae? *The Astrophysical Journal* **631**(1), L89-L92.

Nittler L. R., Hoppe P., and Stroud R. M. (2007) Elemental heterogeneity in an isotopically homogeneous SiC aggregate from a supernova. *Lunar and planetary science conference* **38**, 2321.

Nollett K. M., Busso M., and Wasserburg G. J. (2003) Cool bottom processes on the thermally pulsing asymptotic giant branch and the isotopic composition of circumstellar dust grains. *The Astrophysical Journal* **582**, 1036-1058.

Rauscher T., Heger A., Hoffman R. D., and Woosley S. E. (2002) Nucleosynthesis in massive stars with improved nuclear and stellar physics. *The Astrophysical Journal* **576**, 323-348.

Stadermann F. J. and Floss C. (2008) Abundance of presolar grains in comet Wild 2 and implications for transport and mixing in the Solar Nebula. *Lunar and planetary science conference* **39**, 1889.

Straniero O., Chieffi A., Limongi M., Busso M., Gallino R., and Arlandini C. (1997) Evolution and Nucleosynthesis in Low-Mass Asymptotic Giant Branch Stars. I. Formation of Population I Carbon Stars. *The Astrophysical Journal* **478**, 332-339.

Timmes F. X. and Clayton D. D. (1996) Galactic evolution of silicon isotopes: application to presolar SiC grains from meteorites. *The Astrophysical Journal* **472**, 723-741.

Timmes F. X., Woosley S. E., and Weaver T. A. (1995) Galactic Chemical Evolution: Hydrogen through Zinc. *The Astrophysical Journal Supplement Series* **98**, 617-658.

Travaglio C., Gallino R., Amari S., Zinner E., Woosley S., and Lewis R. S. (1999) Low-density graphite grains and mixing in type II supernovae. *The Astrophysical Journal* **510**, 325-354.

Vollmer C., Hoppe P., Brenker F. E., and Holzapfel C. (2007a) A presolar silicate trilogy: condensation, coagulation, transformation - new insights from NanoSIMS/TEM investigations. *Lunar and Planetary Science Conference* **38**, 1262.

Vollmer C., Hoppe P., Brenker F. E., and Holzapfel C. (2007b) Stellar MgSiO3 perovskite: a shock-transformed stardust silicate found in a meteorite. *The Astrophysical Journal* **666**, L49-L52.

Vollmer C., Hoppe P., Brenker F. E., and Palme H. (2006) A complex presolar grain in Acfer 094 - fingerprints of a circumstellar condensation sequence? *Lunar and Planetary Science Conference* **37**, 1284.

Wasserburg G. J., Boothroyd A. I., and Sackmann I.-J. (1995) Deep circulation in red giant stars: a solution to the carbon and oxygen isotope puzzles? *The Astrophysical Journal* **447**(L37-40).

Yada T., Stadermann F. J., Floss C., Zinner E., Nakamura T., Noguchi T., and Lea A. S. (2006) High abundances of presolar silicates in antarctic micrometeorites: implications for their cometary origins. *Lunar and planetary science conference* **37**, 1470.

Yada T., Stadermann F. J., Floss C., Zinner E., Olinger C. T., Graham G. A., Bradley J. P., Dai Z. R., Nakamura T., Noguchi T., and Bernas M. (2005) Discovery of abundant presolar silicates in subgroups of antarctic micrometeorites. *Lunar and Planetary Science Conference* **36**, 1227.

Yoshida T., Umeda H., and Nomoto K. (2005) Si isotopic ratios in Supernovae for Presolar Grains. *The Astrophysical Journal* **631**, 1039-1050.

Zinner E., Amari S., Guiness R., Jennings C., Mertz A. F., Nguyen A. N., Gallino R., Hoppe P., Lugaro M., Nittler L. R., and Lewis R. S. (2007) NanoSIMS isotopic analysis of small presolar grains: Search for Si3N4 grains from AGB stars and Al and Ti isotopic compositions of rare presolar SiC grains. *Geochimica et Cosmochimica Acta* **71**, 4786-4813.

Zinner E., Nittler L. R., Gallino R., Karakas A. I., Lugaro M., Straniero O., and Lattanzio J. C. (2006) Silicon and carbon isotopic ratios in AGB stars: SiC grain data, models and the Galactic Evolution of the Si isotopes. *The Astrophysical Journal* **650**, 350-373.

4 NanoSIMS analysis and high resolution electron microscopy of silicate stardust from the carbonaceous chondrite Acfer 094

Abstract

We have detected 142 presolar silicate and 20 presolar oxide grains within the carbonaceous chondrite Acfer 094 by NanoSIMS oxygen isotope mapping, which were further investigated by scanning / transmission electron microscopy (SEM/TEM) and Auger electron spectroscopy (AES). The majority of analyzed presolar silicates and oxides belong to the O isotope Group I (^{17}O-enriched) and therefore come from $1 - 2.5$ M$_\odot$ red giant stars of close-to-solar or slightly lower-than-solar metallicity. Group II grains seem to be less abundant among presolar silicates compared to Al-rich oxides, but this could be an experimental bias and should be further investigated. About 11 ± 3 % of the presolar silicates can be assigned to Group IV, which are characterized by an enrichment in ^{18}O and close-to-solar ^{17}O/^{16}O and most probably derive from supernovae type II (SNeII). The majority of grains ($70 - 80$ %) are irregular in shape and composed of smaller sub-particles, about $20 - 30$ % display an elongated morphology together with a smooth, platy surface. The grains are evenly distributed within the matrix on a mm scale, but in one case a statistically significant clustering of five grains in one 10x10 μm^2 sized field is observed. This clustering points to an extremely heterogeneous distribution of stardust in the solar nebula or to fragmentation of formerly larger particles shortly before parent body incorporation. The matrix-normalized abundance of silicate stardust in Acfer 094 is 163 ± 14 ppm, of oxide stardust 26 ± 6 ppm, which is among the highest amounts of O-rich stardust in primitive solar system materials. Eight grains were analyzed by TEM and are amorphous, mainly Mg-rich and pyroxene-like in composition. The grains have been rendered amorphous during interstellar passage or by SEM point measurements in the laboratory. Alternatively, they have formed under circumstellar low-temperature conditions. Fe-containing glasses are similar to the "Glass with embedded metal and sulfides" (GEMS) grains, but large Fe-rich inclusions and sulphur > 1 at.% are not present, which indicates a different class of circumstellar grains than presolar GEMS grains. One olivine has a higher Fe content than condensation calculations predict, but is compositionally similar to two other presolar olivines found recently. Crystalline Fe-bearing silicates do therefore indeed form in circumstellar environments. The overall predominance of olivine in crystalline silicate stardust compared to pyroxene could indicate preferential survival of this mineral. Alternatively, this might be the result of different formation pathways. AES of 69 presolar silicates and oxides indicates that most of the grains are Fe-rich (Mg# of 0.82 and lower), which is either due to non-equilibrium condensation, secondary alteration or both. (Mg+Fe)/Si ratios scatter between 1 and 2 and are in most cases characterized by pyroxene- rather than olivine-like compositions, which agrees with the TEM results. Some grains have very low (Mg+Fe)/Si ratios (< 0.5), which could be explained by condensation from a gas with a non-solar composition and a low bulk Mg/Si content. This possibly indicates a low initial metallicity of the parent star or non-equilibrium enrichment of Si-O in the gas from which the grains formed. One grain is extremely rich in Mg (Mg/Si = 3.4) and might be characterized by a heterogeneous Mg distribution. This grain is also special because of its high manganese content (up to 1.4

at.%) similar to "low-iron, manganese-enriched"- (LIME-) silicates indicative of direct condensation processes. Three complex grains consisting of Al-rich oxides and silicate material have been found as well. Refractory Al-rich oxides therefore may serve as seed nuclei for silicate material to condense onto heterogeneously, which is proposed by condensation theory and observational evidence. However, the majority of presolar silicates apparently do not enclose large subgrains.

4.1 Introduction

Silicate dust grains condense in the ejecta of supernova / nova explosions and red giant stars and were part of the molecular cloud, from which our solar system formed. They are detected in-situ by high spatial resolution mass spectrometers such as the NanoSIMS in various primitive solar system materials by their highly anomalous isotopic compositions. These "presolar" or "stardust" signatures can only be explained by nucleosynthetic reactions in stellar interiors. Investigations on these dust grains provide new constraints on stellar evolution and nucleosynthesis, on dust nucleation in circumstellar environments, on dust alteration in the interstellar medium (ISM), on the Galactic chemical evolution (GCE) and on the inventory of dust that formed the solar system (see, e.g., LODDERS and AMARI, 2005 for a review).

A classification scheme developed by NITTLER et al. (1997) based on O isotopic compositions of presolar oxides also applies to presolar silicates. Group I silicates/oxides exhibit enrichments in ^{17}O and close-to-solar or slightly lower-than-solar $^{18}O/^{16}O$ ratios. Most of these grains therefore come from $1 - 2.5\ M_\odot$ asymptotic giant branch (AGB) stars as inferred from a comparison with astronomical observations (HARRIS and LAMBERT 1984) and theoretical considerations (BOOTHROYD and SACKMANN 1999). It is possible, though, that some of the highly ^{17}O enriched silicates ($^{17}O/^{16}O > 3\times10^{-3}$) may have a different stellar source (NITTLER et al. 2008; VOLLMER et al., 2008). Group II silicates/oxides display strong depletions in ^{18}O and most of the grains are thought to come from red giant stars that experienced cool bottom processing (CBP) (WASSERBURG et al., 1995; NOLLETT et al., 2003). Hot bottom burning (HBB) in AGB stars of masses higher than approximately $4\ M_\odot$ (BOOTHROYD et al., 1995) is a distinct possibility to account for low $^{18}O/^{16}O$ ratios in Group II grains, but predicted O isotopic ratios from HBB are different than observed. Group III grains have ^{16}O excesses and might come from stars of lower mass and metallicity compared to the parent stars of the other grains based on GCE considerations. GCE interpretations of the O isotopes are still hampered by uncertainties and some of these grains might as well come from a single SNII (NITTLER, 2007). Group IV grains have moderate to large enhancements in $^{18}O/^{16}O$ and their origins might be best-explained by formation in SNeII (NITTLER et al., 2008; VOLLMER et al., 2008).

Chemical analysis of silicate stardust is a challenging task due to the sizes of the grains (usually smaller than the wavelength of visible light) and the surrounding majority of solar system silicates. For TEM, grains have to be electron transparent. Some presolar silicates were detected in already ultra-microtomed sections of interplanetary dust particles (IDPs), for which no further sample preparation is necessary (MESSENGER et al., 2003; KELLER and MESSENGER 2008). However, most presolar silicates are found in meteorite thin sections and samples pressed into gold foils, which are not accessible to direct TEM

analysis. These grains have to be prepared by the focused ion beam (FIB) technique (e.g. WIRTH, 2004; ZEGA et al., 2007). Alternatively, grains can be analyzed in-situ by Auger electron spectroscopy (AES), where elemental abundances are quantified by a comparison with mineral standards (STADERMANN et al., 2006a). With this technique, larger sample sets can be analyzed, but the mineralogical constitution of the grains remains unclear. Therefore, TEM analysis is essential for a complete characterization. To date, TEM data of presolar silicates have been obtained for 16 grains (MESSENGER et al., 2003; 2005; YADA et al., 2005; FLOSS et al., 2006, NGUYEN et al., 2007, hereafter N07; VOLLMER et al., 2007a; KELLER and MESSENGER 2008; NGUYEN and NITTLER 2008; STROUD et al., 2008). The majority of these grains are amorphous, with only 4 reported olivines (MESSENGER et al., 2003; 2005; KELLER and MESSENGER 2008; NGUYEN and NITTLER 2008). AES as a complementary tool to investigate the compositions of stardust has just started (N07; BOSE et al., 2008a; NGUYEN et al., 2008b) and some rare presolar grain types were already detected by this technique (FLOSS et al., 2008). Here we report on combined investigations on the isotopic compositions, morphologies, distribution, abundances, chemical compositions and mineralogies of stardust silicate and oxide grains from the carbonaceous chondrite Acfer 094 by combined NanoSIMS/ SEM/ AES/ FIB/ TEM analyses.

4.2 Experimental

We chose suitable fine-grained matrix areas in a polished thin section of Acfer 094 for isotopic mapping with the NanoSIMS at the MPI for Chemistry. A focused Cs^+ ion beam (beam diameter < 100 nm, primary current ~ 0.5 – 1 pA) was rastered over a large number of subareas, each 10x10 μm^2 in size, and negative secondary ions of $^{16,17,18}O$, ^{28}Si and $^{27}Al^{16}O$ were simultaneously detected and converted to 256x256 $pixel^2$ images. Total integration time for each ion image was ~1 hour, resulting in a relative counting statistical error for the $^{17}O/^{16}O$ ratio of less than 10% in a typical 300 nm sized grain. All grains with O isotopic anomalies > 4σ away from the isotopically normal background in at least one isotope ratio were defined as being presolar. Only the grains´ innermost 4x4 $pixel^2$ regions of interest (ROIs) were chosen for data reduction in most cases, whereas larger ROIs were integrated over a few grains of larger dimensions. The distinction between a silicate and an Al-rich oxide was mainly based on ^{28}Si and $^{27}Al^{16}O$ ion images compared to the surrounding Si-rich matrix, except for the grains with acquired Auger data. In some cases, primary NanoSIMS identifications had to be corrected after Auger analysis, which means that some Al-rich grains without subsequent Auger analysis could be in fact silicates. Measurements were done with mass resolving powers of m/Δm = 2500 (^{16}O, ^{18}O) and 4500 (^{17}O), sufficient to separate the isobaric interference ^{16}OH from ^{17}O. Identified grains were relocated in the SEM for high-resolution imaging by a comparison between the ion image and the SEM image, were distinctive grains such as Fe-Ni metal grains, sulfides and refractory silicates stand out as orientation marks. Accelerating voltage was 5 kV at a small working distance between 2 and 5 mm to allow for high resolution imaging.

Auger analyses of the grains were then performed with the PHI 700™ Scanning Auger Nanoprobe of Physical Electronics at Washington University in St. Louis (USA). Prior to the analyses, a 2 kV / 1 μA Ar^+ ion beam scans over the sample surface to remove any atmospheric or other contamination, primarily re-deposited carbon. In a first set of analyses, several point measurements on the grains of interest were

performed with 10 kV and 1 – 10 nA for about 10 min per grain. In a second set of analyses, the electron beam was rastered over the grains of interest for about 30 min at 10 kV / 0.3 nA. The acquired spectrum is then differentiated, and by comparison with reference standards, the elemental compositions can be deduced. Because measurement conditions changed between the first and second set of analyses and sensitivity factors for silicate minerals were obtained under measurement conditions similar to the second set of analyses, quantitative results are available only for the second set. The relative uncertainty of reported elemental contents is usually around 10% for major elements. Due to charging effects some spectra are rather noisy, and detection limits for minor elements in these spectra can be as high as several at.% together with a higher relative uncertainty. Relative Auger sensitivity factors on oxides are not precisely known, and identifications of Al-rich oxides therefore bear respective uncertainties. Auger spectroscopic elemental distribution maps were usually acquired with ~5 nA beam current, where the electron beam scans over about 2x2 to 5x5 μm² large areas around the grains of interest and converts the acquired Auger signals into digitized 256x256 pixel² images for previously defined element peaks. These maps can not be quantified, but provide important information on the distribution of measured elements and, therefore, different phases.

To prepare electron transparent sections of the grains, we applied the FIB technique on a Dual Beam Workstation (FEI Strata DB 235) with an attached in-situ lift out tool (Kleindiek MM3A) at the Institute for Functional Materials, University of Saarbrücken. The grain of interest is first relocated and marked with a small Pt spot, which simplifies later re-identification, because this Pt-spot is clearly visible in subsequent TEM analyses. Second, a row of ~100 – 300 nm wide holes are shot into the meteorite along the line of the final section. The section is milled above and below the grain of interest along the line defined by the holes using a 30 kV Ga⁺ ion beam, extracted with the nanomanipulator and welded to a half-cut TEM grid in-situ. The section plane should be aligned parallel to the plane of the TEM grid. During final thinning to ~100 – 150 nm the holes become visible and provide orientation marks to ensure that the section follows the originally intended line. This new preparation technique therefore minimizes the problem to accurately center submicron grains in a FIB section (HOLZAPFEL et al., 2008).

Structural and chemical investigations were mainly performed with a 200 kV TEM (Phillips CM 200) equipped with an ultrathin window EDAX spectrometer and a GATAN image filter at the University of Frankfurt. Two FIB-sectioned grains (14_2_3a and 18_08) were further characterized in two other TEM instruments: Grain 14_No2_3a was fibbed at the Naval Research Lab in Washington, D.C., using a FEI Nova NanoLab 600 and then characterized in a JEOL 2200FS FEG TEM. Grain 18_08 was further analyzed in a FEI Tecnai FEG TEM at the MPI for Polymer Chemistry in Mainz for EDX line measurements and HR imaging. For EDX analysis, the probe was focused onto the grain and spectra were acquired for 30 – 100 s to obtain a relative counting statistical error of less than 5% on major elements and to minimize sample destruction and element diffusion. The spectra were quantified applying standard background correction and Cliff-Lorimer thin-film criteria. K-factors were obtained from mineral standards. It was not possible to quantify the oxygen content, because the exact thickness of the foil could not be measured to correct for self-absorption. Absolute quantification of element concentrations of very

small grains is flawed, therefore only relative abundances of major elements according to integrated peak intensities are reported. Interplanar spacings were calculated from the SAED patterns using a camera constant, that was calibrated against synthetic standards and natural samples within the same FIB section. HR-TEM imaging was not possible in most cases, as FIB sections are usually too thick for this purpose.

4.3 Results and discussion

4.3.1 Oxygen isotopic compositions of silicate and oxide stardust grains

A total of 142 presolar silicate grains were detected within 705 analyzed fields together with 20 Al-rich presolar oxides. Three of the 142 presolar silicate grains contain Al-rich subgrains larger than ~200 nm, which will be discussed later in more detail (Sec. 4.3.6.2). Oxygen isotopic data of the silicate and oxide grains are compiled in Tables 4.1 and 4.2, respectively.

Table 4. 1 Oxygen isotope ratios, sizes and Auger results of presolar silicates from Acfer 094

Auger results in parentheses indicate noisy spectra and thus insecure values. Reported errors are 1σ.

Grain	Group[c]	size (nm) (SEM)	$^{17}O/^{16}O$ (x 10^{-4})	$^{18}O/^{16}O$ (x 10^{-3})	Auger: Mg/(Mg+Fe) (=Mg#) and (Mg+Fe)/Si	Auger: Trace constituents (at.%)
1_07	I[b]	430x230	49.14 ± 3.58	1.36 ± 0.19		
1_08	III	200*	1.91 ± 0.38	2.22 ± 0.13		
1_12	III	290x220*	2.01 ± 0.40	2.07 ± 0.13		
1_15b	I	300	6.75 ± 0.75	2.15 ± 0.13		
4_11	II	370x230	7.60 ± 0.54	0.92 ± 0.06		
4_23	I	230	7.09 ± 0.54	2.09 ± 0.09		
6_06	I	340x180	7.26 ± 0.57	2.02 ± 0.10		
6_09	I	350x300	9.87 ± 0.47	1.90 ± 0.06		
7_03a	II	400x390	8.73 ± 0.65	1.03 ± 0.07		
7_03b	I	160	7.07 ± 0.48	2.09 ± 0.08		
7_04[a]	I	1000x600	5.74 ± 0.15	1.30 ± 0.02		
7_12	I	310x200*	6.74 ± 0.61	1.42 ± 0.09		
7_15a	I	230	7.54 ± 0.61	2.05 ± 0.10		
7_15b	IV	250	3.91 ± 0.42	2.47 ± 0.10		
8_05	I	330	8.92 ± 0.71	1.85 ± 0.10		
8_10	I	810x490	8.07 ± 0.37	1.77 ± 0.05		
8_12	I	470x370	10.21 ± 0.73	1.85 ± 0.09		
8_13	III	350x190*	2.27 ± 0.31	1.95 ± 0.08		
9_15	I	300x270*	5.53 ± 0.36	1.58 ± 0.06		
Chr1_1_2	IV	280x170	4.71 ± 0.28	2.36 ± 0.06		
Chr3_1_8	I	280*	5.79 ± 0.36	1.81 ± 0.06		
Chr3_1_10	I	360x170	6.42 ± 0.42	2.07 ± 0.07		
Chr_2_1_2a	I	280x130	8.84 ± 0.51	2.23 ± 0.08		
Chr_2_1_2b	I	280x200	6.02 ± 0.37	1.30 ± 0.05		
Chr_2_1_6	I	280x230	8.38 ± 0.39	1.84 ± 0.05		

Grain	Group[c]	size (nm) (SEM)	$^{17}O/^{16}O$ (x 10^{-4})	$^{18}O/^{16}O$ (x 10^{-3})	Auger: Mg/(Mg+Fe) (=Mg#) and (Mg+Fe)/Si	Auger: Trace constituents (at.%)
Chr_2_1_7	I	440x420	7.36 ± 0.38	1.49 ± 0.05		
Chr_2_1_8	I	280	5.98 ± 0.32	2.06± 0.06		
Chr_2_2_1	II	440x410	5.48 ± 0.51	0.96 ± 0.06		
10_03	I	300	6.96 ± 0.50	1.66 ± 0.08		
10_06	I	340x250	7.60 ± 0.55	2.22 ± 0.09		
11_05	IV	200x150*	3.96 ± 0.34	2.67 ± 0.09		
11_07	I	450x150	15.82 ± 0.63	2.00 ± 0.07		
11_10	I	450x400	10.35 ± 0.72	1.98 ± 0.10		
12_02	I	400x380	7.36 ± 0.72	1.61 ± 0.07	0.31 / 0.9	Ca 1.5
13_01	I	310x170	6.60 ± 0.43	1.99 ± 0.07	Fe>Mg	
13_04	I	450x380	20.69 ± 0.80	1.68 ± 0.07	(Fe>Mg)	
13_09b	I	240x110	5.85 ± 0.32	1.78 ± 0.05	Fe>Mg, Ca	
13_11	I	320x180	6.33 ± 0.43	1.70 ± 0.07	Si, low Mg+Fe	
13_13	I[b]	300x200	35.53 ± 0.96	2.07 ± 0.07	Mg>Fe	
13_15	I	320x280	6.31 ± 0.40	1.55 ± 0.06	Fe>Mg	
13_16	I[b]	350x220	31.67 ± 0.96	1.97 ± 0.07	Mg>Fe	
13_23	I	350x310	6.87 ± 0.36	1.45 ± 0.05	Mg~Fe, Ca	
14_01	II	420x340	9.08 ± 0.53	1.01 ± 0.05	Fe>Mg, Ca	
14_03	I	280	7.59 ± 0.44	1.70 ± 0.06	Fe>Mg, Ca	
14_09	IV	250x200	4.07 ± 0.39	2.61 ± 0.10	Mg>Fe	
14_11	I	300x320	6.37 ± 0.46	1.40 ± 0.07	Mg>Fe, Ca	
14_2_1	I	350x270	6.02 ± 0.43	1.65 ± 0.07	Si, low Mg+Fe	
14_2_3a	I	470x340	8.22 ± 0.43	1.36 ± 0.05	(Si, Ca, Al, low Mg+Fe)	
14_2_3b	I	400x290	12.49 ± 0.49	1.82 ± 0.06	(Mg>Fe)	
14_2_5	I	370x270	5.84 ± 0.41	1.42 ± 0.06	(Si only, Fe)	
15_2_4	I	400x270	12.58 ± 0.79	1.91 ± 0.10		
15_2_9	I	650x300	6.22 ± 0.53	1.40 ± 0.08		
16_08	I	390x200	7.41 ± 0.70	1.49 ± 0.10	(0.54 / 0.7)	—
16_14	I	320	7.86 ± 0.55	1.92 ± 0.08	0.38 / 1.1	Ca 2.6
17_02	I	300	6.24 ± 0.30	1.67 ± 0.05		
18_08	I	480x420	8.04 ± 0.51	1.93 ± 0.08		
18_14	I	400x280	8.43 ± 0.77	2.08 ± 0.12	Mg~Fe	
19_04a	I	380x350*	7.10 ± 0.58	1.89 ± 0.09		
19_09	I	350x310	8.69 ± 1.00	1.92 ± 0.14		
19_2_1a	IV	330x290*	4.18 ± 0.57	2.82 ± 0.14		
20_08	I	380x340	6.20 ± 0.42	1.98 ± 0.07		
20_11a	IV	350x180	4.22 ± 0.43	2.49 ± 0.10		
20_11b	IV	280x380*	3.73 ± 0.36	2.64 ± 0.09		
20_13	I	300	6.92 ± 0.55	1.95 ± 0.09		
21_06	I	570x360	15.44 ± 0.80	1.94 ± 0.09	Mg>Fe	
21_09	I	380x360	7.47 ± 0.56	1.42 ± 0.08	Fe>Mg, Ca, Al	
21_13a	I	380	16.17 ± 0.71	2.00 ± 0.08	Fe>Mg, Ca	
21_13b	I	300	7.15 ± 0.44	1.81 ± 0.07	Mg>Fe	
22_02	I	380x340	7.62 ± 0.67	1.79 ± 0.10	(Mg~Fe)	
22_03	I	300	4.48 ± 0.49	1.25 ± 0.08		
22_05	II	530x480	10.20 ± 0.61	0.78 ± 0.05	Mg>Fe	

Grain	Group[c]	size (nm) (SEM)	$^{17}O/^{16}O$ (x 10^{-4})	$^{18}O/^{16}O$ (x 10^{-3})	Auger: Mg/(Mg+Fe) (=Mg#) and (Mg+Fe)/Si	Auger: Trace constituents (at.%)
22_09[a]	II	670x480	8.63 ± 0.63	0.79 ± 0.06	Complex (Sec. 4.3.6)	
22_10a	I	450x250	8.34 ± 0.68	1.31 ± 0.08		
22_10b	IV	310x220	4.51 ± 0.51	2.88 ± 0.13		
22_10c	IV	460x260	3.44 ± 0.34	2.99 ± 0.10	Fe>Mg	
22_12	I	300x280	6.98 ± 0.49	2.12 ± 0.08		
22_23	I	300x250	9.26 ± 0.62	2.26 ± 0.10	Fe>Mg, Al	
23_02	I	300x210*	6.78 ± 0.45	1.98 ± 0.07		
23_05	I	400x300	19.12 ± 0.80	1.82 ± 0.08	(Si, low Mg)	
23_06	I	400x330	7.58 ± 0.51	1.34 ± 0.07	Fe>Mg	
23_12a	I	400x310	13.22 ± 0.63	2.04 ± 0.08	Mg>Fe	
23_12b	I	330x320	8.86 ± 0.54	1.91 ± 0.08		
23_15	I[b]	390x240	38.49 ± 1.06	2.04 ± 0.08	Mg~Fe	
24_04	I	250	5.93 ± 0.41	2.03 ± 0.07	Fe>Mg, Ca, S	
24_08	I	340x220	6.89 ± 0.41	1.92 ± 0.07	Fe>Mg	
24_09	I	180x140*	6.40 ± 0.44	1.92 ± 0.08		
24_10	I	270x200	7.01 ± 0.58	2.09 ± 0.10		
24_17	IV	380x300*	4.15 ± 0.34	3.35 ± 0.10		
24_19	I	150*	5.86 ± 0.44	2.01 ± 0.08		
25_03	I	380x360	11.01 ± 0.59	1.98 ± 0.08	Fe>Mg	
25_17	I	240x200	6.07 ± 0.56	1.34 ± 0.08	Mg~Fe	
25_20	I	350x310	8.22 ± 0.61	0.75 ± 0.06	Mg>Fe	
25_22	IV	330x290	3.41 ± 0.35	3.36 ± 0.11	Fe>Mg	
26_06	I	590x350	21.12 ± 0.80	1.63 ± 0.07	0.5 / 0.6	Ca 2.6
26_10a	I	380x200	9.67 ± 0.49	1.81 ± 0.07	0.52 / 1.0	Ca 1.7
26_10b	I	190	6.84 ± 0.41	2.00 ± 0.07		
26_10c	I	270x240	9.78 ± 0.45	2.09 ± 0.06		
26_10d	I	180*	5.76 ± 0.34	2.08 ± 0.06		
26_10e	I	180x60*	5.87 ± 0.38	1.91 ± 0.07		
26_11	I	280	6.11 ± 0.36	1.68 ± 0.06	0.54 / 1.3	Ca 2.1
26_12	I	300x250	6.32 ± 0.40	1.93 ± 0.07	0.75 / 1.3	Ca 1.5
27_02	I	340x220	6.23 ± 0.50	2.05 ± 0.08	0.76 / 2.8	Ca 2.0
27_06	I	610x570	7.89 ± 0.65	1.96 ± 0.10	Rim: 0.79 / 1.5 Core: 0.47 / 2.4	Rim: Ca 1.3 Core: Ca 2.0
27_07	I	320	6.12 ± 0.42	1.64 ± 0.07	0.34 / 0.9	Ca 1.8, Al 3.3
27_09	I	350x190	5.62 ± 0.33	1.97 ± 0.06	0.32 / 1.6	Ca 1.9
27_13	I	300x230	5.66 ± 0.43	2.04 ± 0.08		
27_14	I	310x260	8.68 ± 0.70	1.18 ± 0.08		
27_16	I	270x180	5.90 ± 0.39	1.71 ± 0.06		
28_07	I	270x200	8.39 ± 0.62	1.89 ± 0.09		
29_03	I	270x180	7.23 ± 0.42	1.80 ± 0.06		
29_12a	I	360x260*	5.89 ± 0.36	1.88 ± 0.06		
29_12b	I	280x230	6.71 ± 0.40	1.74 ± 0.06		
29_14	I	220x200	5.78 ± 0.36	1.99 ± 0.06		
30_01	I	340x300	5.37 ± 0.36	1.48 ± 0.06		
30_12	I	340x220	5.14 ± 0.31	1.67 ± 0.05	(0.49 / 0.3)	
30_14a	I	370x280	5.98 ± 0.46	1.58 ± 0.07		

Grain	Group[c]	size (nm) (SEM)	$^{17}O/^{16}O$ (x 10^{-4})	$^{18}O/^{16}O$ (x 10^{-3})	Auger: Mg/(Mg+Fe) (=Mg#) and (Mg+Fe)/Si	Auger: Trace constituents (at.%)
30_14b	IV	180*	4.09 ± 0.31	2.47 ± 0.07		
30_23	I	500x270	10.53 ± 0.63	1.74 ± 0.08	0.67 / 0.3	Ca 0.7
31_02	I	280x170	6.75 ± 0.43	1.88 ± 0.07		
31_04	I	350	8.25 ± 0.39	1.89 ± 0.06		
31_05	I	280x180*	5.05 ± 0.37	1.59 ± 0.06		
31_08a	I	370x340	5.41 ± 0.29	1.75 ± 0.05		
31_08b	I	350*	4.88 ± 0.30	1.73 ± 0.05		
31_09a	I	510x310	9.66 ± 0.54	2.04 ± 0.08	0.76 / 0.5	Ca 4.3
31_09b	I	480x350	7.84 ± 0.52	1.73 ± 0.07	0.76 / 0.7	Ca 0.8
31_09c	I	300x240	4.84 ± 0.38	1.55 ± 0.07	0.5 / 0.5	Ca 1.6, Al 3.2
31_13	II	670x230	5.38 ± 0.34	0.93 ± 0.05	0.64 / 1.2	—
31_16	I	420x350	6.78 ± 0.46	1.94 ± 0.07	0.72 / 1.7	Ca 2.9, Al 6.7
32_03[a]	I	600x500	10.16 ± 0.49	1.79 ± 0.06	Complex (Sec. 4.3.6)	
32_08	I	400	9.26 ± 0.59	1.95 ± 0.08	0.92 / 3.7	Al 3.9
32_11	IV	340x170*	4.69 ± 0.30	2.37 ± 0.07		
32_13	I	650x530	15.67 ± 0.69	2.04 ± 0.08	0.78 / 0.9	Al 5.7
33_11	I	450x350	22.02 ± 0.85	1.92 ± 0.08		
33_12	IV	220x200	3.39 ± 0.33	2.35 ± 0.09		
33_13	I	300x150	6.62 ± 0.48	2.07 ± 0.08	0.51 / 2.4	
33_19	IV	290x210	4.04 ± 0.38	2.66 ± 0.10	0.68 / 1.8	Ca 1.4
34_04	I	270*	5.09 ± 0.28	2.03 ± 0.06		
34_15	I	370x210	5.88 ± 0.43	1.44 ± 0.07	0.82 / 1.7	
35_01	I	250x230	6.00 ± 0.39	2.00 ± 0.07		
35_08	I	240x170	6.76 ± 0.54	1.92 ± 0.09		
35_11	IV	280	4.31 ± 0.44	3.00 ± 0.11	0.45 / 0.6	Ca 1.4
35_19	I	340	6.04 ± 0.35	1.59 ± 0.06	0.32 / 1.1	Ca 0.9
Solar (SMOW)			3.83	2.01		

Table 4. 2 Oxygen isotope ratios, sizes and Auger results of presolar oxides from Acfer 094

Auger results in parentheses indicate noisy spectra and thus insecure values. Reported errors are 1σ.

Grain	Group	size (nm) (SEM)	$^{17}O/^{16}O$ (x 10^{-4})	$^{18}O/^{16}O$ (x10^{-3})	Auger Result (Fe, Mg, Si, Ca, Al)
1_15c	I	310x290*	6.44 ± 0.71	1.76 ± 0.11	
2_11	I	300x190	8.93 ± 0.91	2.04 ± 0.13	
4_28	I	310x210	8.17 ± 0.68	1.90 ± 0.10	
5_01	I	400	16.10 ± 0.75	1.94 ± 0.08	
7_04 (core)	I	500x350	5.74 ± 0.15	1.30 ± 0.02	
7_06	I	320*	7.24 ± 0.53	1.80 ± 0.08	
Chr1_2_15	I	280	13.13 ± 0.47	2.07 ± 0.05	
Chr3_1_14	I	270x220	7.03 ± 0.42	1.48 ± 0.06	
11_14	I	330x280	5.93 ± 0.42	1.85 ± 0.07	
13_09a	I	200x100	5.89 ± 0.32	1.73 ± 0.05	(Al-rich)

Grain	Group	size (nm) (SEM)	$^{17}O/^{16}O$ (x 10^{-4})	$^{18}O/^{16}O$ (x10^{-3})	Auger Result (Fe, Mg, Si, Ca, Al)
13_24	I	320x270	6.60 ± 0.37	1.30 ± 0.05	(Al-rich, Mg)
16_03	I	340x260	7.23 ± 0.60	1.98 ± 0.10	
19_04b	I	450x370	6.17 ± 0.57	1.72 ± 0.09	(Al-rich)
19_2_1b	II	850x280	8.48 ± 1.02	1.00 ± 0.11	(Al-rich, Ca)
22_09 (core)	II	340x200	8.63 ± 0.63	0.79 ± 0.06	Al-rich, Ca (Sec. 4.3.6)
27_05	II	530x400	8.39 ± 0.64	1.05 ± 0.07	4.8, 2.4, 7.3, 1.8, 25.7
28_01	II	540x330	9.67 ± 0.51	0.60 ± 0.04	2.7, 3.3, 7.0, 2.8, 27.1
28_05	I	120*	5.63 ± 0.37	1.98 ± 0.07	
28_10	I	250	6.91 ± 0.41	1.93 ± 0.07	
29_04	I	370x280*	6.70 ± 0.48	1.92 ± 0.08	
31_03	I	350x300*	6.23 ± 0.41	1.59 ± 0.06	
32_03 (core)	I	300x250	10.16 ± 0.49	1.79 ± 0.06	Al-rich, Ca, Mg, Fe, Si (Sec. 4.3.6)
35_17	I	300x250	7.99 ± 0.41	1.93 ± 0.06	5.7, 2.2, 6.2, 0.8, 32.2

Notes: * - grain size determined from the NanoSIMS ion image; a – containing large (> 200 nm) Al-rich subgrains, b – extreme Group I grains ($^{17}O/^{16}O$ > 3 x 10^{-3}), c – Group classification according to NITTLER et al., 1997.

The vast majority of presolar silicate and oxide grains are from Group I (81 ± 7 % of all grains, 81 ± 8 % of the silicate grains, 1σ errors from Poisson statistics throughout this work), which is similar to what has been found by other workers in primitive meteorites (e.g., MOSTEFAOUI and HOPPE, 2004; N07; Fig. 4.1) and what is also observed for presolar oxides (NITTLER et al., 1997; 2008). Four grains have an $^{17}O/^{16}O$ ratio larger than 3 x 10^{-3} (Group I[b]), which might have a different origin than the majority of Group I grains (see below). $^{17}O/^{16}O$ ratios of "normal" Group I grains range from 4.5 x 10^{-4} to 2.2 x 10^{-3} with an arithmetic mean at 8 x 10^{-4}, $^{18}O/^{16}O$ ratios span the range 1.19 – 2.26 x 10^{-3}. It was argued (e.g., NITTLER et al. 1997; 2008) that the bulk of presolar silicates and oxides derives from red giant stars of close-to-solar or slightly lower-than-solar metallicity and about 1.1 – 2.5 $M_{\odot}$ based on comparisons with model predictions for the first and second dredge-up in red giant stars (BOOTHROYD and SACKMANN, 1999). The lower limit is derived from the fact that stars of lower masses would not have evolved to the red giant phase 4.6 Ga ago to inject grains into the solar nebula (e.g., NITTLER and COWSIK, 1997). The upper limit follows the consideration that above this mass ^{17}O is destroyed due to higher temperatures resulting in again lower $^{17}O/^{16}O$ ratios. Therefore, if grains would come from a continuous distribution of stars up to 4 $M_{\odot}$, we would expect a predominance of $^{17}O/^{16}O$ ratios in the 4 – 5 x 10^{-3} range, which is not seen (NITTLER et al., 2008). There are, however, some observations that deserve further attention. NITTLER et al. (2008) already pointed out that red supergiants (M > 8 $M_{\odot}$) might as well reproduce observed oxygen isotopic ratios, and those stars might contribute as much as 2/3 to the O-rich interstellar dust budget (KEMPER et al., 2004). Based on O and Al-Mg data, 15% of the presolar oxide population might originate from red supergiants (NITTLER et al. 2008). This underlines the requirement to measure Al-Mg isotope data to draw more precise conclusions on the origins of presolar oxides and silicates, but this is a complex task in the case of presolar silicates and has been accomplished so far in only one case (NGUYEN and

ZINNER, 2004). Based on our data set, we can not distinguish between a low- and high-mass red giant star origin. If some presolar silicates do indeed derive from red supergiants, we should see evidence for further nucleosynthetic fingerprints in those grains. Future work must focus on additional isotope data of presolar silicates, especially Al-Mg, to answer this question.
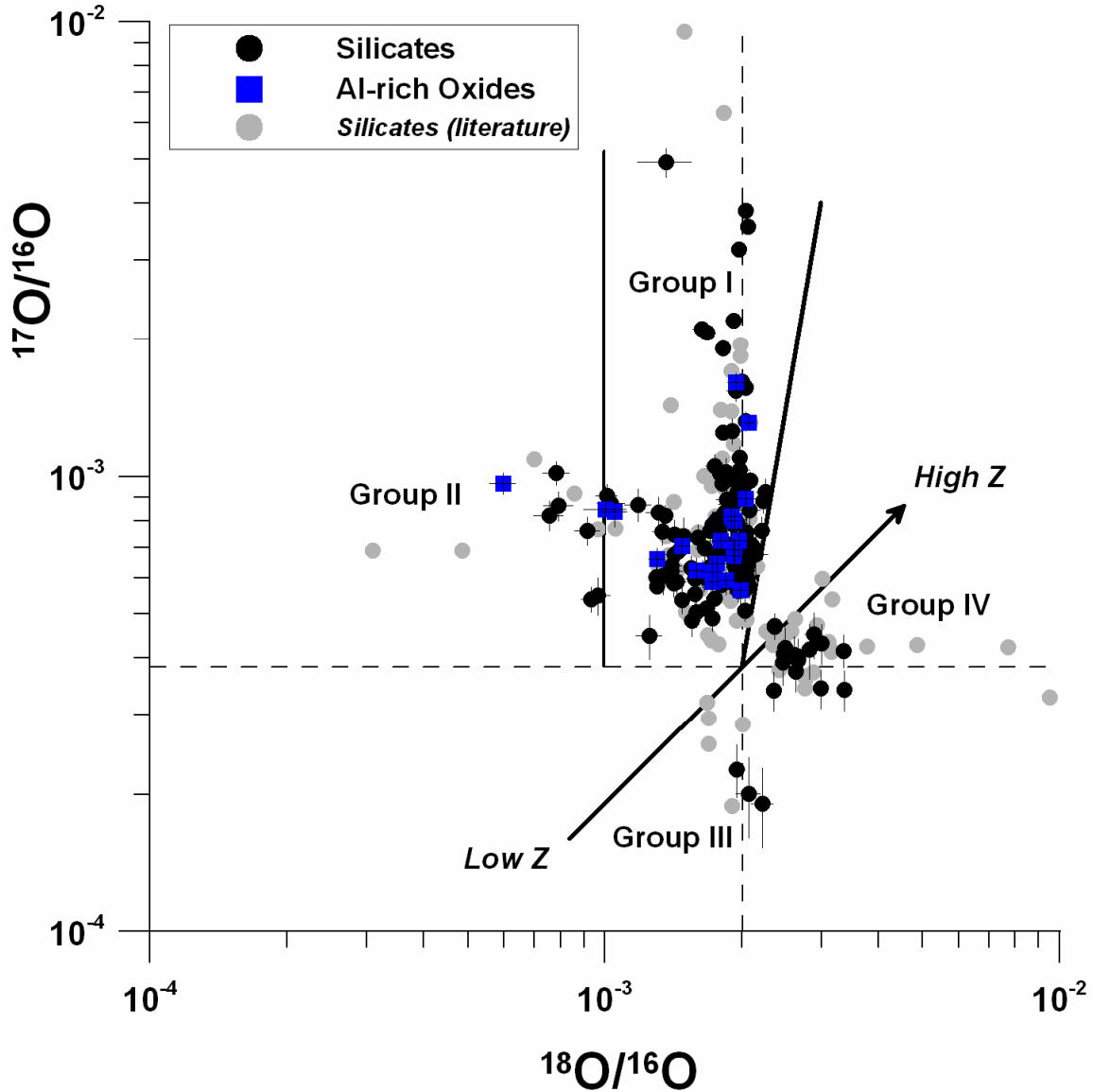

Figure 4. 1 Oxygen isotopic compositions of presolar silicate and oxide grains in Acfer 094

Data from this study are compared to presolar silicate grain data from the literature (NanoSIMS data only: MESSENGER et al., 2003; MOSTEFAOUI and HOPPE, 2004; FLOSS et al., 2006; N07; BLAND et al., 2007; BOSE et al., 2008; YADA et al., 2008). The SN olivine from MESSENGER et al. (2005) is not plotted (off-scale). The approximate ranges of the O isotope groups defined by NITTLER et al. (1997) and the evolution of the O isotopes from low to high metallicity Z based on GCE considerations are shown for comparison.

A recent work by GAIL et al. (2008) indicates that intermediate-mass AGB stars (M = 4 − 8 M$_\odot$) should contribute about half of the presolar oxide and silicate population, as they are as efficient in O-rich dust production as low-mass AGB stars. Such stars experience HBB, which would dramatically change their

isotopic compositions, i.e., lower their $^{18}O/^{16}O$ and raise their $^{17}O/^{16}O$ ratio to levels, which are not observed in presolar O-rich grains. One presolar spinel grain (OC2) might show the effect of HBB (LUGARO et al., 2007), but a recent re-examination of the reaction rate $^{16}O\,(p,\gamma)\,^{17}F$ gave doubt to this interpretation (ILIADIS et al., 2008). To date, there is no explanation to this apparent enigma. It is possible that the stars that contributed grains to the solar nebula were not representative of those stars that deliver material to the ISM (GAIL et al., 2008), maybe due to a speculative galaxy merger scenario that changed the composition of the local ISM (CLAYTON, 2003). Clearly more modelling and further isotope measurements are needed to evaluate the apparent mismatch between predicted dust production rates of intermediate-mass AGB stars, expected HBB effects and observed grain data.

Four grains have an $^{17}O/^{16}O$ ratio higher than 3×10^{-3} (Group I^b), which marks the upper limit of model predictions for the first dredge-up in red giant stars. $^{17}O/^{16}O$ ratios in presolar oxides even extend to higher values (up to 0.02, grain T54 in NITTLER et al. 1997). The missing of presolar silicate grains with this extreme isotopic signature might be due to dilution effects and too few measured silicates. As has been shown by VOLLMER et al. (2008) and NITTLER et al. (2008), combined O- and Si-isotopic data of extremely ^{17}O-rich grains might indicate an origin in binary systems, in which mass was transferred between two companions (one evolved star or white dwarf and one main sequence star). This leads to an enrichment of ^{17}O in the main sequence star, which later evolves into a dust-producing red giant. If mass is lost from the main sequence star, then its envelope is diminished and its ^{17}O abundance therefore less diluted. On the other hand, explosive CNO processing in a nova outburst yields high ^{17}O abundances, which could enrich the envelope of the main sequence star. Clearly, more modelling is needed to explore this possibility. Alternatively, higher mass ($3.5 - 4\ M_\odot$) AGB stars could explain observed O- and Si-isotopic data within the errors, although predicted $^{17}O/^{16}O$ ratios for such stars are lower than actually measured (VOLLMER et al., 2008). A fourth Group I^b grain (1_07), for which no isotope data other than for O are available, has an unusual, high-pressure structure (VOLLMER et al. 2007a), which could furthermore indicate a non-standard origin for these grains.

Seven silicates, three Al-rich oxides and one complex grain (22_09) belong to the ^{18}O-depleted Group II ($^{18}O/^{16}O < 1 \times 10^{-3}$), which represents only about 7 ± 2 % of the whole O-rich stardust population. This is comparable to what has been found by N07, although it was discussed there already that especially Group II grains are more severely diluted by solar system material. Indeed, single grain analyses revealed a higher abundance of Group II oxides than in raster ion imaging mode (NITTLER et al. 1997). The true abundance of Group II grains is therefore not determinable in this study, but might be in the $10 - 15$ % range. $^{18}O/^{16}O$ ratios of these grains range from $5.97 - 10.5 \times 10^{-4}$. Low $^{18}O/^{16}O$ ratios are generally explained either by a low initial parent star metallicity or through destruction of ^{18}O by extra mixing processes such as CBP or by HBB, where HBB seems less likely, because its predictions are largely inconsistent with the grain data (NITTLER et al. 2008). A more exotic source of ^{18}O depleted grains are the winds of very massive Wolf-Rayet stars ($> 40\ M_\odot$) during the WN phase (NITTLER et al. 2008), but observationally the dust formation efficiency in such objects seems rather low. It is interesting to note that four (including one complex grain) out of 11 Group II grains are Al-rich oxides, which represents a higher

fraction than Al-rich oxides among the total population of O-rich stardust (1/6 in this work). However, based on our limited data set this has no statistical significance and clearly more data are necessary to follow up on this observation.

Group III grains comprise by far the smallest population of all detected O-rich stardust grains. All three Group III grains are silicates (2% of the whole O-rich stardust population), which is a bit lower than what has been found by N07, and none of them could be further characterized by SEM. This lower abundance compared to presolar oxides (NITTLER et al. 1997) might as well be attributed to dilution effects for the same reasons discussed for low $^{18}O/^{16}O$ ratios (N07). It is therefore not surprising that presolar grains enriched in $^{17,18}O$ compared to solar are over-represented in relation to $^{17,18}O$ depleted ones. The origins of Group III grains are still poorly constrained, but possible stellar sources are red giant stars of lower mass and metallicity than the parent stars of the other grains and/or a single SNII, especially of those grains that lie below the predicted GCE line (NITTLER et al. 2008). Further isotope systems have to be measured to evaluate this question.

Group IV grains exhibit an ^{18}O enrichment relative to solar and comprise 10 ± 3 % of the whole O-rich stardust population (11 ± 3 % of the presolar silicate population), which is less than what has been found by N07. This is also in contrast to IDPs and Antarctic micrometeorites (AMMs), where a higher fraction of presolar silicates derive from this O isotope group (MESSENGER et al., 2003; MESSENGER et al., 2005; FLOSS et al., 2006; YADA et al., 2008). All Group IV grains in this study are silicates, which is surprising as Group IV oxides have indeed been found (e.g., CHOI et al., 1998). But given the limited data set of only 23 Al-rich oxide grains this observation has limited statistical significance. As is evident from previous studies there is a clear distinction between presolar Group IV oxides and silicates: Group IV oxides lie predominantly on a mixing line between ^{16}O-rich material located in the lower left quadrant of the three-isotope-plot and $^{17,18}O$ enriched material in the upper right quadrant (NITTLER et al. 1997). Group IV silicates, on the other hand, show enrichments in ^{18}O to more extreme values than the Group IV oxides, but do not show a distinctive ^{17}O enrichment or depletion. The only exception to this is the SN olivine found by MESSENGER et al. (2005). The O isotope data of Group IV silicates from this study are only moderately enriched in ^{18}O, but overlap with literature data of Group IV silicates (Fig. 4.1). The enigmatic Group IV grains have drawn considerable attention in recent years (NITTLER, 2007; BOSE et al., 2008b), because their origins have been poorly constrained from the O isotope data alone. Early dredge-up of He-burnt material after a few thermal pulses could enrich ^{18}O in the envelope, synthesized through the $^{14}N+\alpha$ reaction, before it is again destroyed in later thermal pulses. This possibility seems unlikely, because stellar models to not predict early TDU events after only a few thermal pulses (e.g., STANCLIFFE and JEFFERY, 2007). The higher-than-solar $^{18}O/^{16}O$ ratio could also be due to a higher-than-solar metallicity AGB star, but this interpretation fails to explain the close-to-solar $^{17}O/^{16}O$ ratios of most Group IV grains (NITTLER et al. 2008). Also, the very high $^{18}O/^{16}O$ ratios of some presolar silicates (MOSTEFAOUI and HOPPE, 2004; BLAND et al., 2007) would require very high metallicity stars of maybe 2 $Z_{\odot}$ (NITTLER et al. 2008), whose existence is hard to explain at the time of solar system formation. There is now support from additional Si, Mg and Ca isotope measurements that Group IV grains more likely originate in SNeII (NITTLER et al.,

2008; VOLLMER et al., 2008), which has been proposed already 10 years ago (CHOI et al., 1998), but was hard to prove from available data and remained uncertain. The measured ^{28}Si-enriched compositions of some of these grains compared to solar (VOLLMER et al., 2008) point to contribution of material from inner SNII zones, where ^{28}Si is produced in large quantities through O burning.

The fact that some Group IV (and Group III) silicates and oxides lie on a single mixing line connecting a ^{16}O-enriched and a ^{17,18}O-enriched reservoir could point to the origin of these grains in a single SNII (NITTLER, 2007), which is an exciting, but still speculative interpretation. This could also be the reason for the heterogeneous distribution of Group IV grains in various primitive solar system samples (YADA et al., 2008). Isotopic data from SNII carbonaceous grains (TRAVAGLIO et al., 1999; HOPPE et al., 2000) do not support such a single source scenario, and we would expect not only O-rich dust from a single SNII. Furthermore, the compositions of some highly ^{18}O-enriched silicates, of the SN olivine found by MESSENGER et al. (2005) and of the extremely ^{16}O-rich oxide grain T84 (NITTLER et al., 1998) point to origins not consistent with a single source scenario. However, compositions of grains formed in SNeII ejecta are very sensitive to the details of mixing, and it is in principle possible to attain a large range of compositions by appropriate mixing of matter from different SNII zones. Also, whereas SNII SiC and seemingly also silicate grains are characterized by an enrichment of ^{28}Si from the inner SNII zones, there is no indication of a parallel ^{16}O enrichment in most of the silicate grains, which is also a highly abundant isotope in inner SN zones. This under-abundance of ^{16}O in grains supposed to have come from SNeII is hard to explain, because massive stars going supernova should be the most effective contributors to the interstellar ^{16}O budget. Only those Group IV oxide grains, for which several isotope systems have been measured, could be unambiguously attributed to a SNII source, as has been successfully demonstrated by NITTLER et al. (2008) for three grains. Unfortunately, for multi-element isotope studies, presolar silicates are usually too small, and their measured compositions are always diluted by surrounding grains of solar system origin. It is therefore desirable for the clarification of different origins of presolar oxides and silicates to measure further isotope systems such as Si, Al-Mg or Fe, because O isotope data alone often yield equivocal results.

4.3.2 Morphologies of silicate stardust grains

120 grains of the total number of 142 presolar silicates could be documented by HR-SEM. Most of the grains are irregular in shape, but about 20 − 30 % display an elongated morphology. Only a few grains exhibit a rounded or isometric shape, but these may be also elongated grains viewed along the major axis. There is an apparent distinction between smooth/platy grain surfaces, which stick out of the surrounding matrix and thus appear brighter, and irregular grains that seem to consist of smaller particles similar to GEMS (Fig. 4.2).

Figure 4. 2 Different morphologies of presolar silicate grains in this study documented by HR-SEM

Polyaggregate grains similar to GEMS in appearance: a – grain 14_09, b – grain 27_09, c – grain 33_19, one smooth grain with visible cracks: d – grain 26_06, and two smooth, platy grains: e – grain 30_12 f – grain 30_23. Scale bar represents 200 nm in each image.
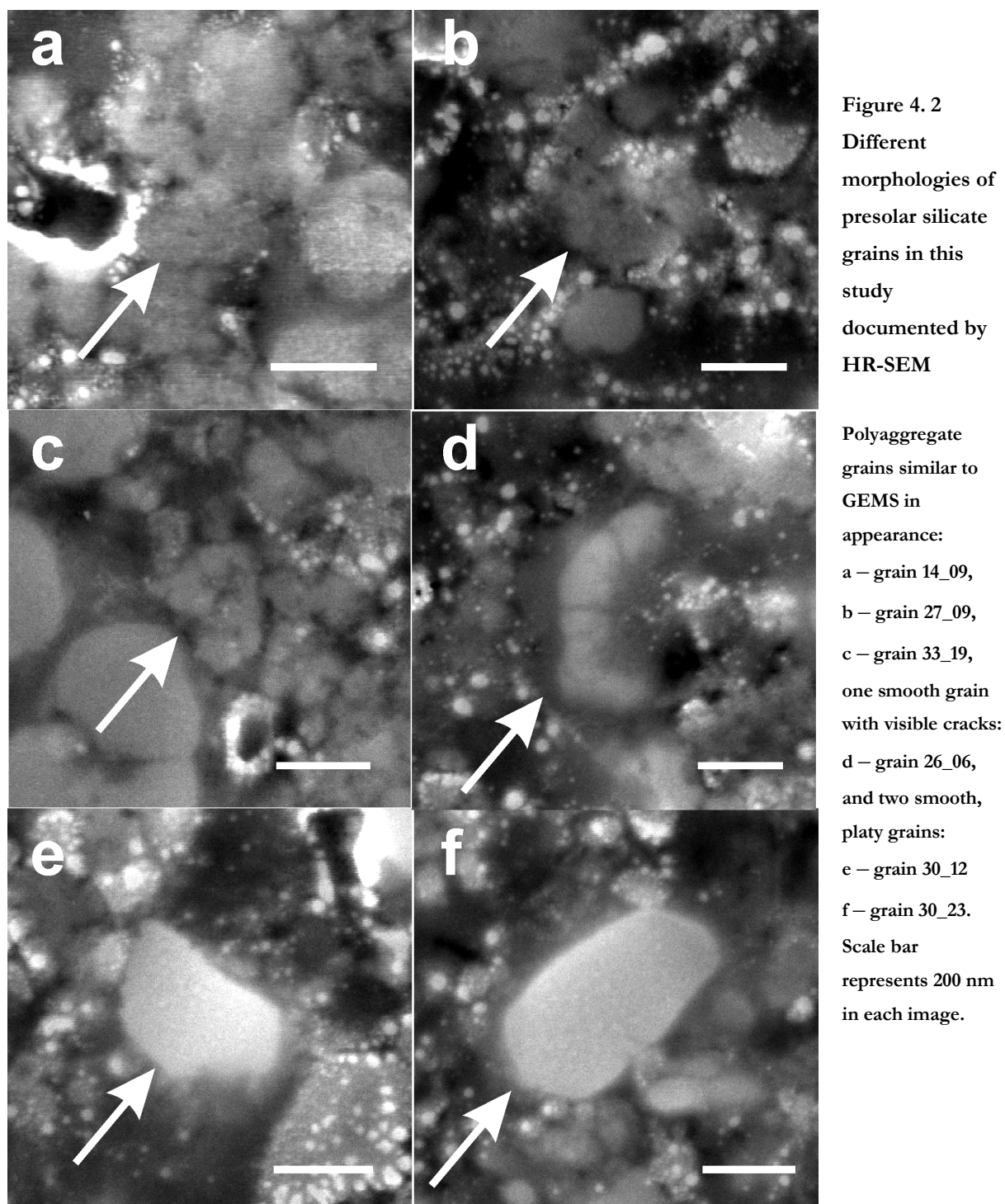
Those irregular grains and "polyaggregates" dominate the whole silicate stardust population (~70 – 80%), but are harder to locate within the matrix, which mainly consists of amorphous silicates of comparable appearance. A similar observation has been recently made for presolar silicates in IDPs (FLOSS et al., 2006). The presolar silicates (as well as solar system silicates) are often surrounded by tiny (< 10 nm) Fe-rich grains (sulfides, oxides or metal) having a bright contrast in the SEM. In some cases, the Fe-rich material seems to infiltrate the presolar grain (e.g., grain 27_06, Fig. 4.3), but this apparently did not erase the isotopic anomaly. However, O isotopic compositions of these grains might be altered to some extent.
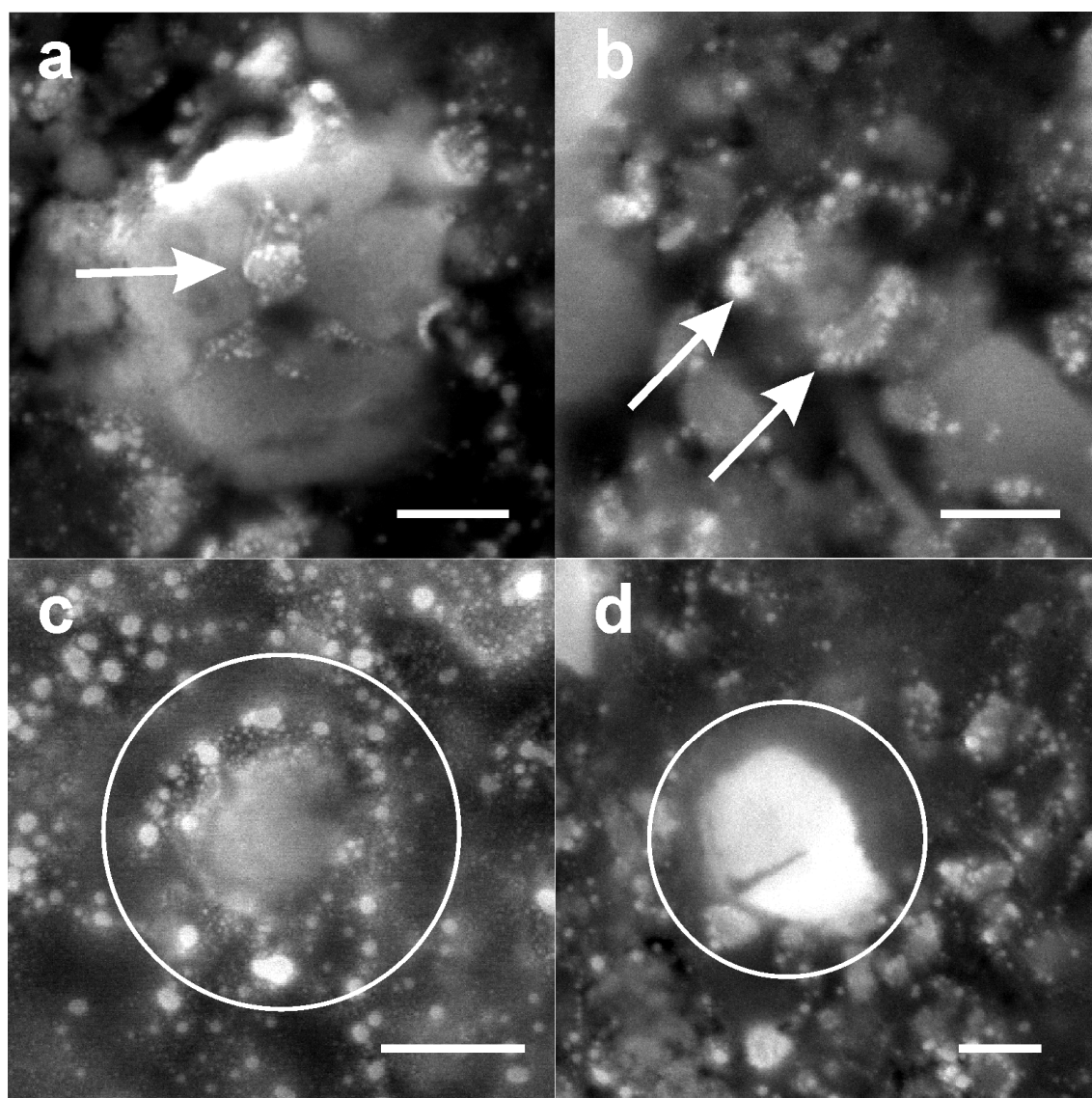
Figure 4. 3 HR-SEM documentation of specific features of presolar silicates

a – grain 27_06 with infiltrated Fe-rich material (arrow-marked), b – grain 31_02 with an accreted Fe-rim (arrows), c – grain 13_15 surrounded by Fe-particles, d – grain 31_09b disrupted by a crack. Scale bars represent 200 nm.

Some grains (31_09b, 26_06, Fig. 4.2 and 4.3) exhibit tiny cracks and fissures different from the polyaggregate morphology mentioned above. The sub-class (Group I^b) of extremely ^{17}O-enriched silicates (^{17}O/^{16}O > 3 x 10^{-3}) was particularly difficult to locate within the matrix compared to grains of less anomalous compositions, because these grains are generally smaller than 300 nm.

In the following we want to discuss observed physical and chemical features of presolar silicates. Laboratory studies of synthetic analogues have shown that silicate condensates often consist of rounded particles bound to fluffy fractal-like structures (COLANGELI et al., 2003). A further topic in condensation experiments is the influence of single grain shapes on IR spectra, and condensing forsterite crystals may be elongated along the crystallographic c-axis (FABIAN et al., 2001). Recent experiments have also shown preferential condensation along one axis, which could explain ellipsoidal shapes of single crystals (TAKIGAWA et al., 2008). Therefore, detected ellipsoidal or rounded grain shapes in this study might

indicate such a condensation pathway leading to single phases, although we do not know the grains´ crystallinities in most cases, and a rounded shape does not necessarily indicate formation by condensation. But if we assume that these grains have not been strongly altered since their circumstellar formation, an ellipsoidal or rounded shape could indicate a primary feature in agreement with laboratory predictions for single crystals. However, the majority of analyzed grains in this study display a highly irregular and polyaggregate-like morphology, which is consistent with condensation experiments as well, if we look at irregular aggregates and not single crystals like above (RIETMEIJER et al., 2002; COLANGELI et al., 2003). Their irregular morphologies would then be explained by smaller particles bound to similar fractal-like structures. On the contrary, irregular particle shapes could be the result of severe fragmentation during ISM passage, which has been proposed to be the dominant modification process of interstellar grains (JONES et al., 1996). Finally, these grains might have been altered by secondary processes in the solar nebula (see below). It is therefore not clear, to what extent irregular, polyaggregate-like morphologies are a primary condensation feature similar to the fluffy aggregates from experiments, or the result of secondary alteration in the ISM or the solar nebula.

There seems to be a clear connection between a smooth, platy surface and a low Fe content, whereas polyaggregate-like grains can be either Fe- and Mg-rich based on combined SEM/AES results. It is not clear whether the high Fe content of very small polyaggregate-like grains is due to tiny Fe-rich distinct particles or to Fe cations within the lattice. The Fe-rich material can be clearly recognized in large grains, (grain 27_06, Fig. 4.3), where the secondary nature seems more obvious than in smaller grains. Fe-poor grains with fissures and cracks or Fe-poor polyaggregate-like grains might then represent an intermediate position between smooth, unaltered and strongly infiltrated Fe-rich grains (Fig. 4.2 and 4.3). Similar cracks have also been observed in presolar SiC grains analyzed in-situ in two CM chondrites (ALEXANDER et al., 1990) and might be due to stress on the meteorite parent body or the solar nebula. A lot of grains in the matrix of Acfer 094 are fragments of formerly undisturbed dust grains (hence the name "breccia" for this meteorite) (NEWTON et al., 1995). Smooth grains with a low Fe content also seem to be harder than the surrounding matrix, as they stick out in SEM images and are easy to locate. These grains apparently have not suffered from strong alteration and might have preserved their original circumstellar appearance. We therefore might see an evolution of Fe-poor unaltered to Fe-rich strongly altered silicates, although some fraction of the Fe might be of primary character.

The origin of Fe-rich material within and around presolar silicates is a major question in this respect. It could be a primary condensation feature, i.e., the Fe-rich material could have condensed together with the silicates in circumstellar environments. Fe metal grains cannot be detected directly in the ejecta of evolved stars due to missing active vibrational modes (MOLSTER and KEMPER, 2005), although they are predicted to exist according to condensation calculations (GAIL and SEDLMAYR, 1999) and due to a high opacity in the near IR (KEMPER et al., 2002). To explain the IR spectra, Fe could be present either as cations in the crystal lattice, as isolated dust grains or as particles surrounded by a glassy matrix ("astronomical/dirty silicates"). Condensation calculations also show that non-equilibrium conditions lead to more Fe-rich silicates at lower temperatures (e.g., GAIL, 2003) and astronomical observations indicate that the majority

(~80%) of circumstellar silicates in most dust shells are amorphous and Fe-rich (MOLSTER and KEMPER, 2005). Interestingly, the fraction of polyaggregate-like grains in this study, which are dominantly Fe-rich, is also ~80%, which could support the conclusion that observed morphologies and Fe contents represent unaltered circumstellar material. Secondary processing in the ISM, the solar nebula or maybe due to metamorphic reactions on the meteorite parent body could also account for Fe-rich material in presolar silicates (NGUYEN and ZINNER, 2004). Large, infiltrated presolar silicates like grain 27_06 support this view. It is therefore possible that some Fe present as tiny particles or as cations is of primary, distinct Fe-rich grains surrounding or infiltrating the grain of secondary origin. Recent calculations indicate that Fe metal may condense onto forsterite crystals (NAGAHARA and OZAWA, 2008), which prevents the dust grain from further reactions with the gas. This obviously complicates any interpretation inferred from the Fe content of presolar silicates. The fact that many components within the Acfer 094 matrix are similarly surrounded by Fe-rich grains more likely supports a solar nebula origin, at least for the surrounding grains. Still, the origin of Fe contents in presolar silicates in this study remains ambiguous.

We can compare presolar silicates in this study with GEMS grains found in IDPs, which might represent a best match to "dirty/astronomical" silicates described above, but whose origins are still poorly constrained (BRADLEY, 1994; BRADLEY et al., 1999). The majority of GEMS grains have solar isotopic compositions, with only a few of them having a proven circumstellar origin as evidenced from isotopic anomalies (MESSENGER et al., 2003). On the other hand, the solar isotopic composition does not necessarily exclude an interstellar origin (BRADLEY and DAI, 2004; KELLER and MESSENGER, 2008). Morphologies of grains in this study are similar to GEMS grains regarding their polyaggregate- or fractal-like geometry in SEM imaging, but TEM analysis revealed that Fe-rich inclusions here are in general smaller or not present at all (Sec. 4.3.5). However, from SEM imaging alone a clear distinction is not possible, but whereas GEMS grains from IDPs are well-documented by TEM, because they are detected in already ultramicrotomed slices, only a small fraction of all presolar silicates from meteorites have been analyzed by TEM.

There is no clear correlation between isotopic compositions and morphologies of Group I/II grains. Group IV grains, however, are generally smaller and display predominantly a polyaggregate-like morphology, which has been linked to their proposed SNII origin (MESSENGER et al., 2005; FLOSS et al., 2008; VOLLMER et al., 2008). Group III grains, the rarest population of analyzed grains in this study, are even smaller, such that they could not be relocated and documented by SEM. This could be an additional hint that those grains indeed come from SNeII (NITTLER, 2007).

Finally, highly ^{17}O-enriched grains are smaller and harder to locate within the matrix than less anomalous grains (Fig. 4.4). Those grains might originate in binary systems (NITTLER et al., 2008; VOLLMER et al., 2008), but it is not clear why grains that form around red giant stars in binary systems should be smaller than grains from single stars. It is difficult to form such grains directly in nova ejecta, as predicted isotopic compositions are more extreme by at least one order of magnitude (JOSÉ and HERNANZ, 2007). However, if the grains formed in such explosive ejecta, then similar assumptions as for grain formation in SNeII might be valid, leading to generally smaller grain dimensions as well. This is highly speculative, of course, as the condensation efficiency in novae is not well constrained. To date, there is only one TEM study of a

grain of this type (VOLLMER et al., 2007a), which indeed revealed a highly unusual crystal structure not compatible with standard condensation models indicating unusual formation conditions. Future investigations on microstructures and additional isotope data of such highly ^{17}O enriched grains will further enlighten their origins.
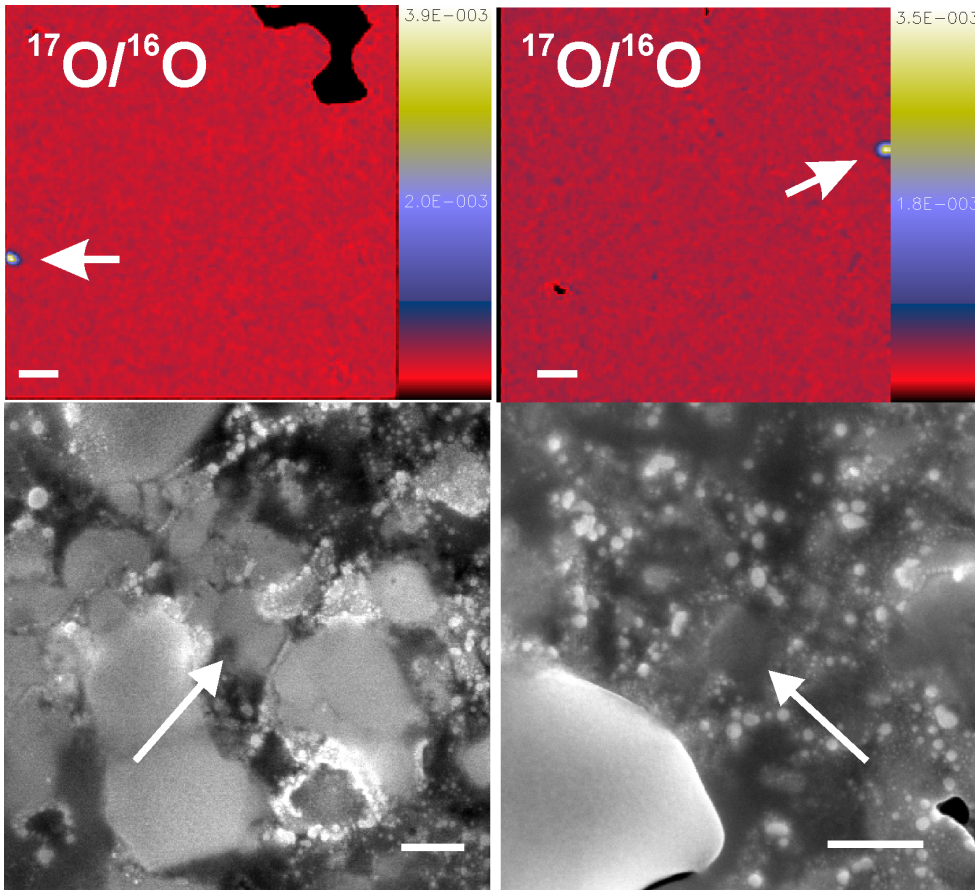

Figure 4. 4 Morphologies of extreme Group I grains NanoSIMS $^{17}O/^{16}O$ ratio images (upper panels) and HR-SEM documentation (lower panels) of the extreme Group I grains 13_13 (left panels) and 13_16 (right panels). Scale bar represents 1 μm in the NanoSIMS ratio images and 200 nm in the SEM images.

4.3.3 Distribution of stardust grains within the matrix of Acfer 094

The first analyses on presolar grains like SiC were performed on chemically separated meteorite samples (BERNATOWICZ et al., 1987), where the original petrographic context between the presolar grains and the surrounding solar system material could not be investigated. ALEXANDER et al. (1990) already showed that the in-situ characterization of presolar phases (SiC grains in that case) provides important constraints on original morphologies and surrounding matrix which are otherwise lost by the harsh chemical or physical treatment used for the production of grain separates. The investigation of the relationship between the presolar material and the more or less altered matrix is then possible. It has also been unclear to what extent the initial amount of presolar material was higher than what we find in meteorites and IDPs and how it was mixed and homogenized to different degrees during solar system evolution (HUSS and LEWIS, 1995). ALEXANDER (2005) suggested that the matrix in primitive meteorites represents a common presolar reservoir, that has experienced minor to moderate alteration in the solar nebula. In contrast, WASSON (2008) proposed that matrix material may have evolved during chondrule-forming processes, during which all initially present presolar grains were destroyed, and that all presolar grains we

find today were introduced at a very late stage into the solar nebula. Examination of the genetic connections between solar and presolar matter are crucial to investigate these problems.

Just recently the first in-situ SiC grains were identified within IDPs (STADERMANN et al., 2006b) and AMMs (YADA et al., 2008). In carbonaceous chondrites they were characterized in-situ shortly after their discovery (ALEXANDER et al., 1990), but the majority of presolar SiCs are from grain separates. To date, the relationship between presolar silicates and the surrounding solar system matrix or distinct grain associations has not been investigated. Only in IDPs, it is found that some presolar silicates are embedded in ^{15}N-rich molecular cloud material, which could have shielded them from intensive ISM processing (MESSENGER et al., 2005). In the following, we will briefly summarize and discuss our observations on the distribution of the stardust population in Acfer 094.

Most of the grains are randomly distributed in the matrix, and there is no trend or gradient observed between matrix and matrix components such as chondrules and CAIs. Some matrix areas seem to be more enriched with presolar material than others, and the observed abundance varies between < 50 ppm and > 200 ppm in typical 100x100 μm^2 areas, but the overall trend on a mm scale is an even distribution.

We do observe in 17 cases out of 705 fields analyzed a clustering of presolar grains within the matrix on a very small scale, i.e., 2 or more grains within the same analyzed 10x10 μm^2 field. In most cases, the clustered grains are from the same isotope group, which is mostly Group I (26_10, Fig. 4.5). However, mixed clustering is observed as well, i.e., two Group IV grains with one Group I grain (22_10, Fig. 4.5).
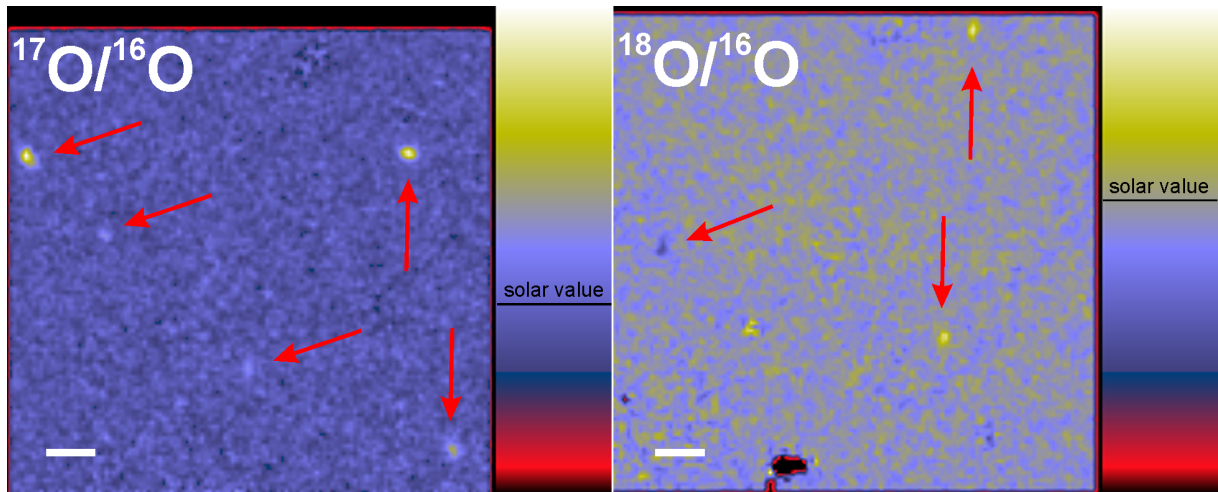

Figure 4. 5 Clustering of presolar silicate and oxide grains

NanoSIMS [17]O/^{16}O and, respectively, ^{18}O/^{16}O ratio images of presolar silicates in fields 26_10 (left) and 22_10 (right). In most such cases the clustered grains are from the same isotope group, but in three cases the grains are from different groups (e.g., Group I and IV in field 22_10). The red and black rim marks the edge of the analyzed area, some other anomalous spots are either artefacts due to morphology effects or do not fulfil the 4σ criterion (this also applies to all following figures). Scale bar represents 1 μm.

To explore the statistical significance of this observation, we calculated the probabilities resulting from a binominal distribution of finding two or more grains in the same analyzed field. We divide the 10x10 μm^2 sized field into squares of 300 nm size (resulting in $(10/0.3)^2$ squares), which is compatible with the typical

diameter of presolar silicate and oxide grains, and assume a probability of 0.000181 of encountering a presolar silicate (142 grains of 0.09 μm^2 size in 70500 μm^2). The probability of finding two presolar silicates in one field is then 1.6 %, i.e., in ~11 of all 705 analyzed fields. We have found 14 of these fields with two grains, which is therefore in reasonable good agreement with the expectations from statistics. We should encounter 0.8 fields with three grains, which compares well with two such fields in our study. Thus, this must be considered as being compatible with the expectations from statistics. The detection of one field with 5 grains (Fig. 4.5), however, is statistically unexpected, as this should happen with a probability of only 0.0002 %. This clustering is thus of high statistical significance. The calculated matrix-normalized abundance of stardust in this highly enriched area is 0.35%. Future improved statistics should shed further light onto this issue.

In six of the observed clustering fields, we see a presolar silicate together with a presolar Al-rich oxide. We also explored the statistical significance of this effect. The coincidence of a presolar silicate with an oxide in the same field should occur in ~3 cases of all 705 analyzed fields. Our finding of 6 cases is about twice as high as expected from statistics. But since it is based on a very restricted sample set of only 20 Al-rich grains a final conclusion is hard to draw. More data are needed to fully explore this effect.

Clustered presolar grains as described above have also been observed in CR chondrites (FLOSS and STADERMANN, 2007) and IDPs (NGUYEN et al., 2007). Also, a recent investigation on the distribution of presolar silicates in AMMs revealed that most of the analyzed grains appeared in a very restricted area, in fact, 11 grains were found in a single 20 x 20 μm^2 area of the AMM (YADA et al., 2008). We can only speculate about the reasons for this clustering. It has been proposed, for instance, that Group IV grains with a likely SN origin might have been injected into the solar nebula in a single event, and that there was not enough time for effective mixing of these phases (NITTLER, 2007; YADA et al., 2008). However, this would only explain the predominance of Group IV, and therefore most likely SN grains, in certain primitive materials, which is indeed observed in AMMs and IDPs (YADA et al., 2008). It does not explain the fact, that we see grains with diverse origins (Group I and Group IV) within a single square of only 10x10 μm^2 size. This could imply that the distribution of presolar materials in the solar nebula was extremely heterogeneous on a very fine scale.

Another, more speculative explanation could be that grains were disrupted from former larger particles shortly before incorporation into the parent body. Of course, this only works for clustered grains with similar isotopic compositions, whose measured differences are then the result of different degrees of dilution (induced by the measurement technique) and homogenization. The discovery of 5 grains in a single 10 x 10 μm^2 field may be explained in this way as their isotopic signatures are similar (Tab. 4.1). In other cases, the isotopic as well as the chemical compositions are similar (31_09), which would further support such a hypothesis. Also, the coincidence of Al-rich oxides together with silicates within about 1/3 of the clustering fields could be explained if these grains represent fragmented particles of former complex grains consisting of refractory oxides and silicates. Those complex grains are also observed intact or slightly fragmented (Sec. 4.3.6). It is possible that both processes played a role in creating the clustered grains.

4.3.4 Abundances of silicate and oxide stardust

The 142 presolar silicate grains in 705 analyzed 10x10 μm² sized fields represent an area of 11.49 μm² giving a matrix-normalized abundance of 163 ± 14 ppm of silicate stardust in Acfer 094. Additionally, 23 Al-rich presolar oxide grains were found and also documented by SEM (including three grains attached to presolar silicates), resulting in an abundance of 26 ± 6 ppm. Grain sizes (maximum widths and lengths) were mainly determined from the HR-SEM images. Only in cases where the grain had already been sputtered away and/or could not be relocated, were the grains´ sizes determined from the NanoSIMS ion images. This occurred for 22 grains, and in these cases the estimated grain sizes are usually larger than the real sizes due to overlap of the Gaussian shaped primary ion beam with surrounding isotopically normal material. Grain areas were calculated as ellipsoids, but a lot of grains exhibit irregular morphologies (Sec. 4.3.2), making a precise measurement difficult. The arithmetic average diameter of all presolar silicates is 307 ± 8 nm, if we re-calculate their cross-sectional areas as circles, those of the Al-rich oxides 308 ± 19 nm, including Al-rich subgrains from three complex grains (Fig. 4.6). The median size of both presolar oxides and silicates is 300 nm. This is different from what is found by N07, where presolar oxides are on average smaller.
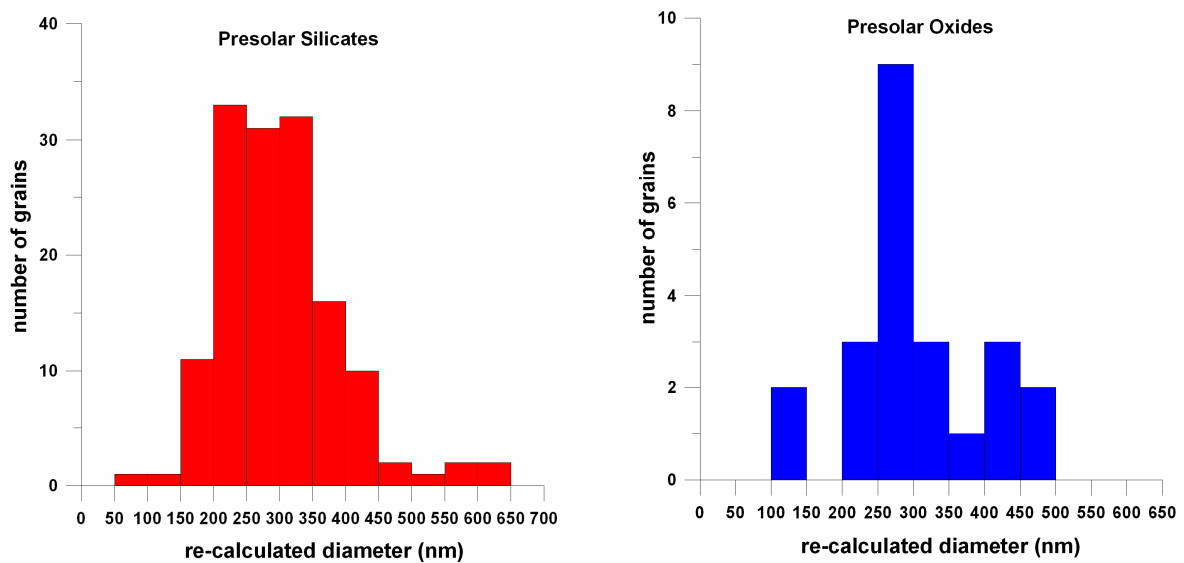
Figure 4. 6 Size distribution of presolar silicates and Al-rich oxides in Acfer 094
The approximate Gaussian distribution is not symmetric, because the smallest grains (< ~150 nm) are not efficiently detected by the NanoSIMS. The re-calculated diameter refers to the diameter of a sphere with the same cross-sectional area as the irregular or ellipsoidal grain.

Determinations of the absolute area fraction of stardust in a fine-grained matrix are hampered by unsystematic uncertainties, which are discussed by N07. These authors calculate a detection efficiency for presolar grains, based on the fact that the smallest grains (< ~150 nm), unless they exhibit very large anomalies, can not be reliably detected in the NanoSIMS, because moderate anomalies are masked by surrounding solar system material. N07 estimated that the determined presolar silicate abundance would

increase by a factor of ~4 if this detection efficiency is taken into account. Reported results here are not, however, corrected for this detection efficiency, and we compare our results only with uncorrected values from other NanoSIMS searches. One uncertainty is the precise measurement of the grains` cross sectional dimensions, because the boundary between a grain of interest and the surrounding matrix is often equivocal, especially with the majority of grains being irregular in shape. We assume that this uncertainty gets less important with increasing grain numbers, because over- and under-measuring the grains´ dimensions should counterbalance itself. We also have to bear in mind, that grains are not perfect ellipsoids, but might be closer to a rectangle, adding another source of unsystematic uncertainty. Our reported error based on counting statistics is therefore only a lower limit to the true uncertainty.

We can compare our matrix-normalized abundance of 163 ± 14 ppm for Acfer 094 with silicate stardust data from the literature (Fig. 4.7).
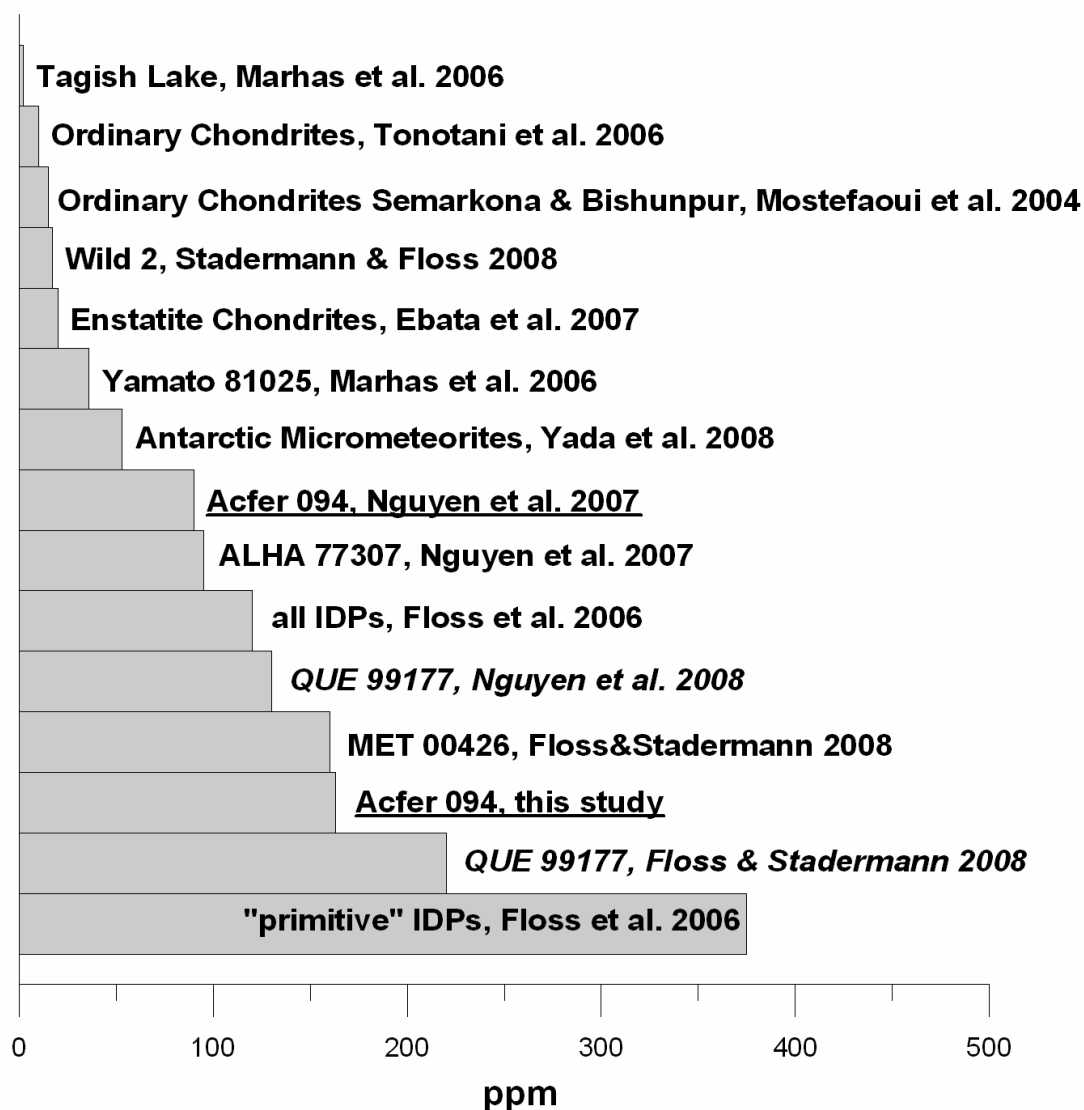
Figure 4. 7 Comparison of presolar silicate abundances for different primitive solar system materials

All abundances are determined by NanoSIMS ion imaging surveys and matrix-normalized (except for the Wild 2 sample, which refers to the bulk material) and not corrected for detection efficiency. Note the differing abundances for QUE 99177 and Acfer 094 in different investigations.

Our value is higher than the one reported by N07 for the same meteorite (90 ± 35 ppm, uncorrected), whereas our presolar oxide abundance is lower (26 ± 6 ppm, compared to 55 ± 20 ppm in N07). However, the values are compatible within 2σ errors. The discrepancy might partly be explained by the fact that presolar grain mineralogies were mostly determined from the grains´ $^{24}Mg^{16}O^-/^{16}O^-$ ratios in N07, whereas a major classification part in this work was done by AES. It is therefore possible that some grains in the work of N07 classified as Al-rich grains might be actually silicate grains, which would increase the silicate and decrease the oxide abundance. Indeed, Auger analyses on grains in N07 indicated that the primary NanoSIMS identification of mineralogies is often misleading. Initial mineralogy classifications by NanoSIMS are complicated by the fact that some silicates contain substantial amounts of Al, either as subgrains or as non-stoichiometric components, deduced from Auger analyses (Sec. 4.3.6). Furthermore, Mg contents of presolar grains are also sometimes non-stoichiometric (Sec. 4.3.6), which makes unambiguous determinations based on $^{24}Mg^{16}O^-$ ion images difficult. Clearly, more accurate mineralogy determinations by AES and TEM are needed to examine this issue. For the purpose of discussion we assume that presolar silicate and oxide abundance determinations by N07 and in this work are the same within errors, but that silicates are ~6 times more abundant than oxides. This is, however, different from the results in N07, which deduce a similar abundance of oxides and silicates based on efficiency corrected values.

Acfer 094 therefore contains among the highest amounts of presolar silicate grains in meteorites reported so far, together with the CR chondrites MET 00426 (160 ppm) and QUE 99177 (130 ppm or 220 ppm) (FLOSS and STADERMANN 2008; NGUYEN et al., 2008a). Lower reported abundances for ordinary chondrites (10 – 20 ppm) (MOSTEFAOUI et al., 2004; TONOTANI et al., 2006), carbonaceous chondrites (2 ppm and 36 ppm) (MARHAS et al., 2006) and enstatite chondrites (20 ppm) (EBATA et al., 2007) most likely result from higher degrees of thermal metamorphism and aqueous alteration, as silicates are easily destroyed by these secondary processes. Destruction processes may have occurred either on the meteorite parent body or as the result of pre-accretionary processing in the solar nebula. This does not exclude an initially largely uniform distribution of presolar silicate and oxide grains throughout the nascent solar nebula, and that any differences we see now are due to different stages of alteration during solar system formation (HUSS and LEWIS, 1995). However, the heterogeneous distribution of presolar grains in some primitive solar system materials provides evidence of some heterogeneity among the building blocks from which the meteorite parent bodies formed (Sec. 4.3.3).

More recently, further discussion on presolar silicate and oxide grain survival was initiated by findings in the CR2 chondrites QUE 99177 and MET 00426 (FLOSS and STADERMANN, 2008; NGUYEN et al., 2008a), which have suffered from very little aqueous, but nearly no thermal alteration. It is up to now difficult to directly compare these CR chondrites with Acfer 094, as statistics are still developing (i.e., ~70 O-rich presolar grains in QUE 99177 compared to over 200 for Acfer 094), but it indicates that presolar silicates can indeed be found in meteorites of petrologic type 2. More strongly aqueously altered CR chondrites, however, also lack presolar silicates. Acfer 094 has suffered from terrestrial alteration as well

(BLAND et al., 2008), whose influence on presolar grain abundances can not be inferred. Apparently, we still find a large fraction of presolar grains despite this terrestrial weathering.

Another point of discussion introduced by these new findings is the relative proportion between presolar silicate and oxide grains. Although we have to be cautious in preliminary mineralogy determinations, as discussed above, there seems to be a difference between the CR chondrites investigated by FLOSS and STADERMANN (2008) and Acfer 094. Even if we assume that some of our Al-rich oxides are in fact silicates and considering a high uncertainty in abundance determinations, silicate/oxide ratios in QUE 99177 and MET 00426 are about three times as high as in Acfer 094 (> 17 compared to ~6 in this work). Mineralogy determinations by FLOSS and STADERMANN (2008) and in this work are reliable as they have been acquired mostly by Auger analyses on the grains. There are several possible scenarios which could explain this observation (see also FLOSS and STADERMANN, 2008):

First, we can consider a heterogeneous distribution of presolar oxides and silicates in the solar nebula, and differences in abundances in different meteorite formation regions reflect this distribution. The heterogeneity would then be observed on a very small scale, i.e., single meteorites. Within the meteorite itself, presolar grains are uniformly distributed in the matrix, although some clustering effects are found in this work as well as by other investigators (Sec. 4.3.3). Still, this only explains heterogeneous distributions of presolar grains as a whole population, but not between different types of grains. Only a few in-situ searches have been performed that can directly compare the distribution of carbonaceous and O-rich grains (NGUYEN et al., 2006), but no obvious trend was observed there. Therefore, an intrinsic heterogeneity of different presolar grain classes within the solar system, as mentioned by FLOSS and STADERMANN (2008), appears improbable. The only exception to this could be grains of possible SN origin, many of which may have been introduced into the solar nebula in a single event (NITTLER, 2007). A high abundance of SN grains found in AMMs (YADA et al., 2008) could be a first hint to this scenario. Otherwise, grains from the other O isotope groups seem to be homogeneously distributed, but the data set is still developing. Second, some yet unknown mechanism has preferentially destroyed oxide grains over silicate grains in QUE 99177 and MET 00426, as CR2 chondrites have suffered from aqueous alteration and display a high volume fraction of hydrated minerals (FLOSS and STADERMANN 2008). Although the influence of parent body or pre-accretionary processing on oxide grains is not well constrained, such a selective destruction or hydration process for oxides in favour of silicates is hard to imagine. Refractory oxide grains are generally more resistant to thermal and aqueous metamorphism than silicates. Third, if silicate/oxide ratios in unaltered CR chondrites reflect true solar nebula proportions, then a substantial amount of presolar silicates must have been destroyed in Acfer 094 (and also in ALHA 77307). This explanation is unsatisfying as well, as Acfer 094 is generally believed to represent one of the least altered meteorites despite some terrestrial impregnation. It is not clear why aqueous alteration should affect silicate abundances in Acfer 094 and the analyzed CR chondrites differently. Clearly, more meteorites have to be analyzed to put further constraint on this issue. A recent re-examination of the presolar silicate and oxide abundance in QUE 99177 (NGUYEN et al., 2008a) revealed a lower silicate to oxide ratio (130 ppm to 40 ppm, i.e., more similar to the value described here), but this data set again

suffers from limitations in mineralogy identifications described above. It is therefore possible that a ratio around 5 represents true nebular proportions. It would be interesting to compare this ratio with values in circumstellar environments, but identification of Al-rich phases by IR spectroscopy is still problematic (POSCH et al., 2007), because those bands are masked by strong silicate features, unless those are highly depleted in stars of unusual chemistry (MALDONI et al., 2008).

The highest presolar silicate abundance has been reported so far for a sub-group of IDPs with ^{15}N enrichments (375 ppm) (FLOSS et al., 2006). These "isotopically primitive" IDPs are characterized by similar components as the matrix of unaltered CR chondrites, although a clear connection between this IDP population and the CR chondrite group is still speculative. IDPs, especially so-called anhydrous cluster IDPs, are generally believed to be associated with material from comets (BRADLEY, 2003), although isotope analyses on cometary matter from the STARDUST mission (MCKEEGAN et al., 2006) revealed a surprisingly low abundance of presolar grains therein (10 – 20 ppm) (STADERMANN and FLOSS, 2008). It is therefore not clear, whether the samples from comet Wild 2 and IDPs share the same origins (ISHII et al., 2008). The abundance within all IDPs, including those samples without distinct N anomalies, is 120 ppm (FLOSS et al., 2006), which is within the range reported for Acfer 094. The search for presolar material in Antarctic micrometeorites (YADA et al., 2008) yielded a presolar silicate abundance of ~50 ppm, which is significantly lower, even within errors, than the Acfer 094 value. Generally, AMMs predominantly show mineralogical and chemical affinities to carbonaceous chondrites and much less to IDPs, which could explain their lower presolar silicate abundance compared to IDPs. Still, they are more severely altered than the primitive chondrites Acfer 094 or ALHA 77307. Acfer 094, ALHA 77307 and the CR chondrites discussed above therefore show stronger affinities to anhydrous cluster IDPs based on presolar silicate and oxide grain abundances. Future comparative studies are needed to examine the relationship between these different primitive solar system materials.

4.3.5 Transmission electron microscopy of silicate stardust

4.3.5.1 Single grains

A total number of 15 grains have been prepared by the FIB technique, of which eight could be successfully analyzed by TEM (Tab. 4.3). One more grain ("1_07") has already been described in VOLLMER et al. (2007a). Four of the six lost grains have been either thinned away during the FIB process due to strong charging effects and a resulting misaligned ion beam or broke off with the FIB section from the Cu grid. Two more grains could not be relocated in the TEM after preparation (7_04, 9_15), because they probably had been sputtered away already after the NanoSIMS measurement. This demonstrates the extreme difficulty in preparing FIB sections of grains in that size range, because the two-dimensional information from the SEM might not be representative of the three-dimensional depth extension of the grain of interest. Furthermore, it is technically challenging to align the FIB slice to such accuracy, that the ~100 – 150 nm thin section really encloses the ~300 nm sized grain. There, it is always possible to miss the grain during final thinning. The efficiency of this process is enhanced by a new marking procedure developed by HOLZAPFEL et al. (2008) for the purpose of this study.

Table 4. 3 FIB/TEM results of presolar silicates in this study

Grain	size (nm) SEM	Auger	TEM BF	TEM EDX (at.%)	TEM SAED
1_07	430x230	–	See Sec. 5, Vollmer et al. 2007a		
4_11	370x230	–	Fe minerals (5 – 20 nm) dispersed (along cracks?) in a homogeneous glass, grain clearly separated from surrounding matrix, no zoning or relict grains, different morphology and composition than GEMS	**Mg/Si** 0.22 – 0.47 (mean 0.42) **Al, Ca, S** < 1 **Fe/Si** 0.02 – 0.1	Amorphous
7_04*	1000x600	–	*Not successful (grain not relocated)*		
8_10	810x490	–	At least 10 ~50 nm large particles, total length ~800 nm, Fe minerals at grain boundaries, clearly separated from surrounding matrix, brighter contrast due to higher Si content or amorphous condition	**Mg/Si** 0.52 – 1.74 **Al** 0.2 – 1.2 **Ca** 0.4 – 4.4 **S** < 1 **Fe/Si** 0.12 – 1.49	Amorphous
9_15	300x270	–	*Not successful (grain not relocated)*		
14_11	300x320	Mg>Fe, Ca	*Not successful (FIB section lost)*		
14_2_3a*	470x340	Si, Ca, Al, low (Mg+Fe)	Homogeneous glass with abundant Fe metal and sulfide grains (~50 nm), 300 x 300 nm, GEMS	**Mg/Si** 0.54 **Fe/Si** 0.88 – 0.97 **S** 2.6 – 3.8 **Al, Ca** ~ 1	Amorphous, Fe minerals crystalline
15_2_9	650x300	–	*Not successful (FIB section lost)*		
18_08	480x420	–	Homogeneous, amorphous grain, size 500x200 nm, relict crystal in center, size 100x50 nm (pseudo-euhedral), fast amorphization under electron irradiation	<u>Center:</u> **Mg/Si** 1.13 – 1.34 **Fe/Si** 0.31 – 0.43 <u>Rim:</u> **Mg/Si** 0.36 – 0.46 **Fe/Si** 0.82 – 0.91 **S** 0.4 – 2.8 **Al** 0.4 – 2.4 **Ca** 0.4 – 3.9	Center crystalline, largest d=3.5 Å (lattice fringes) and d=5.9 Å (SAED), possibly olivine ($d_{120\ or\ 111}$ and d_{001}), rim amorphous
21_06	570x360	Mg>Fe	Cluster of several particles, 250x100 nm, clearly separated from surrounding matrix (brighter contrast), no Fe minerals	**Mg/Si** 0.72 – 1.52 **Fe/Si** 0.03 – 0.17 **Al, Ca, S** < 1	Amorphous
22_05	530x480	Mg>Fe	*Not successful (FIB section lost)*		
22_09*	670x480	complex	*Not successful (FIB section lost)*		
25_20	350x310	Mg>Fe	Amorphous, 400x100 nm, brighter contrast than surrounding matrix, homogeneous, holes from SEM point measurements	**Mg/Si** 0.69 – 1.19 **Fe/Si** 0.02 – 0.09 **Al, Ca, S** < 0.5	Weakly crystalline, probably enstatite
31_13	670x230	Mg# 0.64 (Mg+Fe)/Si 1.2	Section relatively thick, grain has amorphized „canyon" in the center, size 200 x 200 nm, sulfide grain attached on the right side, crystalline region on the left side	<u>In crystalline region:</u> **Mg/Si** 1.75 – 1.78 **Fe/Si** 0.15 – 0.26 (Mg# 0.9) <u>At central canyon:</u> **Mg/Si** 1.07 – 1.33 **Fe/Si** 0.28 – 0.34	Still partly crystalline on left side, d=5.9 Å, olivine (d_{001})
32_08	400	Mg/Si = 3.4	One small region of the grain crystalline, overall homogeneous appearance, 200 x 200 nm	**Mg/Si** 0.86 – 1.37 **Fe/Si** 0.04 – 0.05 **Mn** up to 1.4	Amorphous, crystalline subarea, high Mn content indicates LIME silicate

* – performed at the NRL in Washington, DC

In the following we will describe and discuss features of single grains in more detail. Grain 4_11 is amorphous, highly Si-enriched (Mg/Si down to 0.22) and stands out of the surrounding matrix (Fig. 4.8).
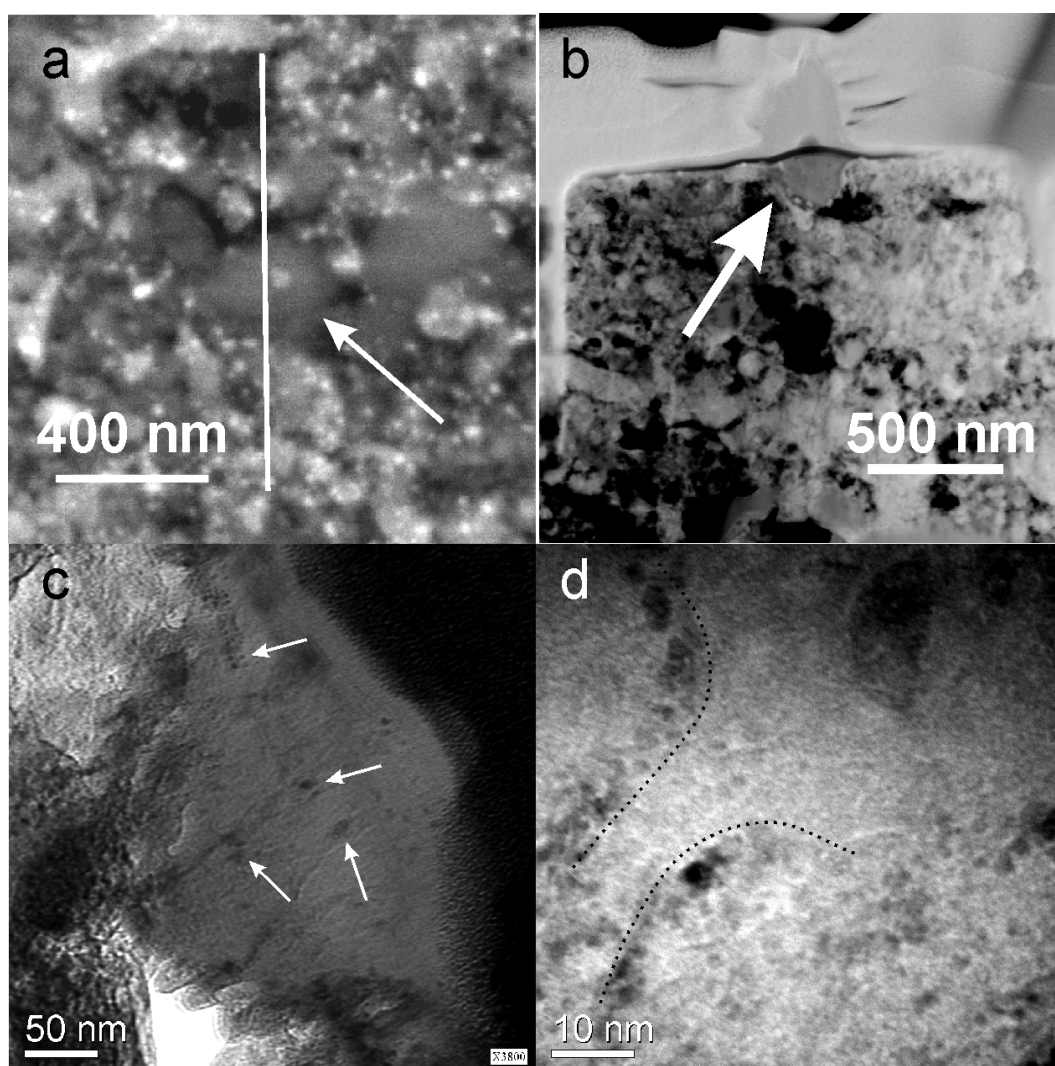

Figure 4. 8 SEM-STEM-TEM images of grain 4_11

a – SEM image with the approximate course of the FIB section, b – STEM image of the final FIB section with the grain of interest underneath the Pt mark, c – Arrows mark locations of Fe minerals in the glassy matrix in the BF-TEM image, d – Fe minerals are not evenly distributed, but occur along lines (marked by the dotted lines).

The glass appears homogeneous in BF imaging mode, but some diffracting Fe minerals (5 – 20 nm in size) are clearly visible. Those crystals are not dispersed homogeneously in grain 4_11, but rather concentrate in discrete subdomains, which seem to be aligned along tiny cracks (Fig. 4.8d). It can not be distinguished whether these Fe particles are a secondary product due to parent body or nebular processing or of interstellar/circumstellar origin. The alignment of Fe minerals does not support a primary circumstellar condensation product, which would lead to an even distribution. Sulfur is not detected at levels > 1 at.% throughout the grain, which indicates that this is not a classical GEMS grain, although Si-normalized contents of Mg and Fe are similarly sub-solar. However, the overall compact appearance of grain 4_11 standing out of the matrix does not resemble the more fragile GEMS, either. Future TEM work on

presolar silicates might reveal, how amorphous glasses like 4_11 with no large Fe minerals and no typical fluffy microstructures are related to the classical GEMS population found in IDPs, and whether an evolutionary sequence exists between these types of grains.

Grain 8_10 consists of a coagulated cluster of at least 10 small (~50 nm) amorphous silicate particles, which form a heterogeneous grain of ~800 nm in diameter (Fig. 4.9).
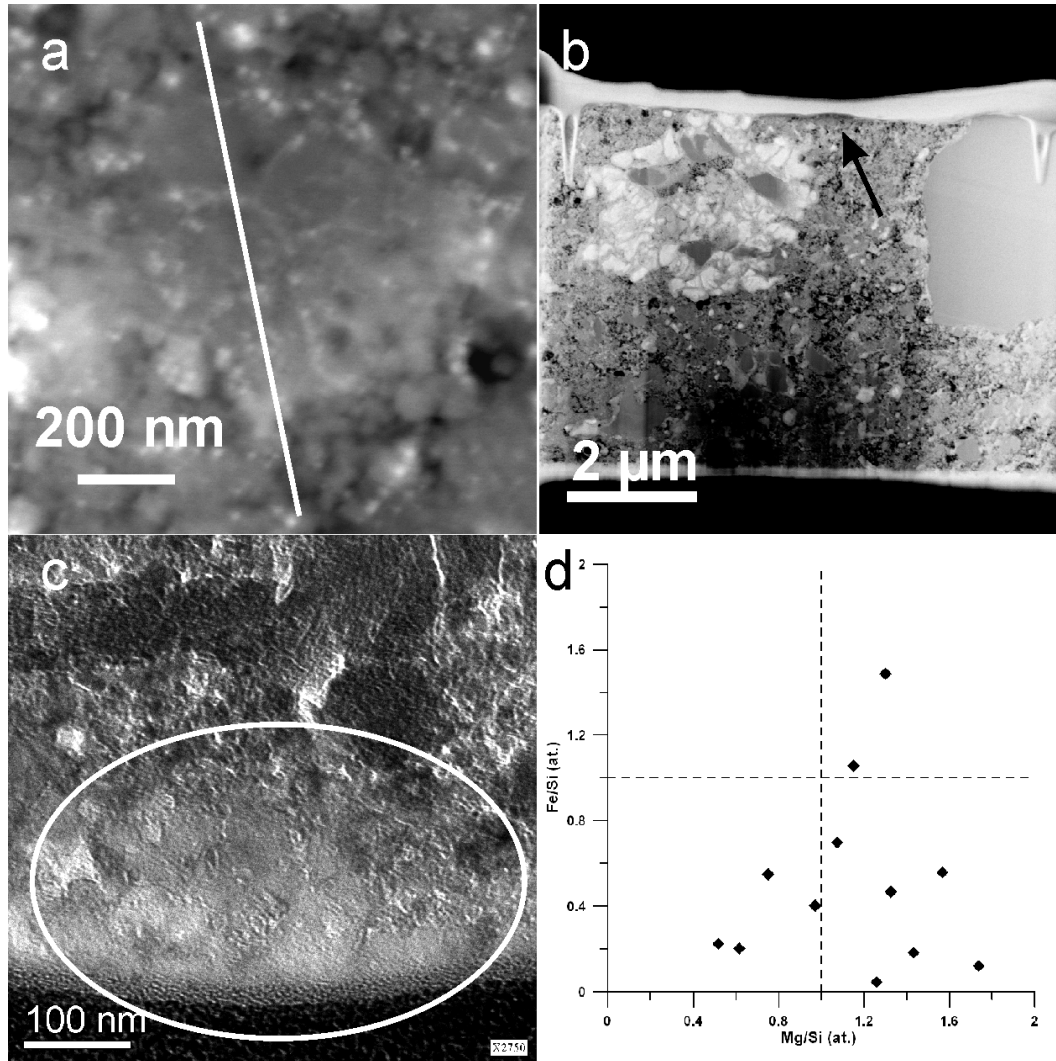
Figure 4. 9 SEM-STEM-TEM images and Mg-Fe-Si compositions of grain 8_10

a – SEM image with the approximate course of the FIB section. The grain can hardly be distinguished from the surrounding matrix, b – STEM image of the final FIB section with the grain of interest marked by the arrow, c – BF-TEM image of grain 8_10 with its brighter contrast compared to the surrounding matrix, d – The extreme elemental scattering throughout the grain. Dashed lines represent chondritic values.

Fe rich particles are present along grain boundaries and might be of secondary, but not circumstellar origin. The grains themselves show a wide compositional range (Mg/Si from 0.52 – 1.74, Fig. 4.9d). This gives support to the view that condensation in the fast cooling winds of AGB stars leads to chemical heterogeneity on a very fine scale, if this compositional spread is of primary origin. This grain could also show that transfer times of presolar silicates are very short, as this fragile aggregate would not have

survived extensive fragmentation processes in the ISM. The appearance of the grain is very similar to GEMS, but sulfur is again < 1 at.% in every analysis. Furthermore, Fe rich minerals are mostly present along grain boundaries, whereas in classical GEMS grains they are dispersed throughout the glassy matrix. This more likely supports a secondary origin of these Fe-rich particles. Therefore, although the aggregate-like structure of grain 8_10 resembles GEMS, its chemical composition is different.

Grain 18_08 consists of a crystalline central grain (~100 nm in size), that partly amorphized during EDX spot measurements, surrounded by an ellipsoidal, amorphous, homogeneous mantle (Fig. 4.10 and 4.11). The largest d-values of the central grain acquired through the measurement of the lattice fringes and one SAED pattern fit to orthorhombic olivine (space group Pbnm). Measured Mg/Si ratios in the central grain do not support this determination as they are too low, but this is most probably due to the small dimensions of the grain.
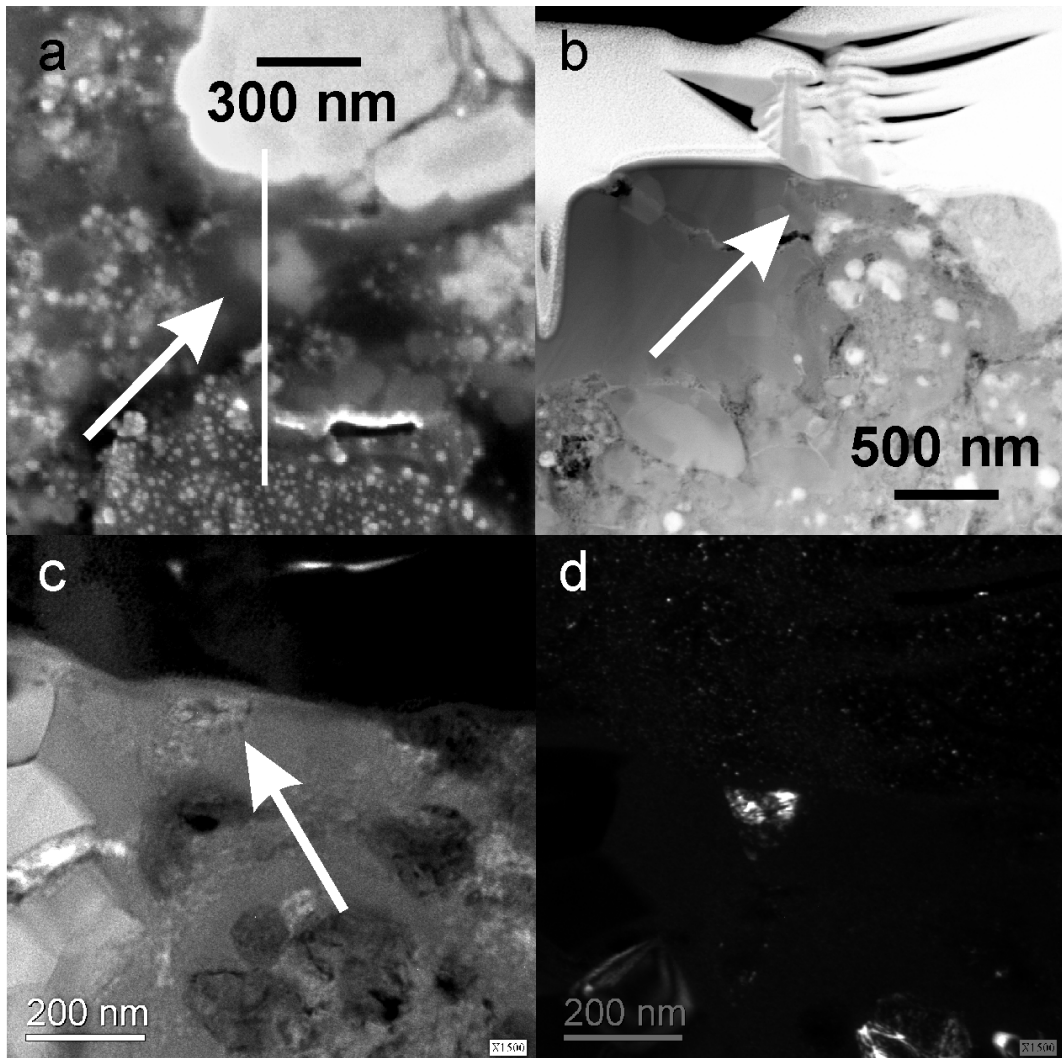
Figure 4. 10 SEM-STEM-TEM images of grain 18_08

a – SEM image with the approximate course of the FIB section, b – STEM image of the final FIB section with the grain of interest marked by the arrow underneath the Pt mark, c – BF-TEM image of grain 18_08 with the crystalline core marked by an arrow, d – DF-TEM image, which clearly demonstrates the crystallinity of the core (partly amorphous already due to EDX measurements).
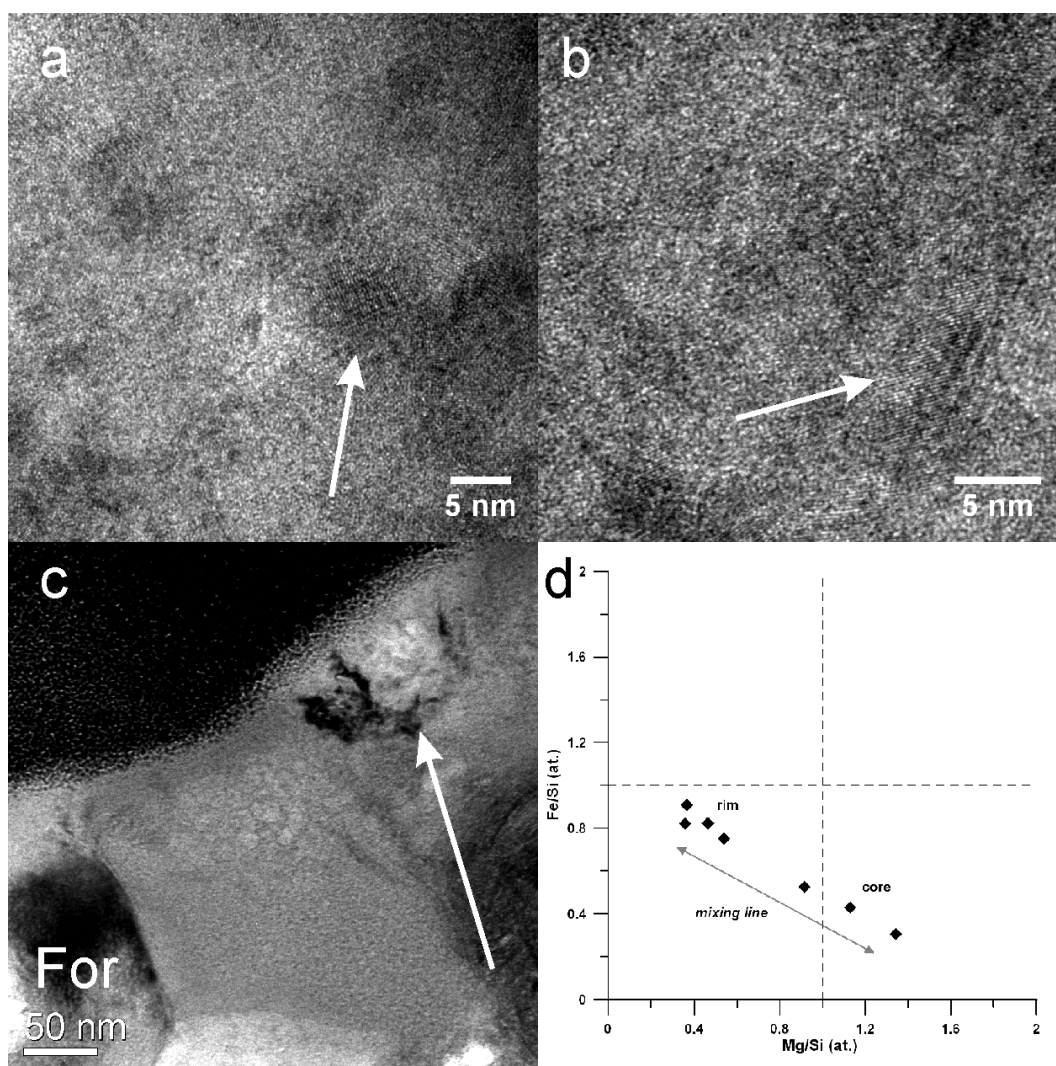
Figure 4. 11 HR-TEM images and Mg-Fe-Si compositions of grain 18_08

a + b – HR-TEM images of the core with crystalline domains still present, c – BF-TEM image with the crystalline core and an adjacent forsterite, d – The evolution of the elemental ratios between the core and the rim indicate a mixing effect. The true composition could be Fe-poor forsterite. Dashed lines are chondritic values.

Contribution from the surrounding and underlying material clearly influences measured abundances, as is also evident from the mixing trend observed in the element plot (Fig. 4.11d). The surrounding amorphous silicate contains less Mg (Mg/Si 0.36 – 0.46) and more Fe (Fe/Si 0.82 – 0.91). Al, Ca and S are present at the 0.4 – 2.4, 0.4 – 3.9 and 0.4 – 2.8 at.% level throughout the grain, respectively, with no difference between the center and the rim.

The outer amorphous region of the grain and the internal crystal display the same ellipsoidal morphological outline, which is a clear indication that these two subareas of grain 18_08 did not form independently, but are genetically connected. There are two main formation possibilities for grain 18_08: First, a formerly completely crystalline grain might have been rendered amorphous in its outer parts due to extensive irradiation sputtering in the ISM. Mg would have been preferentially lost during this process (BRADLEY, 1994). Similar relict grains have been found in irradiated GEMS, which also preserve a morphological and chemical "memory" of the crystal, from which they formed (BRADLEY and DAI,

2004). The second formation mechanism is condensation of the rim onto the crystalline core under low temperature and non-equilibrium conditions. Condensation calculations predict Mg-rich silicates to condense first followed by Fe-rich material at somewhat lower temperatures (e.g., GAIL, 2003). Because the Mg-rich silicates condense above the glass temperature of ~1000 K, they can crystallize in contrast to the Fe-rich silicates condensing at lower temperatures. The Mg-rich silicate might then act as a seed nucleus for the Fe-rich material to accrete onto, which is in accordance to expectations from condensation theory (GAIL, 2003). Those complex grains could also explain the predominance of Fe-rich amorphous silicates in the spectra of evolved stars, because the crystalline silicate fraction might be covered by amorphous mantles. Based on our data we can not definitely exclude one of these possibilities.

Grain 21_06 appears as a cluster of several smaller particles comparable to grain 8_10 and with a similar compositional range although less Fe-rich (Fig. 4.12).
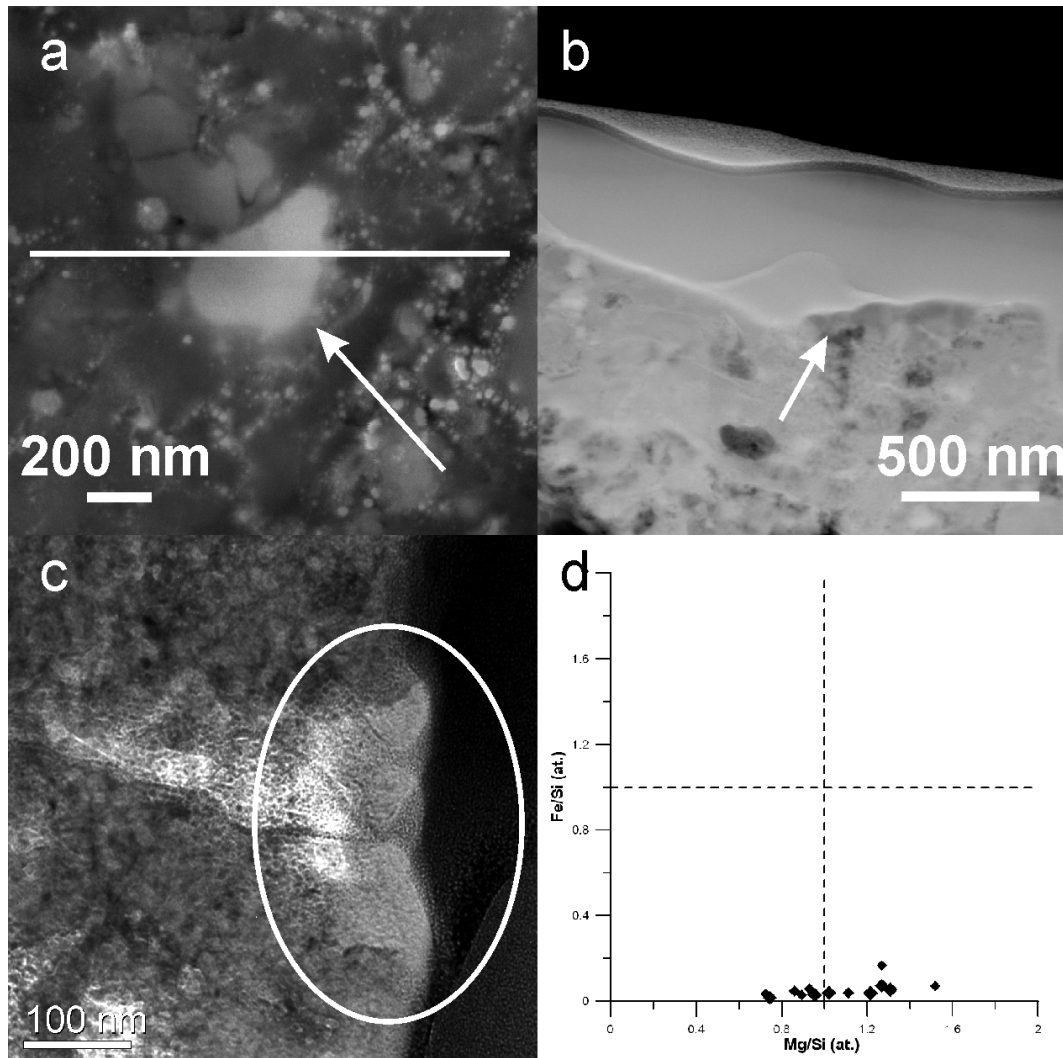
Figure 4. 12 SEM-STEM-TEM images and Mg-Fe-Si compositions of grain 21_06

a – SEM image with the approximate course of the FIB section, b – STEM image of the final FIB section with the grain of interest marked by the arrow underneath the Pt mark (slightly to the right), c – BF-TEM image, d – The scattering of the Mg/Si ratio throughout the grain. Dashed lines are solar values.

Its brighter contrast than the surrounding matrix is probably due to the lower Fe content and/or low crystallinity. Some areas of the grain are crystalline, but it is unclear whether these tiny subareas are still part of the anomalous isotopic signature. Fe contents are very low with the highest Fe/Si ratio at 0.17, Al, Ca and S are similarly below 1 at.%. The composition indicates a non-stoichiometric olivine-like precursor grain, which has been rendered amorphous during interstellar irradiation thereby also explaining the preferential loss of Mg. On the other hand, we do not see a clear trend in Mg values similar to grain 18_08, but rather a heterogeneous Mg distribution. Therefore, the grain could have alternatively condensed under low temperature non-equilibrium conditions from a gas with a low Fe content, such that no complete crystallization and a wide compositional variability was achieved.

Grain 25_20 is located between two large solar system silicates, which are morphologically harder than the presolar grain. Thus, the silicate sits in a tiny valley between these two grains (Fig. 4.13).
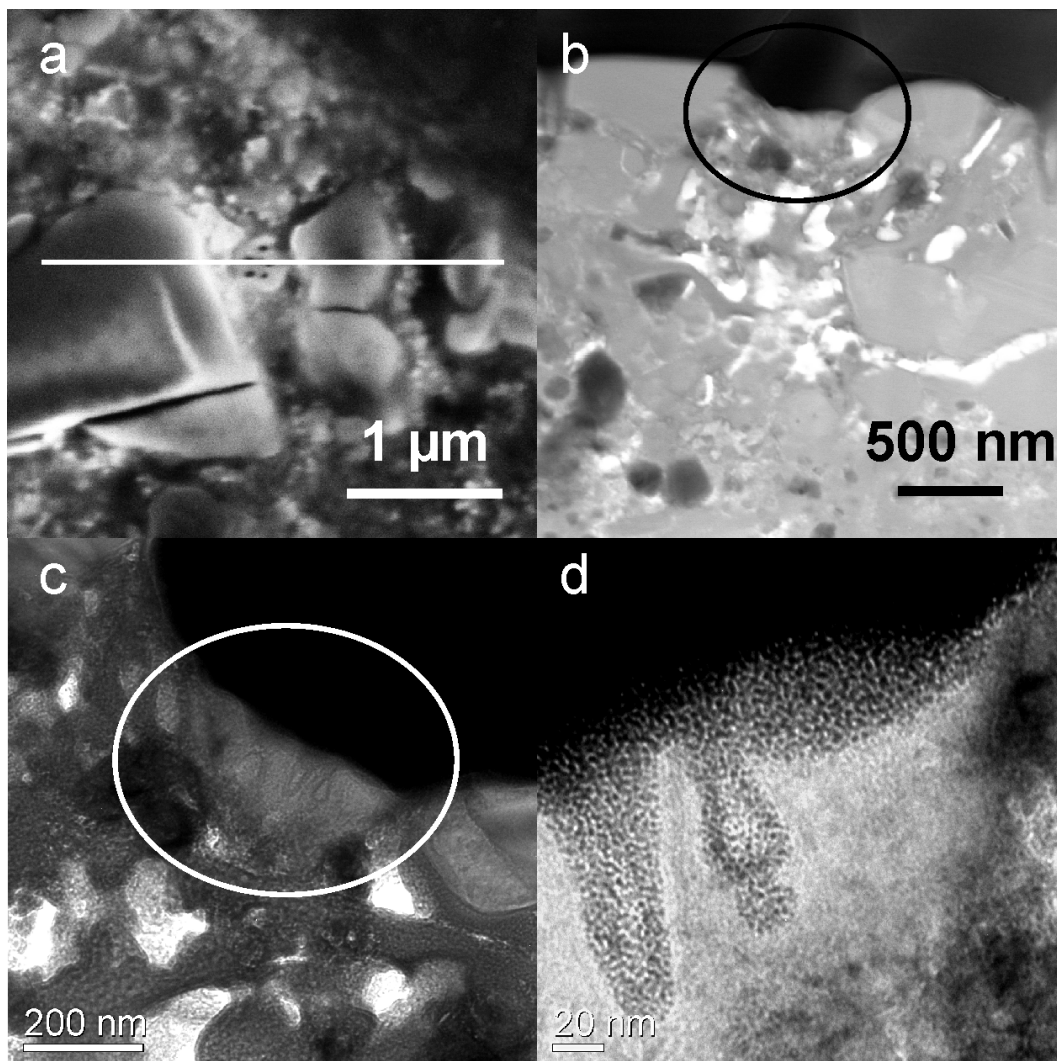
Figure 4. 13 SEM-STEM-TEM images of grain 25_20

a – SEM image with the course of the FIB section. The dark spots are from SEM point measurements, b – STEM image of the FIB section with the grain of interest marked by the circle, c – BF-TEM image: a darker region on the left side of the grain indicates some residual crystallinity, d – BF-TEM image of the SEM-induced holes filled with Pt.

It has again a brighter contrast compared to the surrounding matrix and is mainly amorphous or weakly crystalline. We do not see a strong compositional variability, the grain has a Mg/Si content around 1 (Mg/Si from 0.69 – 1.19) and very low Fe, Al, Ca and S abundances (Fe/Si < 0.1, Al, Ca and S < 0.5). Compositionally it is close to enstatite, but only weakly crystalline as is evident from missing diffraction contrast during tilting. Only in one region, a dark diffraction contrast indicates some residual crystallinity. Tiny holes in the grain are most probably the result of SEM point measurements under high vacuum and high electron current conditions. Particle tracks or similar high energy ion bombardment during interstellar passage should lead to different, i.e., longer and straighter features (e.g., BRADLEY 1994). We therefore conclude that these holes are not a primary feature of the grain of interest, but have been induced during SEM laboratory measurements. The formation mechanism of this grain remains similarly unclear as in the case of grain 21_06: The Fe-poor composition indicates a refractory condensate, but the very low crystallinity points again to formation under temperatures below or around 1000 K, such that the grain remained mainly amorphous. Alternatively, the grain could have been rendered amorphous during interstellar passage and/or SEM point measurements. This is supported by the fact that the region inside the grain that is located away from these holes has a still higher diffraction contrast compared to the material around the holes. Unfortunately, it was not possible to obtain any reliable SAED patterns or HR-TEM images from these regions, but from the EDX point measurements the most probable identification is enstatite.

Grain 14_2_3a has a GEMS-like appearance (Fig. 4.14) containing large Fe-minerals (~50 nm in size) in a glassy matrix with sub-solar Mg/Si (0.54).
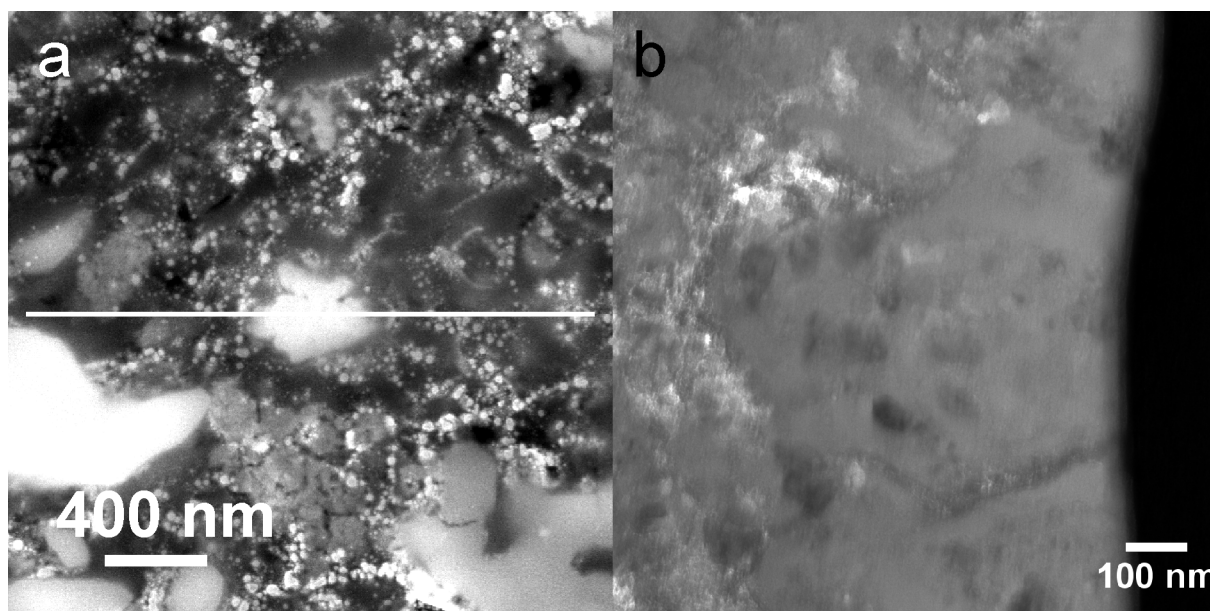

Figure 4. 14 SEM - TEM images of grain 14_2_3a

a – SEM image with the approximate course of the FIB section. The grain appears as a polyaggregate, b – BF-TEM image of grain 14_2_3a with large Fe minerals clearly visible.

The bulk composition is Fe- (Fe/Si 0.88 – 0.97) and also relatively S-rich (2.6 – 3.8 at.%), with Ca, Al contents around 1 at.%. The overall appearance closely resembles GEMS grains from IDPs. However, this grain was not sliced according to the method described by HOLZAPFEL et al. (2008), and therefore we do not have an independent control, such as a marker or holes, to ensure that we did indeed section the intended grain of interest. Unfortunately, it was not possible to verify in a subsequent NanoSIMS analysis, that the grain was included in the FIB section, because it had broken off already after TEM work. Results on this grain should therefore be taken with care.

Grain 31_13 is disrupted by a small canyon in the center (Fig. 4.15b), where Mg contents are lower and Fe contents higher, respectively, compared to the rim (Mg/Si 1.07 – 1.33 and Fe/Si 0.28 – 0.34). The AES and TEM results in this central region are the same within errors.
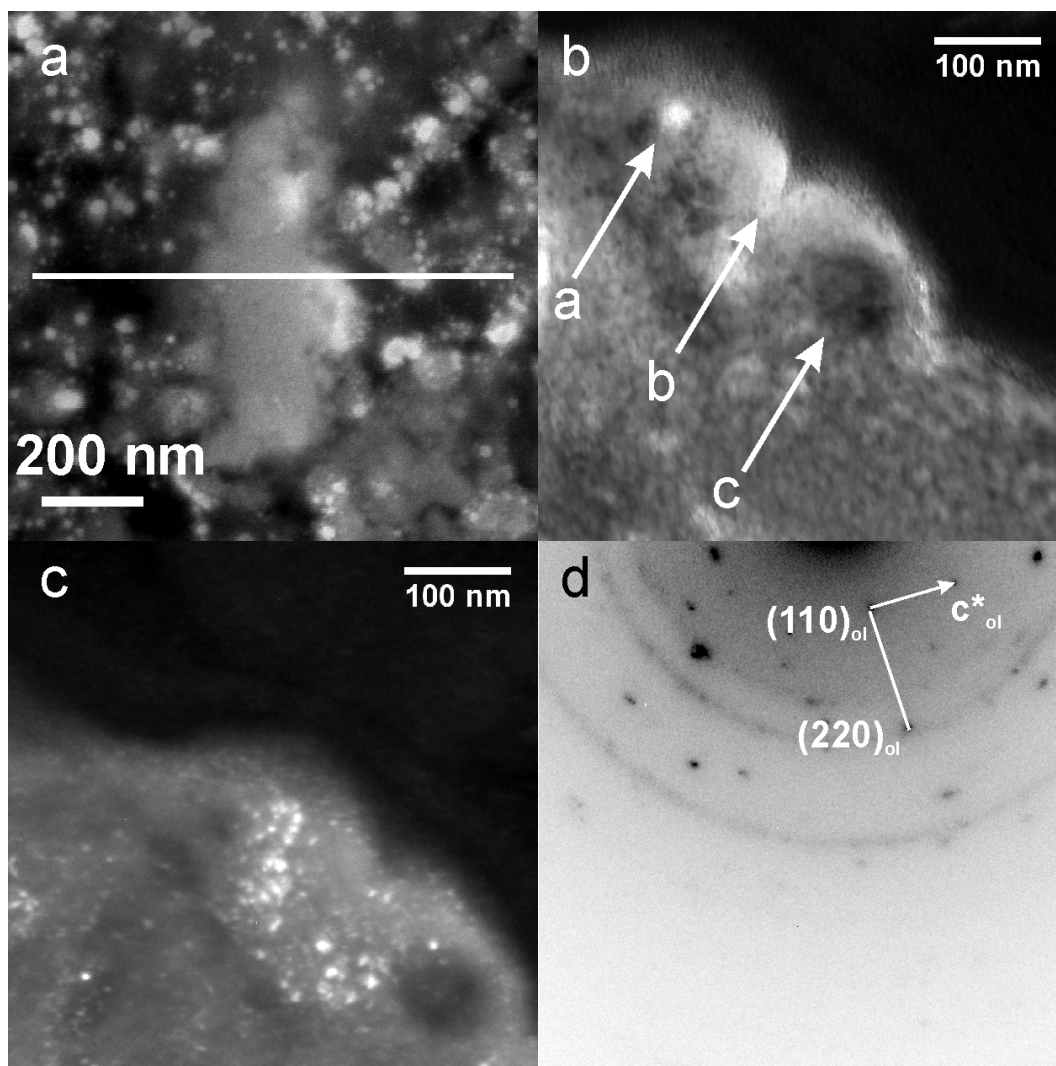
Figure 4. 15 SEM-TEM images and SAED of grain 31_13

a – SEM image with the course of the FIB section, b – BF-TEM image of the grain. (a) marks the spot from the EDX analysis in the crystalline region of the grain, (b) the canyon in the center of the grain, and (c) the position of the Fe sulfide, c – DF-TEM image of the grain, showing the distribution of partly crystalline olivine, d – SAED pattern of the crystalline region with diffraction spots of olivine together with undesired spots from surrounding phases.

On one side of the grain an Fe sulfide is attached to the silicate of interest showing strong diffraction contrast, but we can not decide whether this grain is part of the anomalous feature. On the other side of the canyon, away from the Fe sulfide grain, the grain is partly crystalline, as is also evident from the DF-TEM image. The SAED pattern (with some contribution from surrounding phases) contains major diffraction spots of olivine, which is supported by the EDX point analysis in that region (Mg/Si 1.75 – 1.78 and Fe/Si 0.15 – 0.26). The origin of the canyon remains unclear, but might be due to SEM raster analysis at high electron currents, which has also partly amorphized the formerly completely crystalline olivine and initiated some element evaporation. The amorphous region is then again a laboratory artefact. Formation of the remaining crystalline domains of grain 31_13 can be explained by direct condensation from the gas phase, which leads to forsterite as the first silicate to condense (e.g., GAIL, 2003). However, the Fe content of this grain is a bit too high for a truly refractory forsterite (Mg# 0.9), because condensation calculations and astronomical observations predict almost pure forsterite to form (Mg# ~ 0.99). On the other hand, MESSENGER et al. (2005) have already found an Fe containing olivine from a supernova (Mg# 0.83), explained by a higher abundance of oxidized Fe in the SN gas. In their condensation calculations, the maximum Fe uptake of the condensing olivine leads to a value of Fo_{91} at 950 K, which is similar to what is found here. Another presolar olivine is as well characterized by a similar Fe content (Fo_{90}, KELLER and MESSENGER 2008). Therefore, it remains to be seen whether presolar olivine is more likely characterized by a lower Mg content than theories and observations predict. Further work is necessary to strengthen this hypothesis.

Grain 32_08 finally is characterized by a small crystalline region just below the Pt strap and an otherwise overall weakly crystalline to amorphous contrast in BF imaging mode (Fig. 4.16).
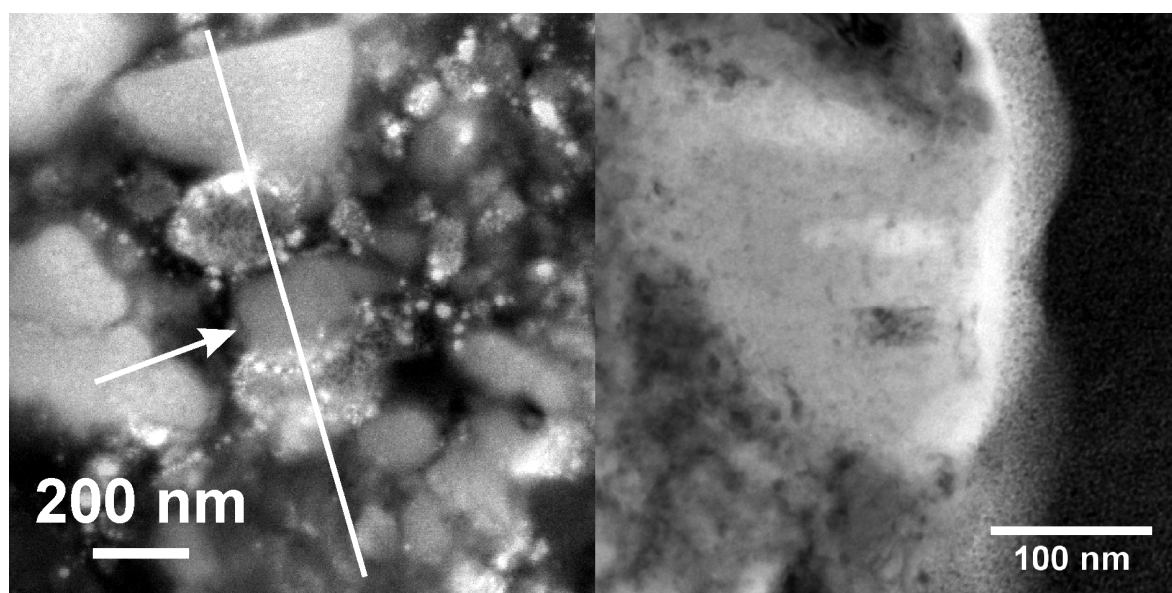

Figure 4. 16 SEM -TEM images of grain 32_08

a – SEM image with the course of the FIB section. The grain is enclosed by heterogeneous Fe-rich material and an Fe sulfide on the northern side, b – BF-TEM image of grain 32_08 with a crystalline subregion and a bright void visible.

Mg/Si ratios range from 0.86 to 1.37 with a very low Fe content (Fe/Si around 0.04), which is different from what has been found by the Auger technique (see Sec. 4.3.6). This could be due to a heterogeneous distribution of Mg inside the grain, which is already evident from the small crystalline subregion inside the grain. Auger analysis only reached about 5 nm deep into the sample, whereas the TEM probed the entire volume of the grain. Another interesting aspect of this grain is the relatively high Mn content (up to 1.4 at.%), which is similar to what has been found in silicates from IDPs and primitive meteorites (KLÖCK et al., 1989). These "low-iron, manganese-enriched"- or "LIME"-silicates are usually explained by condensation from a cooling gas. The detection of a similarly high Mn enrichment in a presolar silicate for the first time, which should represent a relatively undisturbed circumstellar condensate, proves that this process is also applicable in circumstellar environments.

4.3.5.2 Whole population

The majority of presolar silicates analyzed by TEM in this study are Fe-poor (Fe/Si usually < 0.1) and Mg- or Si-rich (Mg/Si between 0.22 and 1.74). This is due to a sampling bias and not representative of the whole silicate stardust population: Fe-poor grains stand out morphologically and are easier to relocate in the SEM (Sec. 4.3.2). They are thus preferred targets for FIB preparation and also easier to analyze in the TEM, because they are clearly separated from the surrounding Fe-rich matrix. Compositions of analyzed grains are mostly non-stoichiometric and variable on a < 50 nm scale (e.g., 8_10, 21_06) and most of them are also amorphous or very weakly crystalline with only two grains being partly crystalline (18_08 and 31_13). Some grains contain trace amounts of Al and Ca in the % range not present in distinct, large subgrains, but as non-stoichiometric components. However, the majority of grains are essentially Ca- and Al-free (< 1 at.%). Most of the grains are ellipsoidal-rounded shaped in agreement with the SEM observations (Sec. 4.3.2) and have a brighter contrast in BF-TEM imaging mode. They seem to be rather sensitive to beam damage: One grain (25_20) has distinct holes and another one (31_13) a large central "canyon", filled with Pt from the FIB preparation. These features are likely the result of electron beam damage during previous SEM point measurements under high vacuum conditions. Fe rich minerals are present as tiny, discrete crystals in two cases (4_11, 14_2_3a), but sulfur is not detected at the > 1 at.% level in all cases except two (grains 14_2_3a and 18_08), indicating a predominance of Fe metal or oxide grains. Therefore, most of the grains, with the exception of grain 14_2_3a and probably 4_11 and 8_10, can not be regarded as classical GEMS grains, which have in general larger Fe metal and sulfide grains and predominantly exhibit a fluffy, sponge-like microstructure (e.g., BRADLEY, 2003). Features from irradiation sputtering, scalloped surfaces or solar flare tracks, which have been found in GEMS grains from IDPs (BRADLEY, 1994), are not observed, which is in agreement with other TEM investigations on stardust grains (STROUD et al., 2004; MESSENGER et al., 2005; KELLER and MESSENGER, 2008).

In the following we will compare TEM characteristics of presolar silicates with astronomical observations and theoretical predictions in general. The majority of circumstellar silicates are Fe-rich and amorphous, whereas a small fraction (usually on the order of 10%, MOLSTER and KEMPER 2005) is crystalline and Mg-rich. This is in agreement with condensation theories, which predict Mg-rich silicates to condense prior to Fe-rich silicates. Because they form at temperatures above the glass temperature, they can crystallize in

contrast to the lower temperature Fe-rich counterparts. Alternatively, former amorphous silicates might crystallize in short term heating events, probably due to shocks (HARKER and DESCH, 2002) or crystalline grains could be rendered amorphous due to irradiation and sputtering processes. However, amorphous Mg-rich silicates have been detected as well (e.g., MARKWICK-KEMPER et al., 2007), but it is difficult to obtain reliable information on the Fe content from the spectra (MOLSTER and WATERS, 2003). In a recent work on results from the *Spitzer Space Telescope*, it was concluded that the enstatite and forsterite populations in protoplanetary systems are clearly separated, with the enstatite grains being larger (up to 1 µm) and forming closer to the central star than the smaller (~0.1 µm) forsterite grains (BOUWMAN et al., 2008). These authors conclude that a localized heating mechanism must be responsible for observed mineral populations and not a large scale mixing transport. Of course, we have to be cautious in comparing formation mechanisms in protoplanetary systems with those in the winds of red giant stars, but the principal condensation paths should be similar.

The majority of the silicate dust population analyzed in this TEM work are amorphous and Mg-rich, with only four grains containing substantial Fe. As mentioned above, this is due to a selection bias and not representative of the whole population. One partly crystalline olivine (31_13) contains more Fe than condensation theories predict, which is in agreement with other investigations on presolar silicates (MESSENGER et al., 2005; KELLER and MESSENGER, 2008). Therefore, condensation conditions in the cooling ejecta of red giant stars may indeed lead to crystalline Fe-containing silicates, if Fe is present in an oxidized form, which is different than inferred from condensation models and also experimental data on synthesized smokes. Alternatively, the Fe abundance is an artefact due to a secondary implantation mechanism similar to SiC-X grains (DENEAULT and CLAYTON, 2003), but it is questionable whether such an exchange mechanism would preserve the crystal structure. It is therefore desirable to check whether measured Fe abundances in presolar olivines are compatible with IR observations within errors. It is an interesting observation that to date only presolar olivine has been detected in the whole crystalline silicate stardust population (MESSENGER et al., 2003; MESSENGER et al., 2005; KELLER and MESSENGER 2008; (NGUYEN and NITTLER, 2008); Grain 31_13), whereas pyroxene is either amorphous or only very weakly crystalline, as is the case in this study. The observed size difference between forsterite and enstatite grains found by BOUWMAN et al. (2008) in protoplanetary systems could indicate different pathways for these two types of grains to form as is discussed in detail by these authors. It is possible that amorphous grains with an pyroxene composition have emerged from former olivine grains during irradiation sputtering or re-condensation combined with a preferential loss of Mg. Clearly, more TEM data on crystalline presolar silicates are needed to further investigate these differences between astronomical observation and determined mineralogical data.

The amorphous, Mg-rich population is similarly difficult to explain, because observational evidence speaks for mostly crystalline Mg-rich silicates as the major mineral species. However, this is based on indirect evidence derived from a high opacity in the near IR explained by Fe (KEMPER et al., 2002). It is not clear from these spectral models, in what form Fe is present, i.e., as inclusions in the silicates or as a separate population (MOLSTER and WATERS, 2003). Therefore, our findings support the view that there are indeed

amorphous Mg-rich silicates without Fe inclusions. These grains then formed under non-equilibrium conditions close to the glass temperature in the circumstellar outflow, which lead to a compositional variability on a fine scale and no or only a weak crystallinity. On the contrary, amorphous Mg-rich grains might be the result of secondary processing, either from SEM point measurements in the laboratory or by sputtering in the ISM. It is therefore not possible to distinguish a primary from a secondary formation mechanism for the amorphous Mg-rich silicate population.

The measured amorphous, Fe-containing silicates (4_11, 8_10, 14_2_3a, rim of 18_08) are similar in morphology and composition to what has been found by other researchers in TEM studies on presolar silicates (MESSENGER et al., 2003; YADA et al., 2005; FLOSS et al., 2006; N07). However, as mentioned earlier, we do not define these grains as classical GEMS grains, because their S contents are lower and they do not exhibit a characteristic fluffy microstructures (see also BRADLEY, 2003). Fe contents might also be partly of secondary nature (Sec. 4.3.2), which makes clear interpretations concerning Fe contents problematic. It is therefore possible that these grains primarily did not contain a lot of Fe and were more similar to the Mg-rich population. This again could be explained by an evolutionary sequence from Mg-rich to more Fe-rich grains during secondary processing.

One particularly Si-rich grain, 4_11, is very similar in composition and appearance to another presolar silicate analyzed by TEM (N07). These two grains are also characterized by an extremely low $^{18}O/^{16}O$ ratio compared to the majority of presolar silicates. Of course, there are other low $^{18}O/^{16}O$ grains with a Mg-rich composition, and – vice versa – Si enriched grains with a Group I signature. But it could be an interesting correlation, if the combination of a low $^{18}O/^{16}O$ ratio and low Mg/Si ratio point to similar formation conditions, as similar grains have been analyzed by AES (Sec. 4.3.1 and Sec. 4.3.6). Astrophysical observations indicate that stars of very low metallicities (< 0.01x solar) have low Mg/Si ratios (FERRAROTTI and GAIL, 2001), which may thus be alternative stellar sources of the grains described here, if the grains´ low $^{18}O/^{16}O$ ratios are coupled to a low initial metallicity. However, the $^{18}O/^{16}O$ ratios of the grains are still too high to support this scenario, even if we consider massive dilution, and it is questionable whether dust grains can form under such low metallicity conditions at all (GAIL et al., 2008). Future work of combined NanoSIMS/TEM investigations on Group II grains could put further constraints on this issue. To date, this correlation is statistically not relevant and highly speculative.

Clearly, TEM work on presolar silicates is still in its infancy and further research is necessary to put new constraints on formation, transformation and survival conditions of circumstellar silicate dust.

4.3.6 Auger electron spectroscopy of silicate and oxide stardust

4.3.6.1 Whole population

We have analyzed 62 presolar silicates and seven presolar oxides by AES. About half of the silicates have a Mg# of 0.5 and lower or a qualitatively low Mg/Fe ratio in the unquantified data set (47 %) (Fig. 4.17). The silicates with a Mg# > 0.5 are still more Fe-rich than expected and the maximum Mg# of the quantified data set is 0.82, excluding one peculiar highly Mg-enriched grain (see below). Not a single, refractory Fe-free silicate has been found.
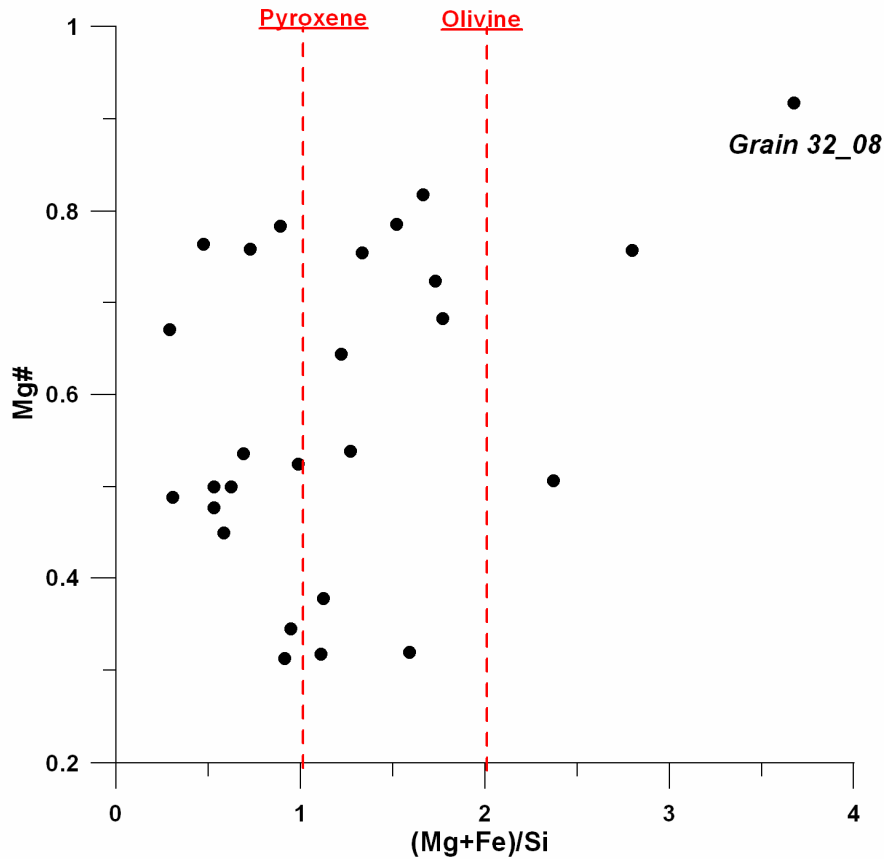
Figure 4. 17 Mg-Fe-Si element abundances of presolar silicates with quantified Auger spectra Most of the grains have non-stoichiometric compositions over a large elemental range and are Fe-rich with the exception of the peculiar grain 32_08.

Eight grains in the quantified data set display atypical major elemental contents with 7 highly Si-enriched grains ($(Mg+Fe)/Si < 0.5$) and one highly Mg-enriched grain. Two grains consist of Ca-, and Al-rich grains attached to silicate material and are referred to as "complex". Another of these complex grains has been found previously ("7_04"), for which no further TEM or Auger data exists (VOLLMER et al., 2006). These grains will be discussed as a separate population in Sec. 4.3.6.2. In the presolar oxide population we find that grains are dominated by Al and contain trace amounts of mostly Ca, but also Fe, Mg and Si. However, relative Auger sensitivity factors for oxides are not precisely known and respective uncertainties must be considered. Only one silicate (24_04) contains sulfur above the detection limit and may thus be regarded as a potential GEMS grain. The majority of grains, however, do not exhibit a resolvable S peak, which is in agreement with the TEM results.

In the following, we will discuss observed compositions in more detail. Ca-bearing Al-rich oxides (Ca content $0.8 - 2.8$ at.% in the quantified data set) could be explained by the fact, that pure Al_2O_3 has a very small condensation window until hibonite condenses out (18 K, compared to over 100 K from hibonite to the next stable condensate grossite) (LODDERS, 2003), which therefore leads to preferential incorporation of Ca into refractory Al-rich oxides. Therefore, observed Ca abundances could reflect initial elemental contents. In chemically processed oxide separates from ordinary chondrites, however, pure Al_2O_3 is the dominant phase (NITTLER et al., 1997; 2008), and single stellar objects with a very high abundance of

Al$_2$O$_3$ have also been analyzed (MALDONI et al., 2008). Still, it is more difficult to locate presolar hibonite grains among the large solar system hibonite background, which is a more common component of primitive meteorites than Al$_2$O$_3$ (CHOI et al., 1999) and might be under-represented in the presolar grain dataset. Alternatively, the Ca content of the oxide grains analyzed here could be of secondary origin due to aqueous alteration on the parent body or terrestrial alteration, which leads to the precipitation of carbonates. As Acfer 094 has not suffered from parent body alteration, as inferred from its low abundance of hydrated silicates (NEWTON et al., 1995), but indeed from terrestrial impregnation (BLAND et al., 2008), this should be considered possible (see also discussion on silicates below).

About half of the Fe- and Mg-rich silicates also contain variable amounts of Ca between 0.7 and 4.3 at.%, and a few grains also Al in the % range, which is similar to what has been found in some grains by TEM. However, Ca and Al have vastly different detection limits in the Auger measurements: whereas the technique is extremely sensitive to Ca, other elements (including Al) cannot be detected even at the sub-3% level. Other Auger investigations on presolar silicates detected smaller contents of these refractory elements (NGUYEN et al., 2008b). It is difficult to speculate about the origins of these constituents. In the TEM, no evident Al- or Ca-rich subdomains could be located, which most likely indicates a non-stoichiometric component. Alternatively, the subdomains may have been too small to distinguish them from the surrounding silicate due to similar contrast. It is also possible that these elements were incorporated into condensing silicates at lower temperatures leading to "chaotic" Mg-Si-Al-O-silicates proposed by astrophysical models (STENCEL et al., 1990). Alternatively, Ca might be again a secondary alteration product similar to Fe. Investigations on grain separates from the same meteorite did not encounter these Ca contents, which indicates that secondary Ca-rich phases attached to the grains of interest were removed during preparation of the grain separate.

As has been discussed earlier (Sec. 4.3.2), Mg-rich grains are best-explained by direct condensation from a gas under high-temperature conditions, although measured Fe contents are too high for truly refractory condensates, but this could be of secondary nature (see below). Preserved elongated and smooth morphologies underline this interpretation. However, TEM investigations have shown (Sec. 4.3.5), that presolar Mg-rich silicates are not necessarily stoichiometric, but display highly variable Mg- and Si-contents on a very fine scale and might be only partly crystalline. Therefore, it is difficult to draw precise conclusions on Mg-rich grains based on AES alone. The most extreme example in this respect is the grain 32_08, which was discussed already in Sec. 4.3.5 in some detail. The Auger quantification yielded a Mg/Si ratio of 3.4 (and a very low Fe content of 2.7 at.%), whereas TEM analysis of the entire grain gave variable ratios between 1 and 2. The only possible explanation to these contradicting results is a heterogeneous distribution of Mg inside the grain, since AES and TEM-EDX measurements determine the compositions of different sub-volumes of the grain. Two more grains of this type have been found in two other meteorites (FLOSS and STADERMANN, 2008). Two other grains yield very high (Mg+Fe)/Si ratios of 2.8 and 2.4, respectively (27_02 and 33_13, Tab. 4.1 and Fig. 4.17), but here secondary Fe-rich material has clearly shifted measured values.

(Mg+Fe)/Si ratios of the majority of measured grains vary around 1, which indicates an over-abundance of pyroxene-like grains compared to olivine-like compositions, which is in agreement with TEM investigations that also dominantly show pyroxene-like stoichiometries. From observations, it is known that amorphous silicates predominantly display an olivine-like stochiometry, whereas in the crystalline silicate fraction enstatite is three times more abundant than forsterite, although these relative abundances heavily depend on the optical reference parameters used (MOLSTER et al., 2002b). This is in contrast to our observations: The only crystalline presolar silicates are olivines (MESSENGER et al., 2003; 2005; KELLER and MESSENGER 2008; NGUYEN and NITTLER 2008; this study), whereas the amorphous or only weakly crystalline silicates predominantly show pyroxene-like stoichiometries. This is also in agreement with Auger analyses on a large number of grains, but we have to be cautious with these interpretations: the large scatter in (Mg+Fe)/Si ratios and Mg# (Fig. 4.17) might indicate, that the investigated grain population has severely suffered from secondary alteration (see discussion on Ca above). If our observed predominance of pyroxene-like grains reflects true nebular proportions, then future observational work must show whether this is also compatible with spectral analyses on relative abundances in stellar atmospheres.

Seven grains are depleted in both Mg and Fe compared to Si ((Mg+Fe)/Si < 0.5), and are thus chemically similar to highly Si-enriched grains like 4_11 described in the TEM section. Other investigators have found grains of this type as well (FLOSS and STADERMANN 2008). As has been discussed already previously (Sec. 4.3.5), those grains might be explained by condensation from a gas with a very low bulk Mg/Si ratio. About 10% of all stars are characterized by such an elemental abundance ratio in their atmospheres (FERRAROTTI and GAIL, 2001). Furthermore, it is possible that a low Mg/Si ratio is coupled to a lower-than-solar metallicity as is evident from observations on Population II stars (FERRAROTTI and GAIL, 2001; GAIL, 2003). Some Mg-depleted grains (silicates and Al-rich oxides) indeed show a very low $^{18}O/^{16}O$ ratio, which might indicate a low metallicity, but it remains to be seen whether this observation has any statistical significance (Sec. 4.3.1). Alternatively, the gas might get successively enriched in Si-O, when the early condensing forsterites are hindered in further reactions to form enstatite due to accreted Fe metal grains (NAGAHARA and OZAWA, 2008). Highly Si-enriched grains would then be the result of strong non-equilibrium condensation conditions. Condensation calculations also indicate that under such low elemental Mg/Si abundance ratios, quartz becomes a stable phase (FERRAROTTI and GAIL, 2001), which has not yet been detected as a presolar phase, but might be attributed to the 20.5 μm feature in IR spectra (MOLSTER et al., 2002a). The grains in this study contain variable amounts of Fe and Mg, which speaks against a pure SiO_2 phase, but this could be due to alteration. It may therefore be only a matter of time until the first presolar quartz grain is identified and measured by AES and TEM.

4.3.6.2 Complex grains

Three grains consist of presolar refractory oxide grains attached to presolar silicate material and are thus described as "complex" (Fig. 4.18).
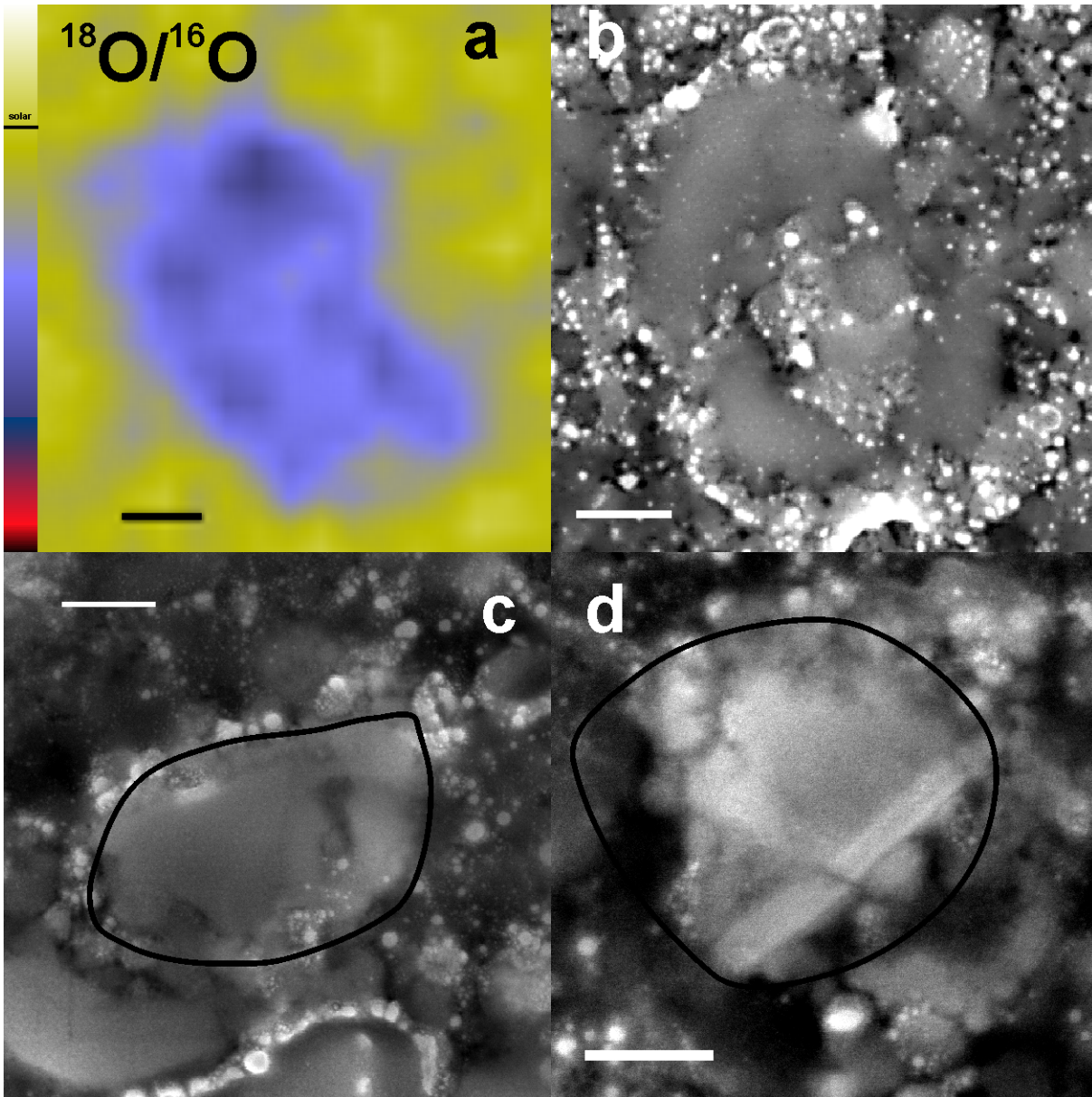
Figure 4. 18 NanoSIMS ratio image of grain 7_04 and HR-SEM images of three complex grains

a – The $^{18}O/^{16}O$ ratio image of grain 7_04 indicates different isotopic compositions in rim and center, b – SEM image of the same area with the triangular shaped core decorated by bright Fe-particles, c – SEM image of grain 22_09 surrounded by Fe particles and the outline of the O isotope anomaly, d – SEM image of grain 32_03 with the outline of the O isotope anomaly. All scale bars represent 200 nm.

Two of these grains have already been reported in conference abstracts (VOLLMER et al., 2006; 2007b). Grain 7_04 was the first grain of this kind to be discovered, but AES was not available to us at that time. Unfortunately, it could not be relocated after FIB preparation in the TEM, leaving its mineralogical constitution unclear. This could either mean that its extension into the matrix was not very deep due to the previous NanoSIMS measurement, which has been observed by other FIB workers as well (STROUD et al., 2008) or that we did not cut the grain exactly in its center. HR-SEM imaging shows that the central grain, ~500x350 nm² in size, is a single triangular crystal, on whose three sides the Si-rich material accreted. In a subsequent NanoSIMS re-examination, count rates for Ca were too low for accurate

statistics, but the central grain itself displays low Mg count rates pointing to a corundum or hibonite rather than spinel. The grain is heavily infiltrated by Fe-rich particles as is evident from the SEM (Fig. 4.18b). The O isotopic composition in the rim is more extreme (i.e., higher $^{17}O/^{16}O$ and lower $^{18}O/^{16}O$ ratios) than in the center even within errors (Fig. 4.18a). This could be explained by the fact that the grain´s rim sampled a different stellar gas reservoir that was more enriched by CNO-processed material, which would imply not well-mixed isotopic reservoirs in the stellar envelope, where this grain formed. More probably, this observation is an artefact due to isotopically normal Fe-rich grains overlaying the core, which diluted the measured O isotopic ratios.

A second grain, 22_09, which also consists of at least three different Ca-Al-Si-bearing subphases, was examined in detail by AES (Fig. 4.18c, Fig. 4.19).
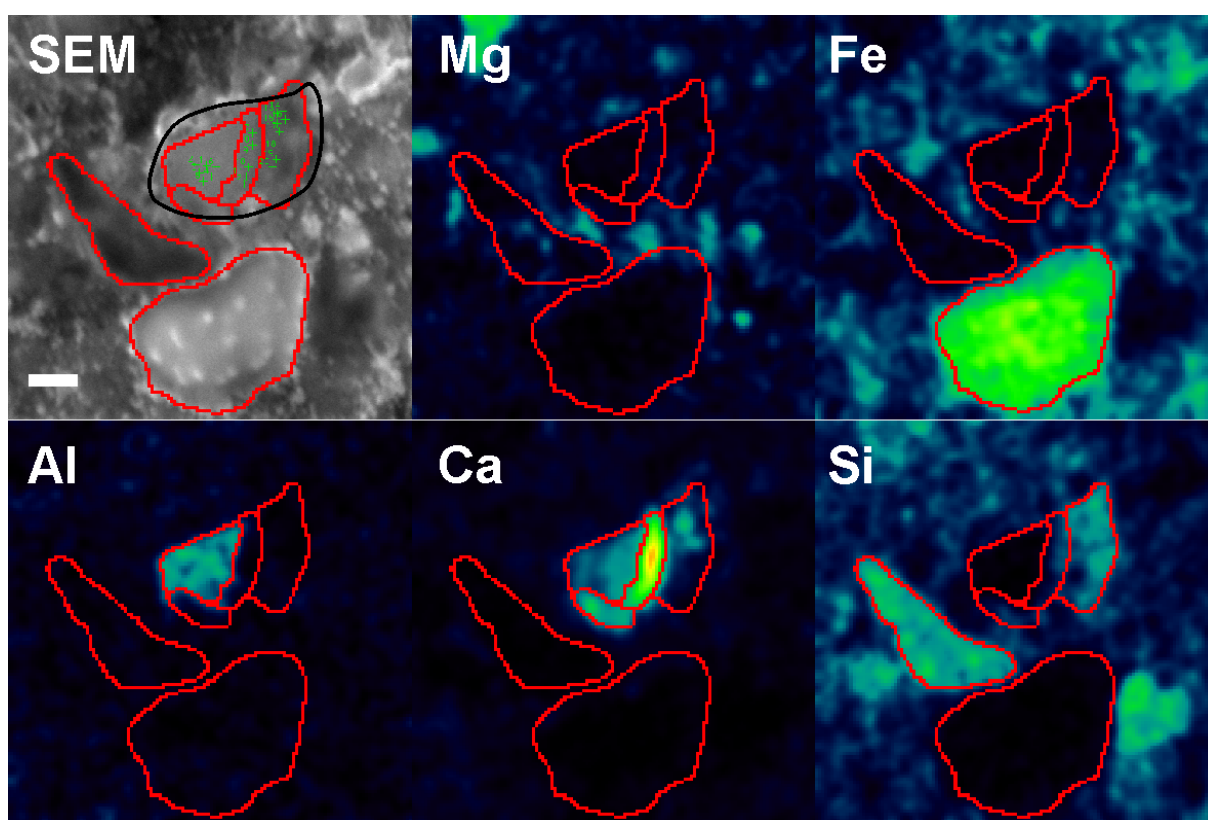
Figure 4. 19 SEM image of the presolar CAI 22_09 and corresponding Auger elemental maps
Locations of point measurements on three zones in the grain are marked by green crosses in the SEM image as well as the outline of the O isotope anomaly. Fe and Mg seem to be missing in the grain, but this is due to the automatic scaling of the colour scheme, which displays the range from lowest to highest abundance for each element in the whole image, that also includes Mg- and Fe-rich regions. Ca and Si are heterogeneously distributed. Scale bar represents 200 nm and refers to all images.

The grain does not exhibit a pronounced rounded shape like 7_04, but the phase on the left is a triangle alike the core in 7_04, which could indicate a similar composition. The phase on the left has a non-stoichiometric composition consisting essentially only of Al, Ca and O (in at%: O 57, Mg 2, Al 24, Si 0, Ca 7, Fe 9), and therefore most likely resembles hibonite or grossite. The Fe content could be due to surrounding or overlying phases that are not necessarily part of the anomaly. The phase in the middle is

dominated by Ca and Si (in at.%: O 53, Mg 6, Al 4, Si 19, Ca 10, Fe 8) and could therefore represent an Ca-silicate like melilite ($Ca_2Al_2SiO_7$, gehlenite endmember – $Ca_2MgSi_2O_7$, åkermanite endmember) or calcic pyroxene ("fassaite", $CaMgSi_2O_6$ – $CaAl_2SiO_6$). However, these quantifications are based on the relative sensitivity factors obtained for Fe-Mg silicates, and must be taken with respective care. The third part of grain 22_09 to the right seems to consist of a complex mixture of non-stoichiometric subphases, as is evident from the Ca-rich "hot spot" in one corner and the heterogeneous distribution of Si (in at.%, "Ca-free region": O 60, Mg 3, Al 0, Si 26, Ca 0, Fe 11; "Ca-hot spot": O 56, Mg 2, Al 0, Si 28, Ca 4, Fe 10). It should therefore be regarded as a non-stoichiometric Fe-rich silicate. The Ca content is similar to what is observed in the majority of presolar silicates. Because minerals of this complex presolar grain are also found in Ca-Al-rich inclusions ("CAIs") from meteorites, it was named the first, presolar CAI (VOLLMER et al., 2007b). Strictly speaking, all presolar hibonite grains are also CAIs (LARRY NITTLER, pers. comm.), but here we are dealing with a true complex phase assemblage typical of solar system CAIs. The third grain (32_03, Fig. 4.20) is characterized by a small heterogeneous area dominated by Al (in at.%: O 54.5, Fe 9.7, Mg 8.5, Si 12.5, Ca 1.6, Al 13.3).
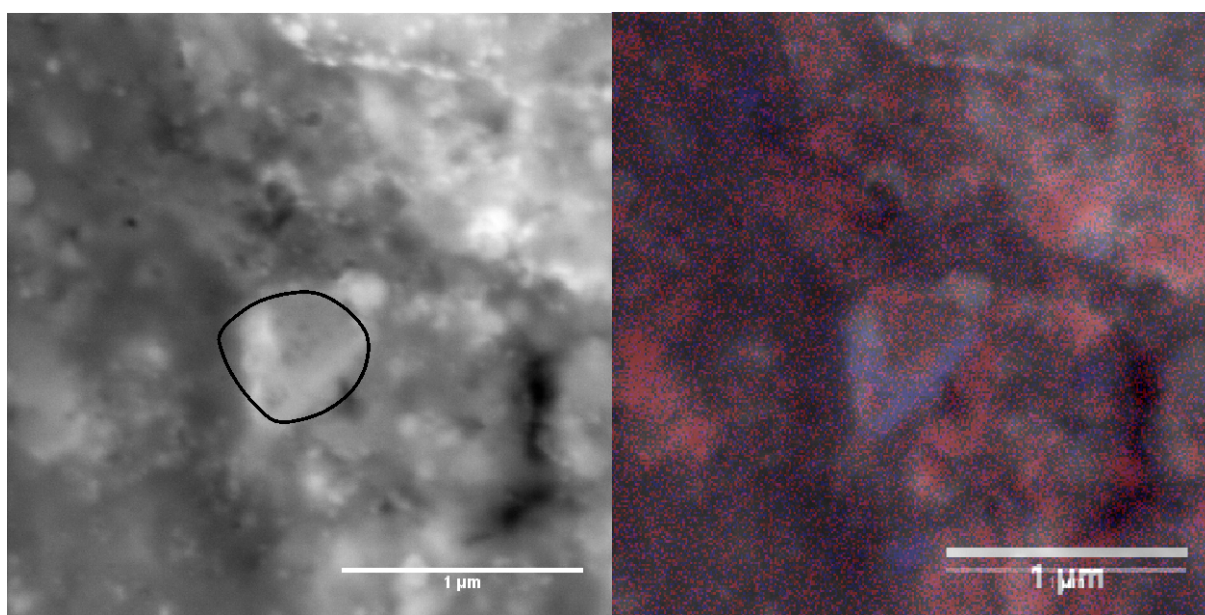

Figure 4. 20 SEM image of grain 32_03 and the corresponding Auger elemental map
The complex nature of this grain (outlined by its O isotope anomaly in the left SEM image) is obvious from the elemental map (Blue – Al, Red – Mg), as at least four different elemental domains < 200 nm in size are visible.

In this case Mg-Fe silicates obviously contribute to the spectrum, because the selected analysis raster was partly in the area of the attached silicate. Quantification is therefore very difficult, but the Ca/Al ratio most likely indicates a hibonite-like phase. The attached silicate to the north of this Al-rich region has approximately equal abundances of Mg and Fe (in at.%: O 56.4, Fe 6.9, Mg 6.3, Si 24.9, Ca 2.4, Al 3.1) and is partly enclosed by the Al-rich phase in two long bars obvious also from the Auger elemental maps (Fig. 4.20). Upon closer inspection, the grain is even more complex on a fine scale: There seems to be a Mg-rich region inside the Al-rich area in the southern part of the grain as well as an Al-rich hot spot to the

left. All in all, this heterogeneity on a fine scale supports a complex formation process for this grain, as Al-rich phases and silicates seem to have condensed in no specific order. This is different from the other two grains, where the silicate phases seem to have accreted onto the Al-rich central grain in a sequence.

In the following we will discuss observed features of complex presolar grains in Acfer 094. It is known from condensation theory that it is thermodynamically difficult to condense silicates directly from the gas phase, therefore imposing the need for seed nuclei such as Al_nO_m or Ti_nO_m (e.g., GAIL, 2003), whose formation themselves is still not well understood. In carbonaceous grains such as graphite and SiC tiny subcrystals of highly refractory carbides (TiC or (Zr,Ti,Mo)C) have been detected, which similarly indicate seed nucleation processes before condensation of the major phase (BERNATOWICZ et al., 1996; CROAT et al., 2003). However, the first TEM analyses on presolar silicates did not identify such tiny sub-crystals (MESSENGER et al., 2003; FLOSS et al., 2006; YADA et al., 2005; N07). The grains described here indicate that silicate material does indeed accrete onto previously condensed more refractory phases. Ca-Al-rich minerals such as corundum, hibonite, grossite, spinel or melilite are expected to condense from a gas of solar composition at higher temperatures until the major silicate phases forsterite and enstatite condense out (e.g., LODDERS, 2003). Highly refractory grains of solar system origin such as corundum aggregates or corundum overgrown by hibonite have been found in the carbonaceous chondrite Acfer 094 (NAKAMURA et al., 2007). Those grains are explained by condensation of pure corundum from the cooling solar gas and subsequent, diffusion-controlled formation of hibonite by reaction with gaseous Ca. These grains then serve as seed nuclei onto which the lower temperature silicates can accrete. This implies that the composition of the gas changes during formation and that the condensing grain and the cooling gas are not in chemical equilibrium, because forming grains are removed kinetically. A similar process could also be imagined for the series of grains in 22_09, which is indeed best-explained by a condensation sequence. The higher-temperature Al-rich oxide forms first followed by the Ca-Si-rich phase and the Fe-bearing silicate condensing at progressively lower temperatures. Theoretically, those composite grains are indeed predicted by theory dependent on different stellar mass loss rates that also influences the silicate crystallinity (SOGAWA and KOZASA, 1999). From an observational point of view they should also exist: detection of Al-rich refractory oxides in IR spectra depends on the mass loss rate, where at higher mass loss rates refractory oxides are coated by silicate mantles (DIJKSTRA et al., 2005). However, in this study only grain 7_04 is completely coated, but the other two complex grains could represent fragments of former intact, larger assemblages.

Still, the number of these complex grains is small compared to the majority of presolar silicates without refractory seed nuclei detected. If these complex grains underline theories on heterogeneous silicate nucleation, then why have the majority of silicate grains apparently condensed homogeneously without obvious subgrains? First, it is possible that those subgrains might be overlooked in a majority of cases, although they are present. The chemically complex nature of most presolar silicates analyzed by TEM makes it very difficult to distinguish Ca- or Al-rich subgrains from the surrounding silicate, because the compositional contrast difference is very weak. Bulk EDX analyses by TEM on presolar silicates indeed showed the presence of refractory elements like Al and Ca in some cases, and AES indicated that about

half of the analyzed grains contain those elements. Therefore, it is still possible that these silicates have indeed condensed heterogeneously, but that seed clusters are just too tiny to be identified, although we have to bear in mind a possible secondary contamination origin for high Ca contents. Second, although it is thermodynamically unfavourable, it may be possible that silicate grains do condense homogeneously. This process depends heavily on the vapour pressure of gaseous Si-O, which could nucleate at higher temperatures than previously thought from a super-saturated gas (NUTH III and FERGUSON, 2006). However, more experimental and theoretical work is necessary to explore the homogeneous growth of silicates. Third, it is possible that a higher fraction of the presolar silicate inventory could originally have formed as complex grains, but was shattered in interstellar shock waves during ISM passage. It was shown that fragmentation due to grain-grain collisions in SN accelerated shock waves is the dominant modification process affecting interstellar dust grains (JONES et al., 1996). This process shifts the size distribution of the interstellar dust inventory to smaller values leaving the total dust mass unaltered. Therefore, what we find today as presolar grains are the remainders of former complex grains that were fragmented into Al-rich oxides such as corundum and hibonite (NITTLER et al., 1997; CHOI et al., 1999) and silicates from former mantles. A tiny fraction of this material might even get converted to high-pressure modifications during this process, which was proposed theoretically (TIELENS et al., 1994) and also detected recently for a presolar silicate (VOLLMER et al., 2007a). This latter possibility is speculative, of course, but might provide an explanation for the under-abundance of O-rich subgrains in presolar silicates, whose formations are otherwise hard to understand from a theoretical point of view.

4.4 Conclusions

We have detected 142 presolar silicate and 20 presolar oxide grains in the carbonaceous chondrite Acfer 094 by NanoSIMS O isotope mapping. The majority of these grains could be documented and their dimensions measured by HR-SEM, 69 grains were investigated by AES for elemental contents, eight grains could be successfully prepared by FIB for further TEM analysis. Our investigations lead us to the following conclusions:

1) The majority of presolar silicates and oxides (81 ± 7 %) belong to the O isotope Group I, which is similar to what has been found by NITTLER et al. (1997; 2008) for oxides only. The bulk of silicate and oxide stardust therefore derives from $1 - 2.5$ M$_\odot$ red giant stars of close-to-solar or slightly lower-than-solar metallicity.

2) The fraction of highly ^{17}O enriched silicates (Group I^b) does not extend to the high values observed for presolar oxides, but this might be an experimental artefact and due to more severe dilution. Still, these oxide and silicate grains might share an exotic, binary star origin (NITTLER et al., 2008; VOLLMER et al., 2008) different from the majority of O-rich stardust, which has to be tested in future studies of several isotope systems on the same grains.

3) Group II grains appear to be less abundant among presolar silicates compared to Al-rich oxides. However, this might be an artefact of the analysis method.

4) About 11 ± 3 % of the presolar silicates can be assigned to Group IV characterized by an enrichment in ^{18}O relative to solar and close-to-solar ^{17}O/^{16}O, whereas Group IV oxides mostly lie on a trend line

between solar O and a ^{16}O-depleted reservoir. It is therefore possible that Group IV silicate and oxide grains do not share the same origins. The Si isotopic compositions (^{28}Si-enriched) of some of the Group IV silicates point to contribution of material from inner SNII zones and those grains therefore most probably derive from such massive star explosions (NITTLER et al., 2008; VOLLMER et al., 2008).

5) The majority of grains (70 − 80 %) are irregular in shape and composed of even smaller sub-particles bound to fractal-like structures known from condensation experiments. About 20 − 30 % of all grains display an elongated or rounded morphology together with a smooth, platy surface, which are harder than the surrounding matrix. These grains appear to represent single, solid phases. It is possible that these grain populations can be assigned to different degrees of secondary alteration.

6) The grains are evenly distributed within the matrix on a mm scale, but in some cases we observe a distinct clustering, i.e., two or more grains in the same 10x10 μm² analyzed field. The abundance of fields with two or three grains in the same field is expected from statistics within errors. However, the clustering in one field with five grains is statistically significant. This clustered field might be the result of an extremely heterogeneous distribution of stardust in the solar nebula or by fragmentation of former larger particles shortly before incorporation into the meteorite parent body.

7) The matrix-normalized abundance of silicate stardust in Acfer 094 is 163 ± 14 ppm, of oxide stardust 26 ± 6 ppm. This meteorite therefore contains among the highest amounts of O-rich stardust together with other primitive carbonaceous chondrites and IDPs.

8)   a. − Most of the grains analyzed by TEM are amorphous or very weakly crystalline (7 out of 8), also the Mg-rich ones, which is in contrast to astronomical observations and theoretical studies which predict mainly crystalline Mg-rich silicates. The grains may have been rendered amorphous during interstellar passage or by SEM point measurements in the laboratory. Alternatively, they could have formed under low-temperature conditions in the circumstellar outflow such that only a weak or no crystallinity was achieved.

           b. − Three Fe-containing glasses with sub-solar Mg/Si ratios are similar to GEMS, but large Fe minerals and the characteristic fluffy morphology are missing here except for grain 14_2_3a. We therefore assume that two of these grains (namely, grains 4_11 and 8_10) represent a different class of circumstellar grains than presolar GEMS grains.

           c. − One partly crystalline olivine has a higher Fe-content than condensation calculations predict (Mg# 0.9), but is compositionally similar to two presolar olivines found recently. Therefore, crystalline Fe-bearing silicates do indeed form in circumstellar environments, in contrast to the observational evidence.

           d. − The overall predominance of olivines among crystalline silicate stardust could indicate preferential survival of this mineral in contrast to pyroxene. Alternatively, olivine formation is favoured, whereas pyroxene, condensing after olivine due to the reaction of olivine with the gas, remains amorphous or is only weakly crystalline. The observed different crystallinity of these two minerals might then be the result of different formation paths.

9)   a. – AES indicates that the majority of grains are Fe-rich (Mg# of 0.82 and lower), which is either due to non-equilibrium condensation, secondary alteration or both. A lot of grains exhibit cracks and Fe-rich particles along their surfaces in SEM imaging, which could support a secondary origin for high Fe contents in those grains.

b. – (Mg+Fe)/Si ratios vary between 1 and 2 and are predominantly characterized by pyroxene- rather than olivine-like compositions. This is in agreement with TEM investigations. These grains might represent unaltered circumstellar material or were subject to secondary processes (sputtering, secondary Fe impregnation).

c. – About half of the grains contain Ca and/or Al in quantifiable amounts, which could indicate the presence of tiny, refractory oxides, non-stoichiometric components or terrestrial alteration.

d. – Some grains have rather low (Mg+Fe)/Si ratios (< 0.5), which could be explained by condensation from a gas with a low Mg/Si, by a low initial metallicity of the parent stars, or by successive enrichment of Si-O in the gas by non-equilibrium condensation due to accreted Fe metal grains.

e. – One grain, similar to two grains from two other meteorites, is extremely enriched in Mg (Mg/Si = 3.4) and is characterized by a heterogeneous Mg distribution. This grain is also special because of its high Mn content (up to 1.4 at.%) similar to LIME silicates.

f. – Al-rich oxides are apparently not pure and contain quantifiable amounts of Ca, but also of Mg, Si and Fe. This could be due to non-stoichiometric components, although contribution from interfering silicate and Fe-rich grains in the surroundings and terrestrial alteration cannot be completely ruled out.

g. – Refractory Al-rich oxides may serve as seed nuclei for silicate material to condense, which is proposed by condensation theory as well as by observation of covered Al-rich oxides depending on the mass loss rate. However, the majority of presolar silicates apparently do not enclose large subgrains.

4.5 References

Alexander C. M. O. D. (2005) Re-examining the role of chondrules in producing the elemental fractionations in chondrites. *Meteoritics and Planetary Science* **40**(7), 943-965.

Alexander C. M. O. D., Swan P. D., and Walker R. M. (1990) In situ measurement of interstellar silicon carbide in two CM chondrite meteorites. *Nature* **348**, 715-717.

Bernatowicz T. J., Cowsik R., Gibbons P. C., Lodders K., Fegley Jr. B., Amari S., and Lewis R. S. (1996) Constraints on stellar grain formation from presolar graphite in the Murchison meteorite. *The Astrophysical Journal* **472**, 760-782.

Bernatowicz T. J., Fraundorf G., Ming T., Anders E., Wopenka B., and Zinner E. (1987) Evidence for interstellar SiC in the Murray carbonaceous chondrite. *Nature* **330**, 728-730.

Bland P. A., Howard K. T., Cressey G., and Benedix G. K. (2008) The terrestrial component of primitive chondrite alteration. *Annual Meeting of the Meteoritical Society* **71**, abstr.#5314.

Bland P. A., Stadermann F. J., Floss C., Rost D., Vicenzi E. P., Kearsley A. T., and Benedix G. K. (2007) A cornucopia of presolar and early solar system materials at the micrometer size range in primitive chondrite matrix. *Meteoritics and Planetary Science* **42**(7/8), 1417-1427.

Boothroyd A. I. and Sackmann I.-J. (1999) The CNO isotopes: Deep circulation in red giants and first and second dredge-up. *The Astrophysical Journal* **510**, 232-250.

Boothroyd A. I., Sackmann I.-J., and Wasserburg G. J. (1995) Hot Bottom Burning in asymptotic giant branch stars and its effect on oxygen isotopic abundances. *The Astrophysical Journal* **442**, L21-L24.

Bose M., Floss C., and Stadermann F. J. (2008a) Iron-enriched Stardust Grains in the Meteorites Acfer 094, QUE 99177 and MET 00426. *Annual Meeting of the Meteoritical Society* **71**, abstr.#5094.

Bose M., Stadermann F. J., and Floss C. (2008b) An investigation into the origin of Group 4 stardust grains. *Lunar and planetary science conference* **39**, 1099.

Bouwman J., Henning T., Hillenbrand L. A., Meyer M. R., Pascucci I., Carpenter J., Hines D., Kim J. S., Silverstone M. D., Hollenbach D. J., and Wolf S. (2008) The Formation and Evolution of Planetary Systems: Grain Growth and Chemical Processing of Dust in T Tauri Systems. *The Astrophysical Journal* **683**, 479-498.

Bradley J. P. (1994) Chemically anomalous, preaccretionally irradiated grains in interplanetary dust from comets. *Science* **265**(5174), 925-929.

Bradley J. P. (2003) The Astromineralogy of Interplanetary Dust Particles. *In: Astromineralogy (ed. Th. Henning)*, 217-235.

Bradley J. P. and Dai Z. R. (2004) Mechanism of formation of glass with embedded metal and sulfides. *The Astrophysical Journal* **617**, 650-655.

Bradley J. P., Keller L. P., Snow T. P., Hanner M. S., Flynn G. J., Gezo J. C., Clemett S. J., Brownlee D. E., and Bowey J. E. (1999) An infrared spectral match between GEMS and interstellar grains. *Science* **285**, 1716-1718.

Choi B.-G., Huss G. R., Wasserburg G. J., and Gallino R. (1998) Presolar Corundum and Spinel in Ordinary Chondrites: Origins from AGB stars and a Supernova. *Science* **282**, 1284-1289.

Choi B.-G., Wasserburg G. J., and Huss G. R. (1999) Circumstellar Hibonite and Corundum and Nucleosynthesis in Asymptotic Giant Branch stars. *The Astrophysical Journal* **522**, L133-L136.

Clayton D. D. (2003) A presolar Galactic Merger spawned the SiC-grain Mainstream. *The Astrophysical Journal* **598**, 313-324.

Colangeli L., Henning T., Brucato J. R., Clément D., Fabian D., Guillois O., Huisken F., Jäger C., Jessberger E. K., Jones A., Ledoux G., Manicó G., Mennella V., Molster F. J., Mutschke H., Pirronello V., Reynaud C., Roser J., Vidali G., and Waters L. B. F. M. (2003) The role of laboratory experiments in the characterization of silicon-based cosmic material. *The Astronomy and Astrophysics Review* **11**, 97-152.

Croat T. K., Bernatowicz T. J., Amari S., Messenger S., and Stadermann F. J. (2003) Structural, chemical and isotopic microanalytical investigations of graphite from supernovae. *Geochimica et Cosmochimica Acta* **67**(24), 4705-4725.

Deneault E. A.-N. and Clayton D. D. (2003) Supernova reverse shocks: SiC growth and isotopic composition. *The Astrophysical Journal* **594**, 312-325.

Dijkstra C., Speck A. K., Reid R. B., and Abraham P. (2005) The 10 μm feature of M-type stars in the large magellanic cloud and the dust condensation sequence. *The Astrophysical Journal* **633**, L133-136.

Ebata S., Fagan T. J., and Yurimoto H. (2007) Identification of silicate and carbonaceous presolar grains in the Type 3 enstatite chondrite ALHA81189. *Annual Meeting of the Meteoritical Society* **70**, abstr.#5150.

Fabian D., Henning T., Jäger C., Mutschke H., Dorschner J., and Wehrhan O. (2001) Steps toward interstellar silicate mineralogy VI. Dependence of crystalline olivine IR spectra on iron content and particle shape. *Astronomy and Astrophysics* **378**, 228-238.

Ferrarotti A. S. and Gail H.-P. (2001) Mineral formation in stellar winds II. Effects of Mg/Si abundance variations on dust composition in AGB stars. *Astronomy and Astrophysics* **371**, 133-151.

Floss C. and Stadermann F. J. (2007) Very high presolar grain abundances in the CR chondrite QUE 99177. *Meeting of the Meteoritical Society* **70**, 5060.

Floss C. and Stadermann F. J. (2008) The Stardust inventory of CR chondrites QUE 99177 and MET 00426, and the distribution of presolar silicate and oxide grains in the early Solar System. *Lunar and planetary science conference* **39**, abstr.-#1280.

Floss C., Stadermann F. J., and Bose M. (2008) Circumstellar Fe oxide from the Acfer 094 carbonaceous chondrite. *The Astrophysical Journal* **672**, 1266-1271.

Floss C., Stadermann F. J., Bradley J. P., Dai Z. R., Bajt S., Graham G., and Lea A. S. (2006) Identification of isotopically primitive interplanetary dust particles: A NanoSIMS isotopic imaging study. *Geochimica et Cosmochimica Acta* **70**, 2371-2399.

Gail H.-P. (2003) Formation and evolution of minerals in accretion disks and stellar outflows. *in: Astromineralogy (ed. Th. Henning)*, 55-120.

Gail H.-P. and Sedlmayr E. (1999) Mineral formation in stellar winds - I. Condensation sequence of silicate and iron grains in stationary oxygen rich outflows. *Astronomy and Astrophysics* **347**, 594-616.

Gail H.-P., Zhukovska S., Hoppe P., and Trieloff M. (2008) Stardust from AGB stars. *The Astrophysical Journal* **submitted**.

Harker D. E. and Desch S. J. (2002) Annealing of silicate dust by nebular shocks at 10 AU. *The Astrophysical Journal* **565**, L109-L112.

Holzapfel C., Soldera F., Vollmer C., Hoppe P., and Mücklich F. (2008) TEM foil preparation of sub-um sized grains by the Focused ion beam technique. *Journal of Electron Microscopy*, in preparation.

Hoppe P., Strebel R., Eberhardt P., Amari S., and Lewis R. S. (2000) Isotopic properties of silicon carbide X grains from the Murchison meteorite in the size range 0.5-1.5 μm. *Meteoritics and Planetary Science* **35**(6), 1157-1176.

Huss G. R. and Lewis R. S. (1995) Presolar diamond, SiC, and graphite in primitive chondrites: abundances as a function of meteorite class and petrologic type. *Geochimica et Cosmochimica Acta* **59**(1), 115-160.

Iliadis C., Angulo C., Descouvemont P., Lugaro M., and Mohr P. (2008) New reaction rate for 16O (p,gamma) 17F and its influence on the oxygen isotopic ratios in massive AGB stars. *Physical Review C* **77**, 045802.

Ishii H., Bradley J. P., Dai Z. R., Chi M., Kearsley A. T., Burchell M. J., Browning N. D., and Molster F. J. (2008) Comparison of Comet 81P/Wild 2 Dust with Interplanetary Dust from Comets. *Science* **319**, 447-450.

Jones A. P., Tielens A. G. G. M., and Hollenbach D. J. (1996) Grain shattering in shocks: The interstellar grain size distribution. *The Astrophysical Journal* **469**, 740-764.

José J. and Hernanz M. (2007) The origin of presolar nova grains. *Meteoritics and Planetary Science* **42**(7/8), 1135-1143.

Keller L. P. and Messenger S. (2008) Coordinated chemical and isotopic studies of GEMS grains in IDPs. *Lunar and planetary science conference* **39**, abstr.#2347.

Kemper F., De Koter A., Waters L. B. F. M., Bouwman J., and Tielens A. G. G. M. (2002) Dust and the spectral energy distribution of the OH/IR star OH 127.8+0.0: Evidence for circumstellar metallic iron. *Astronomy and Astrophysics* **384**, 585-593.

Kemper F., Vriend W. J., and Tielens A. G. G. M. (2004) The absence of crystalline silicates in the diffuse interstellar medium. *The Astrophysical Journal* **609**, 826-837.

Klöck W., Thomas K. L., McKay D. S., and Palme H. (1989) Unusual olivine and pyroxene composition in interplanetary dust and unequilibrated ordinary chondrites. *Nature* **339**, 126-128.

Lodders K. (2003) Solar system abundances and condensation temperatures of the elements. *The Astrophysical Journal* **591**, 1220-1247.

Lodders K. and Amari S. (2005) Presolar grains from meteorites: Remnants from the early times of the solar system. *Chemie der Erde* **65**, 93-166.

Lugaro M., Karakas A. I., Nittler L. R., Alexander C. M. O. D., Hoppe P., Iliadis C., and Lattanzio J. C. (2007) On the asymptotic giant branch star origin of peculiar spinel grain OC2. *Astronomy and Astrophysics* **461**, 657-664.

Maldoni M. M., Ireland T. R., and Robinson G. (2008) IRAS 22036+5306: an Al2O3 oxide-dominated post-AGB star. *Monthly Notices of the Royal Astronomical Society* **386**, 2290-2296.

Marhas K. K., Hoppe P., Stadermann F. J., Floss C., and Lea A. S. (2006) The distribution of presolar grains in CI and CO meteorites. *Lunar and planetary science conference* **37**, abstr.# 1959.

Markwick-Kemper F., Gallagher S. C., Hines D. C., and Bouwman J. (2007) Dust in the Wind: Crystalline silicates, Corundum, and Periclase in PG 2112+059. *The Astrophysical Journal* **668**, L107-L110.

McKeegan K. D., Aléon J., Bradley J. P., Brownlee D. E., Busemann H., Butterworth A., Chaussidon M., Fallon S., Floss C., Gilmour J., Gounelle M., Graham G., Guan Y., Heck P. R., Hoppe P., Hutcheon I. D., Huth J., Ishii H., Ito M., Jacobsen S. B., Kearsley A. T., Leshin L. A., Liu M.-C., Lyon I., Marhas K. K., Marty B., Matrajt G., Meibom A., Messenger S., Mostefaoui S., Mukhopadhyay S., Nakamura-Messenger K., Nittler L. R., Palma R., Pepin R. O., Papanastassiou D. A., Robert F., Schlutter D., Snead C. J., Stadermann F. J., Stroud R. M., Tsou P., Westphal A., Young E. D., Ziegler K., Zimmermann L., and Zinner E. (2006) Isotopic compositions of cometary matter returned by Stardust. *Science* **314**, 1724-1728.

Messenger S., Keller L. P., and Lauretta D. S. (2005) Supernova olivine from cometary dust. *Science* **309**, 737-741.

Messenger S., Keller L. P., Stadermann F. J., Walker R. M., and Zinner E. (2003) Samples of stars beyond the solar system: Silicate grains in interplanetary dust. *Science* **300**, 105-108.

Molster F. J. and Kemper C. (2005) Crystalline Silicates. *Space Science Reviews* **119**, 3-28.

Molster F. J. and Waters L. B. F. M. (2003) The mineralogy of interstellar and circumstellar dust. *in: Astromineralogy (ed. Th. Henning)*, 121-170.

Molster F. J., Waters L. B. F. M., and Tielens A. G. G. M. (2002a) Crystalline silicate dust around evolved stars II. the crystalline silicate complexes. *Astronomy and Astrophysics* **382**, 222-240.

Molster F. J., Waters L. B. F. M., Tielens A. G. G. M., Koike C., and Chihara H. (2002b) Crystalline silicate dust around evolved stars III. A correlations study of crystalline silicate features. *Astronomy and Astrophysics* **382**, 241-255.

Mostefaoui S. and Hoppe P. (2004) Discovery of abundant in situ silicate and spinel grains from red giant stars in a primitive meteorite. *The Astrophysical Journal* **613**, L149-L152.

Mostefaoui S., Marhas K. K., and Hoppe P. (2004) Discovery of an in-situ presolar silicate grain with GEMS-like composition in the Bishunpur matrix. *Lunar and planetary science conference* **35**, abstr.#1593.

Nagahara H. and Ozawa K. (2008) Heterogeneous nucleation and growth of metal on silicates and its astrophysical implication. *Lunar and planetary science conference* **39**, abstr.#1241.

Nakamura T. M., Sugiura N., Kimura M., Miyazaki A., and Krot A. N. (2007) Condensation and aggregation of solar corundum and corundum-hibonite grains. *Meteoritics and Planetary Science* **42**(7/8), 1249-1265.

Newton J., Bischoff A., Arden J. W., Franchi I. A., Geiger T., Greshake A., and Pillinger C. T. (1995) Acfer 094, a uniquely primitive carbonaceous chondrite from the Sahara. *Meteoritics* **30**, 47-56.

Nguyen A., Alexander C. M. O. D., and Nittler L. R. (2008a) An abundant mix of presolar matter in the highly primitive CR chondrite QUE 99177. *Annual Meeting of the Meteoritical Society* **71**, abstr.#5277.

Nguyen A., Busemann H., and Nittler L. R. (2007) Remarkably high abundance of presolar grains in interplanetary dust particles collected from the comet Grigg-Skjellerup dust stream. *Lunar and planetary science conference* **38**, abstr.2332.

Nguyen A. and Nittler L. R. (2008) Laboratory Analysis of Presolar Silicate Stardust: Constraints on Nucleosynthesis and Dust Formation and Processing. *American Astronomical Society Meeting #212, #6.05; Bulletin of the American Astronomical Society* **40**, 196.

Nguyen A., Nittler L. R., and Alexander C. M. O. D. (2006) In situ identification of a presolar SiC X grain, presolar silicates and 13C-rich grains in the Allan Hills 77307 meteorite. *Annual Meeting of the Meteoritical Society* **69**, abstr.# 5355.

Nguyen A., Stadermann F. J., Nittler L. R., and Alexander C. M. O. D. (2008b) Characterization of presolar silicate and oxide grains using Nanosims and Auger Spectroscopy. *Lunar and planetary science conference* **39**, 2142.

Nguyen A. N. and Zinner E. (2004) Discovery of ancient silicate stardust in a meteorite. *Science* **303**, 1496-1499.

Nittler L. R. (2007) Presolar grain evidence for Low-Mass Supernova injection into the Solar Nebula. *Workshop on the Chronology of Meteorites and the Early Solar System, Kauai* **LPI Contribution No. 1374**, 125-126.

Nittler L. R., Alexander C. M. O. D., Gallino R., Hoppe P., Nguyen A. N., Stadermann F. J., and Zinner E. (2008) Aluminum-, Calcium- and Titanium-rich oxide stardust in ordinary chondrite meteorites. *The Astrophysical Journal* **682**, 1450-1478.

Nittler L. R., Alexander C. M. O. D., Gao X., Walker R. M., and Zinner E. (1997) Stellar saphires: The properties and origins of presolar Al2O3 in meteorites. *The Astrophysical Journal* **483**, 475-495.

Nittler L. R., Alexander C. M. O. D., Wang J., and Gao X. (1998) Meteoritic oxide grain from supernova found. *Nature* **393**, 222.

Nittler L. R. and Cowsik R. (1997) Galactic Age Estimates from O-rich Stardust in Meteorites. *Phys Rev Lett* **78**(2), 175-178.

Nollett K. M., Busso M., and Wasserburg G. J. (2003) Cool bottom processes on the thermally pulsing asymptotic giant branch and the isotopic composition of circumstellar dust grains. *The Astrophysical Journal* **582**, 1036-1058.

Nuth III J. A. and Ferguson F. T. (2006) Silicates do nucleate in Oxygen-rich Circumstellar Outflows: New Vapor Pressure Data for SiO. *The Astrophysical Journal* **649**, 1178-1183.

Posch T., Mutschke H., Trieloff M., and Henning T. (2007) Infrared spectroscopy of Calcium-Aluminium-rich inclusions: analog material for protoplanetary dust? *The Astrophysical Journal* **656**, 615-620.

Rietmeijer F. J. M., Nuth III J. A., Karner J. M., and Hallenbeck S. L. (2002) Gas-to-solid condensation in a Mg-SiO-H2-O2 vapor: metastable eutectics in the MgO-SiO2 phase diagram. *Physical Chemistry Chemical Physics* **4**, 546-551.

Sogawa H. and Kozasa T. (1999) On the origin of crystalline silicate in circumstellar envelopes of oxygen-rich asymptotic giant branch stars. *The Astrophysical Journal* **516**, L33-36.

Stadermann F. J. and Floss C. (2008) Abundance of presolar grains in comet Wild 2 and implications for transport and mixing in the Solar Nebula. *Lunar and planetary science conference* **39**, 1889.

Stadermann F. J., Floss C., and Lea A. S. (2006a) Using Auger Spectroscopy to characterize sub-micrometer presolar grains in situ: an overview. *Lunar and Planetary Science Conference*.

Stadermann F. J., Floss C., and Wopenka B. (2006b) Circumstellar aluminum oxide and silicon carbide in interplanetary dust particles. *Geochimica et Cosmochimica Acta* **70**, 6168-6179.

Stancliffe R. J. and Jeffery C. S. (2007) Mass loss and yield uncertainty in low-mass asymptotic giant branch stars. *Monthly Notices of the Royal Astronomical Society* **375**(4), 1280-1290.

Stencel R. E., Nuth III J. A., Little-Marenin I. R., and Little S. (1990) The formation and annealing of circumstellar dust, as gauged by IRAS low-resolution spectra and microwave maser chronology. *The Astrophysical Journal* **350**, L45-L48.

Stroud R. M., Nittler L. R., and Alexander C. M. O. D. (2004) Polymorphism in presolar Al2O3 grains from asymptotic giant branch stars. *Science* **305**, 1455-1457.

Takigawa A., Tachibana S., and Nagahara H. (2008) Effects of anisotropic evaporation of circumstellar forsterite on infrared spectra. *Lunar and planetary science conference* **39**, abstr.# 1523.

Tielens A. G. G. M., McKee C. F., Seab C. G., and Hollenbach D. J. (1994) The physics of grain-grain collisions and gas-grain sputtering in interstellar shocks. *The Astrophysical Journal* **431**, 321.

Tonotani A., Kobayashi S., Nagashima K., Sakamoto N., Russell S. S., Itoh S., and Yurimoto H. (2006) Presolar grains from primitive ordinary chondrites. *Lunar and planetary science conference* **37**, abstr.#1539.

Travaglio C., Gallino R., Amari S., Zinner E., Woosley S., and Lewis R. S. (1999) Low-density graphite grains and mixing in type II supernovae. *The Astrophysical Journal* **510**, 325-354.

Vollmer C., Hoppe P., and Brenker F. E. (2008) Si isotopic compositions of Presolar Silicate Grains from Red Giant Stars and Supernovae. *The Astrophysical Journal* **684**, 611-617.

Vollmer C., Hoppe P., Brenker F. E., and Holzapfel C. (2007a) Stellar MgSiO3 perovskite: a shock-transformed stardust silicate found in a meteorite. *The Astrophysical Journal* **666**, L49-L52.

Vollmer C., Hoppe P., Brenker F. E., and Palme H. (2006) A complex presolar grain in Acfer 094 - fingerprints of a circumstellar condensation sequence? *Lunar and Planetary Science Conference* **37**, 1284.

Vollmer C., Stadermann F. J., Bose M., Floss C., Hoppe P., and Brenker F. E. (2007b) Auger Analysis of Presolar Silicates in Acfer 094 & the Discovery of a Presolar CAI. *Annual Meeting of the Meteoritical Society* **70**, abstr.#5107.

Wasserburg G. J., Boothroyd A. I., and Sackmann I.-J. (1995) Deep circulation in red giant stars: a solution to the carbon and oxygen isotope puzzles? *The Astrophysical Journal* **447**(L37-40).

Wasson J. T. (2008) Evaporation of nebular fines during chondrule formation. *Icarus* **195**, 895-907.

Wirth R. (2004) Focused Ion Beam (FIB): A novel technology for advanced application of micro- and nanoanalysis in geosciences and applied mineralogy. *European Journal of Mineralogy* **16**(6), 863-876.

Yada T., Floss C., Stadermann F. J., Zinner E., Nakamura T., Noguchi T., and Lea A. S. (2008) Stardust in Antarctic Micrometeorites. *Meteoritics and Planetary Science* **in press**.

Yada T., Stadermann F. J., Floss C., Zinner E., Olinger C. T., Graham G. A., Bradley J. P., Dai Z. R., Nakamura T., Noguchi T., and Bernas M. (2005) Discovery of abundant presolar silicates in subgroups of antarctic micrometeorites. *Lunar and Planetary Science Conference* **36**, 1227.

Zega T. J., Nittler L. R., Busemann H., Hoppe P., and Stroud R. M. (2007) Coordinated isotopic and mineralogic analyses of planetary materials enabled by in situ lift-out with a focused ion beam scanning electron microscope. *Meteoritics and Planetary Science* **42**(7/8), 1373-1386.

5 Stellar MgSiO$_3$-Perovskite: a shock transformed stardust silicate found in a meteorite

Christian Vollmer[1*], Peter Hoppe[1], Frank E. Brenker[2] and Christian Holzapfel[3]

[1]Max Planck Institute for Chemistry, Particle Chemistry Dept., 55020 Mainz, Germany; [2]Geoscience Institute / Mineralogy, Goethe-University of Frankfurt, 60054 Frankfurt, Germany; [3]Institute for Functional Materials, Saarland University, 66041 Saarbrücken, Germany, *present address*: Schleifring und Apparatebau GmbH, Am Hardtanger 10, 82256 Fürstenfeldbruck, Germany.

Abstract

We have discovered an isotopically highly anomalous MgSiO$_3$-grain in the ungrouped carbonaceous chondrite Acfer 094 with a perovskite-like crystal structure resembling the dominant high pressure mineral of the Earth`s lower mantle. Oxygen isotopic ratios of the silicate grain are $^{17}O/^{16}O = 4.91 \pm 0.36 \times 10^{-3}$ (12x the solar value) and $^{18}O/^{16}O = 1.36 \pm 0.19 \times 10^{-3}$ (0.4x the solar value). This signature points to condensation in the ejecta of a ~2 M$_\odot$, close-to-solar metallicity red giant branch (RGB) or asymptotic giant branch (AGB) star. Alternatively, the grain could have formed in the ejecta of a nova, in which ^{17}O is highly overabundant. TEM analysis of the grain revealed a high pressure perovskite-like crystal structure not predicted by equilibrium condensation in low pressure stellar environments. A possible formation scenario is transformation of a silicate precursor triggered by a shock wave, either in the interstellar medium (ISM) or originating from the grain`s parent star. Shock waves must thus be considered as a potential mechanism to recrystallize silicates, or even convert them into high pressure structures. Alternatively, non-equilibrium condensation or crystallization by a chemical vapor deposition (CVD)-like process, also invoked for the formation of nanodiamonds, is a distinct possibility, although more speculative.

Subject headings: circumstellar matter --- shock waves --- stars: winds, outflows --- stars: late-type --- astrochemistry --- ISM: kinematics and dynamics

5.1 Introduction

Our solar system formed from the collapse of a molecular cloud to which several stellar sources such as RGB and AGB stars, novae and supernovae contributed dust. Whereas the majority of this circumstellar dust equilibrated isotopically during solar system formation, a tiny portion of grains escaped this homogenization. These "presolar" grains are recognized in primitive meteorites and interplanetary dust particles (IDPs) by their anomalous isotopic compositions. The laboratory study of these pristine samples has provided a wealth of information about their stellar sources (e.g., LODDERS and AMARI, 2005).

Among the presolar grains identified to date are diamond, silicon carbide (SiC), silicon nitride (Si_3N_4), graphite, corundum (Al_2O_3), titanium oxide (TiO_2), hibonite ($CaAl_{12}O_{19}$), spinel ($MgAl_2O_4$), and recently discovered silicates.

Silicates were detected in the disks and outflows of young and evolved stars by infrared spectroscopy over a decade ago (e.g., WATERS et al., 1996). Searches for presolar silicates in primitive solar system materials remained unsuccessful for a long time. Only new developments in high spatial resolution mass spectrometry have made their identification possible (MESSENGER et al., 2003). It is now well established that presolar silicates are the most abundant presolar grain species besides nanodiamonds. Matrix normalized abundances of up to 810 ppm for isotopically primitive IDPs (FLOSS et al., 2006) and of up to 200 ppm for primitive meteorites (NGUYEN et al., 2007; VOLLMER et al., 2007) have been reported.

Presolar grains not only provide isotopic information about their stellar sources, but also allow the testing of grain condensation and transformation models in circumstellar environments and in the ISM. Whereas presolar minerals such as nanodiamond, graphite, SiC and Al_2O_3 have been well-studied by transmission electron microscopy (TEM) (DAULTON et al., 1996; DAULTON et al., 2002; CROAT et al., 2003; STROUD et al., 2004), structural information on presolar silicates is very limited. From more than a hundred presolar silicates found so far, structural information obtained by TEM is available for only nine grains, of which seven are amorphous and two are olivine (MESSENGER et al., 2005 and references therein; FLOSS et al., 2006; VOLLMER et al., 2007). Thermodynamic models for gas-solid condensation of silicates in O-rich stellar ejecta, calculated for low pressure – high temperature conditions, lead to forsterite (Mg_2SiO_4) and enstatite ($MgSiO_3$) as the first silicates to condense (e.g., LODDERS and AMARI, 2005). Astronomical observations can be used to evaluate the predictions of these models. There, chemical and mineralogical information is obtained by comparing infrared spectra with spectra of synthetic particles produced in the laboratory (e.g., RIETMEIJER et al., 2002). The spectra of O-rich stars show the presence of both amorphous and crystalline silicates, though amorphous silicates comprise the larger fraction in most astrophysical settings (MOLSTER et al., 2002). In the ISM, crystalline silicates have not been detected yet and their abundance is estimated not to exceed a few percent (KEMPER et al., 2005). It is unclear whether this is the result of destruction in the ISM (e.g., MOLSTER et al., 2002) or an observational bias. Also, it is still unknown whether silicates nucleate homogeneously from the gas phase, although this is thermodynamically difficult, or whether they accrete onto previously condensed seed nuclei, such as TiO_2 or Al_2O_3. Only microstructural and analytical data acquired in the laboratory from these grains can help to answer these questions. Here we report the results of the first coordinated NanoSIMS/TEM analysis of a presolar crystalline $MgSiO_3$ phase.

5.2 Experimental

The presolar silicate was detected in a thin section of the Acfer 094 meteorite. This ungrouped carbonaceous chondrite has not suffered aqueous or thermal alteration, resulting in an exceptionally good preservation of presolar material (GRESHAKE, 1997; NGUYEN et al., 2007; VOLLMER et al., 2007). The grain was identified by oxygen isotope mapping of a polished thin section of the meteorite with the

NanoSIMS ionprobe at the Max Planck Institute for Chemistry in Mainz. A focused Cs⁺ ion beam (< 100 nm, ~1 pA) was rastered over a large number of fine-grained matrix areas, each 10x10 μm² in size. Negative secondary ions of ^{16,17,18}O, ^{28}Si and ^{27}Al^{16}O were simultaneously detected and converted to 256x256 pixel ion images. The presolar silicate was identified by its anomalous isotopic composition (Fig. 5.1).
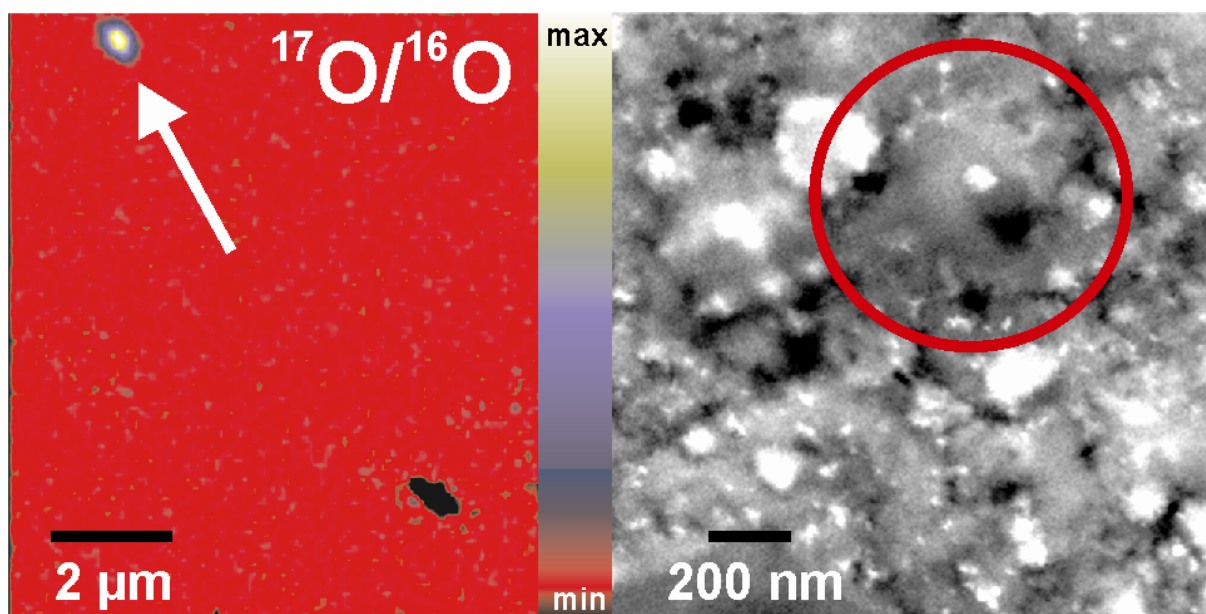

Figure 5. 1 Morphology of grain 1_07

NanoSIMS ^{17}O/^{16}O ion image of a 10x10 μm² field (left) and the corresponding SEM image of the relocated grain (right). Grain 1_07 clearly stands out by its extreme enrichment in ^{17}O.

After NanoSIMS analysis, we prepared the grain for TEM studies with the focused ion beam (FIB) technique. This technique utilizes a Ga⁺ ion beam to remove specimens site-specific on a nanometer scale (e.g., WIRTH, 2004). We worked with a Dual Beam Workstation (FEI Strata DB 235) equipped with an in-situ nanomanipulator (Kleindiek MM3A). Structural and chemical investigations were done on a 200 kV TEM (Phillips CM 200). We performed bright and dark field imaging, selected area electron diffraction (SAED) and energy-dispersive x-ray (EDX) analyses on the grain to identify its crystal structure and to determine its chemistry. For EDX analysis, the probe was focused onto the grain and spectra were acquired for 100 s using an ultra thin window EDX spectrometer (EDAX). The spectra were quantified using standard background corrections and Cliff-Lorimer thin-film techniques. K-factors were obtained from mineral standards. Interplanar spacings were calculated from the SAED patterns using a camera constant, which was calibrated against synthetic standards and a natural clinopyroxene within the same FIB section.

5.3 Results

The ~500 nm sized grain ("1_07") shows an extreme ^{17}O enrichment of 12 times the solar abundance and a moderate ^{18}O depletion ($^{17}O/^{16}O = 4.91 \pm 0.36$ x 10^{-3}, $^{18}O/^{16}O = 1.36 \pm 0.19$ x 10^{-3}). This ^{17}O enrichment is among the highest observed in a presolar silicate found so far. Simultaneously acquired negative secondary ion images of the three O isotopes, ^{28}Si and $^{27}Al^{16}O$ indicate that the grain is a silicate and not an Al-rich oxide such as spinel or corundum.

The strong diffraction contrast of the grain in TEM bright field imaging mode even during tilting of the sample points to a highly crystalline phase (Fig. 5.2).
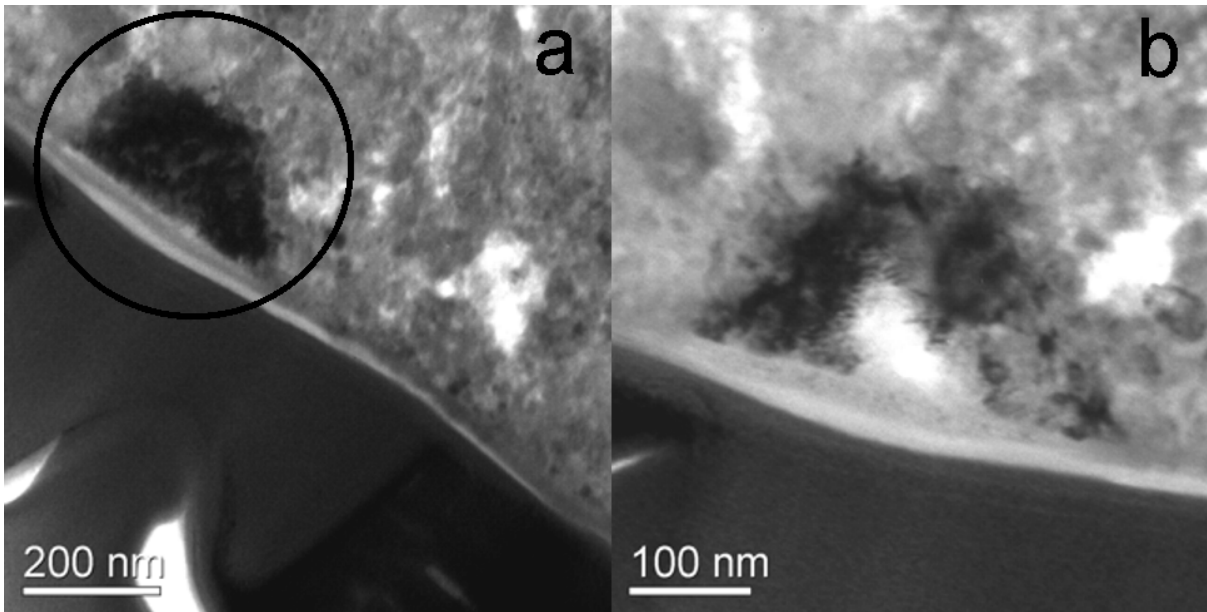
Figure 5. 2 TEM micrograph of grain 1_07 before and after EDX point measurements
It could be easily relocated in the FIB section because of its strong diffraction contrast in the bright field image. A disrupted sputtered edge and some contrast difference in the center is visible. The two amorphized areas of the EDX point measurements can be clearly identified.

Bragg diffraction exhibits sharp and well defined spots indicative of a single crystal (Fig. 5.3). The recorded zone axis pattern (ZAP) could not be indexed to any common pyroxene, olivine modification, or hydrous Mg-Si-O-structure. The best fit was obtained by applying the lattice constants of high pressure MgSi-Perovskite with space group Pbnm (SUGAHARA et al., 2006), the most abundant silicate phase of the Earth´s lower mantle (see e.g., HEMLEY and COHEN, 1992 for review). This MgSiO₃ modification is stable only above ~23 GPa at ~1300 K. The observed b- and c-axis very accurately match the calculated values (Fig. 3). We have to note that it was not possible to obtain a complete set of ZAPs for a comprehensive structural analysis of the grain. However, the observed d-values can be regarded as a clear fingerprint of a silicate perovskite-like structure. The only difference between the silicate grain analyzed here and the lower mantle perovskite structure is the presence of reflections of the type h0l with h+l=2n+1 and 0kl with k=2n+1, which should be absent in a structurally undisturbed MgSi-Perovskite. From dark field imaging, SAED or the recorded lattice fringes, both double diffraction and polysynthetic

twinning (MADON et al., 1989) seem unlikely to account for this observation. Instead, a supercell structure of double-sized cell parameters might be a better explanation. This structure has also been proposed for synthetic MgSiO₃-perovskite from high pressure experiments in order to explain extra peaks (WALTER et al., 2004 and references therein), and is a well known feature of thin film perovskite structures (BANERJEE et al., 2001).
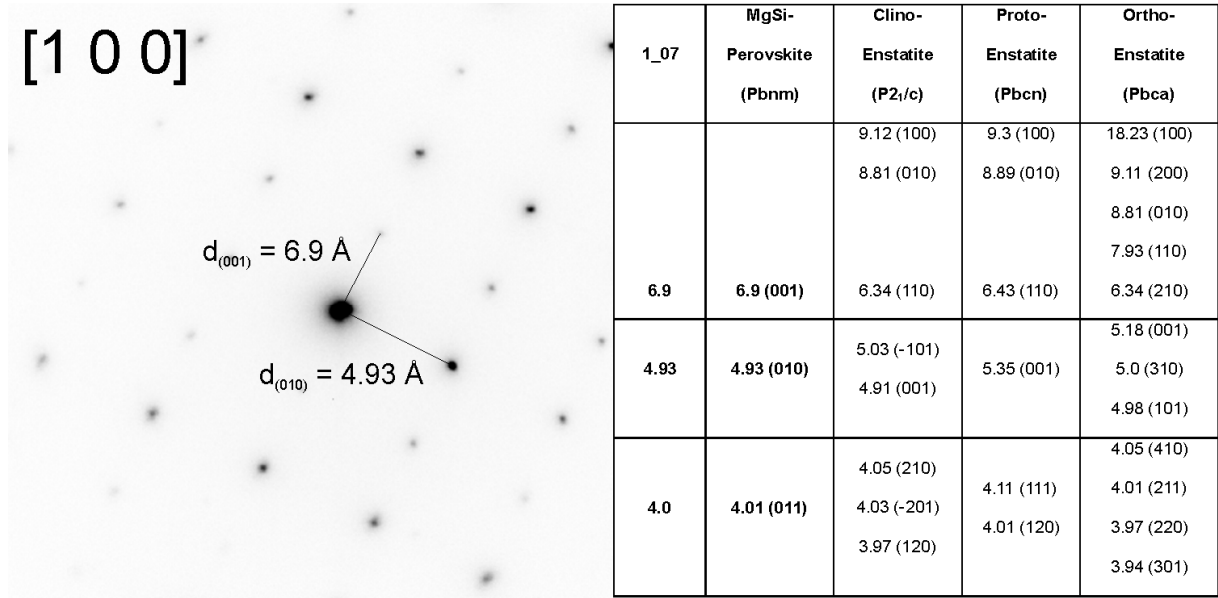

1_07	MgSi-Perovskite (Pbnm)	Clino-Enstatite (P2₁/c)	Proto-Enstatite (Pbcn)	Ortho-Enstatite (Pbca)
		9.12 (100)	9.3 (100)	18.23 (100)
		8.81 (010)	8.89 (010)	9.11 (200)
				8.81 (010)
				7.93 (110)
6.9	6.9 (001)	6.34 (110)	6.43 (110)	6.34 (210)
4.93	4.93 (010)	5.03 (-101)	5.35 (001)	5.18 (001)
		4.91 (001)		5.0 (310)
				4.98 (101)
4.0	4.01 (011)	4.05 (210)	4.11 (111)	4.05 (410)
		4.03 (-201)	4.01 (120)	4.01 (211)
		3.97 (120)		3.97 (220)
				3.94 (301)

Figure 5. 3 SAED pattern of grain 1_07

Bragg diffraction spots are well defined with no sign of a second phase present. The table compares the corresponding d-values (in Å) with those of common MgSiO₃-modifications (space groups in brackets) down to 4 Å. The only possible fit without assuming an extreme distortion of the main axes is MgSi-Perovskite. Measured d-value error is ±0.04 Å.

EDX point measurements on the center and the rim showed that the grain consists of a very pure, nearly FeO-free (~1 mol.% FeO) MgO-silicate. Minor elements expected in presolar silicates, such as Al or Ca, were all below the detection limit of ~0.5 wt.%. Only along the grain rim does EDX analysis give the expected stochiometric Mg:Si ratio of 1:1, whereas the center is characterized by a Mg enrichment relative to Si of ~24%. This Mg enrichment remains unexplained, as the measured ratio does not fit into any common silicate structure. However, given the observation of a possible supercell structure, the grain may not necessarily have a stochiometric composition. Amorphization during EDX point measurements occurred rather rapidly (Fig. 5.2), supporting the absence of common silicates such as olivine or pyroxene, which are stable under electron irradiation.

5.4 Discussion

5.4.1 Isotopic composition

Most presolar silicates and oxides found so far fall within the four O isotope groups defined by NITTLER et al. (1997) and originate mainly from RGB/AGB stars with different masses and metallicities according

to models of stellar nucelosynthesis and evolution (BOOTHROYD and SACKMANN, 1999). In the context of these models, grain 1_07 formed in a star of ~2 times the solar mass and close-to-solar metallicity. As the measured oxygen isotopic ratios of submicrometer-sized presolar grains are usually lower limits due to possible isotopic dilution with surrounding solar system material (NGUYEN et al., 2007), the true isotopic composition is possibly even more extreme. If this were the case, condensation in nova ejecta, in which ^{17}O is highly overabundant (JOSÉ et al., 2004), is an alternative possibility. Analysis of the Si isotopic composition of grain 1_07 could allow to distinguish between an RGB/AGB star or a nova as the stellar source of the grain. Unfortunately, there is no material left for such an analysis. A third possibility is an origin in a very massive (> 4 M$_\odot$) red giant star that has experienced hot bottom burning. This scenario has been proposed for a highly ^{17}O enriched presolar Al$_2$O$_3$ grain (NITTLER et al., 1997) and a presolar spinel grain (LUGARO et al., 2007). However, this process also results in massive destruction of ^{18}O (^{18}O/^{16}O < 10^{-6}), and as such a strong ^{18}O depletion is not seen in grain 1_07, even after considering dilution with surrounding material, this possibility can be excluded.

5.4.2 Mineralogy

The formation of crystalline silicates in diverse astrophysical settings such as protoplanetary disks and ejecta of late-type stars is still a matter of debate (SCOTT and KROT, 2005; BROWNLEE et al., 2007 and references therein). Direct condensation from a vapor phase or annealing in the hot inner regions of the stellar environment, followed by turbulent diffusion, have been proposed by several authors (e.g., GAIL, 2004). Alternatively, annealing of silicate precursors in nebular or circumstellar shock waves at large distances from the central star has been hypothesized as a possible in-situ mechanism to form crystalline silicates (HARKER and DESCH, 2002). A third possibility has been proposed by MOLSTER et al. (1999), who speculate about a low temperature process for silicate crystallization. These authors explain infrared bands of crystalline silicates observed in stellar environments too cold for annealing by an in-situ process probably induced by high energy particles (CARREZ et al., 2002). However, the nature of this process is not specified.

Grain 1_07 does not have a crystal structure predicted by thermodynamic condensation models of low pressure stellar environments. Therefore, the formation of this silicate directly from the gas phase in the hot inner region of the parent star can be ruled out. A stellar high pressure silicate instead points to formation by shock. The origin of the shock pressure regime in which grain 1_07 formed can not be unequivocally constrained from our data. In the following we will discuss potential astrophysical environments in which the shock transformation might have occurred.

Shock transformation on the Acfer 094 parent body due to impacts must be excluded, as extensive studies have shown that the matrix of Acfer 094 is not affected by shock metamorphism (GRESHAKE, 1997). It would also be highly improbable that an impact generated shock would transform only a presolar grain, and not the surrounding matrix. Also, transformation of the grain by accretion shocks in the solar nebula shortly before parent body incorporation is problematic: Shock transformation of isolated grains like 1_07 should have been found in larger quantities of solar system materials.

The dynamics of dust transformation in interstellar shocks has been studied in detail (JONES et al., 1994; TIELENS et al., 1994; JONES et al., 1996; JONES et al., 1997; JONES, 2004). In shock waves, energetic grain-grain collisions and collisions between gas atoms/ions and dust grains lead to the loss of grain mass to the gas, and to changes in the grain size distribution. The evolution of large interstellar dust grains in shocks is dominated by the effects of fragmentation due to grain-grain collisions. Fragmentation may be accompanied by phase transformation because the grains achieve pressures high enough for silicate re-crystallization and transformation, at least for a small fraction of the target grain (TIELENS et al. 1994; JONES et al. 1996). Whether there are specific conditions where this is possible also for complete large grain fragments remains to be seen. Grain 1_07 might be an example of a stellar silicate which was converted to a highly crystalline perovskite-like structure by an interstellar shock. Clearly, more theoretical modeling is needed to explore the possibility of phase transformation in grain-grain collisions for grains of the size of grain 1_07 in more detail.

An alternative to an interstellar origin are shock waves in the direct vicinity of the parent star. Expanding shells around stars in the post-AGB phase drive strong shock fronts through previously expelled dust at velocities similar to interstellar shock waves (see LODDERS and AMARI, 2005 and references therein). The dust is thought to be destroyed effectively, yet it is still observed in the subsequent planetary nebula phase. As for the interstellar shock origin it remains to be seen whether future dust evolution models will be able to account for fragmentation and simultaneous phase transformation of large grains by stellar shock fronts.

Grain 1_07 could also have formed in the ejecta of an ONe or CO nova, thereby explaining the observed high ^{17}O enrichment (JOSÉ et al., 2004). The thermonuclear runaway explosion on the white dwarf of the binary system would drive a strong shock front through previously or simultaneously condensed silicates, allowing possible phase transformations. Enstatite is also expected to be the most abundant silicate phase to condense in nova ejecta (JOSÉ et al., 2004).

During shock, partial vaporization may have altered the grain's chemistry by removing Mg from the grain´s surface which has been observed in irradiated GEMS grains (BRADLEY, 1994). Shock cooling timescales are on the order of ~10^{-12} s (TIELENS et al., 1987), which is too short for diffusive re-equilibration of overabundant MgO with $MgSiO_3$ to form Mg_2SiO_4. Temperature decrease in the post shock must have been sufficiently fast to quench the silicate perovskite structure. It is interesting to note that Mg-rich grains like grain 1_07 are more easily annealed than their Fe-rich counterparts (HARKER and DESCH, 2002). The discovery of $MgSiO_3$-perovskite in a shock vein of the Tenham meteorite (TOMIOKA and FUJINO, 1997) proves that transformation of silicate precursors into the perovskite structure under non-static conditions in a shock front is indeed possible. Shock transformation must therefore be regarded as a viable mechanism for silicate re-crystallization in some parts of the ISM or circumstellar environments.

In contrast to shock, a more speculative mechanism could be specific low temperature formation conditions proposed by MOLSTER et al. (1999). Unusual crystal structures have been found in IDPs (DAI and BRADLEY, 2001), where a cubic sulfide phase documented by TEM presumably condensed from a

low temperature vapor. Recent TEM analysis of a Mg-enriched presolar Al_2O_3 grain also revealed a crystal structure not predicted by equilibrium condensation models (STROUD et al., 2007). Circumstellar nanodiamonds are thought to have formed largely by a non-equilibrium process similar to chemical vapor deposition (CVD) (DAULTON et al., 1996). Certainly, these observations do not indicate that $MgSiO_3$-perovskites behave similarly; however, thin film experiments demonstrate that cubic perovskites can grow onto MgO-periclase seeds (CHERN and CHENG, 1999). Grain 1_07 could have formed in an analogous way, which could explain the enhanced Mg concentration in the center of the grain. A low dust temperature (100 – 250 K) is also a general feature of crystalline silicate observations (MOLSTER et al., 2002) and superlattice structures often indicate low temperature ordering processes (WILLIAMS and CARTER, 1996). To explore the possibility of formation of grain 1_07 by low temperature formation conditions it would be desirable that possible p-T-conditions for silicate perovskite condensation are examined in future studies.

Infrared bands in the spectra of evolved stars and other astrophysical environments are generally attributed to well-known phases. It should be examined whether infrared bands of orthorhombic MgSi-Perovskite could explain unidentified dust features or even infrared bands normally ascribed to orthorhombic enstatite. Furthermore, future TEM investigations of presolar silicates might reveal similar transformed structures. It is therefore possible that grain 1_07 represents a larger population of silicate stardust.

5.5 References

Banerjee R., Purandare S. C., Palkar V. R., and Pinto R. (2001) Effect of silicon on the microstructure of pulsed laser ablated ferroelectric PbTiO3 thin films. *Journal of Physics D: Applied Physics* **34**, 1037-1043.

Boothroyd A. I. and Sackmann I.-J. (1999) The CNO isotopes: Deep circulation in red giants and first and second dredge-up. *The Astrophysical Journal* **510**, 232-250.

Bradley J. P. (1994) Chemically anomalous, preaccretionally irradiated grains in interplanetary dust from comets. *Science* **265**(5174), 925-929.

Brownlee D. E., Joswiak D., Bradley J. P., and Matrajt G. (2007) The origin of crystalline silicates in comets and large scale mixing in the solar nebula. *Lunar and Planetary Science Conference* **38**, abstr.#2189.

Carrez P., Demyk K., Leroux H., and Cordier P. (2002) Low temperature crystallization of MgSiO3 glass under ionizing irradiation. *Lunar and Planetary Science Conference* **33**, abstr.#1459.

Chern G. and Cheng C. (1999) Interface matching in oxides of rocksalt/rocksalt(001) and rocksalt/perovskite (001). *Journal of Vacuum Science and Technology A* **17**(4), 1097-1102.

Croat T. K., Bernatowicz T. J., Amari S., Messenger S., and Stadermann F. J. (2003) Structural, chemical and isotopic microanalytical investigations of graphite from supernovae. *Geochimica et Cosmochimica Acta* **67**(24), 4705-4725.

Dai Z. R. and Bradley J. P. (2001) Iron-nickel sulfides in anhydrous interplanetary dust particles. *Geochimica et Cosmochimica Acta* **65**(20), 3601-3612.

Daulton T. L., Bernatowicz T. J., Lewis R. S., Messenger S., Stadermann F. J., and Amari S. (2002) Polytype distribution in circumstellar silicon carbide. *Science* **296**, 1852-1855.

Daulton T. L., Eisenhour D. D., Bernatowicz T. J., Lewis R. S., and Buseck P. R. (1996) Genesis of presolar diamonds: Comparative high-resolution transmission electron microscopy study of meteoritic and terrestrial nano-diamonds. *Geochimica et Cosmochimica Acta* **60**(23), 4853-4872.

Floss C., Stadermann F. J., Bradley J. P., Dai Z. R., Bajt S., Graham G., and Lea A. S. (2006) Identification of isotopically primitive interplanetary dust particles: A NanoSIMS isotopic imaging study. *Geochimica et Cosmochimica Acta* **70**, 2371-2399.

Gail H.-P. (2004) Radial mixing in protoplanetary accretion disks. IV. Metamorphosis of the silicate dust complex. *Astronomy and Astrophysics* **413**, 571-591.

Greshake A. (1997) The primitive matrix components of the unique carbonaceous chondrite Acfer 094: A TEM study. *Geochimica et Cosmochimica Acta* **61**(2), 437-452.

Harker D. E. and Desch S. J. (2002) Annealing of silicate dust by nebular shocks at 10 AU. *The Astrophysical Journal* **565**, L109-L112.

Hemley R. J. and Cohen R. E. (1992) Silicate Perovskite. *Annual Reviews Earth and Planetary Sciences* **20**, 553-600.

Jones A. P. (2004) Dust destruction processes. *Astrophysics of Dust, ASP conference series, edited by Adolf N. Witt, Geoffrey C. Clayton and Bruce T. Draine*, 347.

Jones A. P., Tielens A. G. G. M., and Hollenbach D. J. (1996) Grain shattering in shocks: The interstellar grain size distribution. *The Astrophysical Journal* **469**, 740-764.

Jones A. P., Tielens A. G. G. M., Hollenbach D. J., and McKee C. F. (1994) Grain destruction in shocks in the interstellar medium. *The Astrophysical Journal* **433**, 797-810.

Jones A. P., Tielens A. G. G. M., Hollenbach D. J., and McKee C. F. (1997) The propagation and survival of interstellar grains. *Astrophysical implications of the laboratory study of presolar materials.*

José J., Hernanz M., Amari S., Lodders K., and Zinner E. (2004) The imprint of nova nucleosynthesis in presolar grains. *The Astrophysical Journal* **612**, 414-428.

Kemper F., Vriend W. J., and Tielens A. G. G. M. (2005) Erratum: The absence of crystalline silicates in the diffuse interstellar medium. *The Astrophysical Journal* **633**(1), 534-534.

Lodders K. and Amari S. (2005) Presolar grains from meteorites: Remnants from the early times of the solar system. *Chemie der Erde* **65**, 93-166.

Lugaro M., Karakas A. I., Nittler L. R., Alexander C. M. O. D., Hoppe P., Iliadis C., and Lattanzio J. C. (2007) On the asymptotic giant branch star origin of peculiar spinel grain OC2. *Astronomy and Astrophysics* **461**, 657-664.

Madon M., Guyot F., Peyronneau J., and Poirier J. P. (1989) Electron microscopy of high-pressure phases synthesized from natural olivine in diamond anvil cell. *Physics and Chemistry of Minerals* **16**, 320-330.

Messenger S., Keller L. P., and Lauretta D. S. (2005) Supernova olivine from cometary dust. *Science* **309**, 737-741.

Messenger S., Keller L. P., Stadermann F. J., Walker R. M., and Zinner E. (2003) Samples of stars beyond the solar system: Silicate grains in interplanetary dust. *Science* **300**, 105-108.

Molster F. J., Waters L. B. F. M., and Tielens A. G. G. M. (2002) Crystalline silicate dust around evolved stars II. the crystalline silicate complexes. *Astronomy and Astrophysics* **382**, 222-240.

Molster F. J., Yamamura I., Waters L. B. F. M., Tielens A. G. G. M., de Graauw T., de Jong T., de Koter A., Malfait K., van den Ancker M. E., van Winckel H., Voors R. H. M., and Waelkens C. (1999) Low-temperature crystallization of silicate dust in circumstellar disks. *Nature* **401**, 563-565.

Nguyen A., Stadermann F. J., Zinner E., Stroud R. M., Alexander C. M. O. D., and Nittler L. R. (2007) Characterization of presolar silicate and oxide grains in primitive carbonaceous chondrites. *The Astrophysical Journal* **656**, 1223-1240.

Nittler L. R., Alexander C. M. O. D., Gao X., Walker R. M., and Zinner E. (1997) Stellar saphires: The properties and origins of presolar Al2O3 in meteorites. *The Astrophysical Journal* **483**, 475-495.

Rietmeijer F. J. M., Nuth III J. A., Karner J. M., and Hallenbeck S. L. (2002) Gas-to-solid condensation in a Mg-SiO-H2-O2 vapor: metastable eutectics in the MgO-SiO2 phase diagram. *Physical Chemistry Chemical Physics* **4**, 546-551.

Scott E. R. D. and Krot A. N. (2005) Thermal processing of silicate dust in the solar nebula: clues from primitive chondrite matrices. *The Astrophysical Journal* **623**, 571-578.

Stroud R. M., Nittler L. R., and Alexander C. M. O. D. (2004) Polymorphism in presolar Al2O3 grains from asymptotic giant branch stars. *Science* **305**, 1455-1457.

Stroud R. M., Nittler L. R., Alexander C. M. O. D., and Zinner E. (2007) Transmission Electron Microscopy and Secondary Ion Mass Spectrometry of an unusual Mg-rich presolar Al2O3 grain. *Lunar and Planetary Science Conference* **38**, abstr.# 2203.

Sugahara M., Yoshiiasa A., Komatsu Y., Yamanaka T., Bolfan-Casanova N., Nakatsuka A., Sasaki S., and Tanaka M. (2006) Reinvestigation of the MgSiO3 perovskite structure at high pressure. *American Mineralogist* **91**, 533-536.

Tielens A. G. G. M., McKee C. F., Seab C. G., and Hollenbach D. J. (1994) The physics of grain-grain collisions and gas-grain sputtering in interstellar shocks. *The Astrophysical Journal* **431**, 321.

Tielens A. G. G. M., Seab C. G., Hollenbach D. J., and McKee C. F. (1987) Shock processing of interstellar dust: diamonds in the sky. *The Astrophysical Journal* **319**, L109-L113.

Tomioka N. and Fujino K. (1997) Natural (Mg,Fe)SiO3-Ilmenite and -Perovskite in the Tenham Meteorite. *Science* **277**, 1084-1086.

Vollmer C., Hoppe P., Brenker F. E., and Holzapfel C. (2007) A presolar silicate trilogy: condensation, coagulation, transformation - new insights from NanoSIMS/TEM investigations. *Lunar and Planetary Science Conference* **38**, 1262.

Walter M. J., Kubo A., Yoshino T., Brodholt J., Koga K. T., and Ohishi Y. (2004) Phase relations and equation-of-state of aluminous Mg-silicate perovskite and implications for Earth´s lower mantle. *Earth and Planetary Science Letters* **222**, 501-516.

Waters L. B. F. M., Molster F. J., De Jong T., Beintema D. A., Waelkens C., Boogert A. C. A., Boxhoorn D. R., De Graauw M. S., Drapatz S., Feuchtgruber H., Genzel R., Helmich F. P., Heras A. M., Huygen R., Izumiura H., Justtanont K., Kester D. J. M., Kunze D., Lahuis F., Lamers H. J. G. L. M., Leech K. J., Loup C., Lutz D., Morris P. W., Price S. D., Roelfsema P. R., Salama A., Schaeidt S. G., Tielens A. G. G. M., Trams N. R., Valentijn E. A., Vandenbussche B., Van den Ancker M. E., Van Dishoeck E. F., Van Winckel H., Wesselius P. R., and Young E. T. (1996) Mineralogy of oxygen-rich dust shells. *Astronomy and Astrophysics* **315**, L361-364.

Williams D. B. and Carter C. B. (1996) *Transmission Electron Microscopy*. Plenum Press.

Wirth R. (2004) Focused Ion Beam (FIB): A novel technology for advanced application of micro- and nanoanalysis in geosciences and applied mineralogy. *European Journal of Mineralogy* **16**(6), 863-876.

A final remark on the discovery of grain 1_07:

There is a philosophical irony in the fact, that a high-pressure mineral, known from the interior of the Earth, is found as a presolar mineral, because:

"We are searching for grains from faraway stars, but what we find, is the most abundant mineral of our planet Earth."

6 Summary and Outlook

In this work, I have analyzed silicate and oxide stardust grains from different stellar sources, detected in the carbonaceous chondrite Acfer 094, by a variety of high spatial resolution analysis techniques: The oxygen and silicon isotopic compositions of a large number of grains have been measured by NanoSIMS, their morphologies and sizes were determined by scanning electron microscopy (SEM), their chemical compositions were analyzed by Auger electron microscopy (AES), and finally, their microstructural constitutions were investigated by combined focused ion beam/transmission electron microscopy (FIB/TEM) studies. This is the first time that such a complete set of silicate and oxide stardust grains from the same meteorite were analyzed by this range of methods. Silicates are the most abundant type of dust grains condensing around oxygen-rich dying stars (red giant stars and nova/supernova explosions) and have been a major constituent of the molecular cloud, from which our solar system formed. Thus, by determining the origins and formation histories of these "stardust" or "presolar" silicates, the evolution and inventory of the material that formed our sun and the planets can be investigated. Their characteristic fingerprints are extreme isotopic anomalies, which can not be achieved by any mechanism in the solar system, but only by nucleosynthetic reactions occurring in stellar interiors. They are true circumstellar condensates, that survived the formation and evolution of the solar system nearly intact and are thus the only samples available to investigate the stellar sources, that injected material into the solar nebula. Furthermore, astrophysical problems, such as dust condensation in circumstellar environments, dust transformation in the interstellar medium, the Galactic chemical evolution of the elements, which are otherwise only accessible by observational and theoretical work, can be tested directly in a terrestrial laboratory by high-precision analytical techniques.

In this work, I have shown that the majority of silicate stardust grains derive from red giant stars of $1 - 2.5$ $M_\odot$ and close-to-solar or slightly lower-than-solar metallicity (=the fraction of elements heavier than He in a star, which is coupled to the age of the Galaxy), and therefore similar sources as the majority of oxide stardust grains. However, by measuring the Si isotopic compositions of 40 presolar silicates, I could show that about 10% of all grains, i.e., silicates with an enrichment in ^{18}O and ^{28}Si relative to solar, most likely originate in type II supernova explosions ("Core Collapse SNe"). This gave strong support to already existing ideas about the origins of this class of presolar silicates and oxides, and also proved that the dust formation efficiency in SNeII, which is a current topic in modern astrophysics, is more effective than previously thought. The Si isotope measurements also quantified the evolution of the secondary isotopes ^{29}Si and ^{30}Si (relative to the primary isotope ^{28}Si) by slow neutron capture reactions ("*s*-process") in asymptotic giant branch stars, which was previously only known from nuclear physics and the measurement of presolar SiC grains. However, comparison of the Si isotopes of presolar silicates from AGB stars with those of presolar SiC grains provide a more direct measure for the quantification of the *s*-process on the Si isotopes. I could also show that there is a sub-class of presolar silicates characterized by an extreme enrichment of ^{17}O and also by a moderate enhancement of ^{30}Si relative to solar, whose origins might be explained by formation in binary systems consisting of a white dwarf or a red giant and a main

sequence star. As binary systems constitute about 50% of all stars (DUQUENNOY and MAYOR, 1991), it is not unrealistic that a small portion of stardust grains derive from such sources.

I also investigated the morphologies, sizes and distribution of silicate and oxide stardust in Acfer 094 and could show, that the majority of grain morphologies are consistent with what is expected from condensation experiments. However, a lot of grains are altered by inclusion of Fe-rich minerals, whose origins can not be constrained on the basis of this work and remain enigmatic. The distribution of stardust grains was investigated for the first time on such a large sample set, and it could be shown that a distinct clustering of stardust grains speaks for an extremely heterogeneous solar nebula or small-scale fragmentation processes. The abundance of silicate stardust in Acfer 094 is among the highest reported so far for any primitive solar system material and furthermore stresses the extraordinary scientific value of this meteorite, which is among the most pristine samples available for studies on the origins of the solar system.

I also measured the elemental contents of 69 grains by AES and could show that the majority of grains are Fe-rich, but this could be due to secondary Fe alteration, and might not necessarily be a primary condensation feature. Some grains were detected with rather atypical, non-stochiometric compositions (i.e., Mg-poor and Mg-rich), which point to unusual formation conditions under non-solar gas compositions. One of the most interesting results of this work was the detection of complex presolar grains consisting of refractory Al-rich grains attached to silicate material. These composite grains most likely represent condensation sequences and have been predicted by condensation theory (SOGAWA and KOZASA, 1999) and observational evidence (DIJKSTRA et al., 2005). These grains were the first findings of this type and gave support to astrophysical assumptions.

Up to this research project, combined NanoSIMS/TEM data on presolar silicates were available for only seven grains (MESSENGER et al., 2003; MESSENGER et al., 2005; NGUYEN, 2005; YADA et al., 2005; FLOSS et al., 2006), by the end of this project this database has increased to 15 grains (KELLER and MESSENGER, 2008; NGUYEN and NITTLER, 2008; STROUD et al., 2008). In this work, nine grains were successfully analyzed by combined NanoSIMS/TEM studies. The majority of grains were found to be Mg-rich and amorphous, which is in contrast to astrophysical evidence, which mainly predict crystalline Mg-rich and amorphous Fe-rich circumstellar condensates. However, the grains might have been rendered amorphous by secondary processes or could have formed under non-equilibrium, low-temperature conditions in the circumstellar outflow. The detected crystalline presolar silicates in this study and in other work are nearly all olivines, whereas the amorphous grains more likely exhibit a pyroxene-like stochiometry. This important result points to different formation pathways for these two types of grains and could be explained by condensation theory: Whereas forsterite is the first stable silicate phase to condense, enstatite forms by reaction of forsterite with gaseous Si-O. This could lead to weak or no crystallinity of the later forming enstatite at lower temperatures. However, the relatively high Fe content of three detected presolar olivines (MESSENGER et al., 2005; KELLER and MESSENGER, 2008; this study) is in contrast to astrophysical evidence and theoretical considerations, which predict essentially Fe-free crystalline grains. This again speaks for different formation pathways than theory and observation expect

and underlines the importance of these microstructural investigations. One important finding in this respect is the discovery of a presolar crystalline silicate with a high-pressure perovskite-like structure (grain 1_07) neither predicted by condensation theory nor by models on dust evolution in the interstellar medium. Usually it is assumed that grains are rendered amorphous, shattered into smaller fragments or completely vaporized during grain-grain or grain-gas collisions in an interstellar shock wave. The discovery of a high-pressure phase of presolar origin shows that dust grains encountering interstellar shocks might not necessarily be destroyed, but can be transformed to high-pressure modifications. This process was also initially proposed as a formation mechanism for presolar nanodiamonds (TIELENS et al., 1987), although further work showed that a chemical vapor deposition (CVD) process might be a more probable formation pathway (DAULTON et al., 1996). A CVD-like process might as well explain the existence of the perovskite-like silicate of presolar origin, which is a highly speculative, but still exciting possibility different from the shock transformation scenario, but this has to be tested by theoretical modeling.

Silicate stardust has been discovered only six years ago and was difficult to detect in primitive solar system samples due to its dimensions (grains are usually smaller than the wavelength of visible light) and the surrounding majority of solar system silicates. Therefore, research on this presolar grain type has just begun, and this work is only a first step to analyze these grains by a variety of microanalytical techniques. Further work on stardust silicates should focus on several issues:

It will be important to obtain high-precision Al-Mg isotope analyses of presolar silicates to put further constraints on their origins, which is often hard to confine from O-Si isotope data alone, but the preparation of grain separates for this purpose will be highly complicated. Especially the origins of extreme Group I and Group III grains need further examination. Additional isotope systems will also help to substantiate the proposed SNII origin for Group IV grains and to disentangle the metallicity vs. extra mixing processes affecting Group II grains. It will be important to identify grains from intermediate mass red giant and red supergiant stars, that are prolific O-rich dust producers and should contribute to the presolar grain inventory. Further TEM investigations on presolar silicates will be important to constrain silicate condensation paths and to reveal additional hints for transformation or low-temperature processes, if grain 1_07 represents a larger population of silicate stardust. Improved statistics on the isotopic compositions and chemistries of Group II grains could tell us, if the over-abundance of Al-rich oxides compared to silicates in this group is an analytical artifact or if this represents true proportions which might be explained by origins in low-metallicity sources. We also need TEM investigations on complex presolar silicates to reconstruct their condensation and to improve theoretical models on heterogeneous silicate nucleation. Future condensation experiments could also provide further ideas to complex condensation sequences. The origin of Fe minerals in presolar silicates (and GEMS) is still an unsolved enigma, and future work should also target this question. The petrographic context of presolar silicates (and presolar grains in total) should be investigated in more detail, as these surveys are important to answer questions on the origins of chondritic matrix, which is still not understood. We also need a larger database on clustered presolar grains to confine the reasons for this effect, which is observed in a variety of primitive solar system materials. Further primitive samples have to be scanned for presolar silicates, as

the abundance of presolar materials in a diverse set of samples yields important information on the distribution of these grains in the solar nebula and also on the evolution of the young solar system.

These future research projects will provide important new aspects about the different stages of the cosmic lifecycle of dust and finally about the stardust, that composed the solar system and our planet Earth.

Danksagung

Lebenslauf

*26. März 1977 in Essen, Staatsangehörigkeit deutsch, Familienstand ledig

Schulbildung

1983-1987	Grundschule Essen-Kettwig
1987-Juni 1996	Gymnasium Essen-Werden
	Abschluss: Hochschulreife

Zivildienst

2. 9. 1996-30. 9. 1997	Familien- und Krankenpflege e.V.
	in Essen-Rüttenscheid

Studium

Oktober 1997-Juli 1999	Studium der **Journalistik** an der Universität Dortmund, ohne Abschluss
Oktober 1999-Mai 2005	Studium der **Geologie** an der Universität zu Köln
	Abschluss: Diplom
	Thema: Charakterisierung von Einschlüssen in ultratiefen Diamanten mit Hilfe zerstörungsfreier in-situ-Methoden (Arbeitsgruppe Herbert Palme, Betreuung: Frank E. Brenker)
Seit Oktober 2005	Doktorarbeit an der Universität Frankfurt / Max-Planck-Institut für Chemie, Mainz
	Thema: Kombinierte isotopische, chemische und mineralogische Studien an präsolaren Körnern (Betreuung: Peter Hoppe und Frank E. Brenker)